Electrochemical Studies of Redox Induced Substitution Reactions

Kenneth Graham Macnamara

Ph.D Thesis

University of Edinburgh

2001

Declaration

Except where specific reference is made to other sources, the work contained in this thesis is the original work of the author. It has not been submitted in whole or in part, for any other degree

Kenneth Macnamara

Acknowledgements

Firstly, thanks must go to Dr Lesley Yellowlees who has been a terrific supervisor and become an excellent friend.

Thanks, to Dr Kenneth Taylor and Dr Alan Brown for starting the work in chapter three and Dr Nicholas Payne for preparing all the complexes in chapter five. Thanks also have to go to the crystallography section, that is, Dr Bob Coxall, Andy Parkin, and Dr Simon Parsons, and to the technical staff, in particular Donald Robertson, and the electrical and mechanical workshops.

In the lab: Thanks to Dr Xiao Ming Liu who first taught me many of the techniques employed in this work. Thanks to Dr Marie Elliot who has been great fun in and out of the lab and has been co-conspirator to many a good story. Thanks to Lorna who has survived three years in the lab with me and a very enjoyable trip to Italy.

Out of the lab: There are too many others to thank but some can't go without a mention: Thanks to Dr Tony Barrett (who better to drink all that champagne with), Mhairi Brunton (wouldn't have got here – or anywhere - without you), Dr Alasdair Graham (great curries and great times), Hilary Hartigan (for Loch Rannoch), the squash boys (champions), and especially Elizabeth Moir (for teaching me how to drink gin and the rest).

I would also like to thank the EPSRC for funding and the University of Edinburgh for my Sports Bursary.

Finally, I'd like to thank my great friend, Dr Eric Farr, who suggested to me that I should do a PhD at a good university and play some good squash – I've done my best.

Abstract

This thesis concerns the reduction induced substitution reactions of three families of transition metal salts: (i) $[MX_6]^{2-}$, where M = Ir, Os, Re and X = Cl^-, Br^-, I^-, (ii) $[OsX_3Y_3]$, where X = Cl^- or Br^- and Y = a tertiary alkyl phosphine or arsine, and (iii) $[Os(NCS)_n(SCN)_{n-6}]^{3-}$, where n = 0 to 6. The substitution reaction has been investigated extensively using electrochemical techniques, in particular double-step chronoamperometry, to elucidate the mechanisms involved and the factors influencing the rate of reaction and the activation energy for the process.

On one-electron reduction, $[MX_6]^{2-}$ undergoes a substitution reaction of one halide, X, for a ligand, L, of less electron donating character. The rate constant and activation energy are largely independent of the nature or the concentration of the entering group, L, and reduced by an increased concentration of the leaving group in solution. The rate limiting step is the loss of a halide. The rate increases $Cl^- < Br^- < I^-$ reflecting leaving group ability and ease of solvation in the organic solvent. On changing the metal centre, the rate of reaction decreases Re >> Os > Ir, rationalised in terms of the nuclear charge of the metal centre: Re(III) is less able to support the electron density from the halides than Os(III) and Ir(III). The activation energy is understood to be the energy required to break the metal-halide bond and represents the extent of orbital overlap between the metal and halide. The nephelauxetic parameter, β, indicates strongly covalent character of the iridium-halide bond reflecting a high overlap of the iridium and halide orbitals. Overall, a Dissociative mechanism has been assigned to the halide loss with the exception of $[OsCl_6]^{2-}$ which can be more adequately described by a dissociative Interchange mechanism with the formation of a pre-equilibrium complex, $\{[OsCl_6]^{3-},L\}$. Digital simulation of the mechanisms supports these findings.

It has been shown that the "inert" supporting electrolyte can play a significant role in the reaction rate of $[OsCl_6]^{3-}$ with L, although the activation energy remains constant.

Thus, the reaction proceeds significantly faster with $NaBF_4$ present than with Adogen 464 (methyltrialkyl(C_8-C_{10})ammonium chloride), due to ion pair formation.

mer-$[OsX_3Y_3]$, when reduced to the Os(II) species in dichloromethane, reacts via a Dissociative mechanism giving a five co-ordinate species by liberation of a ligand. Both the rate of reaction and the activation energy for the process are effected by the nature of the tertiary alkyl phosphine/arsine ligands although no clear trend is evident: both steric and electronic influences are closely involved without either ever being clearly dominant. There is a general trend that as Tolman's electronic parameter for the phosphine ligand, χ_i, tends towards zero, the rate of reaction and activation energy for the process increase. Any *trans effect* or *trans influence* experienced within the complex appears to be less significant than the *cis effect* of the phosphine/arsine ligands. Oxidation of *fac*-$[OsX_3Y_3]$ results in isomerisation to *mer*-$[OsX_3Y_3]^{1+}$. Digital simulation has shown the rate of reaction to be $1900 \pm 120\ s^{-1}$ at 297 K. A relatively low activation energy and the fast rate of reaction suggest the isomerisation reaction goes by an intramolecular rearrangement.

The complexes *cis*-$[Os(NCS)_2(SCN)_4]^{3-}$, *fac*-$[Os(NCS)_3(SCN)_3]^{3-}$, and $[Os(NCS)_6]^{3-}$ have been prepared, isolated, and characterised by electrochemistry, *in situ* uv-vis spectroelectrochemistry, and X-ray crystallography. They have been shown to react on reduction with a ligand, L, of less donating character. Cyclic voltammetric investigations confidently predict the reaction to be the mono-substitution of one thiocyanate ligand for L. The mechanism of reaction is dissociative in nature. A trend is observed whereby the rate constant increases and the activation energy decreases as the number of S-bound ligands increase. The Os(II)-thiocyanate bond is, therefore, weakened by the increase in –SCN ligands, probably due to the increased steric strain introduced to the complex by the non-linear –SCN ligands and their stronger electron donor properties than the –NCS ligands. *In situ* IR spectroelectrochemical studies suggested that an –SCN ligand is lost on substitution.

Contents

Abbreviations

A	Arrhenius pre-exponential factor; Associative mechanism
Adogen 464	methyltrialkyl(C_8-C_{10})ammonium chloride
An	acetonitrile
Ar	aryl group
B	Racah parameter
Bc	benzyl cyanide
Bn	benzonitrile
By	butyronitrile
C	Racah parameter
c_i	concentration of the i^{th} ion
Cy	cyclohexane
CV	cyclic voltammetry
D	Dissociative mechanism
dcm	dichloromethane
dce	dichloroethane
DEAE	diethylaminoethyl
D_i	diffusion coefficient, i
DMSO	dimethylsulfoxide
E	potential
$E_{1/2}$	half-wave potential
e^-	an electron
E_a	activation energy
EC	electrochemical-chemical
E_k	kinetic energy
en	ethylenediamine
E_p^{ox}	potential peak for an oxidation process
E_p^{red}	potential peak for a reduction process
EPR	electron paramagnetic resonance
Et	Ethyl

F	Faraday's constant (96485 C mol^{-1})
f_A	activity coefficient of the ion, A
f_B	activity coefficient of the ion, B
$f_{AB^{\ddagger}}$	activity coefficient of the activated complex, $AB^{\ddagger}$
fac	facial
G	Gibbs free energy (kJ mol^{-1})
GC	gas chromatography
H	enthalpy (kJ mol^{-1})
h	Planck constant (6.626 x10^{-34} J s)
HFB	hexafluorobut-2-yne
HOMO	highest occupied molecular orbital
HPLC	high performance liquid chromatography
I	Interchange mechanism
I_a	associative Interchange mechanism
I_d	dissociative Interchange mechanism
i	current (A)
i_p^{ox}	current peak for an oxidation process
i_p^{red}	current peak for a reduction process
IR	infrared
$K^{\ddagger}$	pseudo equilibrium constant
$K_a^{\ddagger}$	activity equilibrium constant
K_E	equilibrium constant
K_{obs}	observed equilibrium constant
k	rate constant
k_b	rate constant of the back reaction
k_B	Boltzmann constant (1.38 x10^{-23} J K^{-1})
k_f	rate constant of the forward reaction
k_{obs}	observed rate constant
L	ligand
LMCT	ligand to metal charge transfer
LUMO	lowest unoccupied molecular orbital
Me	methyl

mer	meridional
MLCT	metal to ligand charge transfer
n	electron number
NMR	nuclear magnetic resonance
$[N^nBu_4]^+$	tetrabutylammonium ion
OTTLE	optical transparent thin layer electrode
Ph	phenyl
Pn	propionitrile
pp	dmpe dimethylposphinylethane
	depe diethylphophinylethane
	dppe diphenylphosphinylethane
	dppm diphenylphosphinylmethane
Py	pyridine
Q	charge (C)
R	gas constant (8.31451 $J\ K^{-1}\ mol^{-1}$)
r.l.s	rate limiting step
S	entropy ($J\ K^{-1}mol^{-1}$)
t	time (s)
T	temperature (K)
TCNE	tetracyanoethylene
TCNQ	tetracyanoquinodimethane
THF	tetrahydrafuran
uv-vis	ultraviolet-visible
uv-vis-nir	ultraviolet-visible-near infrared
w/v	weight/volume
z	charge of a complex ion
α	transfer coefficient
Å	Angstrom
β	nephelauxetic parameter
Δ_o	ligand field splitting parameter
ΔE	peak to peak separation
ε	molar extinction coefficient ($cm^{-1}\ mol^{-1}\ dm^3$)
$\Delta G^{\ddagger}$	Gibbs free energy of activation

$\Delta H^{\ddagger}$	enthalpy of activation
μ	ionic strength
$\Delta S^{\ddagger}$	entropy of activation
θ	Tolman's cone angle (^{o})
τ	time (s)
$\Delta V^{\ddagger}$	volume of activation
ν	reaction rate; scan rate (V s^{-1})

List of Figures

List of Tables

CHAPTER ONE:

Introduction

1 Introduction

1.1 Introductory Remarks

This thesis concerns the redox-induced substitution reactions of three families of transition metal salts:

(i) $[MX_6]^{2-}$, where M = Os, Ir, Re and X = Cl^-, Br^-, I^-

(ii) $[OsX_3L_3]$, where X = Cl^-, Br^- and L = tertiary alkyl phosphines or arsines

(iii) $[Os(NCS)_n(SCN)_{n-6}]^{3-}$, where n = 0-6.

On reduction, the metal salts undergo substitution of a ligand for one of less electron donating character such as acetonitrile. The substitution reaction has been extensively investigated using electrochemical and spectroelectrochemical techniques to elucidate the mechanisms involved.

By way of introduction a brief over view on the current understanding of rates and reaction mechanisms of inorganic complexes is presented. Thereafter, a number of detailed examples are given of inorganic substitution reactions from the chemical literature illustrating the methods of rate law and reaction mechanism determination and the complex problems therein. A number of factors effect both the rate and reaction mechanism. As with most chemistry, it is often impossible to examine one feature in isolation. Although it is important to understand each effect individually, it is thought to be more fruitful to discuss relevant chosen cases in more detail. Emphasis is given to the platinum group metal complexes.

1.2 Rates and Reaction Mechanisms in Inorganic Complexes

The basic data of chemical kinetics are the concentrations of reactants and products throughout the course of reaction. From this an understanding of the rate laws and the mechanisms of reaction can be developed. Consideration must be taken of various parameters, often most importantly temperature.

1.2.1 The Rates of Reaction

The relationship between reaction rate and concentration of reactants determined experimentally is given by the rate law. For the general reaction,

$aA + bB \rightarrow cC$

reaction rate, $v = k[A]^a[B]^b$

where "k" is the rate constant. The rate law shows that the concentration of reactants is raised to some power, or order. The order is not necessarily the stoichiometric coefficients for the balanced equation. The sum of the order for each species in the rate law gives the overall reaction order, i.e. first, second, and third order. Non-integer values of order are possible. Transient intermediates and side reactions often complicate the experimental determination of a rate law. The process can be simplified by having all but one of the reactants in large excess. For the second order rate law,

$v = k[A][B]$

if the concentration of B is constant then,

$\nu = k'[A]$, where $k' = k[B]_0$

The rate law is now said to be pseudo first order. A similar treatment of a third order rate law, $\nu = k[A]^2[B]$ gives,

$\nu = k'[A]^2$

a pseudo second-order reaction. By isolating each species in turn and evaluating the dependence of the rate to each concentration of species a complete rate law can be determined.

Integration of differential rate laws allows the calculation of concentration at time, t. For the reaction,

$$A \xrightarrow{k} B$$

$$\Rightarrow \nu_A = \frac{d[A]}{dt} = -k[A]$$

$$\Rightarrow \int_{[A]_0}^{[A]} \frac{d[A]}{[A]} = -k\int_0^t dt$$

$$\Rightarrow \ln[A] - \ln[A]_0 = -kt \quad \text{OR} \quad \ln\frac{[A]}{[A]_0} = -kt \qquad \textit{- integrated first order rate law}$$

A plot of $\ln[A]/[A]_0$ against time gives a straight line plot with gradient k. The time dependence of concentration is different for a second order reaction. For example,

$$\frac{d[A]}{dt} = -k[A]^2$$

$$\Rightarrow -\frac{d[A]}{[A]^2} = kdt$$

$$\Rightarrow -\int_{[A]_0}^{[A]} \frac{d[A]}{[A]^2} = \int_0^t k dt$$

$$\Rightarrow \frac{1}{[A]} - \frac{1}{[A]_0} = kt \qquad \textit{- integrated second order rate law}$$

A plot of 1/[A] against time gives the gradient, k, and the intercept $1/[A]_0$. Further calculations can be carried out for other orders of reaction. Advances in graph fitting programs have made it possible to solve increasingly complicated rate laws from experimental data.

1.2.2 Initial Rate Method

It is worth noting that most kinetic studies are made on reactions well before they reach equilibrium. In the initial rate method the rate of reaction is measured at the commencement of reaction when the concentrations are predetermined. If this reaction can be repeated at a number of starting concentrations then the rate law can be determined. The advantages of this approach are two fold; 1) reverse equilibria are unimportant as there are no appreciable amounts of products, and 2) the rate is not complicated by further side reactions. A major disadvantage is that a complex rate law can be disguised.

1.2.3 Transition State Theory

It is found that the rate of most reactions increase with temperature and that for a chemical reaction to be fruitful an energy barrier must be overcome. Transition State

Theory proposed by Eyring in 1935 is the basis for understanding this effect. Reacting molecules must absorb energy from their environment to overcome an energy barrier to go on and react. The energy required is the activation energy, E_a. The reacting molecule with this energy deforms to give a transition state called an activated complex. The theory is depicted in an energy profile, **Figure 1.1**.

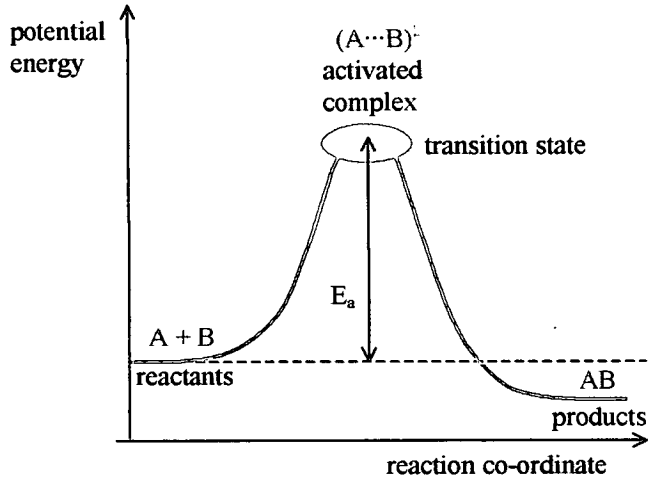

Figure 1.1 Reaction profile for a reaction step

When reactants A + B have the transition state energy they will go on to make products. Similarly in the reverse process when AB has the transition state energy they will fall apart to A + B. This is an important distinction when considering more detailed reaction dynamics discussed later.

1.2.4 Temperature and Reaction Rates

A minimum condition for two molecules to react is that they must collide. It is usually the case that this collision must take place along a particular direction, a reaction co-ordinate. Furthermore, collision will only lead to a reaction if the molecules overcome the activation energy. An increase in temperature will increase the number of collisions, the velocity of collisions and, more importantly, will

increase the fraction of molecules with sufficient kinetic energy to react as illustrated in **Figure 1.2**.

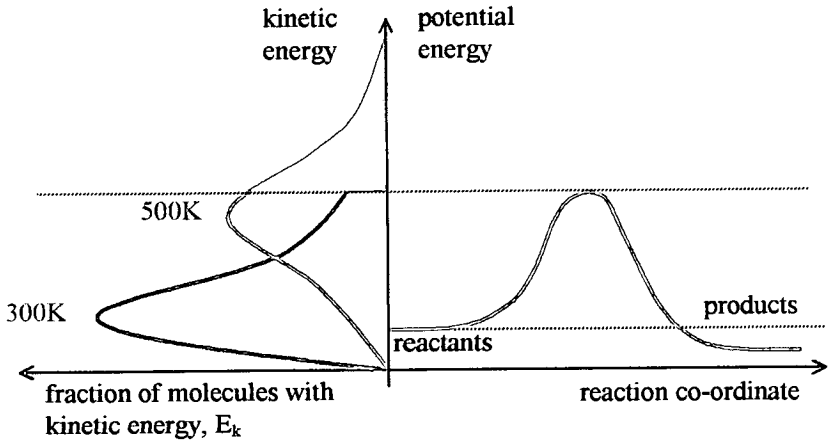

Figure 1.2 Energy diagram of reaction step and fraction of molecules with a particular kinetic energy[1]

The link between reaction rate, energy, and collisions, is made by the Arrhenius equation:

$k = Ae^{-E_a/RT}$ OR $\ln k = \ln A - \frac{E_a}{RT}$ **Equation 1.1**

The term "k" is the reaction rate constant, "A" is the pre-exponential factor or frequency factor, "R" is the gas constant (8.31451 J K^{-1} mol^{-1}), and "T" is temperature in K. "A" can be thought of as describing the frequency of collisions along the reaction co-ordinate. The "$e^{-E_a/RT}$" part describes the fraction of molecules with sufficient energy for reaction. A plot of lnk against 1/T for many reactions gives a straight line with gradient, $-E_a/R$.

1.2.5 Mechanisms of ligand Substitution – General Considerations

In this section reactions of co-ordination compounds in which one ligand is replaced by another are discussed such as:

$$X + M\text{-}Y \rightarrow M\text{-}B + Y$$

Where M is a metal and X and Y are competing ligands The reaction mechanism involves at least one elementary step relating to the *stoichiometric mechanism*. The details of the activated complex in the rate limiting step are considered in the *intimate mechanism*.

There are three paths a stoichiometric mechanism can take; Associative (A), Dissociative (D), and Interchange (I).[2] The energy profiles now roughly take the form shown in **Figure 1.3**.

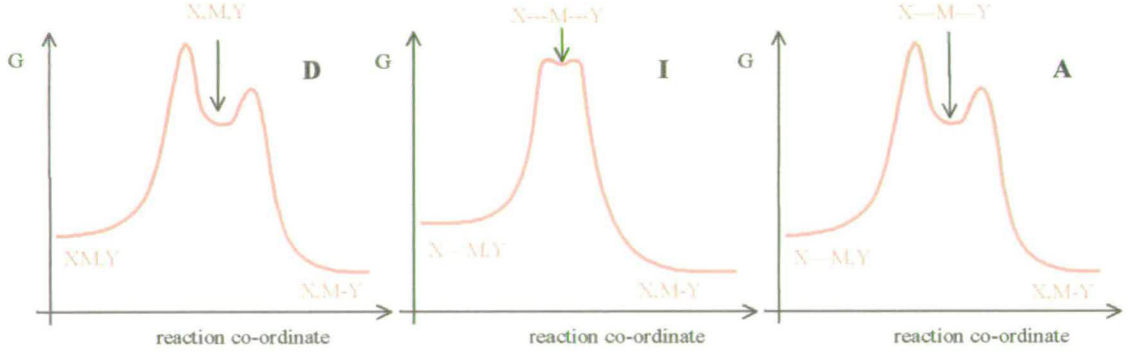

Figure 1.3 Reaction profiles for Dissociative, Interchange, and Associative mechanisms

An Associative mechanism involves at least two elementary steps; a bimolecular step where an intermediate of higher co-ordination number is formed and a unimolecular step where a ligand is displaced. The rate limiting step is the formation of the intermediate and therefore dependent on the entering group. Consequently the rate is independent of the rate of the leaving group. A Dissociative process also goes by at least two elementary steps; one step involves an unimolecular step where an

intermediate of lower co-ordination number is formed and a bimolecular where a new ligand bonds with the intermediate. The rate is independent of the entering group, so that the rate limiting step is the unimolecular step. An Interchange mechanism takes place in one elementary step where no true intermediate is formed. The difference between either Associative or Dissociative and Interchange is loosely determined by whether an intermediate is sufficiently stable to discern between incoming nucleophiles and whether it is present long enough to be detected.[3]

The three mechanisms, A, D, and I, are ideal cases and are useful characterisations of reactions. It is instructive to further elaborate on the formation of the activated complex. Information on the properties of the transition state is commonly obtained from the entropy of activation, $\Delta S^{\ddagger}$, and the volume of activation, $\Delta V^{\ddagger}$. The values of $\Delta S^{\ddagger}$ and $\Delta V^{\ddagger}$ separate the Interchange mechanism into either associative (a) or dissociative (d) sub-classifications, represented as a subscript on the stoichiometric mechanisms, so that the range of mechanisms are described as, A, I_a, I_d, D.

A positive change in entropy shows an increase in disorder of a system indicating a dissociative mechanism. A decrease in disorder will give a negative change in entropy. There are, however, a number of contributions to $\Delta S^{\ddagger}$ making true interpretation difficult.

i) Electrostriction. If there is a change in charge density on creation of an activated complex then there will be a change in ordering in the solvent in a process known as electrostriction. An increase in charge density causes the solvent molecules to order around the activated complex and therefore gives a negative value of $\Delta S^{\ddagger}$. A decrease in charge density causes a less ordered system and gives a positive value of $\Delta S^{\ddagger}$.

ii) Stereo re-organisation. Whether an activated complex undergoes significant stereo re-organisation will influence the $\Delta S^{\ddagger}$. A reorganisation of the complex will increase the disorder.

iii) Translational, rotational, vibrational motion on the reaction co-ordinate.

The volume of activation is the difference in molar volume between the initial reactants and the activated complex. As for $\Delta S^{\ddagger}$, $\Delta V^{\ddagger}$ is closely related to the extent of electrostriction. For this reason the value of $\Delta V^{\ddagger}$ can only be reliable for neutral systems where a rate increase with increasing pressure (a negative value of $\Delta V^{\ddagger}$) implies an associative mechanism. It follows that a positive $\Delta V^{\ddagger}$ implies a dissociative mechanism.

Of the two values it is found that $\Delta V^{\ddagger}$ is more easily interpreted but requires sophisticated high-pressure equipment. $\Delta S^{\ddagger}$ values are more easily obtained, generally from the Eyring relationship (**Equation 1.10**), but perhaps are less useful because of the many contributions making up the final value create increasingly difficult interpretation and because of the non-trivial modifications involved for an ionic reaction in an electrolytic solution.

1.2.6 Reaction Dynamics

The concepts of the activated complex can be developed in an empirical approach, in which the activation process is expressed in terms of thermodynamic functions.[4,5]

A pseudo equilibrium constant, $K^{\ddagger}$, is defined as:

$$K^{\ddagger} = \frac{[A\cdots B]^{\ddagger}}{[A][B]}$$

where $[A\cdots B]^{\ddagger}$ is the concentration of the activated complex. The steady state approximation is made such that during the major part of the reaction the rates of change of all reaction intermediates are negligibly small. The rate equation for the formation of AB can now be given as:

$$\text{Rate} = \nu[A\cdots B]^{\ddagger} = \nu K^{\ddagger}[A][B] \qquad \textbf{Equation 1.2}$$

where ν is the rate at which the complex relaxes from the transition state to the products. It is reasoned that ν is also the vibrational frequency of the A···B bond along the reaction co-ordinate. At the transition state, the energy of bond vibration equals the potential energy of the bond so that

$$E_{vib} = h\nu = E_{pot} = k_B T \qquad \textbf{Equation 1.3}$$

where h is Planck's constant (6.624×10^{-34} Js) and k_B is the Boltzmann constant (1.38×10^{-23}). **Equation 1.3** rearranges to

$$\nu = \frac{k_B T}{h} \qquad \textbf{Equation 1.4}$$

Insertion into **Equation 1.2** gives

$$\text{Rate} = \frac{k_B T}{h} K^{\ddagger}[A][B] \qquad \textbf{Equation 1.5}$$

The rate is also given by, rate = k[A][B] and substitution into **Equation 1.5** gives

$$k = \frac{k_B T}{h} K^{\ddagger} \qquad \textbf{Equation 1.6}$$

The pseudo equilibrium constant is related to the Gibbs energy of activation by

$$\Delta G^{\ddagger} = -RT\ln K^{\ddagger} \qquad \textbf{Equation 1.7}$$

$$\Rightarrow \Delta G^{\ddagger} = -RT\ln\frac{kh}{k_B T} \qquad \textbf{Equation 1.8}$$

Because G = H – TS, the Gibbs energy of activation can be divided into an entropy of activation, $\Delta S^{\ddagger}$, and an enthalpy of activation, $\Delta H^{\ddagger}$.

$\Delta G^{\ddagger} = \Delta H^{\ddagger} - T\Delta S^{\ddagger}$ **Equation 1.9**

Substitution into **Equation 1.8** gives

$$\ln\frac{k}{T} = -\frac{\Delta H^{\ddagger}}{R}\frac{1}{T} + \ln\frac{k_B}{h} + \frac{\Delta S^{\ddagger}}{R}$$ **Equation 1.10**

Equation 1.10 is often described as the *Eyring relationship*. A plot of ln(k/T) against 1/T should give a straight line with a gradient of $-\Delta H^{\ddagger}/R$ and an intercept of $\ln(k_B/h) + \Delta S^{\ddagger}/R$. Rather than extrapolate to obtain a value for $\Delta S^{\ddagger}$, values of $\Delta H^{\ddagger}$ (from the gradient $-\Delta H^{\ddagger}/R$) and $\Delta G^{\ddagger}$ (calculated from **Equation 1.8**) can be inserted into **Equation 1.9** for a given temperature. This equation strictly applies to non-electrolytes in dilute solution and must be modified for ionic reactions in electrolyte solutions.[6] Ions derived from both reactants and from added electrolytes often affect the rate of a reaction. The rate constant for a reaction should be obtained at constant ionic strength (or obtained by extrapolating data at different ionic strengths to a zero ionic strength). This must be allowed for in the derivation of a true rate law or removed by "swamping" with excess electrolyte. For the calculation of kinetic parameters by the Eyring relationship of an ionic reaction in electrolyte solution, the rate constant is modified as in **Equation 1.11**.

$$k = \frac{kT}{h}K_a^{\ddagger}\frac{f_A f_B}{f_{AB^{\ddagger}}}$$ **Equation 1.11**

The term $K_a^{\ddagger}$ is the activity equilibrium constant and $f_{AB^{\ddagger}}, f_A$, and f_B, are the activity coefficients of the activated complex, $AB^{\ddagger}$, and the ions, A and B respectively. Activity coefficients are related to the concentration but for single ions cannot be measured with thermodynamic rigour. They are usually equated to a measurable mean ionic activity coefficient.[7]

1.2.7 Substitution Reactions of Octahedral Complexes

The substitution reactions of octahedral transition metal complexes go by either Interchange or Dissociative mechanisms. The reaction is very much dependent on the leaving group and independent of the entering group. There are ambiguous reports of Associative mechanisms. However any dependence on the entering group can usually be accounted for by a pre-equilibrium interaction between reagents.[8,9]

1.2.7.1 Leaving Group Effect

Since substitution reactions in octahedral complexes are essentially dissociative in nature it is clearly important to understand the effects of the leaving group. A reactivity series for complexes of the type, $[Co(NH_3)_5X]^{n+}$ has been established as $HCO_3^- >> NO_3^- > I^- > H_2O > Br^- > Cl^- > SO_4^{2-} > (S)CN^- > F^- > CH_3COO^- > (N)CS^- > NO_2^- > NH_3 > OH^- > CN^-$.[3] This is quite typical although the series is by no means definitive. We can expect the other ligands of the ligand set, the so-called spectator ligands, to have effects on the rates. Spectator ligands, both *cis* and *trans*, can have the ability of making the leaving group more labile according to their electronic character.

The trans effect

It has long been known that ligand exchange reactions often show a preference for the site *trans* to one ligand rather than another. An approximate ordering of ligands is:

$$CO > CN^- > C_2H_4 > PR_3 > H^- > CH_3^- > C_6H_5^- > NO_2^-$$

$$I^- > (S)CN^- > Br^-, Cl^- > Py, NH_3, OH^-, H_2O$$

There are many explanations for the *trans* effect generally citing π or σ effects, or both. One explanation is that ligands with the most π-acceptor character and which therefore remove most π-electron density from the metal have the strongest *trans* effect.[10] Another explanation notes the order of *trans* effect follows roughly the order of increasing orbital overlap.[2] In either case it is observed that a ligand with a strong *trans* effect reduces the electron density on the ligand opposite (*trans*) and it follows that it is this *trans* ligand which is most open to nucleophilic attack. It can be considered that the *trans* ligand encourages the attachment of a further ligand and in this sense can successfully explain kinetic phenomena such as rates and reaction mechanisms. It should be recognised that the *trans* effect is kinetic, depending on the activation energies and stabilities of both the ground state and activated complex.

The trans influence

The influence of one ligand on the strength of the bond to the ligand that is *trans* to it is called the *trans* influence. A ligand that is a strong σ-donor is expected to produce an axial polarisation of the metal. It is thought a lone pair from one ligand can induce a positive charge on the near side of the metal and a concomitant negative charge on the far side, thus weakening the bond to the ligand in the *trans* position. This is a thermodynamic effect and is a ground state property which may be evaluated from the bond lengths, NMR coupling, or metal-ligand stretching frequencies. The sequence is generally similar to the *trans* effect but with some notable exceptions.

$$C_2H_4 > H^- > PR_3 > (S)CN^- > I^- > CH_3^-, CO, CN^-$$

$$> Br^- > Cl^- > NH_3, > OH^-$$

The exceptions are largely accounted for by π-bonding ability, a likely order for this ability is given as:

$$C_2H_4, CO > CN^- > NO_2^- > (S)CN^- > I^- > Br^- > Cl^- > NH_3 > OH^-$$

The net *trans* effect, therefore, can more or less be rationalised in terms of the strength of the π-bonding and the *trans* influence.

Cis effect

Unlike any thermodynamic *trans* influence or kinetic *trans* effect, there is generally only a small effect on reaction rate due to the electronic properties of the *cis* ligands, however, because of their proximity to the site of replacement steric interactions can play an important role.

1.2.7.2 Steric Effects and Stereochemical Change

Generally, a Dissociative mechanism is favoured by complexes under steric strain from their ligands. A five co-ordinated activated complex will lessen the steric strain promoting dissociative activation and in many cases increasing the rate. There are two stable configurations for a five co-ordinate activated complex; trigonal bipyramidal or tetragonal pyramidal. Retention of the original geometry occurs when substitution goes by a tetragonal pyramidal configuration. A trigonal bipyramidal intermediate, however, can lead to isomerisation of the original complex. A common feature of the ligands that lead to stereochemical change is the ability of the spectator ligands to donate π electrons to the metal. This donation stabilises the intermediate most effectively by adopting trigonal bipyramidal geometry even though crystal field

stabilisation theory suggests square based pyramidal geometry as the more stable (*vide infra*).

1.2.7.3 Rate Laws and Their Interpretation

The rate law of an octahedral substitution by an Interchange mechanism is usually consistent with the Eigen–Wilkins mechanism. The first step in the mechanism accounts for an outer sphere pre-equilibrium between the complex, C, and the entering group, Y, such that:

$$C + Y \rightleftharpoons \{CY\}$$

$$K_E = \frac{[\{CY\}]}{[C][Y]} \qquad \textbf{Equation 1.11}$$

Values of K_E are difficult to measure but will be large for ions of opposite charge which will have stronger bonding between them and small for ions of like charge (and weaker bonding). Large ions will collide more often than smaller ions and will give large and small values of K_E respectively.

The second step in the Eigen-Wilkins mechanism is the rate limiting step where the encounter complex, {CY}, occasionally reacts to give products:

$$\{CY\} \xrightarrow{k} \text{products}$$

$$rate = k[\{CY\}] \qquad \textbf{Equation 1.12}$$

The concentration of the total complex, $[C]_T$, is the sum of that which is free, [C], and that which is in the encounter complex, [{CY}] such that;

$$[C]_T = [C] + [\{CY\}] \qquad \textbf{Equation 1.13}$$

Insertion of **Equation 1.11** into **Equation 1.13** gives;

$$[C]_T = [C] + K_E[C][Y]$$

$$\Rightarrow [C]_T = [C](1 + K_E[Y])$$

$$\Rightarrow [C] = \frac{[C]_T}{1 + K_E[Y]} \qquad \textbf{Equation 1.14}$$

Combining **Equation 1.11** and **Equation 1.12** gives:

$$rate = kK_E[C][Y] \qquad \textbf{Equation 1.15}$$

From **Equation 1.14** and **Equation 1.15** the overall rate law is found to be:

$$rate = \frac{kK_E[C]_T[Y]}{1 + K_E[Y]}$$

A special case arises when the entering group, Y, is the solvent. The encounter complex, {CY}, is saturated because the complex species, C, is associated with (at least) one solvent molecule. $K_E[Y]$ will be much greater than 1 and the rate constant will equal the observed rate of reaction. The mechanism can be applied to all bimolecular reactions in solution that occur at rates less than the limit imposed by diffusion.

1.3 Examples of Inorganic Substitution Reactions

i) Leigh *et al* have presented a wonderfully comprehensive quantitative kinetic study to show the effect of changing the metal centre, spectator ligands, and nucleophile, on the rates and mechanisms of substitution of X_2 in octahedral complexes of the type, $[MH(X_2)(pp)_2]^+$, where M = Fe, Ru, Os; X = H_2, N_2; pp = dmpe ($Me_2PCH_2CH_2PMe_2$), depe ($Et_2PCH_2CH_2PEt_2$); for L, where L = MeCN, PhCN, Cl^-.[11] By reference to work by Basallote *et al* and Albinez *et al* on analogous complexes a large family of complexes are considered showing a range of reaction mechanisms (**Figure 1.4**).[9,12]

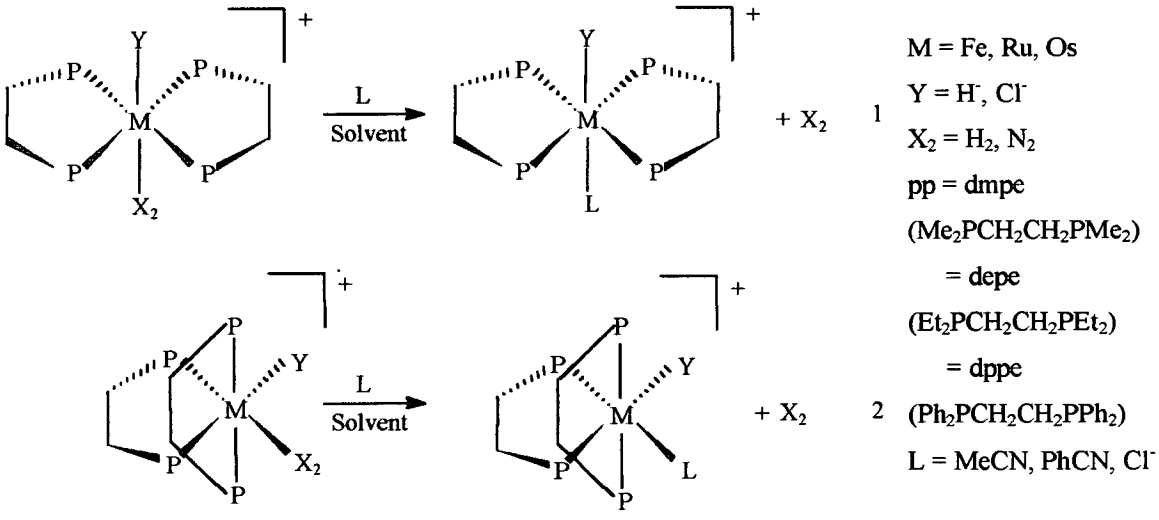

Figure 1.4 Reaction for *trans* (1) and *cis* (2) $[MY(X_2)(pp)_2]^+$

Factors affecting mechanism

In the studies concerning dmpe and depe the kinetics were carried out with a systematic variation of the concentration of the nucleophile, L. There was no appreciable change in the observed rate, k_{obs}, demonstrating that the rate was independent of the concentration of L. The rate was also shown to be independent of the identity of L. The activation parameters, $\Delta H^{\ddagger}$ and $\Delta S^{\ddagger}$, were both large, positive values. The rate limiting step, therefore, was understood to be a unimolecular

reaction liberating X_2 and the mechanisms described as either Dissociative or dissociative Interchange. The Dissociative mechanism is illustrated below.

$$[MH(X_2)(pp)_2]^+ \underset{k_{-1}}{\overset{k_1}{\rightleftharpoons}} [MH(pp)_2]^+ + X_2 \xrightarrow[L]{k_2} [MH(L)(pp)_2]^+$$

The rate limiting step, k_1, gives the five co-ordinate activated complex, $[MH(pp)_2]^+$. This is followed by nucleophile attack, k_2(fast). The first order rate equation was proposed as;

$$\frac{-d[MH(X_2)(pp)_2]^+}{dt} = \frac{k_1 k_2 [L][MH(X_2)(pp)_2]^+}{k_{-1}[X_2] + k_2[L]}$$

But simplifies for the pseudo first order rate when L is in excess to:

$$\frac{-d[MH(X_2)(pp)_2]^+}{dt} = k_1[MH(X_2)(pp)_2]^+$$

Basallote's work on *trans*-$[FeH(H_2)(dppe)_2]^+$, in contrast, showed a surprising change in the mechanism on changing the phosphine ligand to dppe.[9] The reaction still occurred in one measurable step but the rate constant showed some dependence on the concentration and nature of L. The $\Delta S^{\ddagger}$ reflected this change. The mechanism, assigned as an associative Interchange, was found to be more complicated than for dmpe and depe and, as an unusual case, will be discussed later. Overall, it was clearly shown that changing the electronic and steric properties of the phosphine ligands perturbs the lability of both the phosphine ligands themselves and X_2 with the result being a change in mechanism for the overall reaction.

Factors affecting the rate constant, k_{obs}

The largest factor affecting k_{obs} for the reaction $[MH(X_2)(pp)_2]^+ \rightarrow [MH(L)(pp)_2]^+$ was shown to be changing the metal centre of the complex. In this case it was found that the order exists, 4d >> 3d >> 5d which is consistent with other studies of Group

8 complexes.[13,14,*] It was demonstrated that the rate constants were also dependent on the alkyl group on the phosphine ligands; depe was a factor 5 faster than dmpe; Et is a better σ-donor than Me, thus weakening the M-X_2 bond. It was understood that the electronic effects of the alkyl groups are of more importance than any steric effect.[15]

The ligand *trans* to H_2 (the leaving group) is found by Albinez to have a strong effect on k_{obs}. The *trans* ligand competes with H_2 for π electron density through the metal. The series, *trans*-$[RuY(H_2)(pp)_2]^+$ (Y = H^-, Cl^-, pp = depe) is stable to H_2 loss for Y = Cl^- and labile for Y = H^-. Rigo *et al*, however, found the reverse was true for pp = $Cy_2PCH_2CH_2PCy_2$ (Cy = cyclohexyl).[16]

It was concluded, in an open fashion, by Leigh that, "the rate constants for loss of X_2 depend subtly on the metal and on all the ancillary ligands".[11]

A small rate dependence of 15 to 35 % was shown on changing the solvent from acetone to THF although activation parameters remain unchanged. The polarities of the starting complex and of the activated complex are unchanged and are therefore not considered to have an effect, rather it is attributed to small changes in the electron donor power of the individual solvents.

Factors affecting the activation parameters

A summary of activation energies and activation parameters for the substitution of X_2 in complexes of the type $[FeH(X_2)(pp)_2]^+$ in acetone is given in **Table 1.1**. According to Leigh *et al*, values of $\Delta H^{\ddagger}$ and $\Delta S^{\ddagger}$ for the reaction of $[MH(X_2)(pp)_2]^+ \rightarrow [MH(L)(pp)_2]^+$ are larger when $X_2 = H_2$ than N_2.[11] From that, it follows that H_2 complexes experience tighter binding to the metal and are considered more thermodynamically and kinetically stable. It is noteworthy, however, that with consideration of the stated errors in $\Delta H^{\ddagger}$ and $\Delta S^{\ddagger}$ the values are almost the same

* Halpern *et al* found rate constants spanning the remarkable range of 10^{11} for the complexes $[Ru(H_2)_2H(PPh_3)_3]^+$ (10^5 s^{-1}) and $[OsH_3\{P(C_6H_4Me\text{-}p)_3\}_3]^-$ (10 s^{-6}).[13]

within experimental error. Thermodynamic values were shown to increase in line with a decrease in k_{obs}. $\Delta G^{\ddagger}$ was generally invariant with changes in the ancillary ligands.

Complex	E_a kJ mol^{-1}	$\Delta H^{\ddagger}$ kJ mol^{-1}	$\Delta S^{\ddagger}$ J K^{-1} mol^{-1}	$\Delta G^{\ddagger}_{298K}$ kJ mol^{-1}
$[FeH(H_2)(dppe)_2]^+$		86 ± 7	-4 ± 21	
$[FeH(H_2)(depe)_2]^+$	115.1 ± 4.7	112.4 ± 4.7	48 ± 15	98.1 ± 0.2
$[FeH(N_2)(depe)_2]^+$	109.3 ± 4.7	107.2 ± 4.1	40 ± 14	95.2 ± 0.1
$[FeH(N_2)(dmpe)_2]^+$	123.5 ± 3.7	120.8 ± 3.7	73 ± 13	99.2 ± 0.2

Table 1.1 Summary of activation energies and parameters for the reaction of $[FeH(X_2)(pp)_2]^+$ in acetone

Qualitative comparisons of cis and trans

Comparisons were made between the *trans-* and *cis-* complexes of $[MH(X_2)\{P(CH_2CH_2PR_2\}_3]^+$ on their reaction with L. It was found that the *cis* complexes were faster than *trans* at liberating X_2. This effect was described by Bianchini *et al* as an incipient formation of H_3 due to the *cis* arrangement, reportedly significant for $X_2 = H_2$, but no comparable effect could be detected for N_2.[17,18] The trend in reactivity of the metals was found to be the same, Ru >> Fe >> Os.

ii) As discussed earlier, Basallote *et al* have proposed an associative Interchange mechanism for the reaction of the type,

trans-$[FeH(H_2)(dppe)_2]^+ + L \rightarrow$ *trans*-$[FeHL(dppe)_2]^+ + H_2$

where L = MeCN, PhCN, DMSO.[9] As for the analogous dmpe and depe complexes of Leigh, the process took place in one measurable kinetic step. The observed rate

constants, however, demonstrated sensitivity to concentrations of L in some solvents (THF, MeCN) but not in others (acetone). The activation parameters for the reaction with MeCN in these solvents are given in **Table 1.2**.

Solvent	$\Delta H^{\ddagger}$ / kJ mol^{-1}	$\Delta S^{\ddagger}$ / J K^{-1} mol^{-1}	$\Delta V^{\ddagger}$ / cm^3 mol^{-1}
MeCN	78 ± 3	-29 ± 8	-35 ± 2
THF	80 ± 4	-25 ± 13	-23 ± 1
Acetone	86 ± 7	-4 ± 21	-18 ± 1

Table 1.2 Activation parameters for the dihydrogen substitution reaction of *trans*-$[FeH(H_2)(dppe)_2]^+$ for MeCN

The enthalpy of activation, $\Delta H^{\ddagger}$, remained approximately constant while $\Delta S^{\ddagger}$ was negative in all cases and showed some solvent dependence. Once again, it should be noted that the errors in $\Delta S^{\ddagger}$ are very large. The determination of $\Delta V^{\ddagger}$, however, proved to be the decisive tool in elucidating the mechanism. The very negative values of $\Delta V^{\ddagger}$ suggested a definite association character. Two simple associative mechanisms of the type shown below were ruled out.

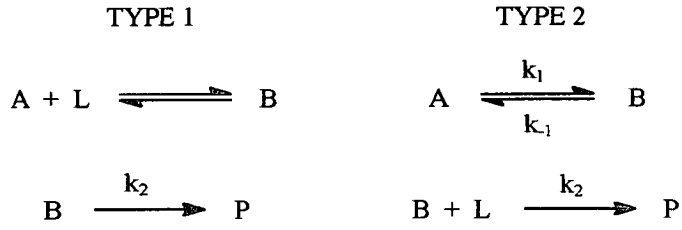

Scheme 1.1 Possible mechanisms of reaction for associative substitution

Type 1 is controlled by the rate k_2 and would build up a significant concentration of the intermediate B. Neither UV-visible or NMR spectra recorded any intermediate however. It was deemed unreasonable to expect a spectrum of the intermediate to be indistinguishable from the starting complex due the fact that $\Delta V^{\ddagger}$ and $\Delta S^{\ddagger}$ are considerably negative.

The rate limiting constant k_1 in Type 2 allows for no build up of intermediate concentration but was ruled out because it was considered unlikely that the process could occur with such a large decrease in volume.

Basallote has proposed a more feasible mechanism illustrated in **Scheme 1.2** accounting for the failures of Type 1 and 2. Noting that complexes of the type *trans*-$[FeH(H_2)(dppe)_2]^+$ can have a certain fluxional behaviour making the H atom homotopic; it was understood that this may stabilise the metal centre inhibiting the dissociation of H_2.[19] It was proposed that the initial step might instead be the opening of one of the chelate rings favoured over dissociation of H_2. This process was not unprecedented with several reports in the literature suggesting dissociation of a spectator ligand is responsible for catalytic processes and substitution reactions.[20,21] Both reaction mechanisms through route A and B are thought to satisfactorily describe the kinetic results. In either case the rate determining step, k_2, for substitution of H_2 for L involves an associatively activated transition state.

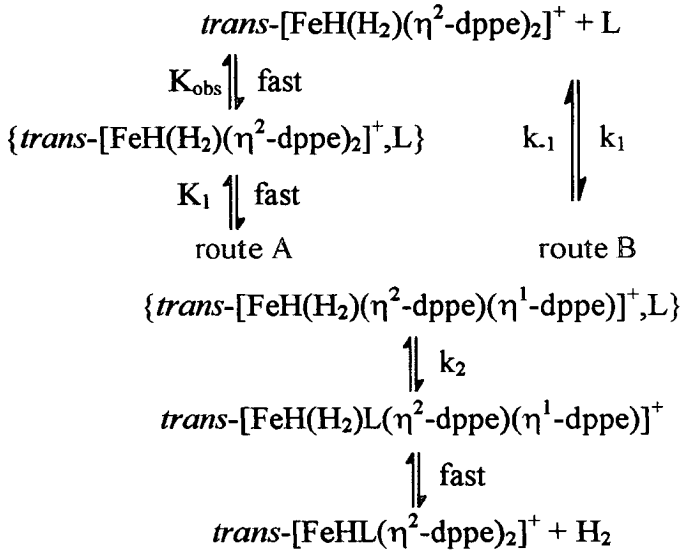

Scheme 1.2 Proposed mechanism for the dihydrogen substitution reaction of *trans*-$[FeH(H_2)(dppe)_2]^+$ for L

In the mechanism proposed it was thought that an initial build up of {*trans*-$[FeH(H_2)(\eta^2\text{-dppe})(\eta^1\text{-dppe})]^+$,L} would have similar spectral properties of the starting complex and would therefore be undetected. The chelate ring opening was understood not to be significant to $\Delta V^{\ddagger}$ as the increased volume in a free end to dppe would be negated by the contraction of a five co-ordinate intermediate and postulated hydrogen bonding between the uncoordinated phosphine and H_2. The measured large negative $\Delta V^{\ddagger}$ was therefore attributed to the association of L to the unsaturated intermediate. The solvent dependence of $\Delta V^{\ddagger}$ and $\Delta S^{\ddagger}$, particularly when

the solvent and L are the same, was more easily accounted for in this way but it was acknowledged that the solvent may also be involved in further specific interactions.

The rate laws for the reactions were given as,

mechanism A, $k_{obs} = \frac{K_1 k_2 K_{obs}[L]}{1 + K_{os}[L]}$ mechanism B, $k_{obs} = \frac{k_2 k_1 / (k_{-1} + k_2)[L]}{1 + k_1 / (k_{-1} + k_2)[L]}$

iii) An excellent kinetic study into the reactions of $M(CO)_4(\eta^2\text{-HFB})$, (HFB = hexafluorobut-2-yne, M = Fe, Fu, Os) with a family of phosphines (PR_3) has been carried out by Jordan *et al.*[22] The general reaction scheme is shown below.

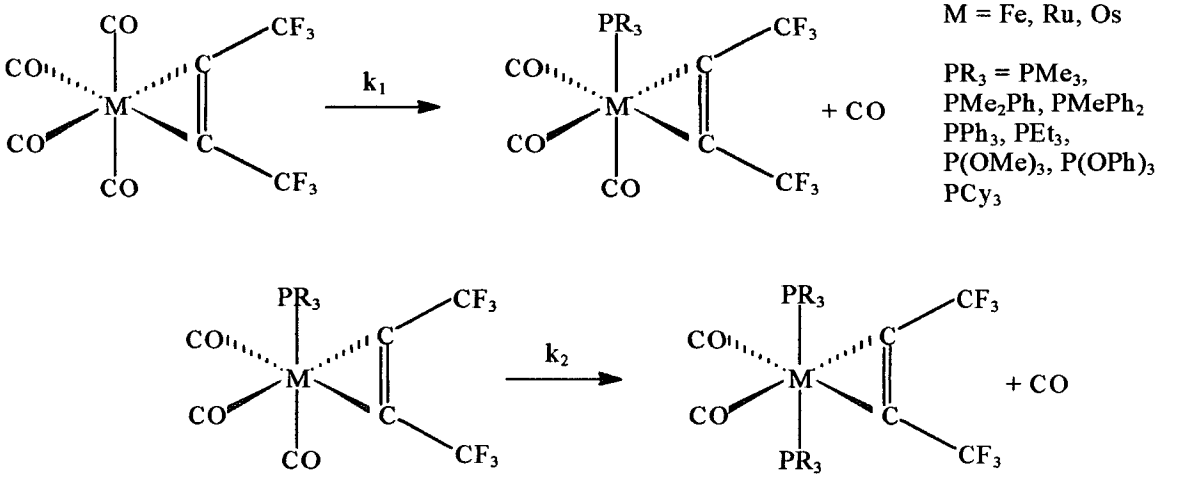

Figure 1.5 Reaction of $[M(CO)_4(\eta^2\text{-HFB})]$ with PR_3

A phosphine group replaces one CO and the second substitution of a phosphine gives a nice example of the influence of the phosphine *trans* to the leaving group. Comparisons to $M(CO)_5$ were made to illustrate the effect of the alkyne group.

Factors affecting the rate constant, k_i

It was found that the rates of all reactions were independent of the concentration of phosphine and the rate laws for both steps given as:

rate = $k_i[M(CO)_4(\eta^2\text{-HFB})]$

where i = 1 or 2. The value of k_1 was found to be independent of the nature of the phosphine. There was a dependence on rate, k_2, according to the π-donor abilities of the phosphine in the *trans* position but was independent of the entering group. The $\Delta S^{\ddagger}$ for each reaction was positive and both reactions understood to go via a five co-ordinate intermediate in the dissociative mechanism shown in **Scheme 1.3**.

Increased reactivity with different ligands was attributed to either or both the destabilisation of the ground state or stabilisation of the transition state.

$$M(CO)_4(\eta^2\text{-HFB}) \underset{k_{-1d}}{\overset{k_{1d}}{\rightleftharpoons}} M(CO)_3(\eta_2\text{-HFB}) + CO$$

$$M(CO)_3(\eta_2\text{-HFB}) + PR_3 \xrightarrow{k_{1s}} M(CO)_3(PR_3)(\eta_2\text{-HFB})$$

$$M(CO_3(PR_3)(\eta^2\text{-HFB}) \underset{k_{-2d}}{\overset{k_{2d}}{\rightleftharpoons}} M(CO)_2(PR_3)(\eta^2\text{-HFB}) + CO$$

$$M(CO)_2(PR_3)(\eta^2\text{-HFB}) + PR_3 \xrightarrow{k_{2s}} M(CO)_2(PR_3)_2(\eta^2\text{-HFB})$$

Scheme 1.3 Dissociative reaction scheme of $M(CO)_4(\eta^2\text{-HFB})$ with PR_3

Jordan cited Takats's work where it was understood that spectator ligands could destabilise the metal centre in $M(CO)_4(\eta^2\text{-alkyne})$ relative to $M(CO)_5$ by repulsion between the filled metal d-orbitals and the alkyne π-orbitals.[23] The same paper also demonstrates the effect of stabilisation of the transition state through π-donation from the alkyne to the vacant co-ordination site illustrated in **Figure 1.6**.

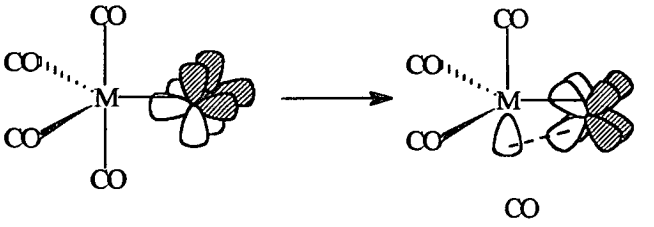

Figure 1.6 Possible stabilisation of the five co-ordinate intermediate by π-donation from the alkyne ligand

Further work by Jordan *et al* with C_2H_2 as the alkyne supported this hypothesis.[24] It was found that the complex, $M(CO)_4(\eta^2\text{-HCCH})$ was more reactive than $M(CO)_4(\eta^2\text{-HFB})$. This was explained in terms of the $\Delta H^{\ddagger}$, on average lower by 9 kJ mol^{-1} than $M(CO)_4(\eta^2\text{-HFB})$ for the same reaction with a phosphine ligand. This *cis*-effect on the rate of reaction is well documented in the literature for similar complexes.[25]

Factors affecting k_2 were shown to be a balance between electronic π-donor/acceptor effects and steric interactions of the phosphines. The rate was found to cover a range from 3 times less than k_1 to 4 times larger. It was argued that since phosphines are better σ-donors than CO they would lessen the stabilisation from π-donation from the alkyne to the vacant co-ordination site in the transition state. In contrast the phosphine may stabilise the transition state because of steric repulsion between the phosphine and the alkyne. No clear trend could be presented. The basicity of the phosphine (evaluated by Bodner *et al* from ^{13}C NMR shifts, or from pK_a) was not an important factor.[26] Both the strongest and weakest bases had relatively fast reactions. Larger steric factors evaluated from Tolman's cone angles showed a tendency to increase the rate.[27] A summary of properties of PR_3 and rate constants k_1 and k_2 are presented in **Table 1.3**. Reactions labelled "fast" were too quick to measure.

PR_3	pK_a	δ / ppm	Cone angle / °	k_1/ 10^{-4} s^{-1}	k_2/ 10^{-4} s^{-1}
PMe_3	8.65	5.05	118	8.54	2.50
PMe_2Ph	6.5	4.76	122	8.58	2.16
$PMePh_2$	4.57	4.53	136	9.11	3.44
PPh_3	2.73	4.30	145	7.33	9.02
PEt_3	8.69	5.54	132	8.46	10.6
$P(OMe)_3$	2.6	3.18	107	8.29	38.7
PCy_3	9.7	6.32	170	8.97	fast
$P(OPh)_3$	-2.0	1.69	128	7.99	fast

Table 1.3 Summary of properties of PR_3 and rate constants k_1 and k_2 for reactions with $Os(CO)_4(\eta^2$-HFB) and $Os(CO)_3(PR_3)(\eta^2$-HFB) in dichloromethane at 288 K.

The effect of the metal centre

The rate constants are of the order Fe >> Ru > Os, inconsistent with $M(CO)_5$ and the general literature.[13,14,25a,28] Jordan takes the view that this is not necessarily surprising considering the previously discussed π-donor ability of the alkyne. However the effect is remarkable in its strength where k_1 for Fe is 10^3 times larger than Os. Theoretical calculations are in agreement with the reactivity order.[29] This effect is rationalised in terms of the lower energy of the 3d metal and their greater general preference for an 18 electron configuration than for Ru or Os.

iv) Flood *et al* has presented some work on phosphine ligand exchange in osmium complexes as examples of anion dissociation and labilisation by ligand π-base effect making marvellous use of ^{31}P NMR.[30,31,32] Osmium complexes, of the type illustrated in **Figure 1.7**, were found to undergo ligand exchange reactions, $P(CH_3)_3$ for $P(CD_3)_3$, at 80 °C. $P(CD_3)_3$ was in solution in a large excess so that it would dominate the association reaction. The rate of substitution and stereochemical change was demonstrated to be significantly affected by the heteroatom group, X. On

the premise of microscopic reversibility it was understood that if dissociation was favoured from a specific site the labelled ligand L' would associate in the same position thus revealing the preference.[32,33,34]

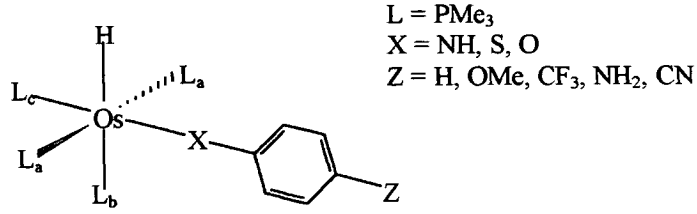

Figure 1.7 *cis*-[$L_4Os(H)X(C_6H_4Z)$]

The rates for dissociation on each site, a, b, c, were similar for both the anilides [$L_4Os(H)(NHC_6H_4Z)$] and thiophenoxides [$L_4Os(H)(SC_6H_4Z)$] with a ratio 4:slow:1 and 3:slow:1 respectively for a:b:c. Quite different rates of dissociation were found for phenoxide [$L_4Os(H)(OC_6H_4Z)$] suggesting an alternative mechanism. Data for the dissociation however, were inconsistent with a square pyramidal or with a trigonal bipyramidal intermediate.

From the ^{31}P NMR analysis, phosphine exchange in the anilides and thiophenoxides complexes was understood to proceed via phosphine dissociation in the *cis* position (to H and X), L_a, followed by subsequent migration. This process is outlined in **Scheme 1.4**.

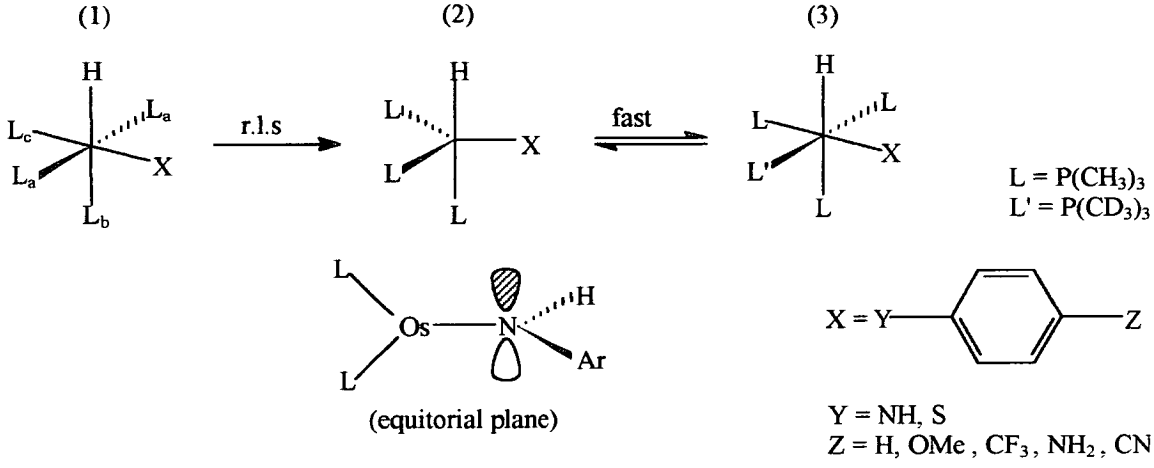

Scheme 1.4 Mechanism for phosphine exchange for [$L_4Os(H)(XC_6H_4Z)$]

L_a dissociates to the five co-ordinated intermediate, (1)→(2), followed by a rapid association of the labelled phosphine, L' (2)→(3). Further dissociation could then lead to sites L_c and L_b of the starting complex being exchanged. Steric considerations suggested the aryl group would orientate toward the hydride. For the anilides it was argued that the intermediate could then be stabilised by the lone pair on the nitrogen aligning along the P-Os-P axis equitorially directing π-symmetry overlap with the developing formation of the vacant osmium orbital. This process explaining the stereospecificity of the reaction was supported by theoretical calculations.[35] Flood believed in a similar stabilisation of the intermediate by a lone pair from the sulphur. It was reasoned that although sulphur has two lone pairs, one is a $3sp^2$ hybrid, and the other is essentially a 3p orbital.[36] The sp^2 orbital is understood to be less basic than the p and point away from the metal. The p orbital on the other hand orientates towards the metal so that it would be able to form a π overlap with the vacant metal orbital as for the nitrogen. The comparative rates of the anilides and thiophenoxides were therefore understood as a reflection of their relative π-donor strength.

In contrast to the ^{31}P NMR for the anilides and thiophenoxides, analysis showed substitution for the phenoxide examples onto all three positions independently with an approximate ratio of 1:0.27:0.27 for a:b:c. The most consistent interpretation of the rate limiting step supported by kinetic simulation is illustrated in **Scheme 1.5**.[37]

The first step was ionisation of the phenoxide (4)→(5). The rate constant for the re-association of the two ions (5)→(4) is much faster than for L' uptake (5)→(6) and assures a fast pre-equilibrium. In a combination of dissociation (6)→(7a/b) and isomerisation (7a/b)→(7c) all three sites could be independently exchanged (7)→(8). Keen observation of the rate in several different solvents showed a dependence on the solvent polarity supporting the supposition of the ion pair $[L_5OsH][OC_6H_4Z]$. It was concluded that this ion pair mechanism was the consequence of phenoxide's lower π-donor ability and the relatively weak Os-O bond.

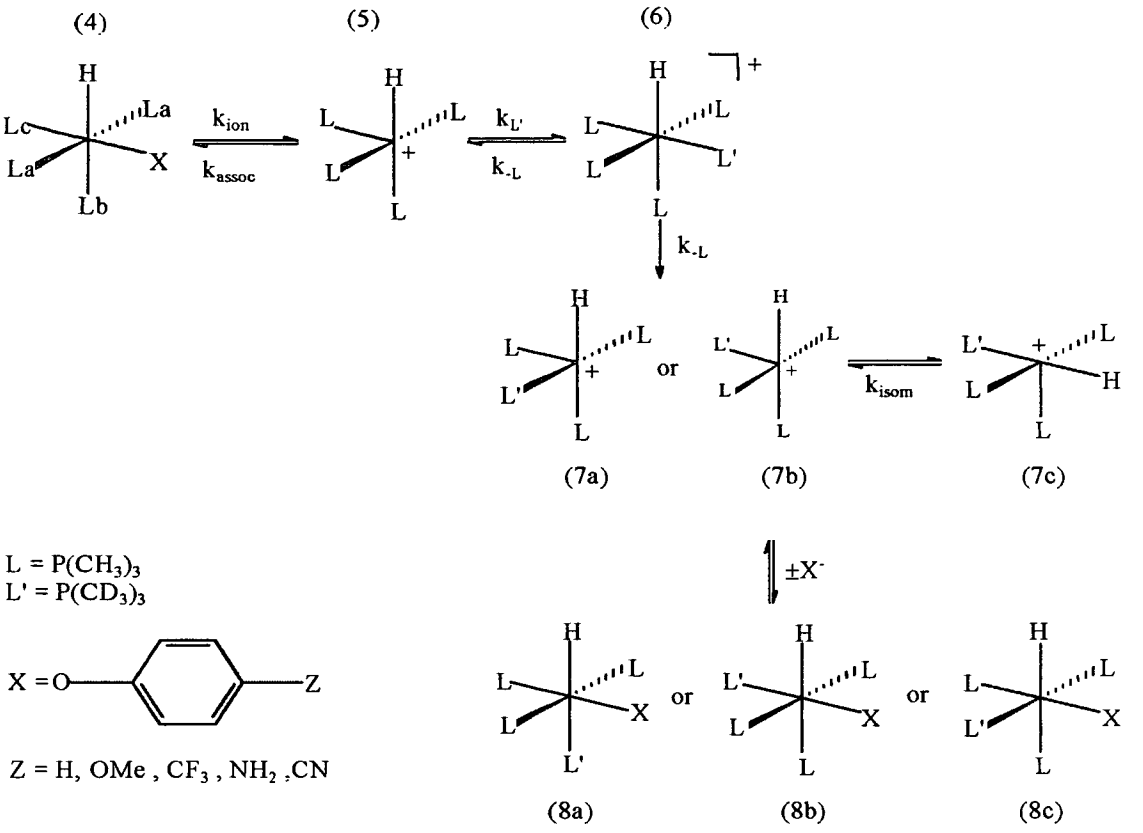

Scheme 1.5 Ion pair mechanism of phosphine exchange in for $[L_4Os(H)(OC_6H_4Z)]$

The rates of dissociation for the anilides, thiophenoxides, and phenoxides were further effected by the group Z, although by a smaller amount. It was clear that as the electron donation from Z increased the rate increased.

1.4 References

[1] Kotz, J. C.; Purcell, K. F.; *Chemistry and Chemical Reactivity,* 2nd edition, Saunders College Publishing, 1991
[2] Shriver, D. F.; Atkins, P. W.; Langford, C. H.; *Inorganic Chemistry*, Oxford University Press, 1990
[3] Haim, A.; Taube, H.; *Inorg. Chem.*, 1963, **2**, 1199
[4] Atkins, P. W.; *Physical Chemistry*, 4th edition, Oxford University Press, 1990
[5] Segel, I. H.; *Enzyme Kinetics*, Willey Classics Library Edition, 1993
[6] Wilkins, R. G.; *The Study of Kinetics and Mechanism of Reactions of Transition Metal Complexes*, Allyn and Bacon, Inc, 1974
[7] Bard, A. J.; Faulkner, L. R.; *Electrochemical Methods, Fundamentals and Applications*, John Wiley & Sons, New York, 1980
[8] Tobe, M. L.; *Inorganic Reaction Mechanisms*, Nelson, 1972
[9] Basallote, M. G.; Duran, J.; Fernandez-Trujillo, M. J.; Gonzales, G.;Manez, M. A.; Martinez, M.; *Inorg. Chem.*, 1998, **37**, 1623
[10] Greenwood, N. N.; Earnshaw, A.; *Chemistry of the Elements,* Pergamon Press, 1984
[11] Helleren, C. A.; Henderson, R. A.;Leigh, G. J.; *J. Chem. Soc., Dalton Trans.*, 1999, 1213
[12] Albinez, A. C.; Heinekey, M.; Crabtree, R. H.; *Inorg. Chem.*, 1991, **29**, 3632
[13] Halpern, J.; Cai, L.S.; Desrosiers, P. J.; Lin, Z. R.; *J. Chem. Soc., Dalton Trans.*, 1991, 717
[14] Amendola, P.; Antiniutti, S.; Albertin, G.; Bordignon, E.; *Inorg. Chem.*, 1990, **29**, 318
[15] Kubas, G. J.; Ryan, R. R.; Unkefer, C. J.; *J. Am. Chem. Soc.*, 1987, **109**, 8113
[16] Mezzetti, A.; Del Zotto, A.; Rigo, P.; Farnettis, E.; *J. Chem. Soc., Dalton Trans.*, 1991, 1525
[17] Bianchini, P. J.; Linn, K.; Masi, D.; Peruzzini, M.; Polo, A.; Vacca, A.; Zanobini, F.; *Inorg. Chem.*, 1993, **32**, 2366
[18] Bianchini, P. J.; Masi, D.; Peruzzini, M.; Casarin, M.; Maccato, C.; Rizzi, G. A.; *Inorg. Chem.*, 1997, **36**, 1061
[19] Bautista, M. T.; Cappellani, E. P.; Drouin, S. D.; Morris, R. H.; Schweitzer, C. T.; Sella, A.; Zubkowski, J.; *J. Am. Chem. Soc.*, 1991, **113**, 4876
[20] a) Aubart, M. A.; Chandler, B. D.; Gould, R. A. T.; Krogstad, D. A.; Schoondergang, M. F. J.; Pignolet, L. H.; *Inorg. Chem.* 1994, **33,** 3724
b) Krogstad, D. A.; Konze, W. V.; Pignolet, L. H.; *Inorg. Chem.* 1996, **35**, 6763
[21] a) Henderson, R. A; *J. Chem. Soc., Dalton Trans.*, 1998, 515
b) Henderson, R. A; *J. Chem. Soc., Dalton Trans.*, 1998, 509
[22] Pearson, J.; Cooke, J.; Takats, J.; Jordan, R. B.; *J. Am. Chem. Soc.* 1998, **120**, 1434
[23] Marinelli, G.; Steib, W. E.; Huffma, J. C.; Caulton, K. G.; Gagné, M. R.; Takats, J.; Dartiguenave, M.; Chardon, C.; Jackson, S. A.; Eisenstein, O.; *Polyhedron*, 1990, **9**, 1867
[24] Moo, T. F.; Zhang, Z. S.; Washington, J.; Takats, J.; Jordan, R. B.; *Organomet.*, 1999, **18**, 2331
[25] a) Lichtenberger, D. L.; Brown, T. L.; *J. Am. Chem. Soc,* 1978, **100**, 366
b) Cotton, F. A.; Darensbourg, D. J.; Kolthemmer, B. W. S.;Kudaroski, R.; *Inorg. Chem,* 1982, **21**, 1656
c) Darensburg, D. J.; Klausmeyer, K. K.; Reibenspies, J. H.; *Inorg. Chem.* 1995, **34**, 4933
[26] Bodner, G. M.; May, M. P.; McKinney, L. E.; *Inorg. Chem.*, 1980, **19**, 1952
[27] Tolman, C. A.; *Chem. Rev.*, 1977, **77**, 313
[28] Huq, R.; Poë, A. J.; Chawala, S.; *Inorg. Chim. Acta.*, 1980, **38**, 121
[29] Klobulkowski, M.; Decker, S.; Cundai, T. R.; *Abstr. Pap. Am. Chem. Soc.*, 2000, 25-COMP, Part 1
[30] Flood, T.C.; Lim, J. K.; Deming, M. A.; Keung, W.; *Organomet.*, 2000, **19**, 1166
[31] Desrosiers, P.J.; Shiinomoto, R. S.; Deming, M. A.; Flood, T. C.; *Organomet.*, 1989, **8**, 2861
[32] Desrosiers, P.J.; Shiinomoto, R. S.; Flood, T. C.; *J. Am. Chem. Soc.*; 1986, **108**, 7964
[33] Atwood, J. D.; Brown, T. L.; *J. Am. Chem. Soc.*, 1976, **98**, 3155
[34] Brown, T. L.; *Inorg. Chem.*, 1989, **28**, 3229

[35]a) Davy, R. D.; Hall, M. B.; *Inorg. Chem.*; 1989, **28**, 3521
b) Riehl, J. F.; Jean, Y.; Eisenstein, O; Plisser, M.; *Organomet.*, 1992, **11**, 729
[36] Ashby, M. T.; Enemark, J. H.; *J. Am. Chem. Soc.*, 1986, **108**, 730
[37] Weigert, F. J.; *Comput. Chem.*, 1987, **11**, 273

CHAPTER TWO:

Experimental Techniques

2 Experimental Techniques

Detailed in this chapter are the experimental techniques for electrochemical and spectroelectrochemical experiments employed throughout this work.

2.1 Electrochemical Techniques

Electrochemical studies for chapters three, four and five, were carried out using a DELL 4466DL PC with General Purpose Electrochemical System (GPES) version 4.5 software connected to an Autolab PGSTAT20 potentiostat. Electrochemical studies for chapter six were performed on an updated system using a DELL GX110 PC with GPES version 4.8 software connected to a PGSTAT30 potentiostat.

All techniques used a three electrode configuration; working electrode, counter electrode, and reference electrode. For cyclic voltammetry, stirred voltammetry, differential pulse voltammetry, and double-step chronoamperometry, experiments were performed in a cell of the type illustrated in **Figure 2.1a**. The working electrode took the form of a 0.2 mm^2 surface area platinum microdisc and the counter electrode a platinum rod with a large surface area. The reference electrode for cyclic voltammetry, stirred voltammetry, and differential pulse was Ag/AgCl against which the ferrocinium/ferocene couple was measured at +0.55 V. The reference electrode was a platinum rod for double-step chronoamperometry experiments. Cyclic voltammetric experiments were carried out at 0.1 V s^{-1} unless otherwise stated. Stirred voltammetry was performed at 0.02 V s^{-1} on a vigorously stirring test solution. The jacketed cell (**Figure 2.1b**) achieved temperature control. The cell can be cooled with methanol down to 223 K or heated with silicon oil up to 498 K. Steady state temperatures below 223 K were achieved using a toluene/liquid N_2 slush

bath. Measurements of temperature were taken from a thermocouple *in situ* prior to the experiment, accurate to ± 0.1 K.

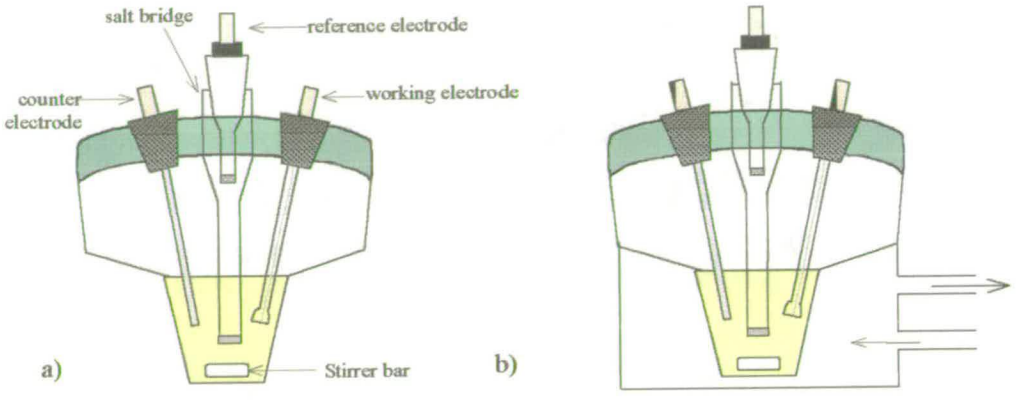

Figure 2.1 a) Schematic of three electrode cell for cyclic voltammetry, stirred voltammetry, differential pulse voltammetry, and chronoamperometric experiments. b) Jacketed cell for temperature controlled experiments

A typical cyclic voltammogram is illustrated in **Figure 2.2**. The oxidation and reduction peak currents and potentials are labelled, i_p^{ox}, i_p^{red}, E_p^{ox}, E_p^{red} respectively. For a reversible process, ΔE = 59 mV (298 K) and $|i_p^{ox}/i_p^{red}|$ is unity at all scan rates, while i_p is proportional to $\nu^{1/2}$, where ν = scan rate.

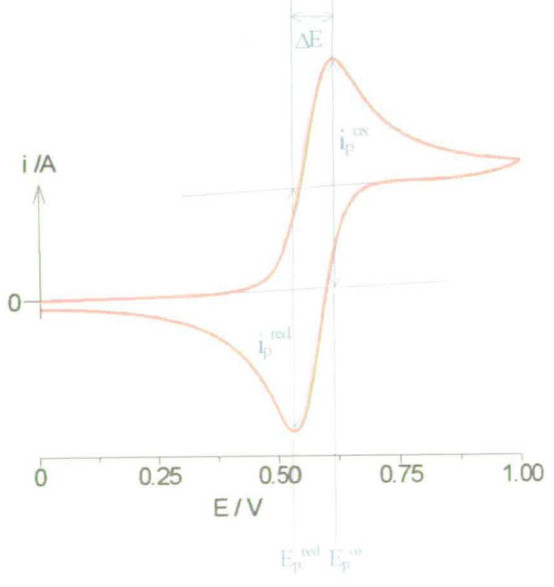

Figure 2.2 Typical cyclic voltammogram for an oxidation process

Bulk electrolysis experiments were carried out in an H-type cell, illustrated in **Figure 2.3**. The working electrode was a large basket of platinum gauze. The platinum gauze counter electrode is separated by sintered glass frits from the test solution. The sintered frits allow current to flow but are impermeable with respect to the test species. The microdisc electrode allows conventional cyclic voltammetric experiments to be carried out monitoring the progress of the electrolysis.

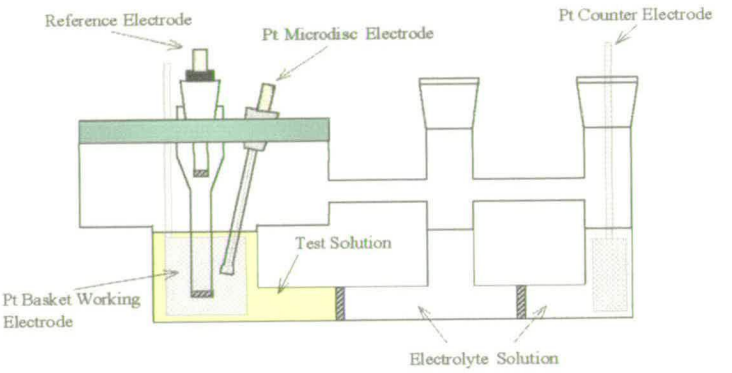

Figure 2.3 H-type cell for bulk electrolysis

The number of electrons involved in a reduction or oxidation process can be calculated from the relationship:

$$Q = n.e.F$$

where Q is the charge in coulombs, n is the number of moles of the electroactive species, e is the number of electrons in the redox process, and F is Faraday's constant (96485 C mol^{-1}). This experiment is usually termed coulometry.

Tetrabutylammonium tetrafluoroborate ($[N^nBu_4][BF_4]$) was used as supporting electrolyte throughout unless otherwise stated. Specific concentrations of electrolyte, temperature and scan rates are given in the text. The solvents were purged with either dinitrogen or argon prior to experiments and a blanket of the inert gas was kept over the solution for the duration of the experiment.

2.2 Kinetic Techniques

Techniques used in kinetic studies must be capable of monitoring the rate of change taking place in the reaction. The time scale of the change is therefore critical in the appropriate choice of technique. It should give as much information about elementary steps, transient intermediates, and overall reaction mechanism as possible. To this end there are many techniques available, some of the most common being spectrophotometry, titration, mass spectrometry, gas chromatography and monitoring pH.

In this work, electrochemical methods have been used to study a number of reduction-induced substitution reactions. The electrochemical techniques used have proven to be a valuable tool because they are capable of monitoring the chemical substitution reaction immediately after the reduction thereby having the advantages of an initial rate method.

2.2.1 Electrochemical kinetic techniques

A chemical reaction can be induced by an electrochemical reaction known as an EC process. Consider the reaction:

$A + e^- \rightleftharpoons B$ - Electrochemical

$B \xrightarrow{k} C$ - Chemical

Generally, the electrochemical transfer is much faster than the chemical reaction so that the rate limiting step is B→C. A typical cyclic voltammogram for an EC process is shown in **Figure 2.4**. Clearly $|i_p^{ox}/i_p^{red}|$ is not unity.

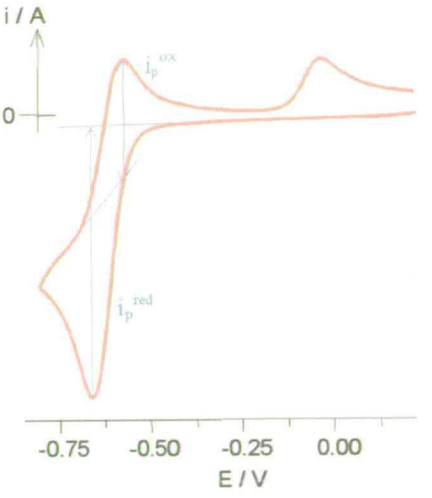

Figure 2.4 Typical cyclic voltammogram for an EC process

There are a number of electrochemical techniques in the literature to measure the rate constant, k. Three main electrochemical kinetic techniques have been previously employed in this laboratory; Nicholson-Shain's method, convolution, and double-step chronoamperometry.[1]

2.2.1.1 Nicholson-Shain approach[2]

The Nicholson-Shain approach is essentially based on the measurements of the peak oxidation and reduction currents and half-wave potential of the cyclic voltammogram. Calculation of the rate constant, k, is somewhat cumbersome involving Laplace transform techniques that can be found in the original paper.[2a] Further drawbacks of this method are the difficulties in accurately measuring both the oxidation and reduction current (often only one can be accurately obtained) and the half-wave potential. Nicholson later proposed a semiempirical procedure that allowed for a more straight forward calculation making the assumption for a simple reversible electron transfer reduction that the half-wave potential occurs at a point where the current is equal to 85.17 % of the reduction peak.[2b] This assumption can lead to associated errors in the calculated rate constant. Furthermore, it is of crucial

importance that the resistance of the solution is completely compensated since failure to do so results in poorly defined waveforms with associated errors in current and potential values.

2.2.1.2 Kinetic convolution[3]

Convolution techniques similarly involve the measurement of a cyclic voltammogram and a mathematical transformation. Woodward *et al* developed a numerical technique to calculate the rate constant for a reversible electron transfer reaction providing that a slight return peak is evident in the return cycle of the cyclic voltammogram.[3a] Problems with this method were evident when the rate constant could be seen to increase with increasing scan rate (theoretically not expected). General improvements were made and are used in GPES software.[3b,3c] The background current must be accurately subtracted and there is often a limited temperature range but an advantage of this technique is the insensitivity to solution resistance.

2.2.1.3 Double-step chronoamperometry[4]

Double-step chronoamperometry was found by Liu[1a] to be the favoured electrochemical technique for studying the EC reaction,

$$[ReCl_5(NCCH_3)]^{1-} + e^- \rightleftharpoons [ReCl_5(NCCH_3)]^{2-} \xrightarrow[\substack{-Cl^- \\ +NCCH_3}]{k} [ReCl_4(NCCH_3)_2]^{1-}$$

Although there is no absolute value for comparison, double-step chronoamperometry was shown to have the least error in both rate constant and activation energy and could be measured over the largest temperature range. For these reasons double-step

chronoamperometry was used in this work and the background to this technique is discussed in some detail.

Consider the reduction-induced reaction,

$$A + e^- \rightleftharpoons B$$

$$B \xrightarrow{k} C$$

The double-step chronoamperometry technique comprises of two electrolysis steps at appropriate controlled potentials. On the first step, E_1/E_2, the electroactive species, A, is instantaneously reduced to B. After a chosen time, τ, the electroactive species, B, is re-oxidised in the second step, E_2/E_1, back to A. E_1 and E_2 are chosen so that both the reduction and oxidation processes are diffusion controlled. The waveform is illustrated in **Figure 2.5**.

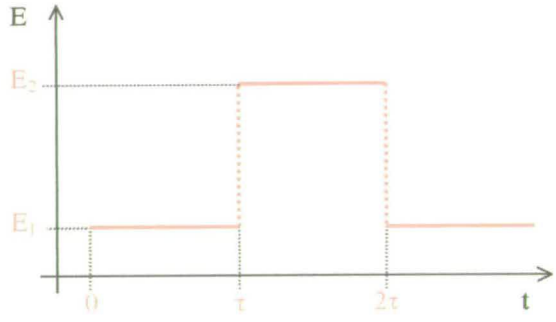

Figure 2.5 General waveform for double-step chronamperometry

Each step is recorded by the current response with time, **Figure 2.6**. The magnitude of the current is controlled by the rate of diffusion of the species at the electrode and is therefore dependent on the time, τ, and dependent on the rate of the chemical reaction, $B \rightarrow C$.

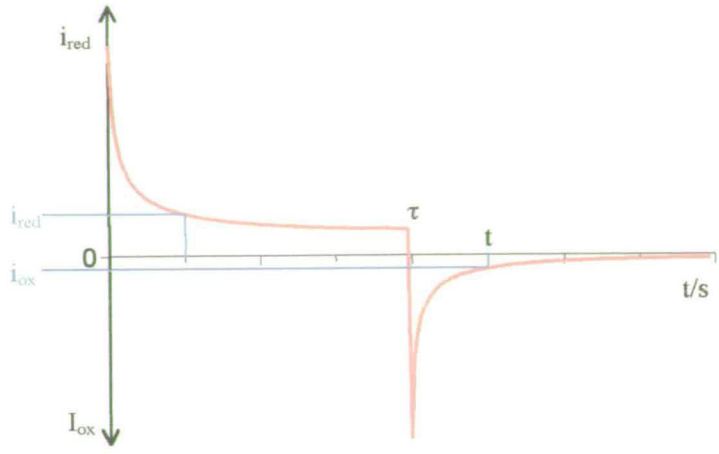

Figure 2.6 Typical reduction-oxidation current-time curves of a reduction-induced EC process for the double-step chronoamperometry experiment

The differences in the current/time responses for the two steps permit the rate constant to be calculated. The non-trivial mathematical treatment can be found in the original paper.[4] From **Equation 2.1**, Schwarz and Shain established a series of theoretical working curves for a first order reaction in which the current ratio $-i_{ox}/i_{red}$ is plotted against $k\tau$ for the time ratio $(t-\tau/\tau)$, **Figure 2.7**.

$$-\frac{i_{ox}}{i_{red}} = \phi[k\tau(t-\tau)/\tau] - \sqrt{\frac{(t-\tau)/\tau}{1+(t-\tau)/\tau}}$$

Equation 2.1

ϕ represents a mathematical function comprising the terms; electrode area, Faraday's constant, k, τ, t, bulk concentration, diffusion coefficients, and number of electrons.

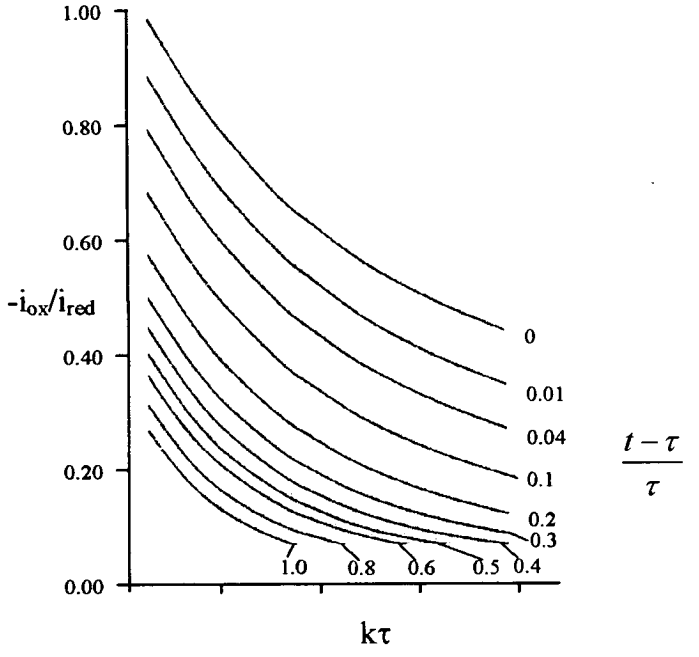

Figure 2.7 Standard working curves for the double-step chronoamperometry experiment of a first order EC reaction[4]

All kinetic measurements in this work used these theoretical working curves to gain values of kτ from the $-i_{ox}/i_{red}$ values obtained from double-step experiments. The value of τ was carefully chosen so that values of $-i_{ox}/i_{red}$ corresponded to the middle part of the working curves assuring the greatest accuracy in the determination of k. Each rate constant reported is the average of at least two independently determined values obtained from a minimum of four different (t-τ)/τ curves. An important advantage of this experiment is that the current ratios are independent of the internal resistance of the solution. It can also be shown that the rate constant is solved independently of electrode area, solution concentration, and diffusion coefficients.

The most consistent results for double-step chronoamperometry were obtained with a platinum quasi-reference electrode. The potential step voltages were chosen by reference to a cyclic voltammogram run prior to the measurements on the same time scale of the proposed chronoamperometric measurement.

2.3 Spectroelectrochemical Techniques

2.3.1 *In situ* uv-vis-nir spectroelectrochemistry

Employing the cell illustrated in **Figure 2.8**, reactions taking place while electron transfer is being executed at the working electrode can be monitored *in situ* by uv-vis-nir absorption spectroscopy.[5] A three electrode electrochemical system is used. The working electrode takes the form of an optically transparent thin layer electrode, OTTLE, and is placed in a quartz cell with a path length of 0.5 mm. The OTTLE is platinum/rhodium gauze with a transparency of *ca.* 40 %. The reference electrode (Ag/AgCl) and counter electrodes are separated from the test solution by porous frits as in the H-type cell. A tight fitting PTFE top prevents solutions, which have been purged of dioxygen, being exposed to the gaseous environment, seals the quartz cell.

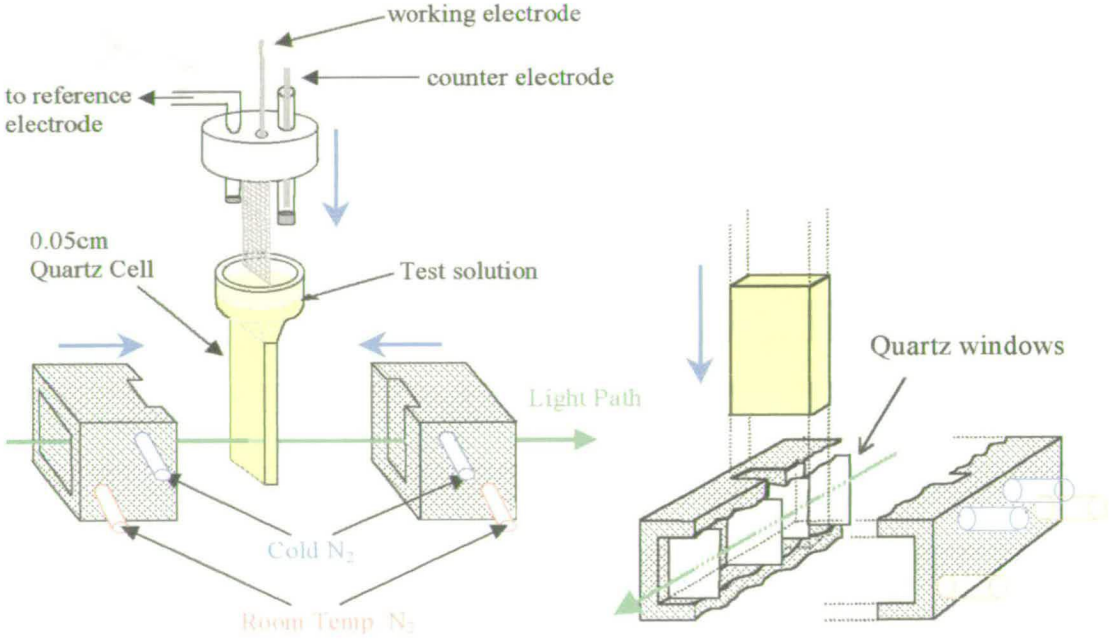

Figure 2.8 Schematic of the experimental setup for *in situ* uv-vis-nir experiments

The quartz cell is placed into a gas tight PTFE block placed in the spectrometer. Temperature control is achieved by passing dry, pre-cooled nitrogen between the inner pair of quartz windows and the cell. To prevent condensation on the windows dry nitrogen is passed between the inner and outer quartz windows and the sample compartment of the spectrometer. The temperature is monitored using a thermocouple connected to a digital thermometer. Uv-vis-nir spectra were recorded on a Perkin-Elmer λ9 spectrophotometer controlled by a Datalink PC running UV Winlab software, version 2.70.01.

2.3.2 *in situ* IR spectroelectrochemistry

The IR cell was designed from a micro-cavity KBr cell consisting of a single block of crystal, 15-22 mm, in which a cavity (0.2 mm x 7 mm x 12 mm) has been formed by ultrasonic machining (Spectra Tech). Special advantages of this type of cell are low volume, easy maintenance, freedom from leaks, and protection of the sample from metal reactions. A three electrode system was used; the working electrode took the form of a platinum wire inserted into the cavity, and the counter and reference electrodes, separated by porous frits, were placed in a well at the top of the cavity (**Figure 2.9**). The PTFE top allows the exclusion of air from the sample.

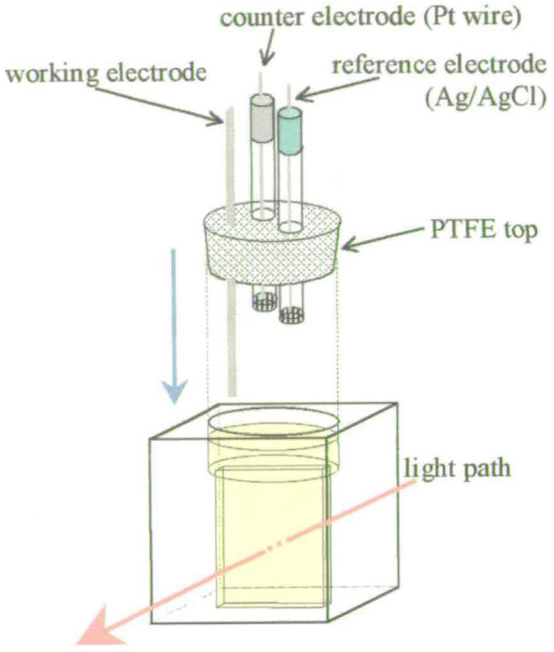

Figure 2.9 Schematic of the experimental setup for the *in situ* IR experiments

All data were recorded on a FTIR 2000 spectrometer (Perkin Elmer). Data was manipulated using the UV Winlab software (version 2.70.01).

2.4 References

[1] a) Xiaoming Liu, PhD Thesis, University of Edinburgh, 1998
b) Payne, N. N.; PhD Thesis, University of Edinburgh, 1997
[2] a) Nicholson, R. S.; Shain, I.; *Anal. Chem.*, 1964, **36**, 706
b) Nicholson, R. S.; *Anal. Chem.*, 1966, **38**, 1406
[3] a) Woodward, F. E.; Goodin, R. D.; Kinlen, P. J.; *Anal. Chem.*, 1984, **56**, 1920
b) Oldham, K. B.; *Anal. Chem.*, 1986, **58**, 2296
c) Myland, J. C.; Oldham, K. B.; Zoski, C. G.; *J. Electroanal. Chem.*, 1985, **182(2)**, 221
[4] Schwarz, W. M., Shain, I.; *J. Phys. Chem.*, 1965, **69**, 30
[5] Heath, G. A.; Yellowlees, L. J.; Braterman, P. S.; *J. Chem. Soc. Chem. Commun.*, 1981, 287

CHAPTER THREE:

Substitution Reactions of Osmium(III), Iridium(III), and Rhenium(III) hexahalides

3 Substitution Reactions of Osmium(III), Iridium(III), and Rhenium(III) hexahalides

"The studies of the rates of reaction of osmium complexes are difficult".[1]

3.1 Introduction

This chapter details a rigorous kinetic study of the reduction-induced substitution reactions of the type;

$$[MX_6]^{2-} + e^- \longrightarrow [MX_6]^{3-} \xrightarrow{L} [MX_5L]^{2-} + X$$

where M = Re, Os, Ir; X = Cl^-, Br^-, I^-; L = acetonitrile (An), propionitrile (Pn), butyronitrile (By), pyridine (Py), benzonitrile (Bn), benzyl cyanide (Bc). By way of introduction the general chemistry of the metalohalogen complexes and the incoming ligand, L, are discussed.

Osmium Complexes

The fourth oxidation state is generally the most stable for osmium complexes.[2] $[OsX_6]^{2-}$ complexes are well known.[3,4,5] All are octahedral, low spin, with two unpaired electrons and well characterised complex anions.[6,7,8] The spectroelectrochemistry of the one electron reduction of $[OsCl_6]^{2-/3-}$ has been published by Heath and Kennedy.[9] $[OsX_6]^{2-}$ complexes are common starting materials and there are many examples of substitution reactions from the literature with phosphine,[10] arsine,[11] thiocyanate,[12] or carbonyl[13] ligands. Various groups have

carried out substitution reactions in aqueous solution.[14,15] Lang *et al* synthesised a number of complexes, $[OsCl_5L]^{2-}$ (L = EtOH, pyridine, pyrazine) via $[OsCl_5(H_2O)]^{2-}$.[15] Preetz *et al* have carried out rigorous studies on successive substitutions of a halide in $[OsCl_6]^{2-}$ and $[OsBr_6]^{2-}$ for H_2O, acetonitrile, and pyridine by photochemical reaction.[16] Successive substitutions of a halide in $[OsX_6]^{2-}$ (where X = Cl^-, Br^-, I^-) for another halide have shown that the kinetic stability of the complex to decrease in the order $Cl^- > Br^- > I^-$. Mixed ligand complexes are strongly influenced by the trans effect.[17,18] The activation energy for the substitution of one Cl^- for I^- in $[OsCl_6]^{2-}$ was found to be 109 ± 7 kJ mol^{-1}.[17]

Os(III) complexes in comparison are distinctly less-common. Komozin has investigated the interaction of Os(III) and Ru(III) complexes with a number of reagents (DMSO, PPh_3, acetonitrile, pyridine) but there has been little other comment in the literature on the reactivity of Os(III) complexes.[19] It is well known that the electrochemical reduction of $[OsCl_6]^{2-}$ in certain inert environments can reversibly generate $[OsCl_6]^{3-}$.[20] In the presence of a less electron donating ligand, L, than chloride this is not the case. One chloride is instead replaced by L, stabilising the lower oxidation state of the metal.[21,22] The resulting solution shows both $[OsCl_5L]^{2-/1-}$ and free chloride oxidations. The former species is oxidised at a potential around 0.5 V more positive than $[OsCl_6]^{3-/2-}$ as expected having replaced a π-donating ligand with a very weak π-acceptor.[23] $[OsBr_6]^{3-}$ and $[OsI_6]^{3-}$ are also known to react with pyridine in a similar fashion.[21] Series of related chlororuthenate(IV) complexes have been synthesised through a stepwise substitution of halide with pyridine, acetonitrile, and benzonitrile.[24,25] A dissociative mechanism has been proposed in the past for the substitution reaction but without definitive experimental evidence.[21] Perhaps the best supporting evidence for this proposition is provided by an analogy with the reduction of *mer*-$[OsCl_3(PMe_2Ph)_3]$, which yields a five co-ordinate neutral osmium(II) species, $[OsCl_2(PMe_2Ph)_3]$, characterised by ^{31}P NMR.[26]

More recently, electrochemical methods have been utilised in the kinetic study of hexachloroosmate with pyridine and various nitriles, seeing little prospect of

spectroscopically observing any intermediates in such a fast reaction.[27] The substitution reactions of electrochemically generated $[OsCl_6]^{3-}$, in the presence of a vast excess of less electron donating ligands, L, were studied using double-step chronoamperometry, and rate constants and activation energies for the process determined. Empirical energies of activation, E_a, for the substitution were derived from Arrhenius plots of the variation in rate with temperature. The average value of E_a found was 57±5 kJ mol^{-1}. The substitution reaction has been found to proceed without significant effect on the rate from the nature of L present. The reaction was found to be first order with respect to hexachloroosmate(IV). The deliberate addition of even one molar equivalent of water to the previously rigorously dried solvents greatly augmented the rate of substitution without altering the final product. Addition of $[N^nBu_4]Cl$ to the solution resulted in a decrease in rate.

Iridium Complexes

Iridium complexes, compared with cobalt and rhodium, show appreciable stability in the fourth oxidation state.[2] Ir(IV) has been studied more extensively than Os(IV). In 1953 Owen and Stevens reported the first unambiguous evidence of metal d electrons moving in molecular orbitals spanning the whole complex from the observation of hyperfine structure of an ESR signal of $(NH_4)_2[IrCl_6]$.[28] From these results they inferred the presence of π-bonding and σ-bonding in $[IrCl_6]^{2-}$. Salts of $[IrX_6]^{2-}$ (X = F^-, Cl^-, Br^-) have been prepared and are relatively stable compared with other platinum group metals.[2] Levason *et al* has synthesised a number of complexes of the type, $[IrCl_5L]^{2-}$ (where L = Py, PPh_3, $AsPh_3$, $SbPh_3$, SMe_2, SPh_2, $SeMe_2$).[29] $[IrCl_6]^{2-}$ is often used as an oxidant for organic substrates involving both outer and inner sphere mechanisms.[30] The spectroelectrochemistry of both the $[IrCl_6]^{2-/3-}$ reduction and the $[IrCl_6]^{2-/1-}$ oxidation have been published.[9,31] There is little mention of $[IrI_6]^{2-}$ in the literature besides a report of a "commercial" sample of $K_2[IrI_6]$ characterised by IR and Raman spectroscopy.[32]

Iridium(III) forms a prolific variety of kinetically inert complexes. $[IrCl_6]^{2-}$ is reported to undergo spontaneous reduction in aqueous solution.[33] The stability of Ir(III) is largely attributed to the large crystal field stabilisation energy of the ground state, t_{2g}^6. The crystal structures $A_3[IrCl_6]^{3-}$, where A = K and NH_4 were determined by Ferguson *et al.*[34] $[IrCl_6]^{3-}$ in water is reportedly in equilibrium with $[IrCl_5(H_2O)]^{2-}$ which reacts with pyridine to give $[IrCl_5py]^{2-}$.[35] The magnetic moment of $[IrCl_5(H_2O)]^{2-}$ and kinetics of the initial aquation and further subsequent aquations have been reported by Garner *et al.*[36,37,38,39] It has been found that substitution reactions of *trans*-$[Ir(en)_2X_2]^+$ ($X = Cl^-$, Br^-, I^-) proceed through rate determining aquation.[40] The reaction is relatively slow and must be carried out above 100 °C. Griffith *et al* have reported the synthesis of $[IrI_6]^{3-}$ characterised by Raman spectroscopy.[41] It is suggested that iodide would be too reducing a ligand for Ir(IV).

Recently, the electrochemical reduction of $[IrCl_6]^{2-}$ in dichloromethane solution to produce $[IrCl_6]^{3-}$ in the presence and absence of pyridine has been investigated.[42] In a solution with an equimolar equivalent of pyridine, $[IrCl_6]^{3-}$ loses chloride to form $[IrCl_5Py]^{2-}$. The $[IrCl_5Py]^{2-/1-}$ couple is observed at approximately 0.5 V positive of the $[IrCl_6]^{3-/2-}$ couple as expected when replacing a π-donor for a very weak π-acceptor.[23] The electrochemical response of $[IrCl_6]^{3-}$ at 261 K under argon in dichloromethane without pyridine slowly changes with time. Two new couples are present after two days; one has been assigned as free chloride, the other couple at +0.01 V has been assigned to the novel five co-ordinate $[IrCl_5]^{2-/1-}$ couple following EXAFS analysis. Upon warming the solution to 293 K there was a colour change from combine harvester yellow to olive green. The uv-vis electronic spectrum of the green solution corresponded to $[Ir_2Cl_9]^{3-}$ prepared by Preetz *et al* and Ferguson *et al.*[43,34]

Rhenium Complexes

Rhenium(IV) complexes are relatively stable. $[ReCl_6]^{2-}$ is well characterised. $K_2[ReCl_6]^{2-}$ has been crystallised.[44,45] Rhenium(III) is readily oxidised unless

stabilised by metal-metal bonds.[46,47,48] Liu has prepared a series of rhenium complexes $[ReCl_{6-n}(Py)_n]^{z-}$ (where n = 0-6) by both electrochemical and chemical reduction-induced substitution.[49] Mono-substituted $[ReCl_5L]^{1-}$ species, where L = acetonitrile and benzonitrile have also been prepared. The half-wave potentials are in good agreement with Lever's ligand additivity theory.[23]

3.2 Experimental

3.2.1 Purification and Drying of Solvents

All solvents were rigorously dried and handled under an atmosphere of dry, oxygen free argon (BOC Gases).

Dichloromethane, (environmental grade, Alfa) was stored over potassium hydroxide pellets for a minimum of two weeks before being refluxed over phosphorus pentoxide (Lancaster) for a minimum of three days and freshly distilled before use.

Acetonitrile (HPLC grade, Aldrich) was refluxed over aluminium chloride (15 g/l) for 1 hour followed by rapid distillation. The distillate was refluxed over alkaline potassium permanganate (10 g potassium permanganate and 10g lithium carbonate per litre) for 15 minutes followed by rapid distillation. The distillate was refluxed over potassium bisulphate (15 g/l) for 1 hour followed by rapid distillation. The distillate was then refluxed over calcium hydride (2 g/l) for 1 hour followed by a careful fractionation from a helice packed column at a high reflux ratio. The middle 80 % fraction was retained and distilled three times from phosphorus pentoxide (1 % w/v). The now purified and dried acetonitrile was freshly distilled from phosphorus pentoxide before use.

Propionitrile, butyronitrile (GC grade, Aldrich) were refluxed over calcium hydride for 48 hours and distilled three times from phosphorous pentoxide, the final time directly on to neutral alumina previously heated at 520-570 K for 24 hours.

Pyridine (GC grade, Aldrich) was stored over potassium hydroxide pellets for 2 weeks, and the supernatant fractionally distilled from, and directly to, freshly roasted type 4 Å molecular sieves.

Benzonitrile and benzyl cyanide (Spectroscopic grade, Acros) were distilled twice under reduced pressure from phosphorous pentoxide directly onto neutral alumina previously heated at 520-570 K for 24 hours.

3.2.2 Synthesis of $[N^nBu_4]BF_4$ and of Osmium, Iridium and Rhenium hexahalides

$[N^nBu_4]BF_4$ was prepared by the neutralisation of tetrabutylammonium hydroxide (40 % w/v, Aldrich) with tetrafluoroboric acid (48 % w/v, Aldrich). The white precipitate was recrystallised twice from a 1:1 water/methanol mixture and dried at 343 K under vacuum for 5 days prior to use.

$[N^nBu_4]_2[OsCl_6]$ was prepared by metathesis from $[NH_4]_2[OsCl_6]$ as follows. $[NH_4]_2[OsCl_6]$ (0.5045 g, 1.15 mmol) (Speciality Chemicals, Johnson Matthey) was dissolved in 1 M hydrochloric acid (60 ml). To this tetrabutylammonium hydroxide solution (40% w/v) was added dropwise until no further precipitation occurred. The resulting solid was filtered and dissolved in dichloromethane. The solution was dried by addition of $MgSO_4$ and filtered. The pure product was obtained by repeated recrystallisation from dissolving in a minimum of dichloromethane and addition of chloroform. The resulting yellow needle crystals were dried under vacuum at 350 K for 48 hours. $[N^nBu_4]_2[OsCl_6]$ was characterised by cyclic voltammetry and uv-vis spectroscopy.

$[N^nBu_4]_2[OsBr_6]$ was previously prepared by Dr Kenneth Taylor, University of Edinburgh, by metathesis from $[NH_4]_2[OsBr_6]$ in solution with hydrobromic acid to which tetrabutylammonium hydroxide solution (40% w/v) was added dropwise until no further precipitation occurred.

$[NH_4]_2[OsI_6]$ was prepared by heating $[NH_4]_2[OsCl_6]$ (0.5 g) in a 1.0 M solution of $[NH_4][I]$ in hydroiodic acid (55 %, 5 ml) at 360 K for 2 hours. The solid $[NH_4]_2[OsI_6]$ produced was filtered and carefully washed with cold water and diethyl ether. The product was dried under vacuum for 48 hours. $[NH_4]_2[OsI_6]$ dissolves slowly in 0.5 M dichloromethane/$[N^nBu_4]BF_4$ at 298 K exchanging counter ions to give the soluble $[N^nBu_4]_2[OsI_6]$. $[N^nBu_4]_2[OsI_6]$ was characterised by cyclic voltammetry and UV-visible spectroscopy.

$[N^nBu_4]_2[IrCl_6]$ was prepared previously by Dr Kenneth Taylor, University of Edinburgh, by addition of chloroiridic acid solution (Johnson Matthey) to a saturated solution of $[N^nBu_4]Cl$ in 4 M hydrochloric acid. The resulting red/brown precipitate was recrystallised by the judicious addition of trichloromethane to a concentrated solution of the salt in dichloromethane.

$[N^nBu_4]_2[IrBr_6]$ was prepared previously by Dr Marie Elliot, University of Edinburgh, by metathesis from the potassium salt in solution with hydrobromic acid to which tetrabutylammonium hydroxide solution (40% w/v) was added dropwise until no further precipitation occurred. $[N^nBu_4]_2[IrBr_6]$ was characterised by cyclic voltammetry and uv-vis spectroscopy.

$[N^nBu_4]_2[ReCl_6]$ was prepared previously by Dr Xiaoming Liu, University of Edinburgh, by metathesis of the potassium salt in solution with hydrochloric acid to which tetrabutylammonium hydroxide solution (40% w/v) was added dropwise until no further precipitation occurred.

3.2.3 Electrochemical Synthesis

It has been found that electrochemical one-electron reduction of $[MCl_6]^{2-}$, where M = Os, Ir, Re, induces substitution for a less electron donating ligand. All bulk electrogeneration experiments were carried out in an H-type cell described in chapter two. All experiments were carried out under an atmosphere of dry, oxygen free argon (BOC gases).

3.2.3.1 Preparation of $[N^nBu_4][OsCl_5L]$, where L = An, Pn, By, Py, Bn, Bc

A solution of 0.5 M $[N^nBu_4]BF_4$/dichloromethane was added to an H-type cell and bubbled through with argon for 15 minutes to displace any dissolved dioxygen. To the main chamber of the H-type cell 30.0 mg (0.0338 mmol) $[N^nBu_4]_2[OsCl_6]$ was added. A 10 fold equivalent of L was then added to the solution and the potential of the basket working electrode held at –0.70 V until the plot of time against charge (Coulombs) levelled off and the current approached zero. A stirred cyclic voltammogram was run at 20 mV s^{-1} to demonstrate complete reduction from Os(IV) to Os(III). The reduction was accompanied by a colour change from bright yellow to pale yellow. The potential of the basket working electrode was then held at +0.20 V in order to oxidise the new complex back to Os(IV). Cyclic voltammetry was carried out at each stage of the process.

The 0.5 M $[N^nBu_4]BF_4$/dichloromethane solution of $[N^nBu_4][OsCl_5Py]$ from the H-type cell was evaporated under vacuum to a minimum volume. In order to separate the electrolyte from the osmium salt the solution was added to a silica gel 60 (Merck) column with 3:1 dichloromethane:ethyl acetate mix as solvent previously bubbled

through with dry N_2 gas to displace any dioxygen. A yellow solution was eluted from the column and evaporated under vacuum. The yellow solid was re-dissolved in dichloromethane and crystallised with slow evaporation of solvent at 288 K ± 5 to give yellow needle-like crystals for study by X-ray diffraction.

X-ray diffraction data were collected on a Stöe Stadi4 diffractometer equipped with Oxford Cyrosystems cryostream and graphite monochromated Mo-K_α radiation using ω-θ scans and the learnt profile method in the range $2.61 \leq \theta \leq 25.08°$. The crystal was a yellow needle of dimensions 0.62 mm x 0.16 mm x 0.16 mm. Of a total 4973 reflection collected, 4969 were independent. The final difference map extrema were 0.977 and -0.986 e.Å^{-3} with a final R of 3.63 % of 4034 strong data. An optimised numerical absorption correction based on face indices was applied (T_{min} = 0.570, T_{max} = 0.628).

Empirical formula	$C_{21}H_{41}Cl_5N_2Os$	a / Å	10.7663(16)
Formula weight	689.01	b / Å	19.013(4)
Crystal system	Monoclinic	c / Å	14.061(3)
Space group	$P2_1/n$	α / °	90
Volume / Å^3	2801.0(10)	β / °	103.299(16)
Z	4	γ / °	90
Temperature	220(2) K	μ(Mo-K_α) / mm^{-1}	5.041
Wavelength / Å	0.71073	R_1[F>4σF]	0.0363
Density calc. / Mg m^{-3}	1.634	wR_2 (all data)	0.0819

Table 3.1 Crystallographic data for [N^{n}Bu$_4$][OsCl$_5$Py]. Full crystal data and structure refinement are given in the Appendices

[N^{n}Bu$_4$][OsCl$_5$An] was isolated from the electrolyte solution by Dr Marie Elliot, University of Edinburgh, on a silica gel 60 column with previously degassed ethyl acetate as the elutant. A yellow band remained on the column once all the supporting electrolyte had been eluted. The solvent was then changed to previously degassed propan-2-ol. A yellow solution was eluted and evaporated under vacuum. The yellow solid was recrystallised from a 1:5 dichloromethane/ether mix at 288 K ± 5 to give yellow needle-like crystals suitable for study by X-ray diffraction.

X-ray diffraction data were collected on a Bruker AXS SMART diffractometer equipped with a CCD area detector, Oxford Cyrosystems cryostream and graphite

monochromated Mo-K_α radiation using ω-θ scans in the range $1.83 \leq \theta \leq 26.40°$. The crystal was a yellow needle of dimensions 0.29 mm x 0.04 mm x 0.04 mm. Of a total 17477 reflection collected, 5242 were independent. The final difference map extrema were 1.885 and -0.553 e.Å^{-3} with a final R of 3.18% of 4430 strong data. An optimised numerical absorption correction based on face indices was applied (T_{min} = 0.652, T_{max} = 0.862).

Empirical formula	$C_{18}H_{39}Cl_5N_2Os$	a / Å	28.116(5)
Formula weight	650.96	b / Å	36.205(7)
Crystal system	orthorhombic	c / Å	10.6385(19)
Space group	Fdd2	α / °	90
Volume / Å^3	10829(3)	β / °	90
Z	16	γ / °	90
Temperature / K	150(2)	μ(Mo-K_α) / mm^{-1}	5.210
Wavelength / Å	0.71073	R_1[F>4σF]	0.0318
Density calc. / Mg m^{-3}	1.597	wR_2 (all data)	0.0636

Table 3.2 Crystallographic data for [N^{n}Bu$_4$][OsCl$_5$An]. Full crystal data and structure refinement are given in the Appendices

Separation of other complexes of the type [N^{n}Bu$_4$][OsCl$_5$L] (L = Pn, By) were carried out as for [N^{n}Bu$_4$][OsCl$_5$Py] all yielding a yellow solution in dichloromethane. Although separation from the supporting electrolyte was accomplished, growing crystals suitable for X-ray analysis has proved an elusive task. The complexes have shown some air sensitivity in solution. Elemental analyses of [N^{n}Bu$_4$][OsCl$_5$L] were inconclusive due to this instability in air.

Negative ion electrospray mass spectrometry was performed on a Research Platform II Mass Spectrometer using MassLynx Operating System. Samples of [N^{n}Bu$_4$][OsCl$_5$L], where L = An, Pn, By, were prepared in approximate 10 ng/µl concentrations in the solvent L. Samples of [N^{n}Bu$_4$][OsCl$_5$L] where L = Bn, Bc, were prepared in acetonitrile because of the relatively low volatility of benzonitrile and benzyl cyanide. Evidence of OsCl$_4$By was obtained but only a suggestion of the appropriate masses for the other species could be obtained. Fragmentation into OsCl$_5$ and OsCl$_4$ and other species readily occurred under a number of experimental conditions.

All $[N^nBu_4][OsCl_5L]$ compounds were characterised through cyclic voltammetry and uv-vis spectrometry.

3.2.3.2 Preparation of $[N^nBu_4][MX_5L]$, where M = Os, Ir, Re and X = Cl, Br, I and L = An, Pn, By

Metal salts of the type $[N^nBu_4][MX_5L]$ were prepared by the same route as for the complexes, $[N^nBu_4][OsCl_5L]$. A solution of 0.5 M $[N^nBu_4]BF_4$/dichloromethane was added to an H-type cell and bubbled through with argon for 15 minutes to displace any dissolved dioxygen. To the main chamber of the H-type cell a known weight of $[N^nBu_4]_2[MX_6]$ was added and the cyclic voltammogram recorded. At a chosen temperature a 10 fold equivalent of L was added to the solution and the potential of the basket working electrode held so that the metal salt was reduced. A stirred cyclic voltammogram was run at 20 mV s^{-1}. Upon complete reduction of the solution the potential of the basket working electrode was altered and held in order to oxidise the new complex back to M(IV). Cyclic voltammetry was carried out at each stage to investigate the process. The mono-substituted metal salts were characterised by cyclic voltammetry and uv-vis spectroscopy. The relevant temperatures, reducing/oxidising potentials and prepared compounds are shown below.

Complex	Amount (mmol)	Temp. (K)	Reducing Potential (V)	Oxidising Potential (V)	Prepared compound
$[N^nBu_4]_2[OsCl_6]$	0.0338	298	-0.70	+0.20	$[N^nBu_4][OsCl_5L]$
$[N^nBu_4]_2[OsBr_6]$	0.0217	298	-0.50	0.00	$[N^nBu_4][OsBr_5L]$
$[N^nBu_4]_2[OsI_6]$	0.0280	223	-0.40	+0.30	$[N^nBu_4][OsI_5L]$
$[N^nBu_4]_2[IrCl_6]$	0.0281	298	-0.20	+1.00	$[N^nBu_4]_2[IrCl_5L]$
$[N^nBu_4]_2[IrBr_6]$	0.0217	233	-0.10	+1.00	$[N^nBu_4]_2[IrBr_5L]$
$[N^nBu_4]_2[ReCl_6]$	0.0283	233	-1.45	0.00	$[N^nBu_4][ReCl_5L]$

Table 3.3 Temperature, reducing/oxidising potentials and prepared compounds for the reduction-induced substitution of $[N^nBu_4]_2[MX_6]$.

3.2.4 Double Step Chronoamperometry

The most consistent results for double step chronoamperometry experiments were obtained with a platinum quasi-reference electrode. The potential step voltages were chosen by reference to a cyclic voltammogram run prior to the measurement on the same time scale of the proposed chronoamperometric measurement. Reproducibility of results has been found to be adversely affected by trace amounts of water. As a result, all solvents were combined with electrolyte at known concentrations (0.2 M $[N^nBu_4]BF_4$ unless otherwise stated) and introduced to an argon filled electrochemical cell through a short column of activated alumina as a final drying step (neutral alumina was activated by heating at 520-570 K under vacuum for 24 hours). Unless otherwise stated the concentration of metal salt was kept at 0.0020 M $\pm$ 0.0002. It should be noted that the typical concentration of 0.2 M electrolyte swamps the concentration of the metal salt and ensures electroneutrality is maintained. In this way electric fields do not build up in the solution as electrolysis proceeds and transport effects are almost completely blind to the small charge "injection" that arises.

3.2.5 Simulation

Experimental cyclic voltammograms of $[N^nBu_4]_2[OsCl_6]$ in 0.5 M $[N^nBu_4]BF_4$/butyronitrile have been simulated using the software, Digisim 2.1©. The accuracy of the simulations was tested by comparison of the fit over a number of scan rates. The full input data for the simulated Dissociative and dissociative Interchange mechanisms, discussed in section 3.3.1.5, are shown in **Table 3.4** and **Table 3.5**. The electron transfer rates, diffusion coefficients, and transfer coefficient (α) for each process were not measured and were left as the Digisim default,

1 x10^4 cm^{-1}, 1 x10^{-5} cm^2 s^{-1}, and 0.5, respectively. There is no reason to believe they should be significantly different from these figures. The transfer coefficient, α, reflects the sensitivity of the transition state to the drop in electrical potential between the metal electrode and solution taking a value $0 < \alpha < 1$. The value of α approaches zero when the transition state resembles the reactants in its potential dependence and conversely, α approaches 1 when the transition state behaves in a product-like manner. In practise the transfer coefficient is typically close to 0.5 for many electrochemical reactions.[50]

Known parameters		Diffusion	Semi-infinite	
Electrode area	0.020 cm^2	Start potential	0.30 V	
Electrode Geometry	planar	End potential	-1.30 V	
Temperature	298 K	Concentration [A]	0.0028 M	
		Resistance	1.1 x10^4 Ω	
Charge transfer reactions		Charge transfer parameters		
Reaction 1	A + e = B	$E_{1/2}$ 1	-0.66 V	
Reaction 2	E + e = D	$E_{1/2}$ 2	0.08 V	
		α 1 and 2	0.5	
		Rate 1	10000 cms^{-1}	
		Rate 2	10000 cms^{-1}	
Homogeneous chemical reactions		Chemical reaction parameters		
		K_E	k_f	k_b
Reaction 1	B = C	0.01	0.50	50
Reaction 2	C = D	500	1	0.06
Diffusion coefficients				
A	1.00x10^{-5} cm^2 s^{-1}	D	1.00x10^{-5} cm^2 s^{-1}	
B	1.00x10^{-5} cm^2 s^{-1}	E	1.00x10^{-5} cm^2 s^{-1}	
C	1.00x10^{-5} cm^2 s^{-1}			

Table 3.4 Input parameters for simulated cyclic voltammetry for a Dissociative mechanism on Digisim 2.1

Known parameters		Diffusion	Semi-infinite	
Electrode area	0.020 cm^2	Start potential	0.30 V	
Electrode Geometry	planar	End potential	-1.30 V	
Temperature	298 K	Concentration [A]	0.0028 M	
		Resistance	1.1 x10^4 Ω	
Charge transfer reactions		Charge transfer parameters		
Reaction 1	A + e = B	$E_{1/2}$ 1	-0.66 V	
Reaction 2	F + e = E	$E_{1/2}$ 2	0.08 V	
		α 1, 2, and 3	0.5	
		Rate 1	10000 cms^{-1}	
		Rate 2	10000 cms^{-1}	
Homogeneous chemical reactions		Chemical reaction parameters		
		K_E	k_f	k_b
Reaction 1	B = C	20	10000	500
Reaction 2	C = D	50	0.50	0.01
Reaction 3	D = E	1000	1000	1
Diffusion coefficients				
A	1.00x10^{-5} $cm^2 s^{-1}$	D	1.00x10^{-5} $cm^2 s^{-1}$	
B	1.00x10^{-5} $cm^2 s^{-1}$	E	1.00x10^{-5} $cm^2 s^{-1}$	
C	1.00x10^{-5} $cm^2 s^{-1}$			

Table 3.5 Input parameters for simulated cyclic voltammetry for a dissociative Interchange mechanism on Digisim 2.1

3.2.6 *in situ* spectroelectrochemical uv-vis

In situ spectroelectrochemical uv-vis experiments were carried out using the optically transparent thin layer electrode (OTTLE) described in chapter two. A 0.5 M $[N^nBu_4]BF_4$/dichloromethane solution was used after being bubbled with argon to displace any dissolved dioxygen. The appropriate metal salts, $[N^nBu_4]_2[MX_6]$ (M = Os, Ir, Re and X = Cl, Br, I,) were weighed into a 1 ml standard flask and dissolved in the 0.5 M $[N^nBu_4]BF_4$/dichloromethane solution. The cell was assembled and placed in the spectrophotometer cavity and cooled to the appropriate temperature. The working electrode potential was set to either reduce or oxidise and the process followed by uv-vis spectroscopy every five minutes. Where a salt of the

general formula $[N^nBu_4][MX_5L]$ (where M= Os, Ir, Re; X = Cl, Br, I; L = An, Pn, By, Py, Bn, Bc) was to be investigated, spectroelectrochemical experiments were carried out in 0.1 M $[N^nBu_4]BF_4$/L solution. Redox-induced substitution was carried out with $[N^nBu_4][MX_6]$ as for the H-type cell using the same reduction/oxidation potentials (see 3.2.3) *in situ* of the uv-vis spectrophotometer at a chosen temperature. The reaction was followed by uv-vis spectrometry every 5 minutes. The solutions were then cooled further, when necessary, and the new salts were reduced and oxidised, followed by uv-vis spectrometry every five minutes. The relevant concentrations, potentials and temperatures are recorded in **Table 3.6**.

Compound	Concentration (mmol dm^{-3})	Temperature (K) of reduction induced substitution	Temperature of reduction/ oxidation (K)	Reduction Potentials (V)	Oxidation Potentials (V)
$[N^nBu_4]_2[OsCl_6]$	3.94	x	223	-0.70	-0.20
$[N^nBu_4][OsCl_5An]$	3.15	273	223	-0.70	+0.20
$[N^nBu_4][OsCl_5Pn]$	3.45	273	223	-0.70	+0.20
$[N^nBu_4][OsCl_5By]$	3.27	273	223	-0.70	+0.20
$[N^nBu_4][OsCl_5Py]$	3.11	273	223	-0.70	+0.20
$[N^nBu_4][OsCl_5Bn]$	3.15	273	223	-0.70	+0.20
$[N^nBu_4][OsCl_5Bc]$	3.46	273	223	-0.70	+0.20
$[N^nBu_4]_2[OsBr_6]$	3.90	x	223	-0.50	0.00
$[N^nBu_4][OsBr_5An]$	3.95	273	223	-0.50	+0.30
$[N^nBu_4][OsBr_5Pn]$	3.77	273	223	-0.50	+0.30
$[N^nBu_4][OsBr_5By]$	3.91	273	223	-0.50	+0.30
$[N^nBu_4]_2[OsI_6]$	3.13	x	203	-0.40	+0.10
$[N^nBu_4][OsI_5An]$	3.01	223	223	-0.20	+0.40
$[N^nBu_4][OsI_5Pn]$	2.98	223	223	-0.20	+0.40
$[N^nBu_4][OsI_5By]$	3.33	223	223	-0.20	+0.40
$[N^nBu_4]_2[IrCl_6]$	3.50	x	223	-0.10	+0.30
$[N^nBu_4][IrCl_5An]$	3.59	293	213	-0.10	+1.25
$[N^nBu_4][IrCl_5Pn]$	3.69	293	213	-0.10	+1.30
$[N^nBu_4][IrCl_5By]$	3.52	293	213	-0.10	+1.30
$[N^nBu_4]_2[IrBr_6]$	4.32	x	223	-0.10	+0.40
$[N^nBu_4][IrBr_5An]$	4.31	273	223	-0.10	+0.95
$[N^nBu_4][IrBr_5Pn]$	4.10	273	223	-0.10	+1.00
$[N^nBu_4][IrBr_5By]$	4.11	273	223	-0.10	+1.00
$[N^nBu_4]_2[ReCl_6]$	2.75	x	183	-1.45	-0.60
$[N^nBu_4][ReCl_5Pn]$	2.88	263	223	-1.45	0.00

Table 3.6 Concentration, temperature of electrochemical synthesis and reduction/oxidation potentials for *in situ* uv-vis spectroelectrochemistry. x = no chemical reaction

3.3 Results and Discussion

3.3.1 $[OsCl_5L]^{2-}$, L = An, Pn, By, Py, Bn, Bc

The CV of $[N^nBu_4]_2[OsCl_6]$ in 0.5 M $[N^nBu_4]BF_4$/dcm at 293 K (**Figure 3.1**) shows a reduction at –0.57 V (ΔE = 80 mV) and an oxidation at +1.38 V (ΔE = 75 mV); both are one electron processes as determined by coulometry and electron transfer rates are diffusion limited, i.e. $i_p \alpha \nu^{1/2}$. The reduction process is not chemically reversible at 0.1 V s^{-1}, 293 K, since $i_p^{red} > i_p^{ox}$.

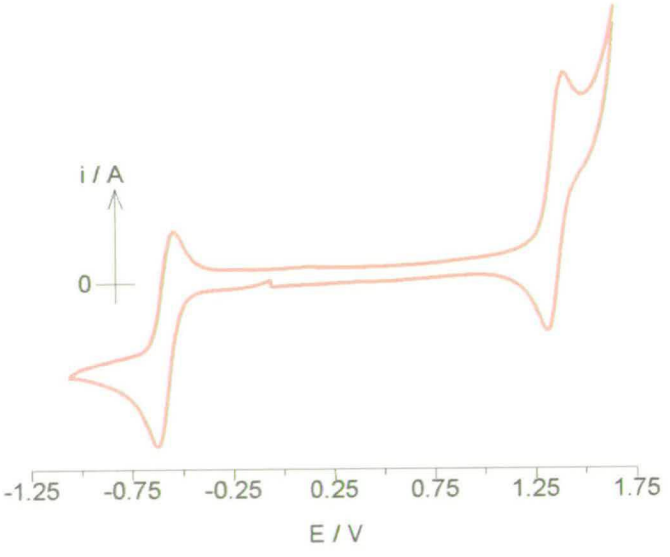

Figure 3.1 CV of $[OsCl_6]^{2-}$ in 0.5 M $[N^nBu_4]BF_4$/dcm at 0.1 V s^{-1}, 293 K

At 223 K, however, $[OsCl_6]^{2-}$ can be reduced in bulk with chemical reversibility. The spectroelectrochemical uv-vis spectrum of the III/IV redox couple of $(N^nBu_4)_2[OsCl_6]$ in 0.5 M $[N^nBu_4]BF_4$/dcm at 223 K is shown in **Figure 3.2**. The spectra of the $[OsCl_6]^{2-}$ and $[OsCl_6]^{3-}$ species are dominated by two strong bands. Both bands are assigned as $Cl^-\pi \rightarrow Os(IV/III)d\pi(t_{2g})$ transitions involving different chloride based orbitals.[6,51] As expected for a ligand to metal charge transfer (LMCT)

the Os(III) transitions are at a higher energy on addition of an electron to the metal centre. The clear isosbestic points indicate a chemically reversible process at this temperature.

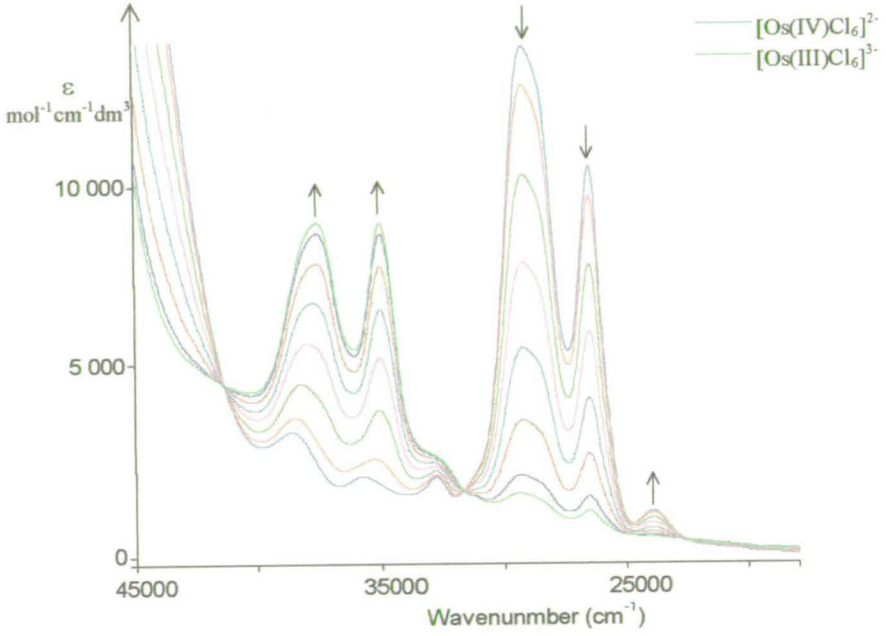

Figure 3.2 *In-situ* uv-vis spectroelectrochemical reduction spectra of $[OsCl_6]^{2-}$ in 0.5 M $[N^nBu_4]BF_4$/dcm at 223 K, electrogeneration potential -0.70 V

In the presence of a less electron donating ligand than chloride, reduction induces substitution of a chloride. Two successive CV's of $[N^nBu_4]_2[OsCl_6]$ in 0.1 M $[N^nBu_4]BF_4$/butyronitrile at 293 K are shown in **Figure 3.3**.

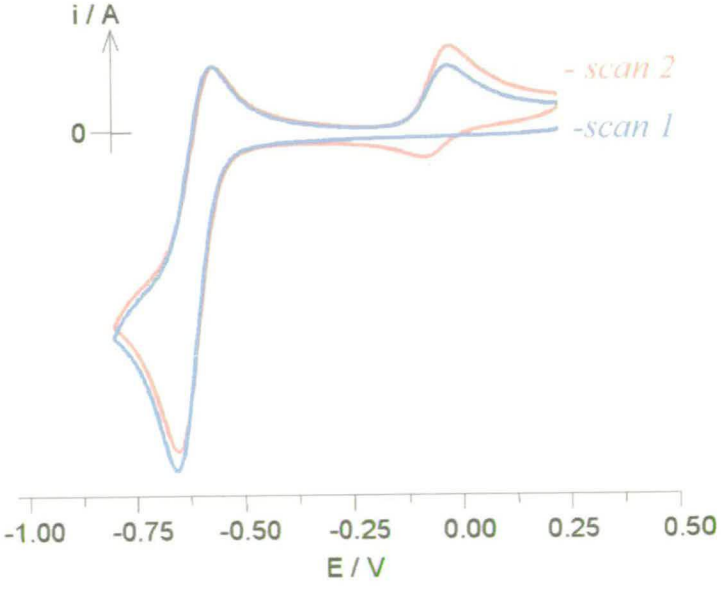

Figure 3.3 CV of $[OsCl_6]^{2-}$ in 0.1 M $[N^nBu_4]BF_4$/butyronitrile at 0.1 V s^{-1}, 293 K

On the time scale of the experiment the Os(III) species reacts, in part, with butyronitrile. The redox chemistry of the daughter product can be seen at approximately 0.5 V positive of the $[OsCl_6]^{3-/2-}$ redox couple. It should be emphasised this substitution reaction is never observed for the Os(IV) species at room temperature without photochemical initiation.[16] The butyronitrile ligand can be thought of as stabilising the Os(III) metal centre by relieving the increase in electron density. Butyronitrile is less electron donating than the chloride it has replaced and can accept electron density from the metal centre. The modelling program, CAChe 3.2, illustrates the electron density on the ligand increasing on ligation to the metal centre (**Figure 3.4**).

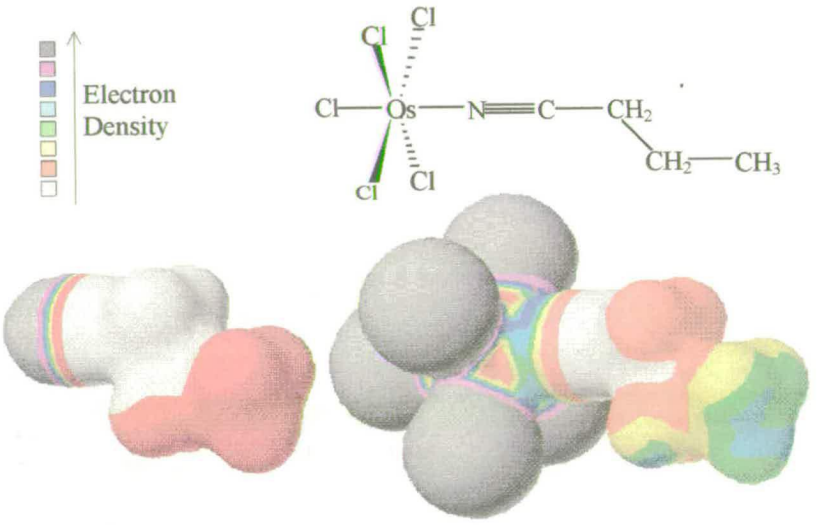

Figure 3.4 Electron density map of free By and $[OsCl_5By]^{2-}$ using EHMO calculations (CAChe 3.2)

A range of complexes has been synthesised by the bulk reduction of $[OsCl_6]^{2-}$ to $[OsCl_6]^{3-}$ in the presence of L in an H-type cell leading to the complete mono-substitution of a chloride to form $[OsCl_5L]^{2-}$, where L = acetonitrile (An), propionitrile (Pn), butyronitrile (By), pyridine (Py), benzonitrile (Bn), benzyl cyanide (Bc). The half wave potentials for the IV/III and V/IV redox couples are shown in **Table 3.7**. The substituted products have an electrochemically reversible reduction at *ca.* 0 V and oxidation at *ca.* +1.85 V. Neither is chemically reversible at 298 K. The redox couples can be considered metal based as neither chloride nor L exhibits redox chemistry in this region.

Compound	$E_{1/2}$ (IV/III) / V	ΔE / mV	$E_{1/2}$ (V/IV) / V	ΔE / mV
$[OsCl_6]^{z-}$	-0.57	80	+1.38	75
$[OsCl_5An]^{z-}$	+0.10	79	+1.89	92
$[OsCl_5Pn]^{z-}$	-0.03	70	+1.82	88
$[OsCl_5By]^{z-}$	-0.08	71	+1.80	89
$[OsCl_5Py]^{z-}$	-0.02	72	+1.83	87
$[OsCl_5Bn]^{z-}$	+0.04	72	+1.87	88
$[OsCl_5Bc]^{z-}$	+0.05	75	+1.87	88

Table 3.7 Half-wave potentials for $[OsCl_5L]^{z-}$ at 298 K

Molecular orbital calculations using CACh e 3.2 show both the HOMO and LUMO of the Os(IV) complex to be based on the metal (**Figure 3.5**).

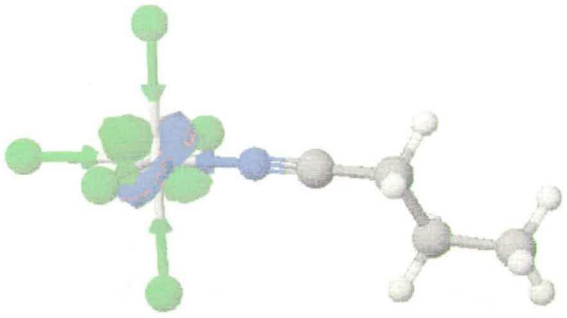

Figure 3.5 HOMO of $[OsCl_5By]^{1-}$, using EHMO calculations (CACh e 3.2)

The differences in half wave potentials can be attributed to the relative electron donor/acceptor properties of the ligands. In this regard acetonitrile, propionitrile, and butyronitrile show a stepwise destabilisation of the metal based Os(IV/III) couple due to the increasing electron donor properties of the alkyl groups. Further reduction-induced processes have been shown to occur with time to yield more substituted products. Taylor has prepared the complete series $[OsCl_{6-n}Py_n]^{z-}$ (n = 0-6), their half-wave potentials increasing positively in step with Lever's ligand addititivity theory.[21,23] Duff and Heath noted similar changes in the series $[RuX_{6-n}L_n]^{z}$, X = Cl^-, Br^-, L = An, Bn, n = 0-6.[52] The IV/III redox couple of the complexes $[RuCl_5L]^{2-/1-}$ L = An, Bn are 0.60 V and 0.64 V positive of the $[RuCl_6]^{3-/2-}$ species. For the reaction $[OsCl_6]^{3-} \rightarrow [OsCl_5L]^{2-}$ no intermediate is observed on the cyclic voltammetry

measured over the course of the reaction. Likewise the *in situ* spectroelectrochemical uv-vis spectrum does not demonstrate any appreciable build up of an intermediate (**Figure 3.6**). The main bands at 26600 cm^{-1} and 29200 cm^{-1} of the $[OsCl_6]^{2-}$ spectrum fall away with bands at 32900 cm^{-1} and 40000 cm^{-1} (shoulder) of the new substituted complex, $[OsCl_5An]^{2-}$ growing in. Note, however, the lack of isosbestic points indicating that $[OsCl_5An]^{2-}$ forms from $[OsCl_6]^{2-}$ via at least one intermediate species.

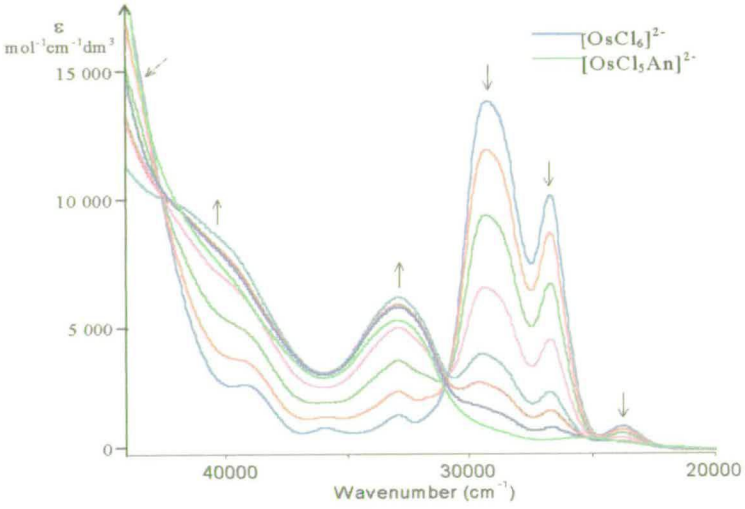

Figure 3.6 Uv-vis spectroelectrochemical reduction spectra of $[OsCl_6]^{2-} \rightarrow [OsCl_5An]^{2-}$ at 273 K in 0.1 M $[N^nBu_4]BF_4$/An at 223 K, electrogeneration potential -0.70 V

3.3.1.1 Uv-vis spectra and spectroelectrochemical uv-vis spectra of $[OsCl_5L]^{2-/1-}$

The uv-vis spectra and *in situ* spectroelectrochemical uv-vis spectra of the mono substituted products $[OsCl_5L]^{2-/1-}$ where L = An, Pn, By, Py, Bn and Bc are shown in **Figures 3.7** and **3.8**. The assignment of absorption bands to specific electronic transitions is notoriously difficult. The comparative study of spectra of closely related species has been helpful in this regard. In the series of complexes $[OsCl_5L]^{z-}$ the osmium metal centre is always in an octahedral co-ordination site and hence the d orbitals will be split into two subsets, t_{2g} or $d\pi$ orbitals, and e_g or $d\sigma$ orbitals, in pseudo O_h symmetry. Some degeneracy of the t_{2g} and e_g orbitals is removed by the

lower symmetry of the mono-substituted species but the "t_{2g}" and the "e_g" sets may still be regarded as dπ and dσ orbitals. Orbital non-degeneracy tends to result in broader bands of similar energy. On comparison with $[OsCl_6]^{3-/2-}$, the transitions of $[OsCl_5L]^{2-/1-}$ must also generally correspond to LMCT transitions. The $[OsCl_5L]^{1-}$ complexes are dominated by a transition at *ca.* 27000 cm^{-1} which is assigned to a $Cl^-\pi \rightarrow$ Os(IV)dπ charge transfer transition. The less intense band or shoulder at lower energy (*ca.* 23000 cm^{-1}) maybe assigned to the spin forbidden LMCT triplet transition. The third row transition metal, osmium, will exhibit strong spin orbit coupling and hence normally weak triplet electronic transitions will be more intense.

Reduction of $[OsCl_5L]^{1-}$ to $[OsCl_5L]^{2-}$ generally results in the move to higher energy of LMCT transitions as observed in the isoelectronic $[OsCl_6]^{3-/2-}$ spectra. The main LMCT transitions tend to shift by almost 6000 cm^{-1} to around 33000 cm^{-1}. In $[OsCl_5Py]^{2-}$ and $[OsCl_5Bn]^{2-}$, however, there is an added complication. Low energy bands at around 25000 cm^{-1} grow in on reduction, for these two complexes only, and may be seen most clearly on the spectroelectrochemical spectra. The bands centred around 25000 cm^{-1} in $[OsCl_5Py]^{2-}$ and $[OsCl_5Bn]^{2-}$ must therefore be assigned to metal to ligand charge transfer (MLCT) transitions, Os(III)dπ $\rightarrow$ (Py/Bn)π*. More than one band is observed because orbital degeneracy has been removed on mono-substitution. Similar transitions are not observed for the other Os(III) complexes since the π*-orbitals for pyridine and benzonitrile lie at lower energy than in the other ligands; certainly pyridine is acknowledged as a very weak π-acceptor.

Jørgensen suggested the bands of weaker absorption in the $[OsCl_6]^{2-}$ spectra at 32800 cm^{-1}, 35800 cm^{-1}, and 38800 cm^{-1} were due to dπ $\rightarrow$ dσ transitions.[6] The molar absorption coefficients are, however, high for this assignment. Comparing the spectrum to those of $[OsCl_5L]^{1-}$ the broad band at *ca* 34000 cm^{-1} probably has the same electronic origins. This band, particularly in $[OsCl_5Pn]^{1-}$, has an absorption far higher intensities than could be expected for a dπ $\rightarrow$ dσ transition. The band moves to higher energy on reduction to the Os(III) species (*ca* 40000 cm^{-1}). Thus the high energy transitions in both $[OsCl_6]^{3-/2-}$ and $[OsCl_5L]^{2-/1-}$ are assigned as further $Cl^-\pi \rightarrow$

Os(IV/III)dπ transitions. The transition band positions, extinction coefficients, and probable electronic assignments are given in **Table 3.8**.

The *in situ* spectroelectrochemical uv-vis spectra, at 223 K, all show precise isosbestic points demonstrating the reversible electrochemical and chemical behaviour of the $[OsCl_5L]^{2-/1-}$ oxidation/reduction, that is, there are no intermediates formed in the redox process.

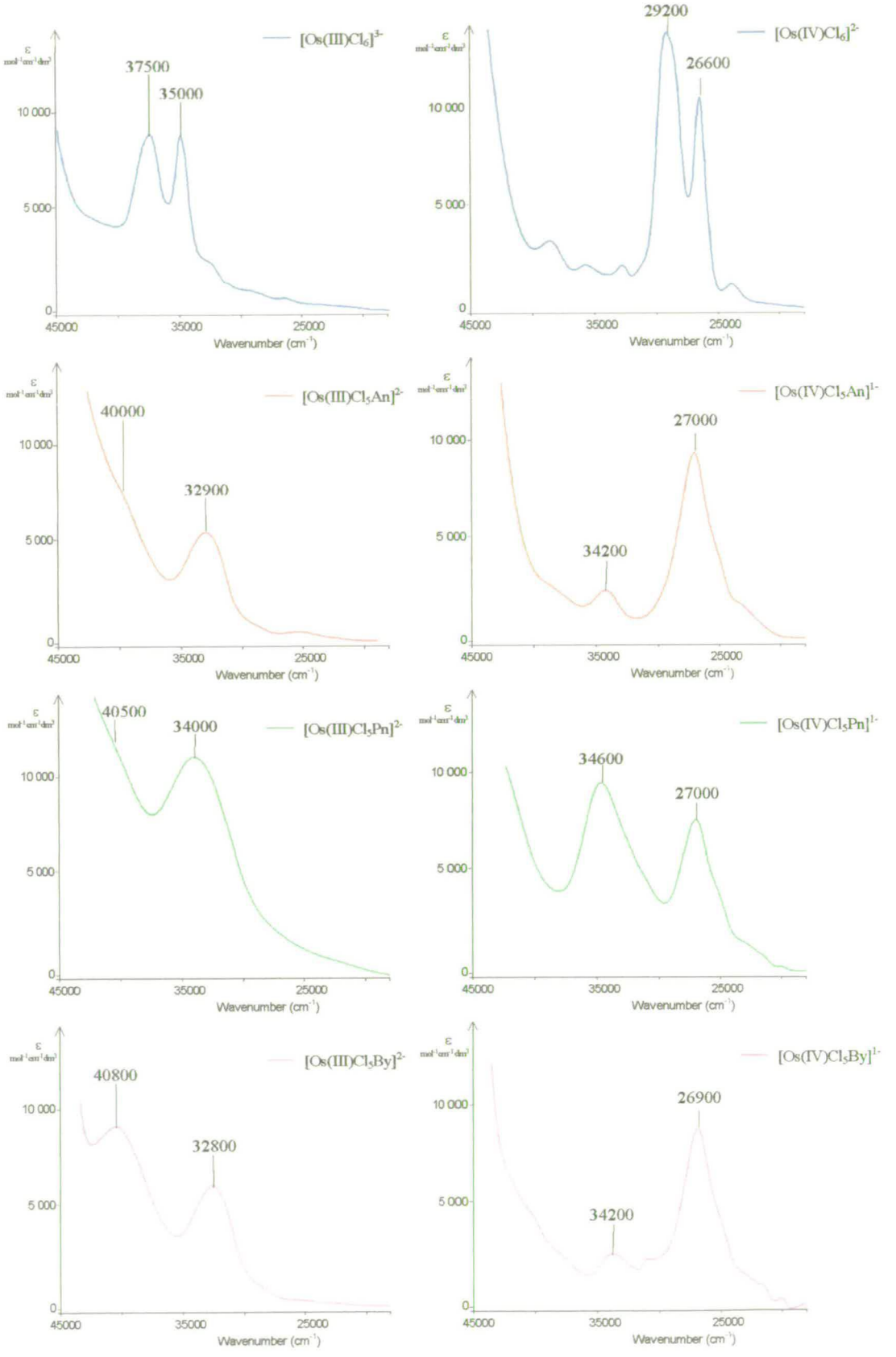

Figure 3.7 Uv-vis spectra of of $[OsCl_6]^{z-}$ in 0.5 M $[N^nBu_4]BF_4$/dcm at 223 K, and $[OsCl_5L]^{z-}$, L = An, Pn. By, Py, Bn, Bc, in 0.1 M $[N^nBu_4]BF_4$/L at 223 K

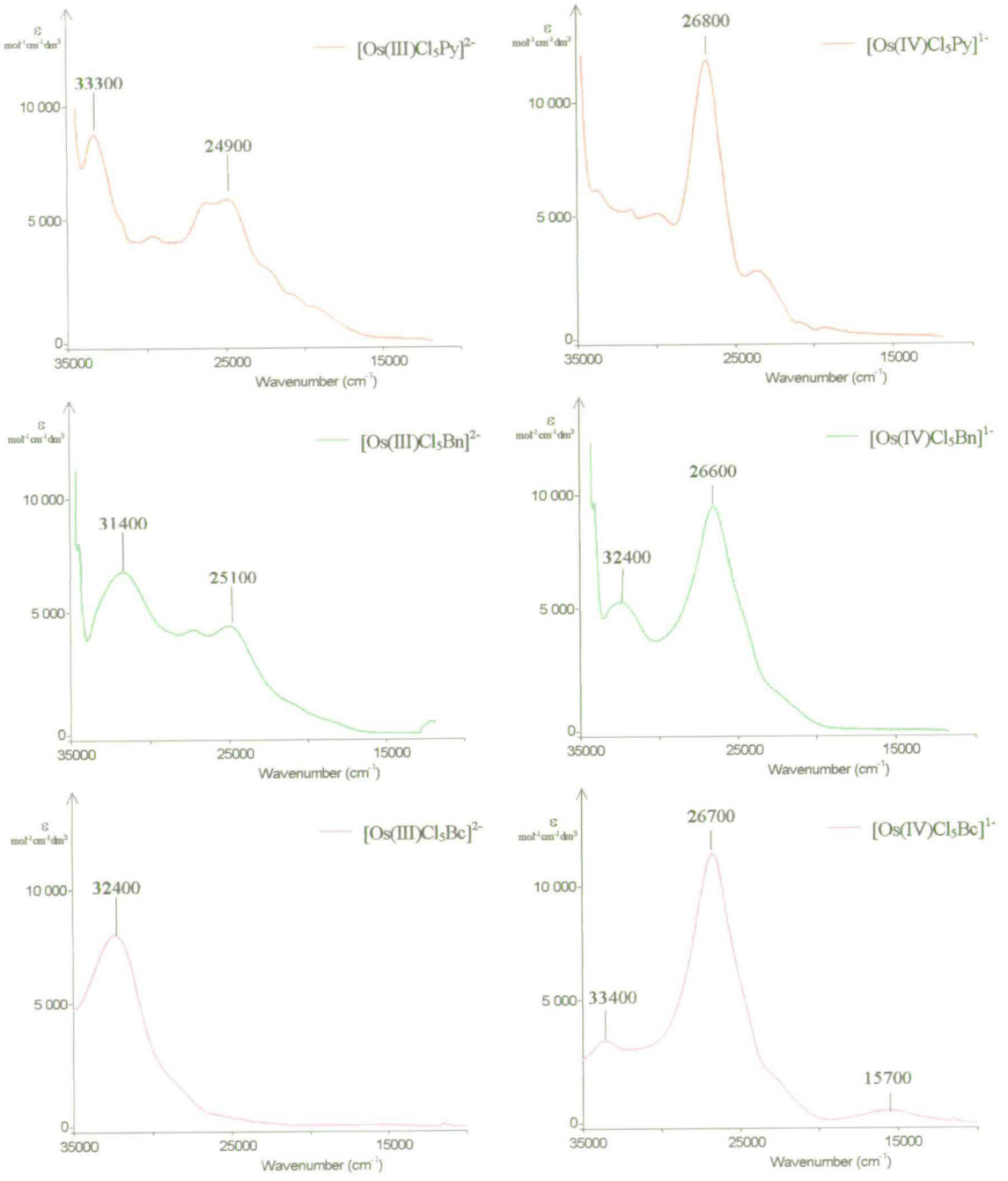

Figure 3.7 Uv-vis spectra of $[OsCl_6]^{z-}$ in 0.5 M $[N^nBu_4]BF_4$/dcm at 223 K, and $[OsCl_5L]^{z-}$, L = An, Pn, By, Py, Bn, Bc, in 0.1 M $[N^nBu_4]BF_4$/L at 223 K

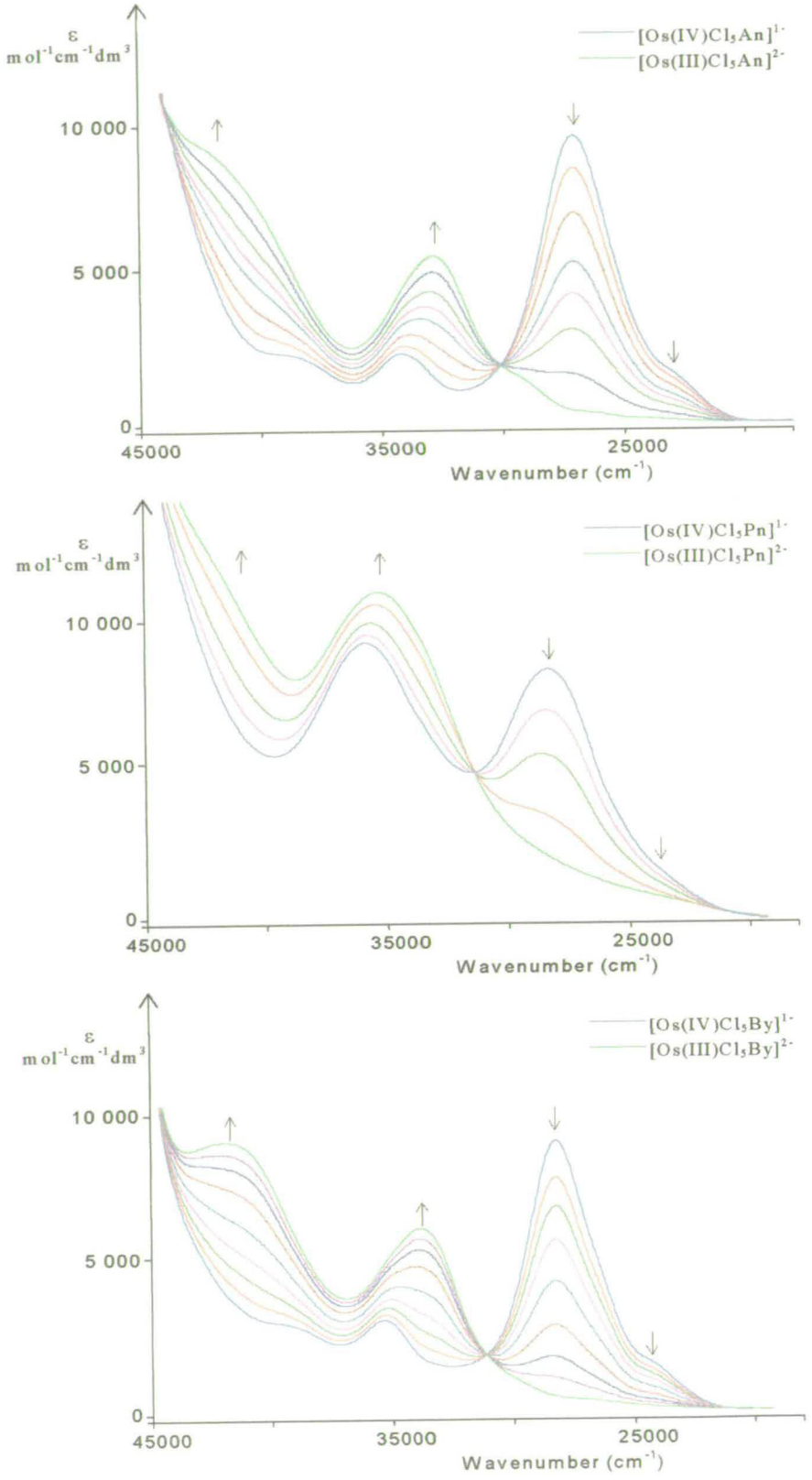

Figure 3.8 Uv-vis spectroelectrochemical reduction spectra of $[OsCl_5L]^{z-}$, L = An, Pn, By, Py, Bn, Bc, in 0.1 M $[N^nBu_4]BF_4$/L at 223 K, electrogeneration potential -0.70 V

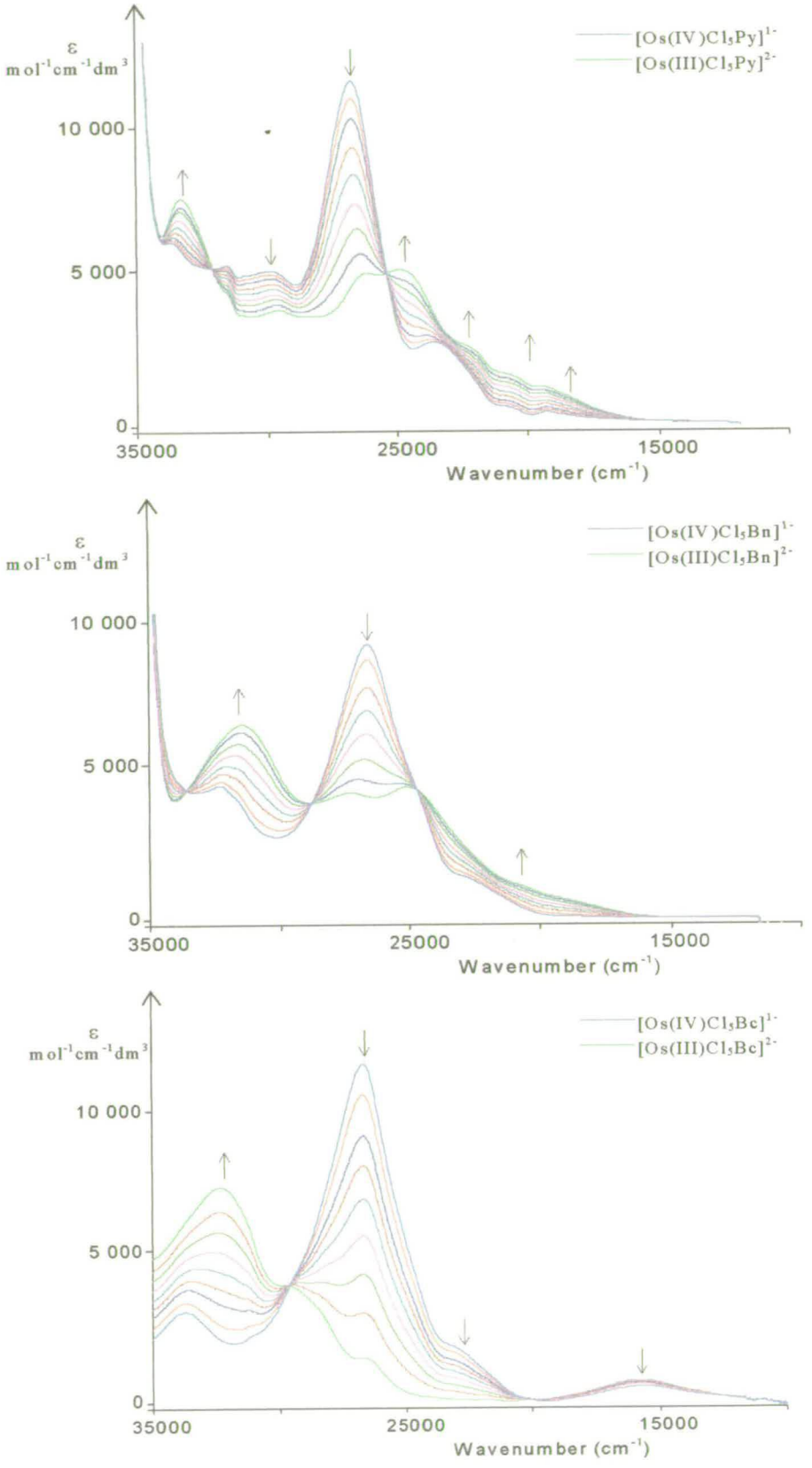

Figure 3.8 Uv-vis spectroelectrochemical reduction spectra of $[OsCl_5L]^{z-}$, L = An, Pn, By, Py, Bn, Bc, in 0.1 M $[N^nBu_4]BF_4$/L at 223 K, electrogeneration potential -0.70 V

Compound	Peak max (cm-1)	ε (mol^{-1} cm^{-1} dm^3)	Assignment
$[Os(IV)Cl_6]^{2-}$	23 700	1 000	$Cl^-\pi \rightarrow Os(IV)d\pi$
	26 600	9 900	$Cl^-\pi \rightarrow Os(IV)d\pi$
	29 200	13 100	$Cl^-\pi \rightarrow Os(IV)d\pi$
	32 800	1 100	$Cl^-\pi \rightarrow Os(IV)d\pi$
	35 800	800	$Cl^-\pi \rightarrow Os(IV)d\pi$
	38 800	2 100	$Cl^-\pi \rightarrow Os(IV)d\pi$
$[Os(III)Cl_6]^{3-}$	32 800	3 100	$Cl^-\pi \rightarrow Os(III)d\pi$
	35 000	8 600	$Cl^-\pi \rightarrow Os(III)d\pi$
	37 500	8 600	$Cl^-\pi \rightarrow Os(III)d\pi$
$[Os(IV)Cl_5An]^{1-}$	23 300sh	1 300	$Cl^-\pi \rightarrow Os(IV)d\pi$
	25 600sh	5 000	$Cl^-\pi \rightarrow Os(IV)d\pi$
	27 000	9 300	$Cl^-\pi \rightarrow Os(IV)d\pi$
	34 200	2 300	$Cl^-\pi \rightarrow Os(IV)d\pi$
$[Os(III)Cl_5An]^{2-}$	29 000sh	1 000	$Cl^-\pi \rightarrow Os(III)d\pi$
	32 900	5 300	$Cl^-\pi \rightarrow Os(III)d\pi$
	40 000sh	7 300	$Cl^-\pi \rightarrow Os(III)d\pi$
$[Os(IV)Cl_5Pn]^{1-}$	23 000sh	1 000	$Cl^-\pi \rightarrow Os(IV)d\pi$
	27 000	8 000	$Cl^-\pi \rightarrow Os(IV)d\pi$
	34 600	9 200	$Cl^-\pi \rightarrow Os(IV)d\pi$
$[Os(III)Cl_5Pn]^{2-}$	34 000	10 900	$Cl^-\pi \rightarrow Os(III)d\pi$
	40 500sh	11 200	$Cl^-\pi \rightarrow Os(III)d\pi$
$[Os(IV)Cl_5By]^{1-}$	23 100sh	1 200	$Cl^-\pi \rightarrow Os(IV)d\pi$
	25 300sh	3 600	$Cl^-\pi \rightarrow Os(IV)d\pi$
	26 900	8 800	$Cl^-\pi \rightarrow Os(IV)d\pi$
	34 200	2 300	$Cl^-\pi \rightarrow Os(IV)d\pi$
	37 700sh	2 000	$Cl^-\pi \rightarrow Os(IV)d\pi$
$[Os(III)Cl_5By]^{2-}$	32 800	5 900	$Cl^-\pi \rightarrow Os(III)d\pi$
	40 300sh	8 100	$Cl^-\pi \rightarrow Os(III)d\pi$
	40 800	9 000	$Cl^-\pi \rightarrow Os(III)d\pi$
$[Os(IV)Cl_5Py]^{1-}$	23 500	2 400	$Cl^-\pi \rightarrow Os(IV)d\pi$
	26 800	11 800	$Cl^-\pi \rightarrow Os(IV)d\pi$
	30 400	5 100	$Cl^-\pi \rightarrow Os(IV)d\pi$
$[Os(III)Cl_5Py]^{2-}$	24 900	5 200	$Os(III)d\pi \rightarrow Py\ \pi^*$
	26 300	5 000	$Os(III)d\pi \rightarrow Py\ \pi^*$
	29 500	3 700	$Cl^-\pi \rightarrow Os(III)d\pi$
	33 300	8 500	$Cl^-\pi \rightarrow Os(III)d\pi$
$[Os(IV)Cl_5Bn]^{1-}$	22 400sh	1 300	$Cl^-\pi \rightarrow Os(IV)d\pi$
	26 600	9 300	$Cl^-\pi \rightarrow Os(IV)d\pi$

Compound	Peak max (cm-1)	ε (mol^{-1} cm^{-1} dm^3)	Assignment
$[Os(III)Cl_5Bn]^{1-}$ (cont.)	32 400	4 500	$Cl^-\pi \rightarrow Os(IV)d\pi$
$[Os(III)Cl_5Bn]^{2-}$	25 100	4 500	$Os(III) \rightarrow Bn\ \pi^*$
	27 200	4 400	$Os(III) \rightarrow Bn\ \pi^*$
	31 400	6 600	$Cl^-\pi \rightarrow Os(III)d\pi$
$[Os(IV)Cl_5Bc]^{1-}$	15 700	500	$Os(IV) \rightarrow Bc\ \pi^*$
	23 100sh	1 600	$Cl^-\pi \rightarrow Os(IV)d\pi$
	26 700	11 200	$Cl^-\pi \rightarrow Os(IV)d\pi$
	33 400	3 200	$Cl^-\pi \rightarrow Os(IV)d\pi$
$[Os(III)Cl_5Bc]^{2-}$	32 400	7 800	$Cl^-\pi \rightarrow Os(III)d\pi$

Table 3.8 Transition bands, molar extinction coefficients, and assignment for $[OsCl_5L]^{z-}$

3.3.1.2 Crystal Structures $[OsCl_5L]^{2-/1-}$, L = Py, An

The crystal structure determinations of $[OsCl_5L]^{1-}$, L = An, Py, were undertaken to confirm the identity of the product species of the one electron reduction-induced substitution reactions of $[OsCl_6]^{2-}$ with L. The structure of $[OsCl_5py]^{1-}$ is illustrated in **Figure 3.9**. The osmium metal centre is in an octahedral geometry surrounded by five Cl^- ligands and one pyridine ligand bound through the nitrogen atom. Relevant bond lengths and angles are given in **Table 3.9**. The metal-ligand distances are all as expected for chloride and nitrogen ligands bonded to Os(IV).[5,21]

Interestingly, the Os-Cl bond distance where the chloride is *trans* to pyridine is not significantly different from the *cis* Os-Cl(4) bond. In other chloro-pyridine osmate complexes, e.g. *mer*-$[OsCl_3Py_3]$, the Os-Cl bond *trans* to the Os-N is longer than the other Os-Cl bonds.[21] A possible explanation may be that in $[OsCl_5Py]^{1-}$ the metal centre is in the (IV) oxidation state whereas in $[OsCl_3Py_3]$ the osmium is in the (III) oxidation state where the π-acceptor properties of pyridine may become important. The structure helps to rationalise why the disubstituted products *trans* and *cis* $[OsCl_4Py_2]^{1-}$ form in almost equal amounts via reduction-induced substitution of

$[OsCl_5Py]^{1-}$ as there is no obvious long Os-Cl bond in $[OsCl_5Py]^{1-}$. The plane of the pyridine ring bisects the Cl(2)-Os-Cl(5) angle probably due to steric constraints between the hydrogen's on C2 and C6 on the pyridine ring and the chlorides in the *cis* position. A consequence of this geometry will be poor interactions between the π-orbitals on the metal and pyridine ligand, and therefore bonding of this ligand to the metal will be predominantly through σ-donation. In any case, the metal centre is Os(IV) and π-interactions will therefore be less important.

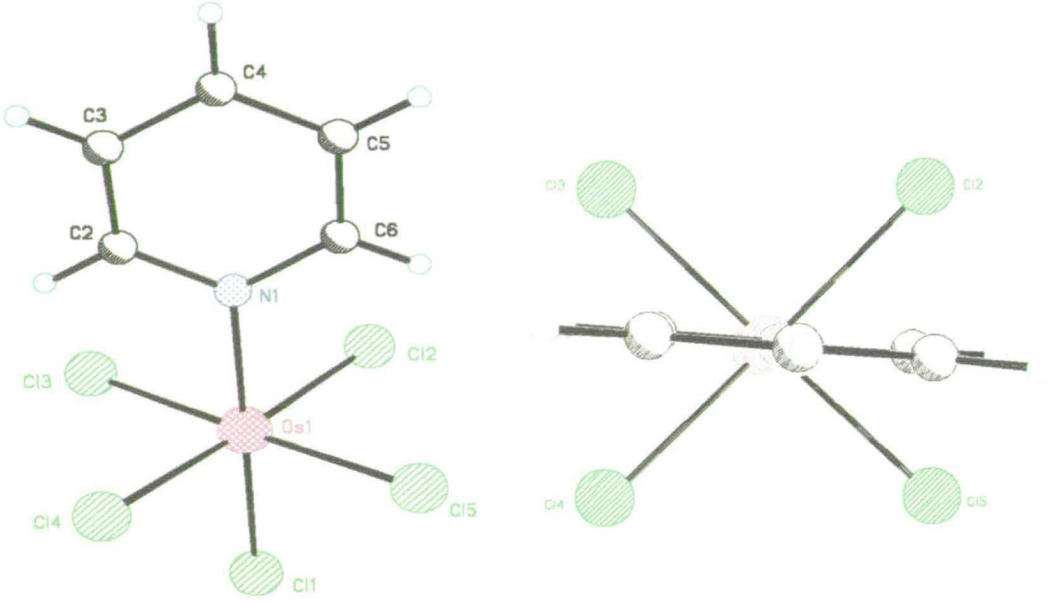

Figure 3.9 Crystal structure of $[OsCl_5Py]^{1-}$

Bond Lengths / Å		Bond Angles / °	
Os(1)-N(1)	2.115(5)	N(1)-Os(1)-Cl(1)	178.30(13)
Os(1)-Cl(1)	2.3204(15)	N(1)-Os(1)-Cl(2)	88.96(13)
Os(1)-Cl(2)	2.3266(18)	N(1)-Os(1)-Cl(4)	88.54(13)
Os(1)-Cl(3)	2.3445(15)	N(1)-Os(1)-Cl(3)	89.71(14)
Os(1)-Cl(4)	2.3175(16)	N(1)-Os(1)-Cl(5)	88.79(14)
Os(1)-Cl(5)	2.3308(16)		

Table 3.9 Selected bond lengths and angles for $[OsCl_5Py]^{1-}$

The crystal structure of $[OsCl_5An]^{1-}$ is shown in **Figure 3.10**. Relevant bond lengths and angles are given in **Table 3.10**. The osmium is octahedral in geometry with five chlorides and an acetonitrile ligand bound to the metal through the nitrogen. All metal-ligand bond lengths are as expected for chloride and nitrogen to Os(IV).[5,21]

The Os-N bond is slightly shorter than for $[OsCl_5Py]^{1-}$ despite pyridine being a stronger base than acetonitrile. In $[OsCl_5An]^{1-}$ the nitrogen donor is sp hybridised whilst in $[OsCl_5Py]^{1-}$ the nitrogen donor atom is sp^2 hybridised which will result in a longer Os-N bond since the greater amount of s character present in a donating atom orbital will shorten the bond.[53] Once more there is no significant difference in the Cl-Os bond length *trans* to the acetonitrile compared with the *cis* bound ligands. Os-N1-C2-C3 is almost linear.

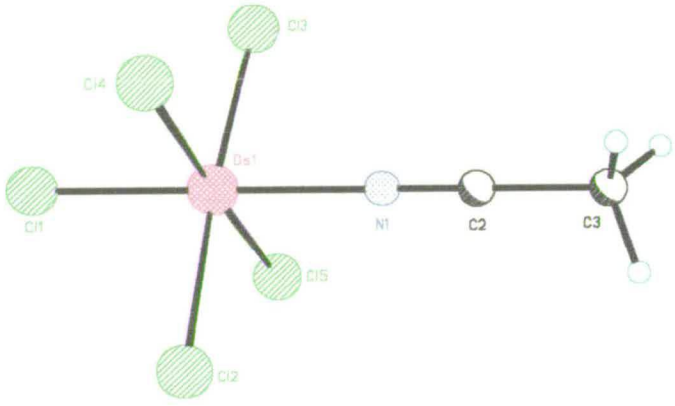

Figure 3.10 Crystal structure of $[OsCl_5An]^{1-}$

Bond Lengths / Å		Bond Angles / °	
Os(1)-N(1)	2.054(6)	N(1)-Os(1)-Cl(1)	178.39(19)
Os(1)-Cl(1)	2.3089(18)	N(1)-Os(1)-Cl(2)	86.62(17)
Os(1)-Cl(2)	2.3450(17)	N(1)-Os(1)-Cl(3)	88.81(17)
Os(1)-Cl(3)	2.3136(18)	N(1)-Os(1)-Cl(4)	87.64(17)
Os(1)-Cl(4)	2.3102(17)	N(1)-Os(1)-Cl(5)	90.19(17)
Os(1)-Cl(5)	2.3388(18)	Os(1)-N(1)-C(2)	175.0(6)
		N(1)-C(2)-C(3)	178.7(9)

Table 3.10 Selected bond lengths and angles for $[OsCl_5An]^{1-}$

3.3.1.3 Rate constants, activation energies and activation parameters for the substitution reaction of $[OsCl_6]^{3-}$ with L

The pseudo first order rate constants, k, for the substitution reactions of electrochemically generated $[OsCl_6]^{3-}$ with L, have been studied using double-step chronoamperometry in 0.1 M $[N^nBu_4]BF_4$/L. The rate constant at 298 K, the activation energy, E_a, and the activation parameters, $\Delta H^{\ddagger}$, $\Delta G^{\ddagger}$, $\Delta S^{\ddagger}$, for the reactions are presented in **Table 3.11**. The rate constants were determined from data over the temperature range 260-310 K. The activation energies, E_a, were calculated from the Arrhenius relationship (**Figure 3.11**) and the activation parameters, $\Delta H^{\ddagger}$, $\Delta G^{\ddagger}$, $\Delta S^{\ddagger}$, from the Eyring relationship without modification for an ionic reaction in electrolyte solution (**Equation 1.10**). The rate constants at 298 K were determined from the linear regression fit from the Arrhenius plots of lnk against 1/T. Errors in k were calculated from the average error for each point determined from the average measured value for each experiment and the statistical errors involved in their calculation. The errors given for E_a and $\Delta H^{\ddagger}$ are the standard deviations from the linear regression fits. Errors given for $\Delta G^{\ddagger}$ and $\Delta S^{\ddagger}$ are calculated from the statistical errors involved in their calculation. Note that trace amounts of water present in the solvent increase the rate dramatically. These results were recorded under a strictly water free environment.

Complex/L	k_{298} / s^{-1}	E_a kJ mol^{-1}	$\Delta H^{\ddagger}$ kJ mol^{-1}	$\Delta G^{\ddagger}_{298K}$ kJ mol^{-1}	$\Delta S^{\ddagger}_{298K}$ J K^{-1} mol^{-1}
$[OsCl_6]^{3-}$/An	1.90 ± 0.20	52.0 ± 2.0	49.7 ± 2.0	71.3 ± 0.3	-72 ± 7
$[OsCl_6]^{3-}$/Pn	1.06 ± 0.22	54.5 ± 2.0	51.1 ± 2.0	72.8 ± 0.3	-73 ± 7
$[OsCl_6]^{3-}$/By	0.51 ± 0.14	55.1 ± 0.7	52.6 ± 0.7	74.6 ± 0.2	-74 ± 6
$[OsCl_6]^{3-}$/Py	4.22 ± 0.27	52.3 ± 2.6	49.9 ± 2.6	69.3 ± 0.3	-65 ± 9
$[OsCl_6]^{3-}$/Bn	0.64 ± 0.12	60.3 ± 0.7	57.9 ± 0.7	74.0 ± 0.2	-54 ± 6
$[OsCl_6]^{3-}$/Bc	0.12 ± 0.01	65.3 ± 2.5	62.6 ± 2.5	77.6 ± 0.3	-50 ± 8

Table 3.11 Rate constants, activation energies, and activation parameters for $[OsCl_6]^{3-} \rightarrow [OsCl_5L]^{2-}$

The rate constants show some dependence on the ligand, L, varying between 0.12 s^{-1} and 4.22 s^{-1} for substitution of a chloride ligand by benzyl cyanide and pyridine respectively. There is a stepwise decrease in the rate constant in the nitrile series, An > Pn > By.

Both the activation energy and intuitively the enthalpy of activation for each ligand are similar in energy, on average 56.6 kJ mol^{-1} and 54.0 kJ mol^{-1} respectively.

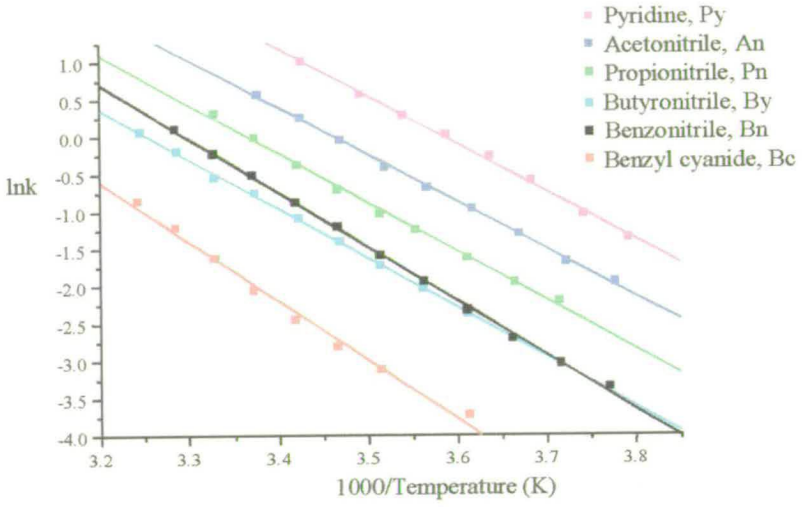

Figure 3.11 Arrhenius plots for the substitution reaction of $[OsCl_6]^{3-}$ with different entering ligands, L

Closer inspection of the activation energy data reveals the possibility of a relationship between the activation energy and the number of carbon atoms in each ligand which may infer that steric bulk of the incoming ligand for the nitriles is important (**Figure 3.12**).

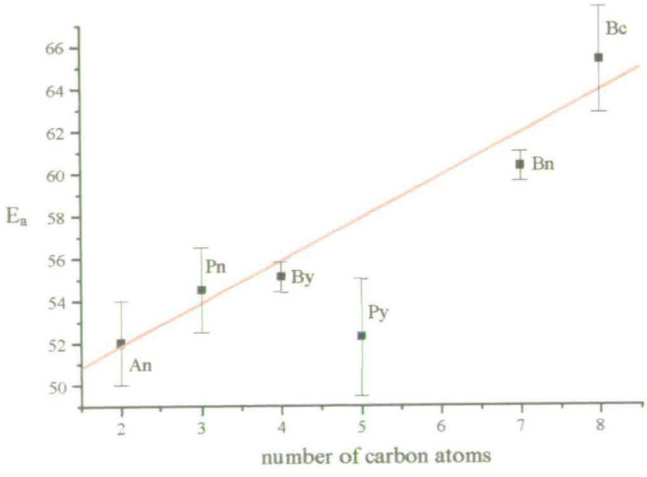

Figure 3.12 Graph of number of carbon atoms against activation energy.

This is consistent with a slight associative character to the activation process and is supported by the entropies of activation: all strongly negative, in the range -52 to -74 J K^{-1} mol^{-1}. This is inconsistent, however, with a process previously found to be first order with respect to the concentration of $[OsCl_6]^{3-}$ and zero order with respect to [L].[27]

When the reaction is carried out in 0.5 M $[N^nBu_4]BF_4$/dichloromethane doped with a ten molar equivalent of butyronitrile the rate constant is slower, however, the activation energy and activation parameters are the same within experimental error (**Table 3.12**). Clearly the rate constant has some dependence on the solvent.

Compound	k_{298} / s^{-1}	E_a kJ mol^{-1}	$\Delta H^{\ddagger}$ kJ mol^{-1}	$\Delta G^{\ddagger}_{298K}$ kJ mol^{-1}	$\Delta S^{\ddagger}_{298K}$ J K^{-1} mol^{-1}
$[OsCl_5By]^{2-}$	0.23 ± 0.11	55.0 ± 0.5	52.5 ± 0.5	76.3 ± 0.2	-80 ± 6

Table 3.12 Rate constant, activation energy and activation parameters for the substitution reaction of $[OsCl_6]^{3-}$ with By in 0.5 M $[N^nBu_4]BF_4$/dichloromethane doped with a ten molar equivalent of butyronitrile

Brown and Taylor measured the rate constant of the reaction of $[OsCl_6]^{3-}$ in $[N^nBu_4]BF_4$/dichloromethane doped with ten molar equivalents of pyridine as a function of the concentration of $[N^nBu_4]Cl$, the sum total of the concentrations of $[N^nBu_4]BF_4$ and $[N^nBu_4]Cl$ being kept constant in each case.[27] Although the final product, established by cyclic voltammetry, was unaffected, the rate was seen to be approximately halved on addition of 250 molar equivalents of $[N^nBu_4]Cl$ (**Figure 3.13**). This is indicative of the rate limiting step being the dissociation of chloride. Intuitively, it would seem likely that the rate should be influenced by the ability of the solvent to solvate Cl^-.

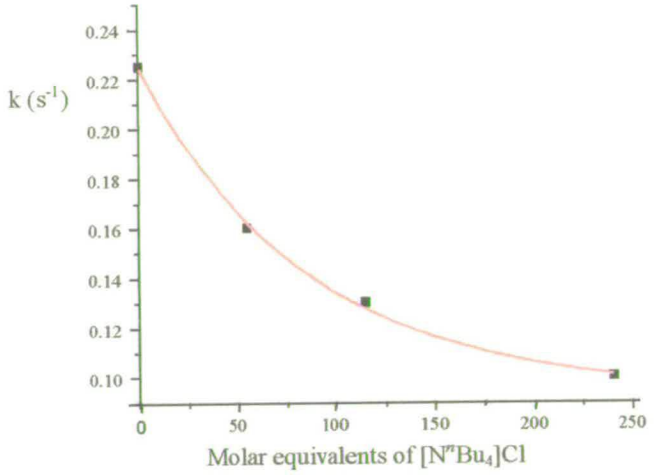

Figure 3.13 Graph of variation of the rate constant for the disappearance of $[OsCl_6]^{3-}$ in 0.5 M $[N^nBu_4]BF_4$/dcm doped with ten molar equivalents of pyridine, as a function of the concentration of $[N^nBu_4]Cl$ at 298 K. ref 27

There is some dependence between the rate constant and the dielectric constants in neat solvents as shown in **Figure 3.14**. A point corresponding to the substitution reaction in butyronitrile-doped dichloromethane as previously described has also been included (DCM).

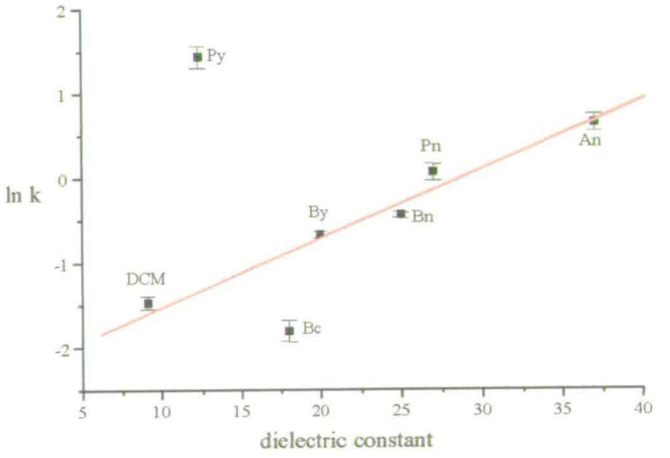

Figure 3.14 Graph of ln k against dielectric constant at 298 K.

It can be seen that there is a reasonable correlation between the natural logarithm of the rate of reaction and the dielectric constant of the bulk medium. This is consistent with a mechanism in which the activated complex is more polar than the reactants.[54] An increase in charge density of the activated complex will usually increase the order of the transition state (electrostriction) and thus can result in a misleadingly negative value for $\Delta S^{\ddagger}$.

3.3.1.4 Reaction Mechanism

On the basis that the rate constant is largely independent of the nature or of the concentration of nucleophile, L, and that the rate is inhibited by chloride ions in solution, the simplest (and most likely) mechanisms are the Dissociative (D) mechanism and the dissociative Interchange mechanism (I_d). For a Dissociative mechanism as shown in **Scheme 3.1**, rate limiting dissociation of Cl^- generates the co-ordinatively unsaturated intermediate, $[OsCl_5]^{2-}$, which is rapidly attacked by the nucleophile, L, to form $[OsCl_5L]^{2-}$.

$$[OsCl_6]^{3-} \underset{k_{-1}}{\overset{k_1}{\rightleftharpoons}} [OsCl_5]^{2-} + Cl^- \xrightarrow[L]{k_2} [OsCl_5L]^{2-}$$

Scheme 3.1

The rate expression associated with this mechanism is derived by treating $[OsCl_5]^{2-}$as a steady-state intermediate (an assumption that no appreciable concentration of $[OsCl_5]^{2-}$ builds up during the reaction which is supported by experimental observation). The resulting rate expression is given in **Equation 3.1**.

$$\frac{-d[OsCl_6]^{3-}}{dt} = \frac{k_1 k_2 [L][OsCl_6]^{3-}}{k_{-1}[Cl^-] + k_2[L]}$$

Equation 3.1

When $k_2[L] >> k_{-1}[Cl^-]$, a condition fulfilled when there is an excess of nucleophile present, Equation 3.1 simplifies to **Equation 3.2**.

$$\frac{-d[OsCl_6]^{3-}}{dt} = k_1[OsCl_6]^{3-}$$

Equation 3.2

This rate expression is largely consistent with the kinetic data since it dictates that the rate of reaction is independent of the concentration of nucleophile providing it is in excess and that k_1 is independent of the nature of nucleophile.

The alternative I_d mechanism is shown in **Scheme 3.2**. A pre-equilibrium is established where there is an outer-sphere association of the nucleophile with the

complex prior to dissociation of the leaving group. Upon dissociation of Cl^-, the nucleophile present in the outer-sphere association is advantageously positioned to bind to the vacant site.

Scheme 3.2

$$[OsCl_6]^{3-} + L \underset{k_{-3}}{\overset{k_3}{\rightleftharpoons}} \{[OsCl_6]^{3-},L\} \xrightarrow{k_4} \{[OsCl_5L]^{2-},Cl^-\} \xrightarrow{fast} [OsCl_5L]^{2-} + Cl^-$$

Assuming that association of L is a rapidly established equilibrium (K_3) and that k_4 represents the rate limiting dissociation of the Os-Cl bond, the I_d mechanism gives the rate law (**Equation 3.3**). Equation 3.3 represents the rate expression for an Eigen-Wilkins mechanism, usually consistent with the Interchange mechanism.[55] If $K_3[L] >> 1$, Equation 3.3 simplifies to **Equation 3.4**, which, is again, largely consistent with the observed kinetics.

$$\frac{-d[OsCl_6]^{3-}}{dt} = \frac{k_4 K_3 [OsCl_6]^{3-}[L]}{1 + K_3[L]}$$

Equation 3.3

$$\frac{-d[OsCl_6]^{3-}}{dt} = k_4[OsCl_6]^{3-}$$

Equation 3.4

For this rate law, it would be expected that k_4 would have some dependence on the nature of the nucleophile because of the presence of the nucleophile within the outer-sphere association during this reaction step: a situation that is experimentally observed. For the assumption, $K_3[L] >> 1$, to hold at low concentrations of L, there must be the unlikely situation of tight binding between the neutral nucleophile, L, and the highly charged $[OsCl_6]^{3-}$. The formation of an outer-sphere association may be queried due to the time the Os(III) species is present in solution as part of the chronoamperometic experiment. In order to have pre-equilibrium, there must be diffusion of L to the newly reduced species. However if pre-equilibrium takes place at diffusion controlled limits then formation of the outer-sphere association is plausible as the rate of diffusion (typically 10^{-5} s^{-1}) is much faster than the time scale of experiment (no less than 0.01 seconds).

A clearer picture of a possible mechanism helps to rationalise the marked effect of trace amounts of water on the reaction rate. Presumably H_2O could initially form an outer-sphere association with the charged metal complex rather than the neutral ligand, L. On reduction of the complex to Os(III), H_2O will be in a preferential position to form $[OsCl_5(H_2O)]^{2-}$. H_2O donates through the oxygen whereas all L are considered nitrogen donors. Os(III) is a relatively soft metal centre to oxygen and will prefer the softer nitrogen donating ligand resulting in the metathesis of $[OsCl_5(H_2O)]^{2-}$ to $[OsCl_5L]^{2-}$. Excess water will also encourage the solvation of free chloride, and thus increase the reaction rate.

An argument of a clear difference between Dissociative and dissociative Interchange may be one of semantics. A feature of five co-ordinate complexes (such as an intermediate in a Dissociative reaction) is that they are often found to have an additional weakly co-ordinated solvent molecule observed by small changes in the uv-vis spectrum in different solvents.[56] An effort to make clear distinctions in the two mechanisms therefore, especially in the case where the solvent is also the entering ligand, may be of limited value.

Strongly negative values of $\Delta S^{\ddagger}$ suggest an associative character in the reaction mechanism. The values of $\Delta S^{\ddagger}$ are open to question however with respect to their notoriously difficult interpretation and without modification of the Eyring relationship for ionic reactions in electrolyte solutions (see chapter 1). Certainly variation within the calculated rate constants and activation as a function of incoming ligand, L, is not significant enough to support an alternative, I_a mechanism and must be ruled out.

3.3.1.5 Simulation

Both Dissociative and dissociative Interchange mechanisms for the substitution of one chloride ligand in $[OsCl_6]^{3-}$ have been simulated using Digisim 2.1. A good fit (**Figure 3.15**) is obtained for the chemical reaction parameters shown in **Table 3.13**.

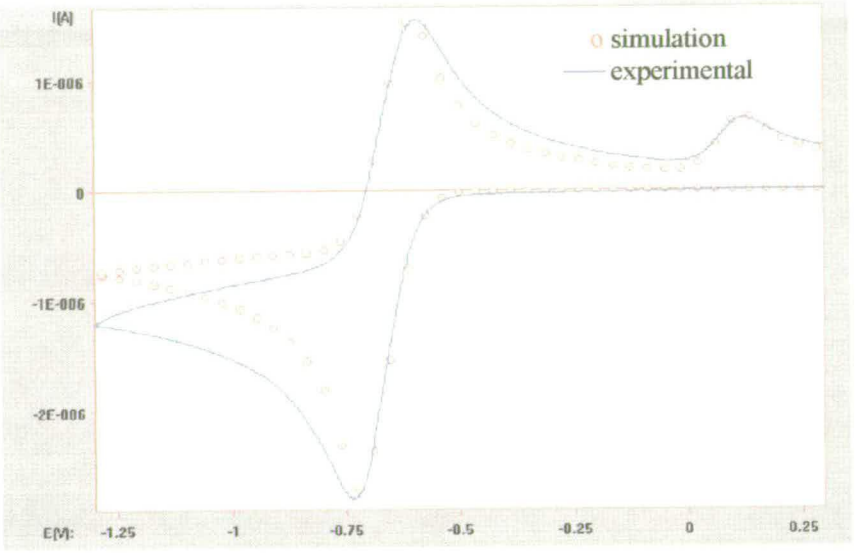

Figure 3.15 Simulated and experimental cyclic voltammograms for a Dissociative mechanism for the reduction-induced substitution reaction of $[OsCl_6]^{2-}$ with butyronitrile at 298 K, 0.4 V s^{-1}

Homogeneous chemical reactions		Chemical reaction parameters		
		K_E	k_f	k_b
Reaction 1	$[OsCl_6]^{3-} \underset{k_b}{\overset{k_f}{\rightleftharpoons}} [OsCl_5]^{2-} + Cl^-$	0.01	0.50	50
Reaction 2	$[OsCl_5]^{2-} + L \underset{k_b}{\overset{k_f}{\rightleftharpoons}} [OsCl_5L]^{2-}$	500	30	0.06

Table 3.13 Chemical reaction parameters for the simulated Dissociative mechanism. Full input data given in Table 3.4

The rate limiting dissociation of chloride (k_f, Reaction 1) matches well with the experimentally measured value of 0.51 s^{-1}. The other rate constants do not seem unreasonable. The back reaction of Cl^- with $[OsCl_5]^{2-}$ (k_b, Reaction 1) is faster than the forward reaction of Cl^- loss from $[OsCl_6]^{3-}$. This is consistent with the fact that

there is no appreciable build up of the five co-ordinate intermediate, $[OsCl_5]^{2-}$, even when $[OsCl_6]^{2-}$ is reduced in bulk at 233 K in 0.5 M $[N^nBu_4]BF_4$/ dichloromethane at 223 K. The rate of association of L to $[OsCl_5]^{2-}$ (k_f, Reaction 2) is significantly faster than for the rate of chloride loss which supports the experimental results that show Cl^- loss to be the rate limiting step. The back reaction of $[OsCl_5L]^{2-}$ to $[OsCl_5]^{2-}$ + L (k_b, Reaction 2) is sufficiently slow so that the overall mono-substitution reaction of $[OsCl_6]^{3-}$ to $[OsCl_5L]^{2-}$ is driven close to completion.

The simulated and experimental cyclic voltammograms do not fit well at potentials below –0.75 V following the electrochemical reduction. This is a common problem in simulating cyclic voltammograms.[57] When electrolytic reactions are induced to occur rapidly, mass transport effects may become important for the successful interpretation of experimental results. There are three significant contributions to mass transport, (i) diffusion, (ii) convection and (iii) migration. An uneven concentration distribution triggers diffusion in order to maximise entropy. Convection occurs from either a natural force (thermal gradients and/or density differences) or an applied external force (gas bubbling or stirring). Hence extra electroactive material is brought to the electrode surface and the currents that flow are larger than those observed when diffusion alone operates. An external electric field results in a drop in electrical potential between the electrode/solution interface and leads to migration mass transport of the redox active species. The movement of ions in solution is therefore induced to or from the electrode. The Digisim software is based on diffusion controlled mass transport.[58] Although the addition of supporting electrolyte, in excess, in the main part negates migration controlled mass transport it may still play some role, especially in highly charged species. Simulated compensation for internal resistance has been used and is effective in fitting the peak to peak separation of the experimental and simulated voltammograms but only has very limited effect on the shape of the wave after the reduction. There are numerical methods in the literature incorporating both diffusion and migration modes of mass transport but these are not explored here.[59] Allowing for both migration and diffusion effects, Bond *et al*, have recently found density–induced convection provides a credible explanation for the major part of the current offset observed when

comparing experimental and theoretical voltammograms.[57] At present, simulations involving diffusion, migration, and convection contributions to the current are not available.

The simulation of the dissociative Interchange mechanism is shown in **Figure 3.16** for the same reaction. The input chemical reaction parameters are in **Table 3.14**.

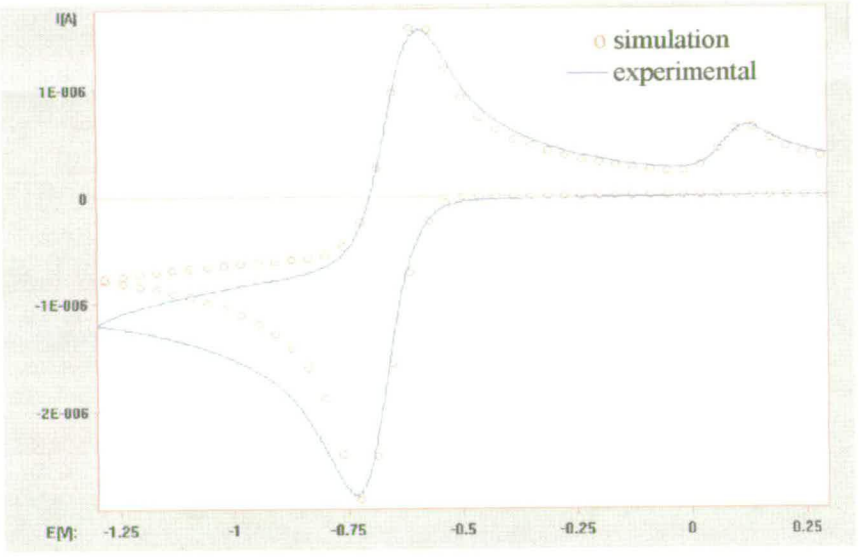

Figure 3.16 Simulated and experimental cyclic voltammograms for a dissociative Interchange mechanism for the reduction-induced substitution reaction of $[OsCl_6]^{2-}$ with butyronitrile at 298 K, 0.4 V s^{-1}

Homogeneous chemical reactions		Chemical reaction parameters		
		K_E	k_f	k_b
Reaction 1	$[OsCl_6]^{3-} + L \underset{k_b}{\overset{k_f}{\rightleftharpoons}} \{[OsCl_6]^{3-},L\}$	20	10000	500
Reaction 2	$\{[OsCl_6]^{3-},L\} \underset{k_b}{\overset{k_f}{\rightleftharpoons}} \{[OsCl_5L]^{2-},Cl^-\}$	50	0.50	0.01
Reaction 3	$\{[OsCl_5L]^{2-},Cl^-\} \underset{k_b}{\overset{k_f}{\rightleftharpoons}} [OsCl_5L]^{2-} + Cl^-$	1000	1000	1

Table 3.14 Chemical reaction parameters for the simulated dissociative Interchange mechanism. Full input data is given in Table 3.4

A slightly better match between experimental and simulated voltammograms is obtained. The set up of an outer sphere association (k_f, Reaction 1) is rapidly achieved well within the time scale of the chronoamperometry experiment. The

equilibrium constant for the formation of the outer-sphere association (K_E, Reaction 1) is high and supports the assumption made in Equation 3.4, that $K_3[L] >> 1$ so that the rate expression can simplify to $-d[OsCl_6]^{3-}/dt = k_4[OsCl_6]^{3-}$ (Equation 3.4). The rate limiting step (k_f, Reaction 2) again compares well with the experimentally measured rate of 0.51 s^{-1}.

3.3.2 $[OsX_5L]^{2-}$, X = Br^-, I^- and L = An, Pn, By, Py, Bn, Bc

The osmium hexabromide and hexaiodide analogues of $[OsCl_6]^{2-}$ were prepared in order to compare their chemistry and further illuminate the redox behaviour and characteristics of the osmium-halogen family of complexes.

3.3.2.1 Osmium hexabromide, $[OsBr_6]^{2-}$

The cyclic voltammogram of $[N^nBu_4]_2[OsBr_6]$ in 0.5 M $[N^nBu_4]BF_4$/dcm at 294 K (**Figure 3.17**) shows a reduction at –0.39 V (ΔE = 140 mV), and an oxidation at +1.38 V (ΔE = 110 mV); both are one electron processes as determined by coulometry and electron transfer rates are diffusion limited, i.e. $i_p \alpha \nu^{1/2}$. The reduction process is not chemically reversible at 0.1 V s^{-1}, 294 K, since $i_p^{red} > i_p^{ox}$. The half-wave potential for $[OsBr_6]^{3-/2-}$ is 0.18 V positive of that of $[OsCl_6]^{3-/2-}$.

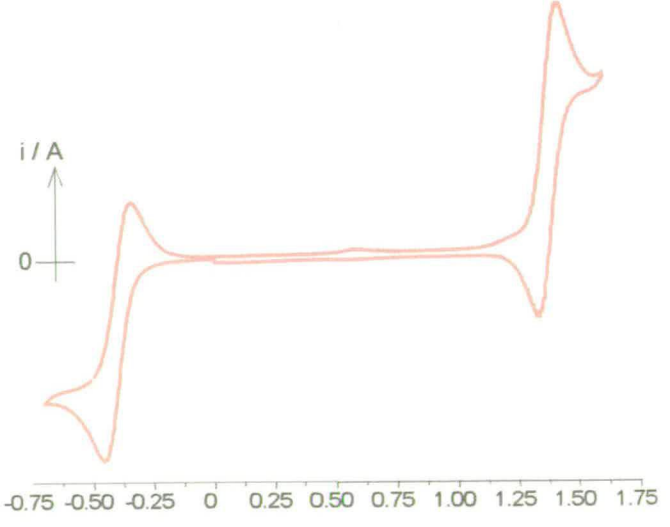

Figure 3.17 CV of $[OsBr_6]^{2-}$ in 0.5 M $[N^nBu_4]BF_4$/dcm at 0.1 V s^{-1}, 294 K

At 223 K, $[OsBr_6]^{2-}$ can be reduced in bulk with chemical reversibility. The uv-vis spectra of the Os(IV) and Os(III) species and the spectroelectrochemical uv-vis spectrum of the III/IV reduction at 223 K are shown in **Figure 3.18**.

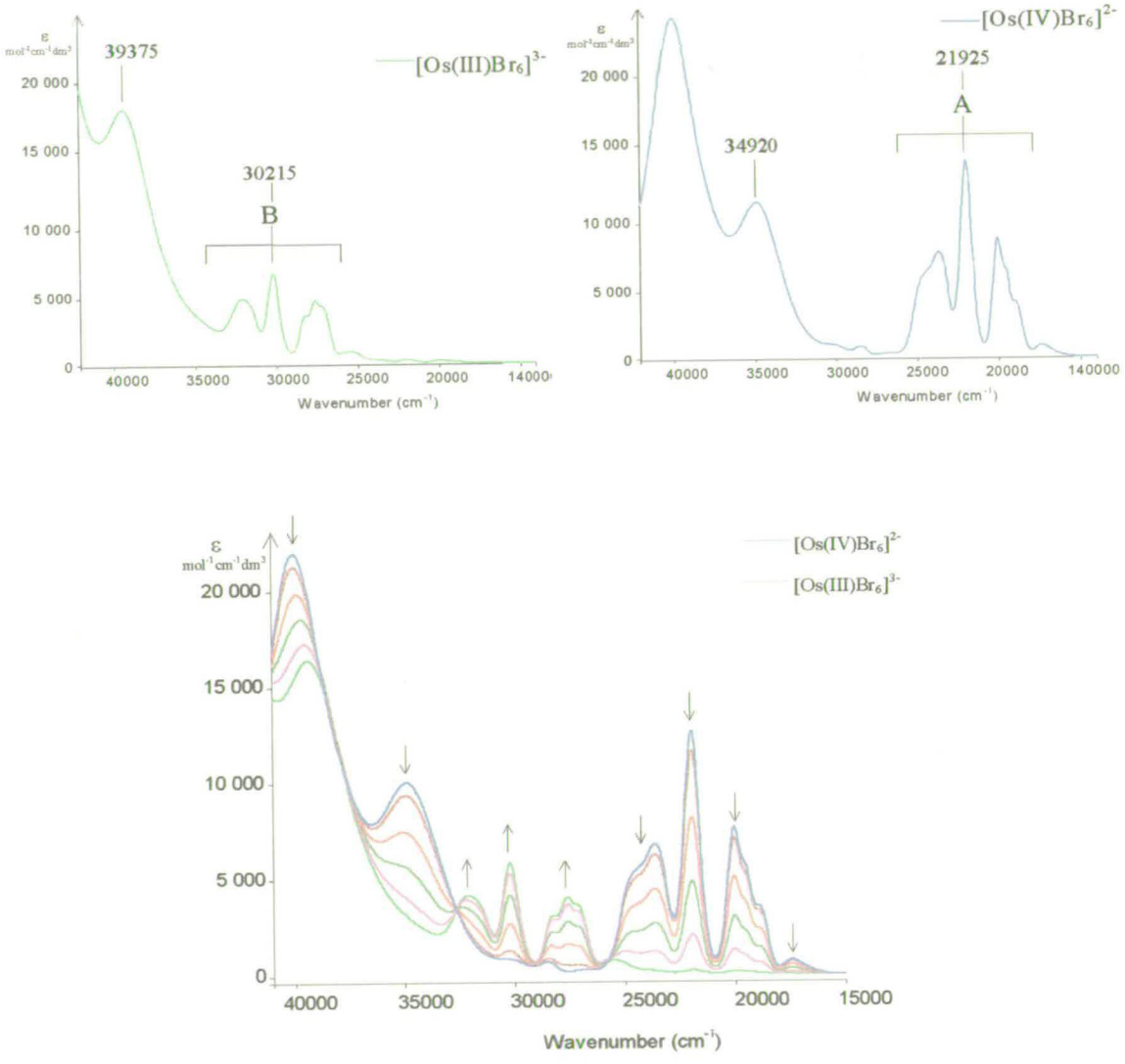

Figure 3.18 Uv-vis spectra of $[OsBr_6]^{3-}$ and $[OsBr_6]^{2-}$ and *in-situ* spectroelectrochemical reduction spectra of $[OsBr_6]^{2-}$ in 0.5 M $[N^nBu_4]BF_4$/dcm at 223 K, electrogeneration potential -0.50 V

The spectrum of the Os(IV) species shows three characteristic bands centred around 21925 cm^{-1} (A). These bands have been assigned as $Br^-\pi \rightarrow Os(IV)d\pi\ t_{2g}$ transitions involving different bromide based orbitals.[6] The bands at 34920 cm^{-1} and 39865 cm^{-1} have been assigned by Jørgensen as $Br^-\pi \rightarrow Os(IV)d\sigma\ e_g$ transitions. This assignment seems unlikely since this would give a value of Δ_0 for $[OsBr_6]^{2-}$ of less than

20000 cm^{-1}, whereas the value of Δ_o of Os(IV)complexes is known to be *ca* 30000 cm^{-1}.[60] They are therefore here assigned as further $Br^-\pi \rightarrow Os(IV)d\pi$. On reduction to Os(III) the spectrum shows the same characteristic bands at higher energy, A → B. The bands move to higher energy as is expected for LMCT transitions as the metal centre is reduced. The spectroelectrochemical spectrum shows clear isosbestic points at 25800 cm^{-1}, 32675 cm^{-1}, and 41250 cm^{-1} indicating a chemically reversible process. Full transition band maxima, molar extinction coefficients, and assignments are given in **Table 3.16**.

Electrogenerated $[OsBr_6]^{3-}$ reacts in the presence of acetonitrile, propionitrile, and butyronitrile giving a new redox couple at approximately +0.1 V and an oxidation at +1.08 V is observed corresponding to the oxidation of free Br^-. Taylor has shown that $[OsBr_6]^{2-}$ undergoes reduction-induced substitution in the presence of pyridine forming $[OsBr_5Py]^{2-}$.[21] For this reason, and by comparison with osmium hexachloride, the new redox couple at +0.1 V is assigned to the mono-substituted product $[OsBr_5L]^{3-/2-}$ couple. The half-wave potentials for the mono-substitution reactions with acetonitrile, propionitrile and butyronitrile are given in **Table 3.15**.

Complex	$E_{1/2}$ (IV/III) / V
$[OsBr_6]^{3-/2-}$	-0.39
$[OsBr_5An]^{2-/1-}$	+0.16
$[OsBr_5Pn]^{2-/1-}$	+0.06
$[OsBr_5By]^{2-/1-}$	+0.02

Table 3.15 Half-wave potentials for $[OsBr_5L]^{z-}$, L = Br^-, An, Pn, By

The potential of the $[OsBr_5L]^{2-/1-}$ redox couple shifts *ca* 0.5 V positive of the $[OsBr_6]^{3-/2-}$ redox couple. The half-wave potentials of the nitriles represent a stepwise destabilisation of the metal based Os(IV/III) couple due to the increasing electron donor properties of the alkyl groups; An > Pn > By. The potential of $[OsBr_5Py]^{2-/1-}$ redox couple is at +0.10 V. No intermediate species in the substitution reaction is observed either by cyclic voltammetry or spectroelectrochemically. The uv-vis spectra of the substituted Os(III) and (IV) species are compared with that of $[OsBr_6]^{3-/2-}$ in **Figure 3.19** and the spectroelectrochemical uv-vis spectra at 223 K are

shown in **Figure 3.20**. Full transition band maxima, molar extinction coefficients, and assignments are given in **Table 3.16**.

As with the osmium chloride series, with ligand substitution, the complex loses symmetry and thus orbital degeneracy of the metal based d-orbitals. The result is broader, less defined bands of similar energy. The bands, on comparison to the spectra of $[OsBr_6]^{3-/2-}$ and $[OsCl_5L]^{2-/1-}$ must correspond to LMCT transitions. On reduction the main transitions $Br^-\pi \rightarrow Os(IV)d\pi$ (A') of $[OsBr_5L]^{1-}$ shift to higher energy by *ca* 5000 cm^{-1} in $[OsBr_5L]^{2-}$ (B') corresponding to the $Br\pi \rightarrow Os(III)d\pi$ electronic transitions. Note that the LMCT transitions in the bromide complexes are all lower in energy than similar transitions in the analogous chloride containing complexes. The lowest energy LMCT transitions of bromide complexes will involve electrons from orbitals where the principal quantum number, n, equals four, rather than three for chloride. The lowering of energy of the observed LMCT transitions is therefore as expected. The spectrum of $[OsBr_5By]^{2-}$ shows an additional absorption at 35390cm^{-1} which is assigned to a MLCT, $Os(III)d\pi \rightarrow By\pi^*$.

The *in-situ* spectroelectrochemistry uv-vis spectra all show clear isosbestic points demonstrating the reversible electrochemical and chemical behaviour of $[OsBr_5L]^{2-/1-}$ at 223 K, on the time scale of the experiment, typically 6 hours.

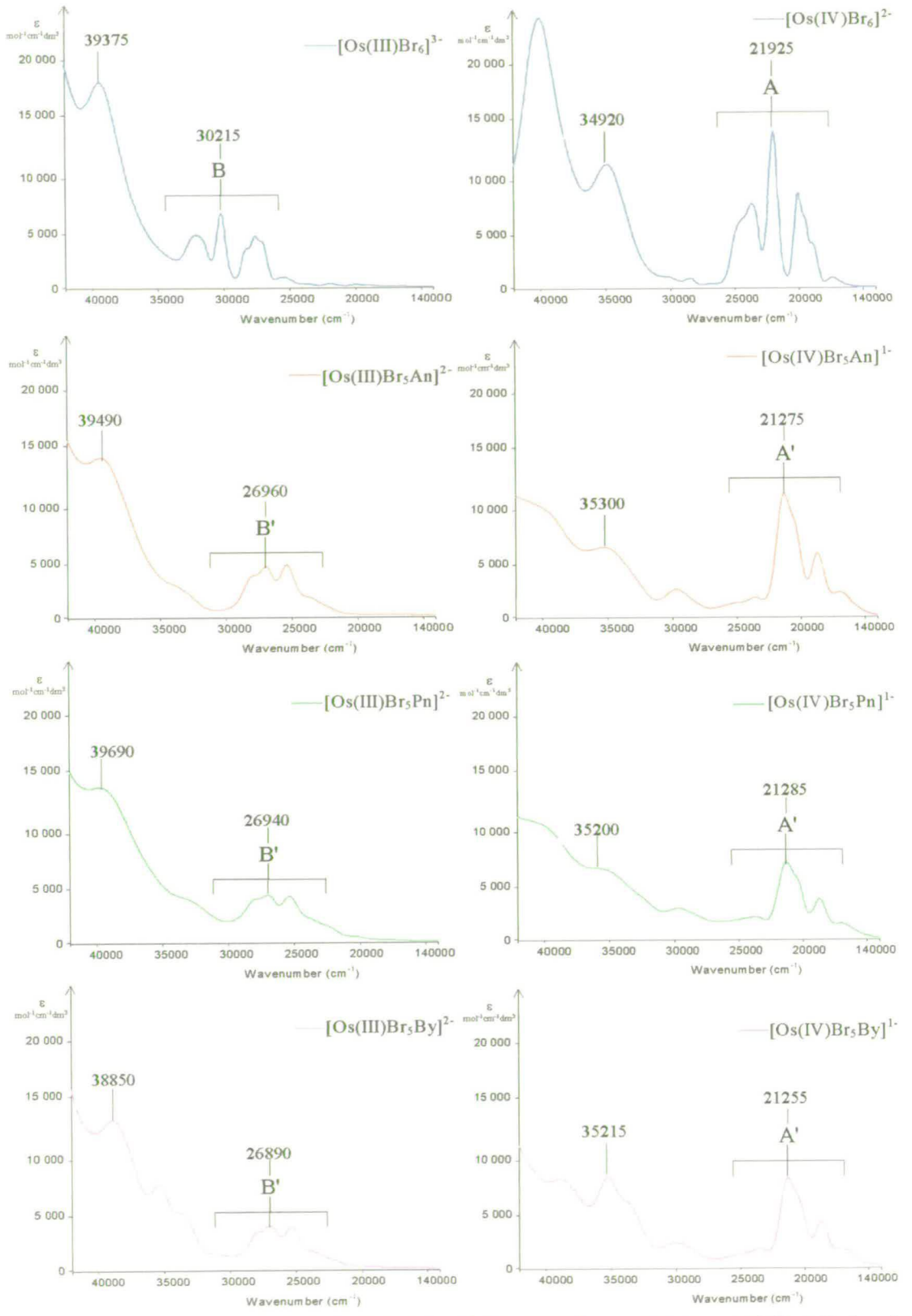

Figure 3.19 Uv-vis spectra of $[OsBr_6]^{z-}$ in 0.5 M $[N^nBu_4]BF_4$/dcm at 223 K, and $[OsBr_5L]^{z-}$, L = An, Pn, By, in 0.1 M $[N^nBu_4]BF_4$/L at 223 K

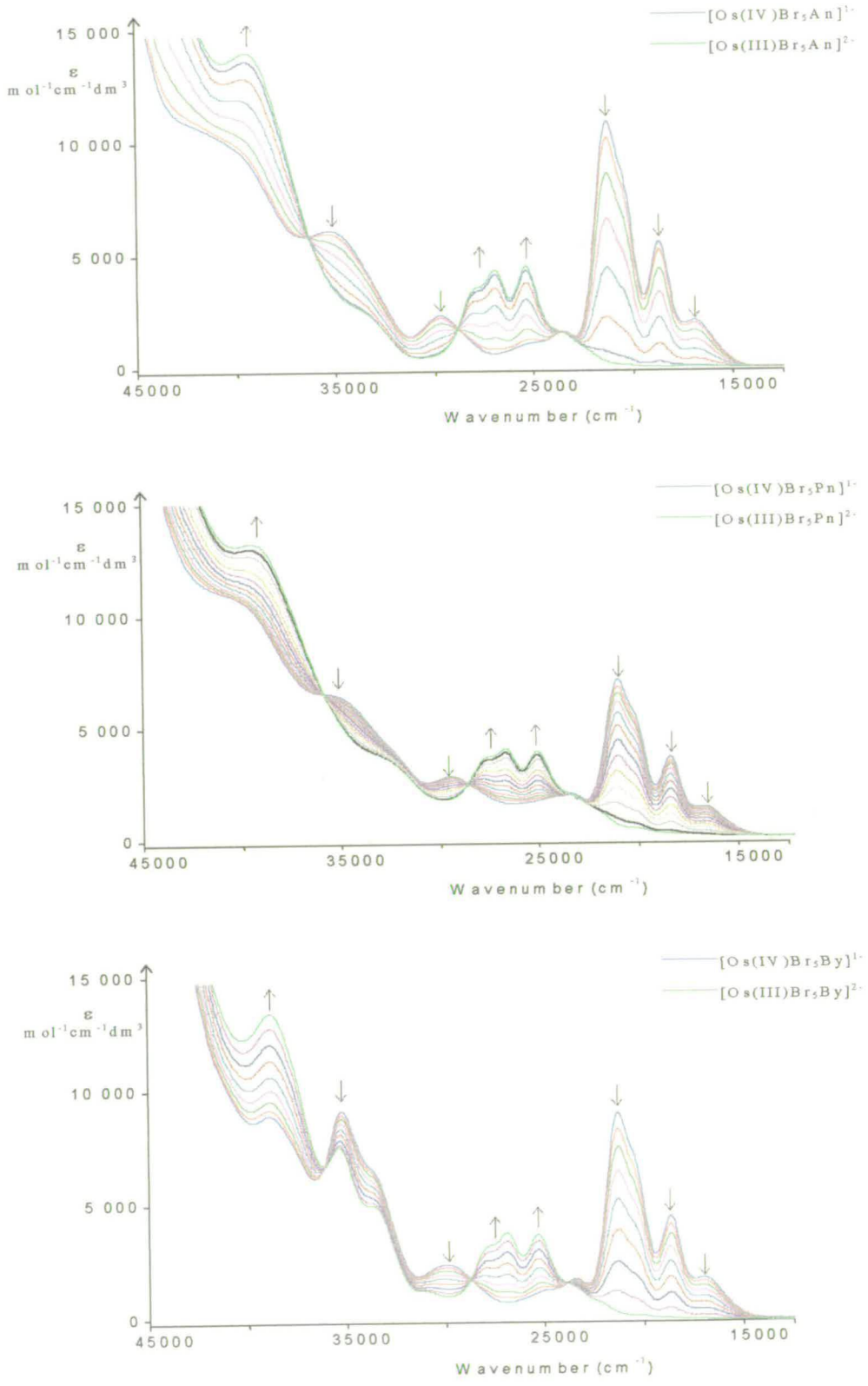

Figure 3.20 *In-situ* uv-vis spectroelectrochemical reduction spectra of $[OsBr_5L]^{z-}$, L = An, Pn, By in 0.1 M $[N^nBu_4]BF_4$/L at 223 K, electrogeneration potential -0.50 V

Complex	Peak max (cm^{-1})	ε ($mol^{-1}\ cm^{-1}\ dm^3$)	Assignment
$[Os(IV)Br_6]^{2-}$	17 235	900	$Br^-\pi \rightarrow Os(IV)d\pi$
	18 800	3 300	$Br^-\pi \rightarrow Os(IV)d\pi$
	19 585sh	6 000	$Br^-\pi \rightarrow Os(IV)d\pi$
	20 080	7 600	$Br^-\pi \rightarrow Os(IV)d\pi$
	21 925	12 400	$Br^-\pi \rightarrow Os(IV)d\pi$
	23 610	7 000	$Br^-\pi \rightarrow Os(IV)d\pi$
	24 790sh	5 300	$Br^-\pi \rightarrow Os(IV)d\pi$
	34 920	10 000	$Br^-\pi \rightarrow Os(IV)d\pi$
	39 865	21 100	$Br^-\pi \rightarrow Os(IV)d\pi$
$[Os(III)Br_6]^{3-}$	25 515	900	$Br^-\pi \rightarrow Os(III)d\pi$
	27 175	4 200	$Br^-\pi \rightarrow Os(III)d\pi$
	27 620	4 800	$Br^-\pi \rightarrow Os(III)d\pi$
	28 245	3 700	$Br^-\pi \rightarrow Os(III)d\pi$
	30 215	6 500	$Br^-\pi \rightarrow Os(III)d\pi$
	32 130	4 400	$Br^-\pi \rightarrow Os(III)d\pi$
	39 375	17 900	$Br^-\pi \rightarrow Os(III)d\pi$
$[Os(IV)Br_5An]^{1-}$	16 950	2 100	$Br^-\pi \rightarrow Os(IV)d\pi$
	18 680	5 700	$Br^-\pi \rightarrow Os(IV)d\pi$
	21 275	11 000	$Br^-\pi \rightarrow Os(IV)d\pi$
	23 540	1 700	$Br^-\pi \rightarrow Os(IV)d\pi$
	29 725	2 400	$Br^-\pi \rightarrow Os(IV)d\pi$
	35 300	6 200	$Br^-\pi \rightarrow Os(IV)d\pi$
	39 865sh	9 800	$Br^-\pi \rightarrow Os(IV)d\pi$
$[Os(III)Br_5An]^{2-}$	25 380	4 600	$Br^-\pi \rightarrow Os(III)d\pi$
	26 960	4 400	$Br^-\pi \rightarrow Os(III)d\pi$
	28 030	3 600	$Br^-\pi \rightarrow Os(III)d\pi$
	39 490	14 100	$Br^-\pi \rightarrow Os(III)d\pi$
$[Os(IV)Br_5Pn]^{1-}$	17 025	1 400	$Br^-\pi \rightarrow Os(IV)d\pi$
	18 675	3 700	$Br^-\pi \rightarrow Os(IV)d\pi$
	20 410sh	5 600	$Br^-\pi \rightarrow Os(IV)d\pi$
	21 285	7 300	$Br^-\pi \rightarrow Os(IV)d\pi$
	23 355	2 000	$Br^-\pi \rightarrow Os(IV)d\pi$
	29 700	2 900	$Br^-\pi \rightarrow Os(IV)d\pi$
	35 200sh	6 500	$Br^-\pi \rightarrow Os(IV)d\pi$
	40 060sh	10 900	$Br^-\pi \rightarrow Os(IV)d\pi$
$[Os(III)Br_5Pn]^{2-}$	25 345	4 000	$Br^-\pi \rightarrow Os(III)d\pi$
	26 940	4 100	$Br^-\pi \rightarrow Os(III)d\pi$
	27 955	3 700	$Br^-\pi \rightarrow Os(III)d\pi$
	32 940	3 700	$Br^-\pi \rightarrow Os(III)d\pi$
	39 690	13 600	$Br^-\pi \rightarrow Os(III)d\pi$
$[Os(IV)Br_5By]^{1-}$	17 000	1 800	$Br^-\pi \rightarrow Os(IV)d\pi$
	18 655	4 500	$Br^-\pi \rightarrow Os(IV)d\pi$

Complex	Peak max (cm^{-1})	ε ($mol^{-1} cm^{-1} dm^3$)	Assignment
$[Os(IV)Br_5By]^{1-}$ (cont.)	20 435sh	6 900	$Br^-\pi \rightarrow Os(IV)d\pi$
	21 255	8 800	$Br^-\pi \rightarrow Os(IV)d\pi$
	23 435	1 800	$Br^-\pi \rightarrow Os(IV)d\pi$
	29 920	2 400	$Br^-\pi \rightarrow Os(IV)d\pi$
	33 460sh	6 200	$Br^-\pi \rightarrow Os(IV)d\pi$
	35 215	9 000	$Br^-\pi \rightarrow Os(IV)d\pi$
	38 885	8 800	$Br^-\pi \rightarrow Os(IV)d\pi$
$[Os(III)Br_5By]^{2-}$	25 320	3 700	$Br^-\pi \rightarrow Os(III)d\pi$
	26 890	3 800	$Br^-\pi \rightarrow Os(III)d\pi$
	27 965	3 100	$Br^-\pi \rightarrow Os(III)d\pi$
	31 005	1 100	$Br^-\pi \rightarrow Os(III)d\pi$
	33 620sh	4 900	$Br^-\pi \rightarrow Os(III)d\pi$
	35 390	7 400	$Os(III)d\pi \rightarrow Br^-\pi^*$
	38 850	13 100	$Br^-\pi \rightarrow Os(III)d\pi$

Table 3.16 Transition bands, molar extinction coefficients, and assignment for $[OsBr_5L]^{2-}$

3.3.2.2 Rate constants, activation energies, and activation parameters for the substitution reactions of $[OsBr_6]^{3-}$

The pseudo first order rate constants, k, for the substitution reactions of electrochemically generated $[OsBr_6]^{3-}$ with L, have been studied using double-step chronoamperometry in 0.1 M $[N^nBu_4]BF_4$/L. The rate constants were determined from data over the range 245-315 K. The rate constant at 298 K, the activation energy, E_a, and the activation parameters, $\Delta H^{\ddagger}$, $\Delta G^{\ddagger}_{298K}$, $\Delta S^{\ddagger}_{298K}$, for the reactions are presented in **Table 3.17**. The activation energies, E_a, were calculated from the Arrhenius relationship (**Figure 3.21**) and the activation parameters, $\Delta H^{\ddagger}$, $\Delta G^{\ddagger}$, $\Delta S^{\ddagger}$, from the Eyring relationship without modification (Equation 1.10). The rate constants at 298 K were determined from the linear regression fit from the Arrhenius plots of lnk against 1/T. Errors in k were calculated from the average error for each point determined from the average measured value for each experiment and the statistical errors involved in their calculation. The errors given for E_a and $\Delta H^{\ddagger}$ are the standard deviations from the linear regression fits. Errors given for $\Delta G^{\ddagger}$ and $\Delta S^{\ddagger}$ are

calculated from the statistical errors involved in their calculation. As for $[OsCl_6]^{2-}$ trace amounts of water critically effects the results. These results were recorded under a strictly water-free environment.

Complex/L	k_{298} / s^{-1}	E_a kJ mol^{-1}	$\Delta H^{\ddagger}$ kJ mol^{-1}	$\Delta G^{\ddagger}_{298K}$ kJ mol^{-1}	$\Delta S^{\ddagger}_{298K}$ J K^{-1} mol^{-1}
$[OsBr_6]^{3-}$/An	54.6 ± 3.7	63.6 ± 3.0	61.1 ± 2.9	63.0 ± 0.2	-6.4 ± 10
$[OsBr_6]^{3-}$/Pn	39.0 ± 2.0	63.7 ± 1.7	61.3 ± 1.7	63.8 ± 0.2	-8.4 ± 6
$[OsBr_6]^{3-}$/By	22.1 ± 0.9	65.1 ± 1.0	62.8 ± 1.0	65.2 ± 0.1	-8.2 ± 4

Table 3.17 Rate constants, activation energies, and activation parameters for $[OsBr_6]^{3-} \rightarrow [OsBr_5L]^{2-}$

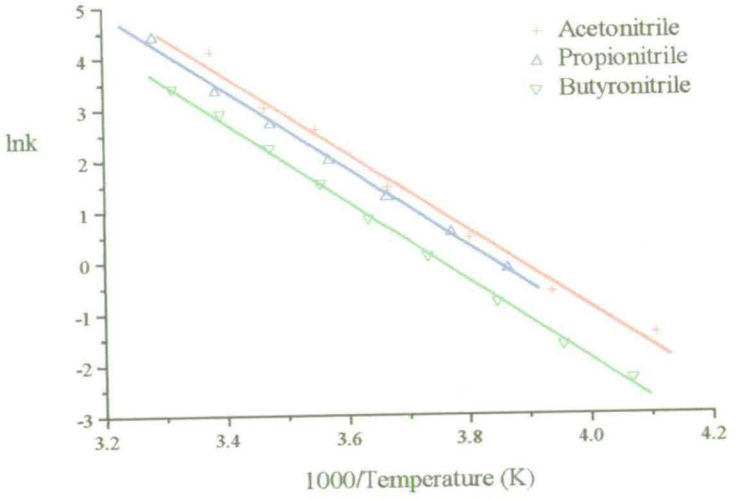

Figure 3.21 Arrhenius plot for the substitution reaction of $[OsBr_6]^{3-}$ with An, Pn, By

The rate constants at 298 K are approximately 35 times faster than the chloride analogues and follow the same stepwise decrease, An > Pn > By. The activation energies are the same within experimental error, on average 64.1 kJ mol^{-1}. It is perhaps of note that the activation energies again follow the pattern of the number of carbon atoms, By > Pn > An. Activation energies and $\Delta H^{\ddagger}$ energies are approximately 10% larger than for chloride, $\Delta G^{\ddagger}$ energies are smaller, and therefore $\Delta S^{\ddagger}$ energies are much less negative.

3.3.2.3 Osmium Hexaiodide, $[OsI_6]^{2-}$

The cyclic voltammogram of $[OsI_6]^{2-}$ in 0.5 M $[N^nBu_4]BF_4$/dcm at 294 K is shown in **Figure 3.22**. The reduction is electrochemically reversible and clearly chemically irreversible at 294 K, 0.1 V s^{-1}. The oxidations are more complex.

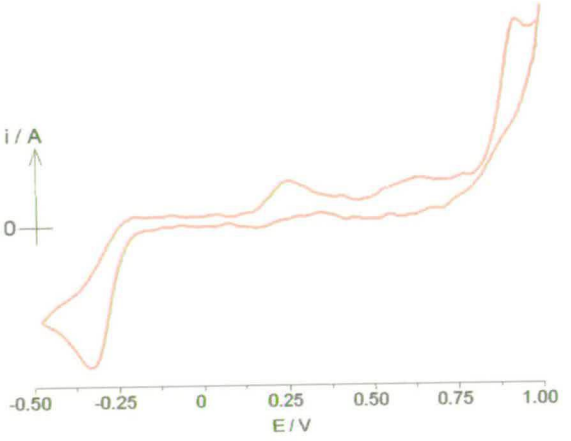

Figure 3.22 CV of $[OsI_6]^{2-}$ in 0.5 M $[N^nBu_4]BF_4$/dcm at 0.1 V s^{-1}, 294 K

The oxidation at +0.25 V was found to be a daughter product of the reduction but remains unidentified. Over time it was found to increase without prior reduction illustrating less stable behaviour of $[OsI_6]^{2-}$ than the chloride or bromide Os(IV) complexes. On cooling to 223 K the reduction process at –0.31 V shows a greater chemically reversibility (**Figure 3.23**). The oxidations retain their complexity.

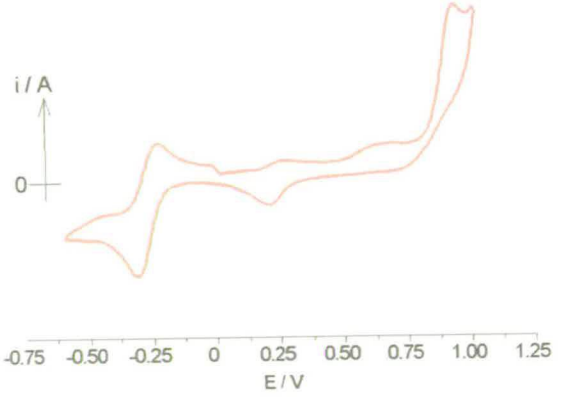

Figure 3.23 CV of $[OsI_6]^{2-}$ in 0.5 M $[N^nBu_4]BF_4$/dcm at 0.1 V s^{-1}, 223 K

The reduction was examined spectroelectrochemically at 203 K in 0.5 M $[N^nBu_4]BF_4$/dcm (**Figure 3.24**).

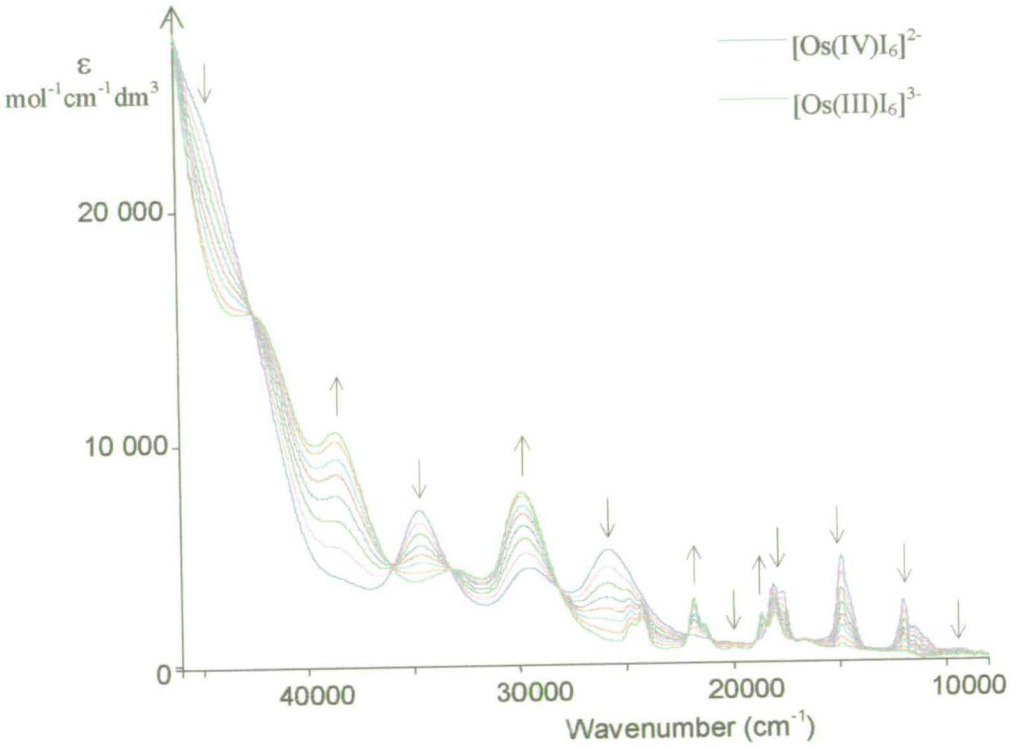

Figure 3.24 *In-situ* uv-vis spectroelectrochemical reduction spectrum of $[OsI_6]^{2-}$ in 0.5 M $[N^nBu_4]BF_4$/dcm at 203 K, electrogeneration potential -0.40 V

The original spectra of $[OsI_6]^{2-}$ was regenerated on oxidation and displays clear isosbestic points at 18475, 19050, 20950, 22200, 28200, 33300, 36025, 42450, and 46025 cm^{-1} indicating a chemically reversible process. The spectra show many transitions, which are more clearly observed in **Figure 3.25**.

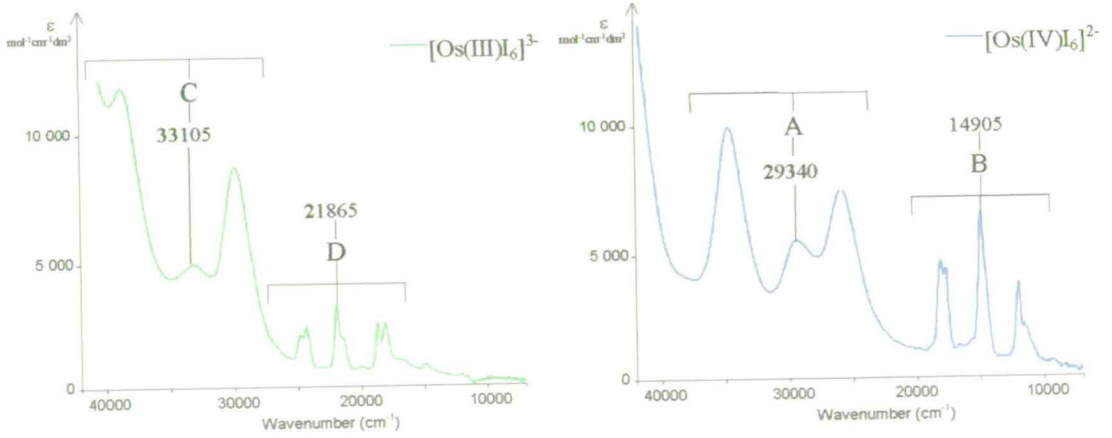

Figure 3.25 Uv-vis spectra of $[OsI_6]^{3-/2-}$ in 0.5 M $[N^nBu_4]BF_4$/dcm at 203 K

The two sets of absorption bands A and B of $[OsI_6]^{2-}$ have been assigned by Jørgensen as $I^-\pi \rightarrow Os(IV)d\pi(e_g)$ and $I^-\pi \rightarrow Os(IV)d\pi(t_{2g})$ respectively.[6] As for $[OsBr_6]^{2-}$ the former assignment seems unlikely. Band set A is assigned here as further $I^-\pi \rightarrow Os(IV)d\pi(t_{2g})$ transitions. On reduction the bands move to higher energy, C and D. These changes are similar to those observed for $[OsCl_6]^{2-}$ and $[OsBr_6]^{2-}$ and on this basis the reduction is attributed to a one electron metal based process. Hence the transitions of the reduced species are assigned as $I^-\pi \rightarrow Os(III)d\pi(t_{2g})$.

Observing the cyclic voltammogram of $[OsI_6]^{2-}$ in the presence of acetonitrile, propionitrile, and butyronitrile at room temperature the Os IV/III redox couple at –0.31 V was seen to diminish over time and a new redox couple grow in at *ca.* +0.15 V (**Figure 3.26**). Below 223 K $[OsI_6]^{2-}$ demonstrated more stable behaviour. Nevertheless $[OsI_6]^{2-}$ clearly shows a greater reactivity than $[OsCl_6]^{2-}$ or $[OsBr_6]^{2-}$.

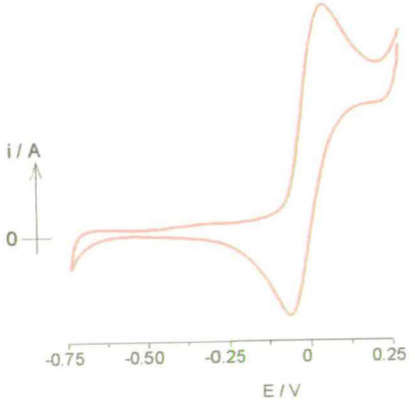

Figure 3.26 CV of $[OsI_6]^{2-}$ after three hours in 0.1 M $[N^nBu_4]BF_4$/acetonitrile at 0.1 V s^{-1}, 295 K

On reduction to Os(III) at 223 K a similar reaction took place; the new redox couple at *ca* +0.15 V replaced the $[OsI_6]^{3-/2-}$ couple, growing in at the same potential as the new product species from the reaction of Os(IV) in acetonitrile at 295 K. Taylor has shown that reduction-induced substitution of $[OsI_6]^{2-}$ to $[OsI_6]^{3-}$ in the presence of pyridine leads to substitution of one I^- for a Py, $E_{1/2}$ = +0.04 V.[21] Thus, and on comparison to osmium hexachloride and hexabromide, the new redox couple is attributed to mono-substituted $[OsI_5L]^{3-/2-}$, where L = An, Pn, By. The half-wave

potentials are shown in **Table 3.18**. The half-wave potentials show the same stepwise destabilisation as seen previously for $[OsCl_5L]^{2-/1-}$ and $[OsBr_5L]^{2-/1-}$. The electronic character of $[OsX_5L]^{2-/1-}$ becomes increasingly similar in the order $X = I^- > Br^- > Cl^-$. Thus the difference in redox potential between $[OsX_5L]^{2-/1-}$ is 180 mV where $X = Cl^-$, L = An and By but only 20 mV where $X = I^-$, L = An and By. This can be explained by the increasing π-donor strength of $I^- > Br^- > Cl^-$ swamping the σ-donor properties of L (An < Pn < By).

Complex	$E_{1/2}$ (IV/III)/V
$[OsI_6]^{3-/2-}$	-0.31
$[OsI_5An]^{2-/1-}$	+0.18
$[OsI_5Pn]^{2-/1-}$	+0.17
$[OsI_5By]^{2-/1-}$	+0.16

Table 3.18 Half-wave potentials for $[OsI_5L]^{2-}$, $L = I^-$, An, Pn, By

The uv-vis spectra of $[OsI_5L]^{2-/1-}$ complexes are compared to that of $[OsI_6]^{3-/2-}$ in **Figure 3.27** and the *in-situ* uv-vis spectroelectrochemical reduction of $[OsI_5L]^{1-} \rightarrow [OsI_5L]^{2-}$ at 203 K is shown in **Figure 3.28**. Full transition band maxima, molar extinction coefficients, and electronic assignments are given in **Table 3.19**.

The uv-vis spectra compare favourably with those of osmium hexachloride and osmium hexabromide ions. On substitution of an iodide the bands become broader and less defined but of similar energy. The two sets of bands are still distinguishable, A' and B', for $[OsCl_5L]^{2-}$ and C' and D', for $[OsI_5L]^{3-}$. It is noteworthy that the spectrum $[OsX_5L]^{3-/2-}$ are increasingly similar when $X = I^- > Br^- > Cl^-$. The spectra of $[OsI_5L]^{2-}$ in particular show little difference in the energy of individual transitions or in their molar extinction coefficients. On reduction the spectra become more clearly individual in character. The increasing similarities are again explained by the increasing π-donor strength of $I^- > Br^- > Cl^-$ swamping the σ-donor properties of L. The *in-situ* uv-vis spectroelectrochemical reductions $[OsI_5L]^{2-} \rightarrow [OsI_5L]^{3-}$ spectra all show neat isosbestic points demonstrating the reversible electrochemical and chemical behaviour at 203 K on the time scale of the experiment.

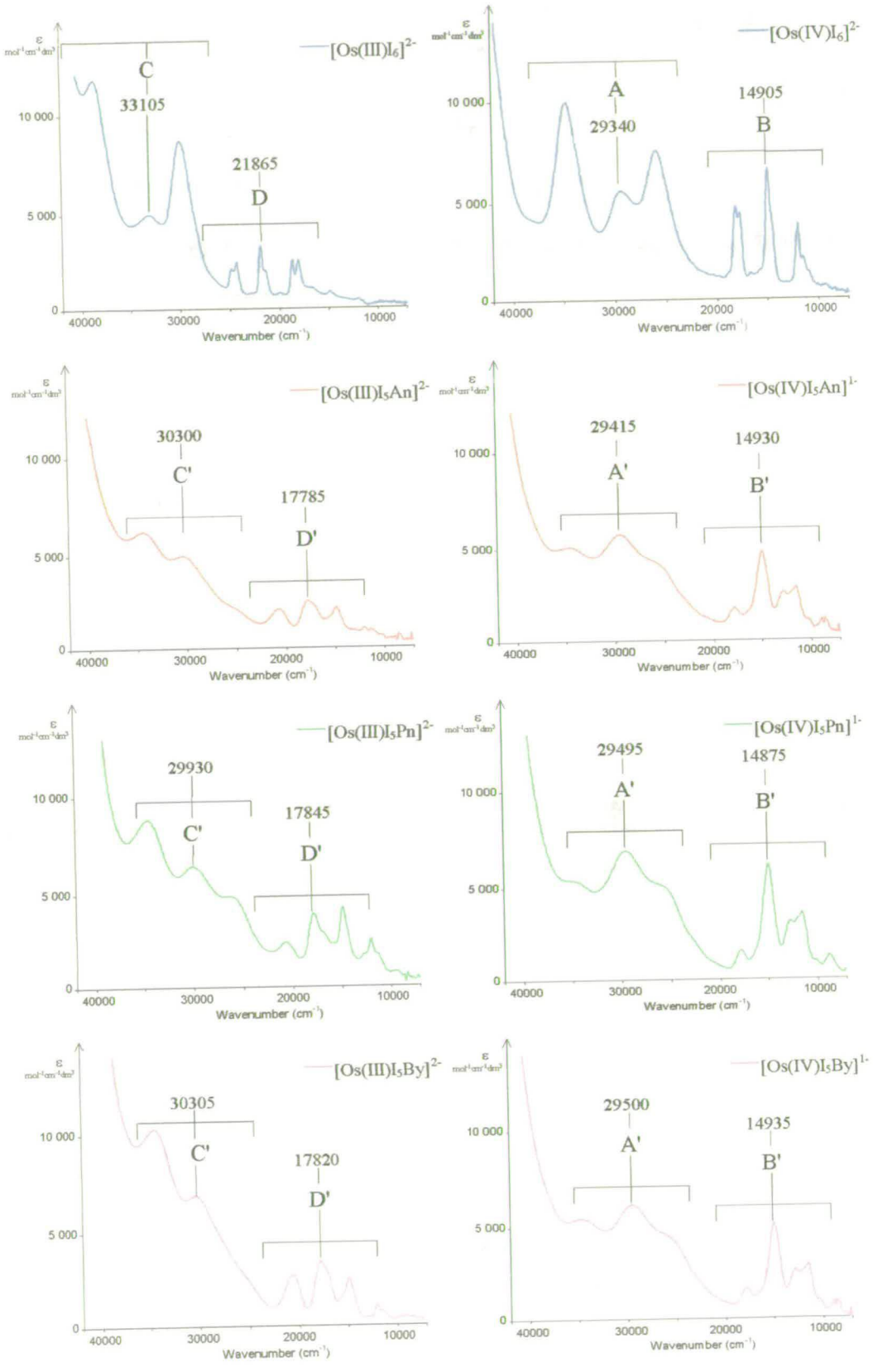

Figure 3.27 Uv-vis spectra of $[OsI_6]^{z-}$ in 0.5 M $[N^nBu_4]BF_4$/dcm at 203 K, and $[OsI_5L]^{z-}$, L = An, Pn, By, in 0.1 M $[N^nBu_4]BF_4$/L at 223 K

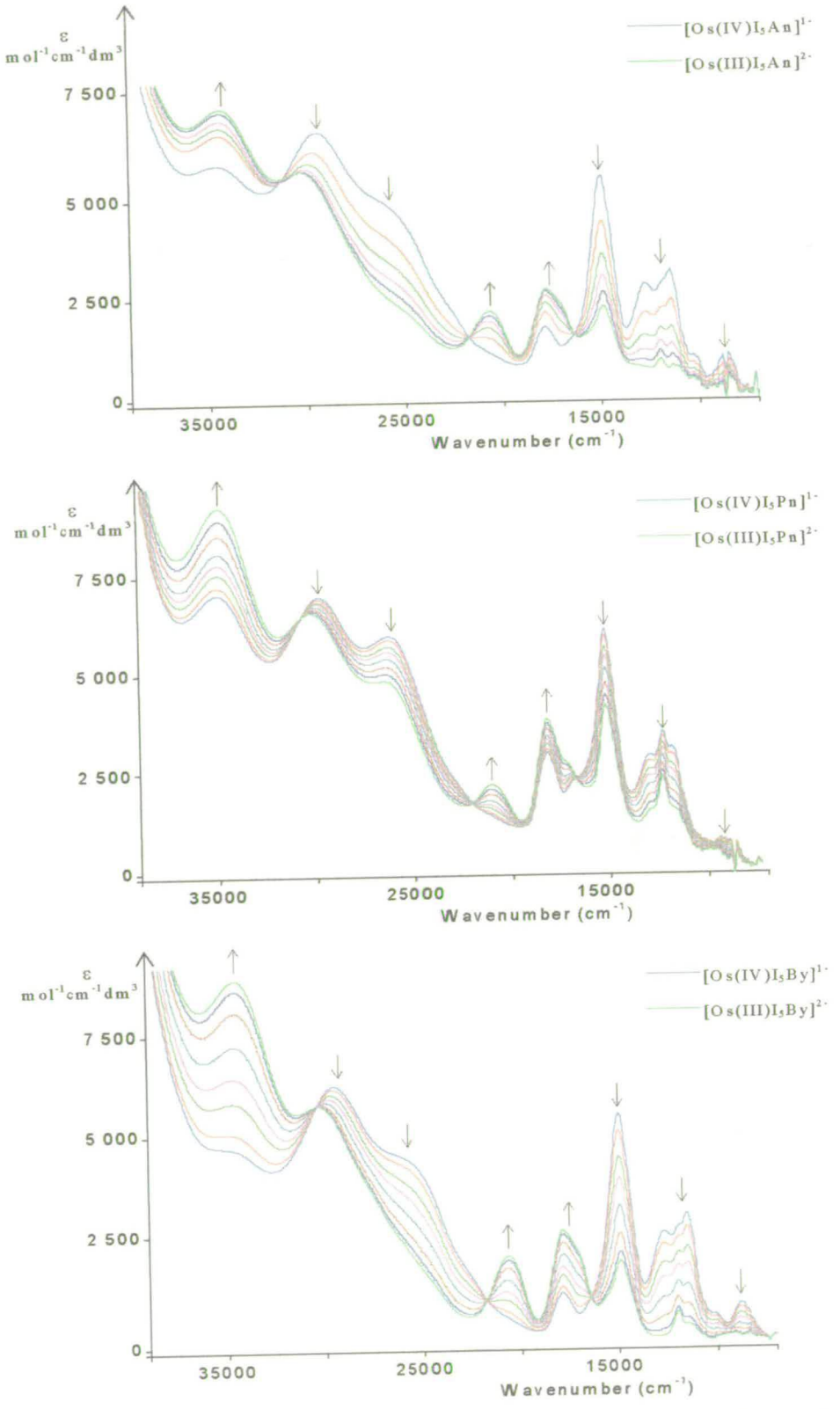

Figure 3.28 *In-situ* uv-vis spectroelectrochemical reduction spectra of $[OsI_5L]^{z-}$, L = An, Pn, By, in 0.1 M $[N^nBu_4]BF_4$/L at 223 K, electrogeneration potential -0.20 V

Complex	Peak max (cm^{-1})	ε (mol^{-1} cm^{-1} dm^3)	Assignment
$[Os(IV)I_6]^{2-}$	11 500	2 300	$I^-\pi \rightarrow Os(IV)d\pi$
	11 985	3 900	$I^-\pi \rightarrow Os(IV)d\pi$
	14 905	6 200	$I^-\pi \rightarrow Os(IV)d\pi$
	17 710	4 100	$I^-\pi \rightarrow Os(IV)d\pi$
	18 120	4 400	$I^-\pi \rightarrow Os(IV)d\pi$
	25 890	7 400	$I^-\pi \rightarrow Os(IV)d\pi$
	29 340	5 500	$I^-\pi \rightarrow Os(IV)d\pi$
	34 610	10 100	$I^-\pi \rightarrow Os(IV)d\pi$
	44 800sh	27 000	$I^-\pi \rightarrow Os(IV)d\pi$
$[Os(III)I_6]^{3-}$	18 080	2 000	$I^-\pi \rightarrow Os(III)d\pi$
	18 670	2 000	$I^-\pi \rightarrow Os(III)d\pi$
	21 420sh	1 500	$I^-\pi \rightarrow Os(III)d\pi$
	21 865sh	2 700	$I^-\pi \rightarrow Os(III)d\pi$
	24 280	1 800	$I^-\pi \rightarrow Os(III)d\pi$
	24 795	1 500	$I^-\pi \rightarrow Os(III)d\pi$
	29 845	8 200	$I^-\pi \rightarrow Os(III)d\pi$
	33 105	4 900	$I^-\pi \rightarrow Os(III)d\pi$
	38 635	11 200	$I^-\pi \rightarrow Os(III)d\pi$
	42 650	17 100	$I^-\pi \rightarrow Os(III)d\pi$
$[Os(IV)I_5An]^{1-}$	8 880	700	$I^-\pi \rightarrow Os(IV)d\pi$
	10 360	900	$I^-\pi \rightarrow Os(IV)d\pi$
	11 470	2 500	$I^-\pi \rightarrow Os(IV)d\pi$
	12 765	2 300	$I^-\pi \rightarrow Os(IV)d\pi$
	14 930	4 600	$I^-\pi \rightarrow Os(IV)d\pi$
	17 840	2 200	$I^-\pi \rightarrow Os(IV)d\pi$
	25 625sh	3 900	$I^-\pi \rightarrow Os(IV)d\pi$
	29 415	5 600	$I^-\pi \rightarrow Os(IV)d\pi$
	34 595	5 000	$I^-\pi \rightarrow Os(IV)d\pi$
$[Os(III)I_5An]^{2-}$	12 020	600	$I^-\pi \rightarrow Os(III)d\pi$
	14 885	1 800	$I^-\pi \rightarrow Os(III)d\pi$
	17 120	1 900	$I^-\pi \rightarrow Os(III)d\pi$
	17 785	2 200	$I^-\pi \rightarrow Os(III)d\pi$
	20 695	1 700	$I^-\pi \rightarrow Os(III)d\pi$
	30 300	4 800	$I^-\pi \rightarrow Os(III)d\pi$
	34 355	6 100	$I^-\pi \rightarrow Os(III)d\pi$
$[Os(IV)I_5Pn]^{1-}$	9 140	1 000	$I^-\pi \rightarrow Os(IV)d\pi$
	11 570	3 100	$I^-\pi \rightarrow Os(IV)d\pi$
	12 005	3 500	$I^-\pi \rightarrow Os(IV)d\pi$
	12 665	2 900	$I^-\pi \rightarrow Os(IV)d\pi$
	14 875	6 000	$I^-\pi \rightarrow Os(IV)d\pi$
	16 515sh	2 200	$I^-\pi \rightarrow Os(IV)d\pi$
	17 860	3 000	$I^-\pi \rightarrow Os(IV)d\pi$
	25 965	5 900	$I^-\pi \rightarrow Os(IV)d\pi$
	29 495	6 800	$I^-\pi \rightarrow Os(IV)d\pi$

Complex	Peak max (cm^{-1})	ε ($mol^{-1} cm^{-1} dm^3$)	Assignment
$[Os(IV)I_5Pn]^{1-}$ (cont.)	34 690	5 300	$I^-\pi \rightarrow Os(IV)d\pi$
$[Os(III)I_5Pn]^{2-}$	9 365	700	$I^-\pi \rightarrow Os(III)d\pi$
	11 465sh	1 600	$I^-\pi \rightarrow Os(III)d\pi$
	12 020	2 400	$I^-\pi \rightarrow Os(III)d\pi$
	12 740sh	1 500	$I^-\pi \rightarrow Os(III)d\pi$
	14 855	4 300	$I^-\pi \rightarrow Os(III)d\pi$
	16 815sh	2 700	$I^-\pi \rightarrow Os(III)d\pi$
	17 845	3 800	$I^-\pi \rightarrow Os(III)d\pi$
	20 700	2 200	$I^-\pi \rightarrow Os(III)d\pi$
	26 285	4 800	$I^-\pi \rightarrow Os(III)d\pi$
	29 930	6 500	$I^-\pi \rightarrow Os(III)d\pi$
	34 505	10 100	$I^-\pi \rightarrow Os(III)d\pi$
$[Os(IV)I_5By]^{1-}$	8 875	900	$I^-\pi \rightarrow Os(IV)d\pi$
	11 510	2 800	$I^-\pi \rightarrow Os(IV)d\pi$
	12 000sh	2 500	$I^-\pi \rightarrow Os(IV)d\pi$
	12 705	2 400	$I^-\pi \rightarrow Os(IV)d\pi$
	14 935	5 000	$I^-\pi \rightarrow Os(IV)d\pi$
	17 865	1 100	$I^-\pi \rightarrow Os(IV)d\pi$
	25 680sh	4 500	$I^-\pi \rightarrow Os(IV)d\pi$
	29 500	5 700	$I^-\pi \rightarrow Os(IV)d\pi$
	34 810	5 300	$I^-\pi \rightarrow Os(IV)d\pi$
$[Os(III)I_5By]^{2-}$	12 030	700	$I^-\pi \rightarrow Os(III)d\pi$
	14 900	1 800	$I^-\pi \rightarrow Os(III)d\pi$
	17 090sh	700	$I^-\pi \rightarrow Os(III)d\pi$
	17 820	2 500	$I^-\pi \rightarrow Os(III)d\pi$
	20 625	1 900	$I^-\pi \rightarrow Os(III)d\pi$
	30 305	6 200	$I^-\pi \rightarrow Os(III)d\pi$
	34 480	10 000	$I^-\pi \rightarrow Os(III)d\pi$

Table 3.19 Transition bands, molar extinction coefficients, and assignment for $[OsI_5L]^{z-}$

The halide to metal charge transfer transitions in the spectra of the hexahalide osmates and the mono-substituted series $[OsX_5L]^{z-}$ move to lower energy along the series Cl^-, Br^-, I^-. This is a result of the increase in the energy of the ligand based π-electrons: 3rd row < 4th row < 5th row, thereby reducing the energy gap between the metal based dπ orbitals and the ligand orbitals. The form of the spectra also becomes more complicated as the halide becomes heavier. Increased spin orbit coupling will result in formally spin forbidden transitions becoming partially allowed, which results in a greater number of electronic transitions being observed.

3.3.2.4 Rate constants, activation energies, and activation parameters for the substitution reactions of $[OsI_6]^{3-}$

The pseudo first order rate constants, k, for the substitution reactions of electrochemically generated $[OsI_6]^{3-}$ with L, have been studied using double-step chronoamperometry in 0.1 M $[N^nBu_4]BF_4$/L. The rate constants were determined from data over the range 175-225 K. The rate constant at 198 K, the activation energy, E_a, and the activation parameters, $\Delta H^{\ddagger}$, $\Delta G^{\ddagger}$, $\Delta S^{\ddagger}$, for the reactions are presented in **Table 3.20**. The activation energies, E_a, were calculated from the Arrhenius relationship (**Figure 3.29**) and the activation parameters, $\Delta H^{\ddagger}$, $\Delta G^{\ddagger}_{198K}$, $\Delta S^{\ddagger}_{198K}$, from the Eyring relationships without modification (Equation 1.10).

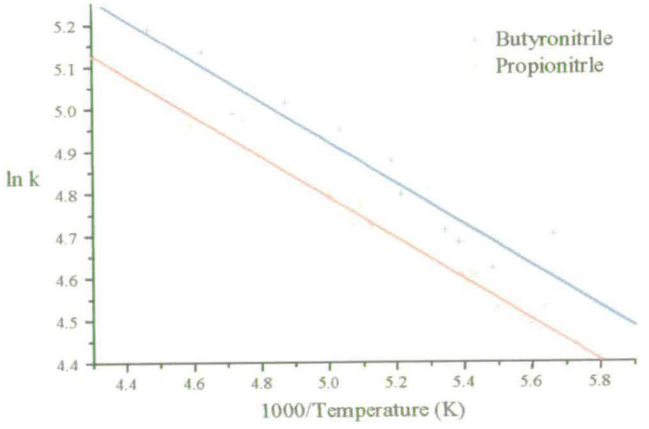

Figure 3.29 Arrhenius plot for the substitution reaction of $[OsI_6]^{3-}$ with Pn and By

The rate constants were determined from the linear regression fit from the Arrhenius plots of lnk against 1/T. Errors in k were calculated from the average error for each point determined from the average measured value for each experiment and the statistical errors involved in their calculation. The errors given for E_a and $\Delta H^{\ddagger}$ are the standard deviations from the linear regression fits. Errors given for $\Delta G^{\ddagger}$ and $\Delta S^{\ddagger}$ are calculated from the statistical errors involved in their calculation. The rate of substitution of $[OsI_6]^{2-}$, even at 225 K, was at the limit of experimental measurement for the double step chronoamperometric technique. **Figure 3.29** clearly shows a

greater scattering of data points than previously shown. Nevertheless by repeated measurement, confidence in the analysis is high and reflected in the calculated errors. Acetonitrile as an electrochemical solvent offers an advantage over propionitrile and butyronitrile because its lower viscosity leads to substantially lower resistivities (resistance within butyronitrile at lower temperatures begins to rise sharply below 233 K).[61] However precipitation of electrolyte from acetonitrile begins around 218 K and leads to freezing of the solution making data unobtainable. Lower temperatures are more accessible without precipitation of electrolyte in propionitrile and butyronitrile. This is a clear case where double-step potentiometry has an advantage over other electrochemical methods in determining the rate constant because compensation for internal resistance is not necessary. It should be noted that k and hence $\Delta G^{\ddagger}$ and $\Delta S^{\ddagger}$ are calculated at 198 K rather than 298 K because of a reluctance to extrapolate the rate constant data to obtain a value of k at 298 K.

Compound/L	k_{198K} / s^{-1}	E_a kJ mol^{-1}	$\Delta H^{\ddagger}$ kJ mol^{-1}	$\Delta G^{\ddagger}_{198K}$ kJ mol^{-1}	$\Delta S^{\ddagger}_{198K}$ J K^{-1} mol^{-1}
$[OsI_6]^{2-}$/Pn	110 ± 6	4.0 ± 0.2	2.5 ± 0.17	40.1 ± 0.2	-188 ± 3
$[OsI_6]^{2-}$/By	134 ± 8	4.0 ± 0.4	2.5 ± 0.36	39.7 ± 0.2	-189 ± 3

Table 3.20 Rate constants, activation energies, and activation parameters for $[OsX_6]^{3-} \rightarrow [OsX_5L]^{2-}$

The rate constants at 198 K are twice as fast as $[OsBr_6]^{3-}$ at 298 K. They show the opposite trend of $[OsCl_6]^{3-}$ and $[OsBr_6]^{3-}$; butyronitrile is faster than propionitrile allowing for experimental error. The activation energies are the same within experimental error. The much lower value of the activation energy perhaps explains the substitution of the Os(IV) species at room temperature. The value of $\Delta G^{\ddagger}$, although smaller than previously seen, is much larger than $\Delta H^{\ddagger}$ and leads to a much more negative value of $\Delta S^{\ddagger}$.

3.3.2.5 Discussion of $[OsX_5L]^{z-}$ kinetic parameters

There is a clear and considerable increase in the rate constant for the reduction-induced substitution reaction of $[OsX_6]^{2-}$ in the presence of a ligand, L, where X = $Cl^- < Br^- < I^-$ (**Figure 3.30**). A detailed study of $[OsCl_6]^{2-}$ has revealed that the rate limiting step in formation of $[OsCl_5L]^{2-}$ is the dissociation of the chloride ligand. Complexes of the type $[OsX_6]^{3-/2-}$, where X = Cl^-, Br^-, I^-, all show consistent electrochemical behaviour both in their half wave potentials and the half-wave potentials of their mono-substituted daughter products, $[OsX_5L]^{2-/1-}$ (**Table 3.21**).

L	$[OsCl_5L]^{3-/2-}$ $E_{1/2}$ (V)	$[OsBr_5L]^{3-/2-}$ $E_{1/2}$(V)	$[OsI_5L]^{3-/2-}$ $E_{1/2}$ (V)
Cl^-	-0.57	-0.39	-0.31
An	+0.10	+0.16	+0.18
Pn	-0.03	+0.06	+0.17
By	-0.08	+0.02	+0.16

Table 3.21 Table of half-wave potentials for $[OsX_5L]^{z-}$, where X = Cl^-, Br^-, I^-, and L = X^-, An, Pn, By

The $[OsX_6]^{3-/2-}$ and $[OsX_5L]^{2-/1-}$ redox couple for each halide is assigned as metal based and substitutions for L are as expected by Lever's ligand additivity theory.[23] When a halide is replaced by a nitrile, in each case, there is a stepwise destabilisation of the Os(IV)/(III) couple relative to their σ-donor abilities, By > Pn > An. This electronic effect is lessened on going down the halide group, so that for $[OsI_5L]^{3-/2-}$ there is only 20 mV between half-wave potentials for acetonitrile and butyronitrile. This effect is understood in terms of the relative π-donor strengths, where I^- dominates over the σ-donor influence of ligand, L. The half-wave potentials are related to the empirical energies of the molecular orbitals by the Nernst equation whilst in the uv-vis spectra electronic transitions relate to the differences in energies between orbitals. The uv-vis band positions mirror the changes in half-wave potentials demonstrating consistent electronic behaviour. It is suggested therefore, that the rate limiting step for the substitution reactions of $[OsBr_6]^{3-}$ and $[OsI_6]^{3-}$, is

also that of the dissociation of the halide. It is well known that iodide is a better leaving group than chloride and in addition free iodide ions have an increased solubility in organic solvents over free chloride.[62,63] Thus the increase in rate constant for the mono-substituted reaction of $[OsI_6]^{3-}$ over $[OsCl_6]^{3-}$ is as expected.

The activation energies of hexahalide-osmates for halide loss is the cleavage of the osmium-halogen bond. $[OsBr_6]^{3-}$ exhibits a 10 % larger activation energy than $[OsCl_6]^{3-}$. The $[OsI_6]^{3-}$ activation energy is significantly less than that of chloride and bromide.

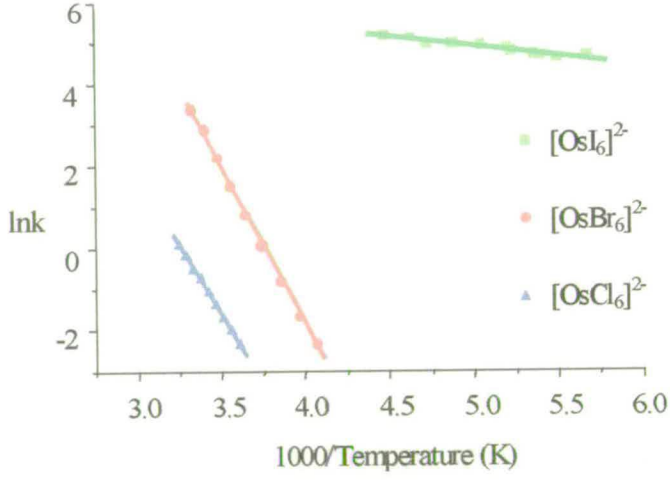

Figure 3.30 Arrhenius plots of the substitution reactions of $[OsX_6]^{3-}$ (X = Cl^-, Br^-, I^-) in 0.1 M $[N^nBu_4]BF_4$/butyronitrile

Crystallographic data for Os(IV) shows the osmium-halide bond lengths and the halide-halide distances increase with the Van der Waals radii of the halide (**Table 3.22**).

X	M-X bond length for $[OsX_6]^{2-}$ / Å[5]	M-X bond length for $[OsX_4(C_2O_4)]^{2-}$ / Å[64]	X-X distance / Å	Van der Waals Radii / Å
Cl^-	2.34	2.34	3.32	1.75
Br^-	2.49	2.48	3.52	1.85
I^-	2.69*	2.69	3.80	1.98

Table 3.22 Average metal-halide bond lengths, halide-halide distances, and Van der Waals radii of halides. *Bond length of Os-I bond is inferred from the analogous series $[OsX_4(C_2O_4)]^{2-}$.

Crystallographic data for $[OsX_6]^{3-}$ are not available, however the metal-halide bond length should increase compared to that of the Os(IV) species and it is therefore hard to envisage steric crowding problems that may effect the metal-halide bond strength. The activation energies are therefore interpreted as an indication of orbital overlap between the metal d-orbitals and the halides. In terms of Lewis acid/base theory, Os(III) is a relatively strong Lewis acid (although not as strong as Os(IV)) and will bond more effectively with the corresponding strong Lewis base. Iodide is a weak Lewis base and will form only a weak bond in comparison to the stronger Lewis bases, bromide and chloride. Furthermore, an argument could be made that the polarisable nature of iodide would enhance the dissociation of an iodide by stabilising an unsaturated, five co-ordinate intermediate thus increasing the rate constant and lowering the activation energy. The activation energies lose their slight dependence on L for $[OsBr_6]^{3-}$ and $[OsI_6]^{3-}$ (they are the same within experimental error). This could indicate an increasingly Dissociative mechanism rather than dissociative Interchange mechanism.

There is no obvious explanation of the values of $\Delta S^{\ddagger}$ calculated for $[OsI_6]^{3-}$. Such a negative value of $\Delta S^{\ddagger}$ implies an associative reaction mechanism, which would require a sterically crowded seven co-ordinate intermediate and would be inconsistent with the observed kinetic behaviour. It is surmised that no clear information can be obtained from direct interpretation of the Eyring relationship. Whether more reliable data can be obtained by the modification to the Eyring relationship for ionic reactions in electrolyte solutions (see chapter 1) is in doubt and beyond the scope of this work. The necessary calculation of the activity coefficients of the activated complex cannot be measured with thermodynamic rigour.[65]

In conclusion the reduction-induced substitution reactions of $[OsX_6]^{2-}$, where X = Cl^-, Br^-, I^-, to yield $[OsX_5L]^{2-}$ have been shown to proceed *via* a Dissociative mechanism (although the osmium hexachloride analogue does show some evidence for a dissociative Interchange pathway). The osmium hexaiodide complex reacts very much faster than the chloride or bromide and in all cases the rate limiting step involves the cleavage of an osmium-halide bond.

3.3.3 $[MX_5L]^{2-}$, M = Re, Ir and X = Br^-, I^- and L = An, Pn, By

Iridium hexachloride, iridium hexabromide, and rhenium hexachloride were prepared in order to investigate the effect the metal centre has on electrochemical response.

3.3.3.1 Iridium hexachloride, $[IrCl_6]^{2-}$

The cyclic voltammogram of $[N^nBu_4]_2[IrCl_6]$ in 0.5 M $[N^nBu_4]BF_4$/dcm at 294 K (**Figure 3.31**) shows a reduction at +0.12 V (ΔE = 100 mV) and an oxidation at +1.87 V (ΔE = 90 mV); both are one electron processes as determined by coulometry and electron transfer rates are diffusion limited, i.e. $i_p \alpha v^{1/2}$, at room temperature and a scan rate of 0.1 V s^{-1}.

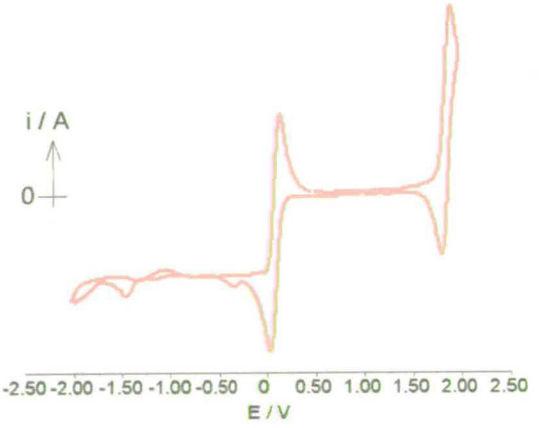

Figure 3.31 CV of $[IrCl_6]^{2-}$ in 0.5 M $[N^nBu_4]BF_4$/dcm at 0.1 V s^{-1}, 273 K

The voltammogram displays some complicated behaviour following the $[IrCl_6]^{3-/2-}$ reduction which is not observed at 203 K. It is unclear what is responsible for this behaviour. Chloride ions do not show any redox chemistry in the region of either redox couples. Cache calculations show the HOMO and LUMO to be based on the

metal. Therefore, both the oxidation and reduction processes are assigned as metal based. The half-wave potential is 0.69 V positive of that of $[OsCl_6]^{3-/2-}$ redox couple, representing a considerable stabilisation of the third oxidation state. Iridium is considered to be more capable of stabilising the electron donation from the chlorides because of the increased nuclear charge.

The uv-vis spectra of the Ir(III) and Ir(IV) species and the spectroelectrochemical uv-vis spectrum of the III/IV reduction at 223 K are shown in **Figure 3.32**.

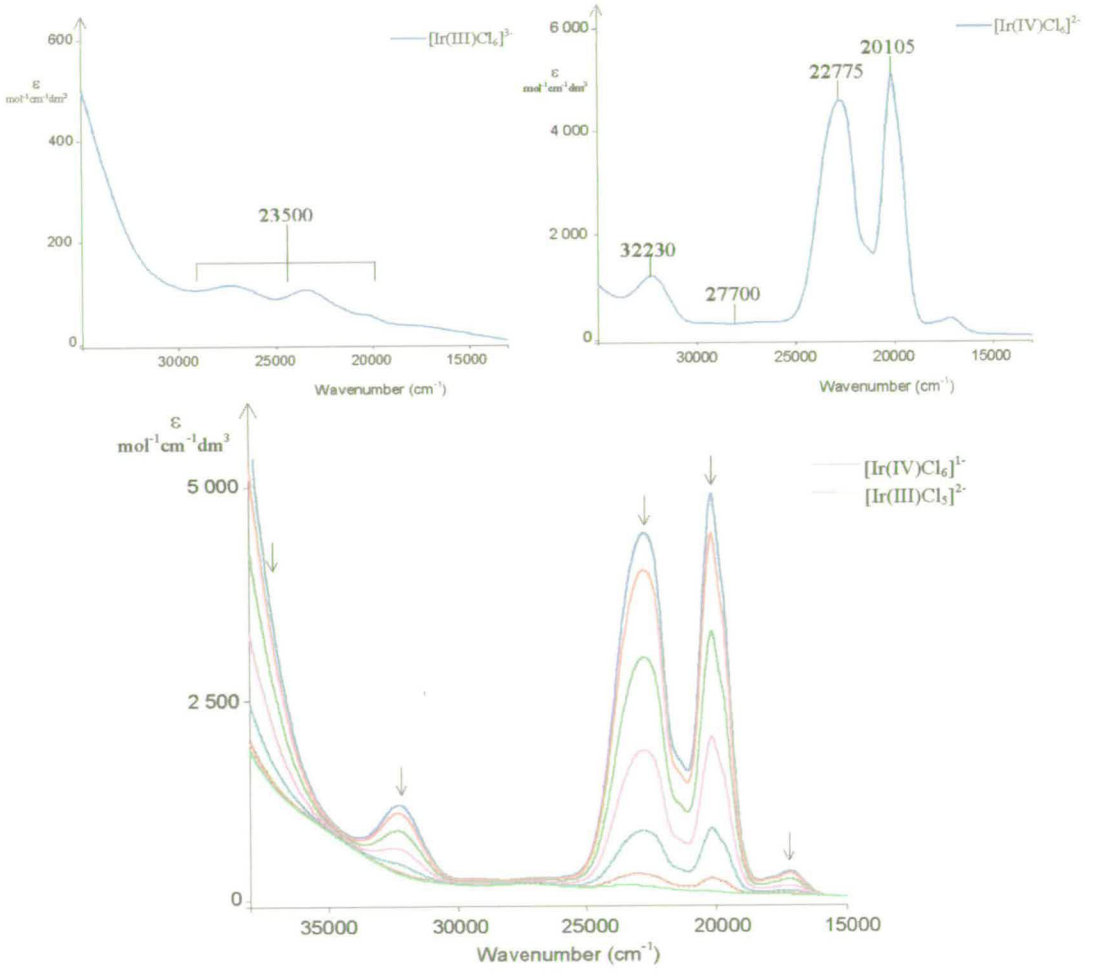

Figure 3.32 Uv-vis spectra of $[IrCl_6]^{3-}$ and $[IrCl_6]^{2-}$ and *in situ* spectroelectrochemical reduction spectrum of $[IrCl_6]^{2-}$ in 0.5 M $[N^nBu_4]BF_4$/L at 223 K, electrogeneration potential -0.70 V

Jørgensen has assigned the main bands at 20100 cm^{-1} and 22800 cm^{-1} as $Cl^-\pi \rightarrow$ Ir(IV)d$\pi(t_{2g})$ transitions and the bands at 27700 cm^{-1} and 32200 cm^{-1} were tentatively assigned as d$\pi(t_{2g}) \rightarrow$ d$\sigma(e_g)$ transitions.[6] Another band at 41800 cm^{-1} was assigned

as $Cl^-\pi \rightarrow Ir(IV)d\sigma(e_g)$. The difference of approximately 20000 cm^{-1} between $d\pi$ and $d\sigma$ orbitals, however, is not as high as might be expected for Ir(IV).[23]

The bands in the Ir(III) absorption spectrum at 20385 cm^{-1}, 23500 cm^{-1}, and 27365 cm^{-1} are much weaker and were not observed by Jørgensen. The band at 20385 cm^{-1} probably arises from a small amount of the Ir(IV) species still present in solution (~1 %) and the two bands at 23500 cm^{-1}, and 27365 cm^{-1} are of the energy expected for a transition within the metal d-orbitals and are confidently assigned as $d\pi(t_{2g}) \rightarrow d\sigma(e_g)$ transitions.[56]

The d-d band maxima can be analysed according to Lever to give values of Δ and B, where Δ is the ligand field splitting parameter between t_{2g} and e_g orbitals and B is the Racah parameter for Ir(III) in $[IrCl_6]^{3-}$.[60] Lever states that the energy of the ground state for low spin d^6 metal centres ($^1A_1$) may be expressed as:

$$^1A_1 = -2.4\Delta + 5B + 8C \qquad \textbf{Equation 3.5}$$

where C is a further Racah parameter and is usually approximated to $4B$. The energy of the first spin allowed excited state, $^1T_1$, electronic configuration $t_{2g}^5e_g^1$, may be expressed as:

$$^1T_1 = -1.4\Delta + 5B + 7C \qquad \textbf{Equation 3.6}$$

The energy of the second excited state, $^1T_2$, electronic configuration $t_{2g}^5e_g^1$, may be expressed as

$$^1T_2 = -1.4\Delta + 21B + 7C \qquad \textbf{Equation 3.7}$$

The experimentally obtained d-d band positions of 23500 cm^{-1} and 27365 cm^{-1} therefore give values of Δ = 24465 cm^{-1} and B = 242 cm^{-1}. This value of Δ goes some way to confirming the 41800 cm^{-1} band in $[IrCl_6]^{2-}$ as a $Cl^-\pi \rightarrow Ir(IV)d\pi(e_g)$ transition. The B value for the free ion Ir(III) is 660 cm^{-1}, which gives a value of 0.37

for the nephelauxetic parameter, β ($\beta = \frac{B_{complex}}{B_{free-ion}}$). This very low β value indicates that the Ir-Cl bands in $[IrCl_6]^{3-}$ are very covalent.

A transition band at 48600 cm^{-1} in the Ir(III) spectrum was assigned by Jørgensen as $Cl^-\pi \rightarrow Ir(III)d\sigma(e_g)$. Low spin Ir(III), d^6, will have electron full $d\pi$ orbitals so clearly no $Cl^-\pi \rightarrow Ir(III)d\pi(t_{2g})$ transitions are possible. The shift of *ca.* 7000 cm^{-1} is similar to that observed for LMCT transitions in Os(IV) and Os(III) spectra and supports the assignment. Full transition band maxima, extinction coefficients, and transition band assignment are given in **Table 3.24**. The spectroelectrochemical reduction spectrum of Ir(IV) to Ir(III) is not remarkably revealing. Nevertheless, by being reproducible on oxidation from Ir(III) to (IV), it demonstrates chemical reversibility at 223 K of the $[IrCl_6]^{3-/2-}$ couple.

Electrogenerated $[IrCl_6]^{3-}$ reacts in the presence of acetonitrile, propionitrile and butyronitrile, with a new redox couple growing in at *ca.* 0.7 V positive of the diminishing $[IrCl_6]^{3-/2-}$ redox couple. An irreversible oxidation at *ca.* +1.4 V corresponds to a molar equivalent of free chloride. This compares with Brown *et al*'s work, where $[IrCl_6]^{3-}$ reacts with pyridine giving $[IrCl_5Py]^{2-}$.[42] The new redox couple in this work is confidently assigned to $[IrCl_5L]^{2-/1-}$ in an analogous manner to the $[OsCl_5L]^{2-/1-}$ processes. The IV/III half-wave potentials for the mono-substituted products are given in **Table 3.23**.

Complex	$E_{1/2}$ (IV/III) / V
$[IrCl_6]^{3-/2-}$	+0.12
$[IrCl_5An]^{2-/1-}$	+0.80
$[IrCl_5Pn]^{2-/1-}$	+0.79
$[IrCl_5By]^{2-/1-}$	+0.79

Table 3.23 Half-wave potentials for $[IrCl_5L]^{z-}$, L = Cl^-, An, Pn, By

The Ir based redox processes of the mono-substituted complexes are approximately 700 mV more positive than their Os analogues reflecting the increased nuclear

charge in Ir compared to Os. Unlike $[OsCl_5L]^{2-/1-}$, there is no significant difference between the half-wave potentials of the mono-substituted species. This is mirrored in their uv-vis spectra (**Figure 3.33** and **Figure 3.34**). Both Ir(IV) and Ir(III) species of acetonitrile, propionitrile, and butyronitrile, have very similar band positions. The extinction coefficients represent the clearest difference between them. As has been observed for the osmium analogue, the transition bands are of similar energy to the hexahalide complex, but with broader and less defined bands. The most interesting changes in the spectra are of the Ir(IV) species. A band at 27700 cm^{-1}, very weak in $[IrCl_6]^{2-}$, was postulated as a $d\pi \rightarrow d\sigma$ by Jørgensen. In the mono-substituted species the transition at *ca* 27000 cm^{-1} has an extinction coefficient of between 1000 and 1700 mol^{-1} cm^{-1} dm^3; rather high for a $d\pi \rightarrow d\sigma$ transition. On mono-substitution, however, the centre of symmetry of the complex is removed and therefore gerade and ungerade subscripts ("g" and "u") on orbitals are not applicable. One consequence of this is that Laporte's Rule for allowed electronic transitions (i.e. g→g or u→u transitions are forbidden) does not have to be obeyed and thus d-d transitions become more intense. The Ir(III) species all show a set of three weak transitions around 27000cm^{-1} (A). A strong band is observed for the propionitrile and butyronitrile species at 42670 cm^{-1} and 48100 cm^{-1} respectively (neither is shown for clarity). The weak bands are of the intensity expected of a metal-based transition and are assigned as $d\pi \rightarrow d\sigma$ transitions. These bands cannot be observed in the Os(III) species due to them being masked by the much more intense $Cl^-\pi \rightarrow Os(III)\pi$ transitions: not possible in the fully occupied Ir(III), d^6 species. The splitting parameter, Δ, derived from the energy of the d-d bands is very similar for $[IrCl_5L]^{2-}$, L = Pn, By, as for $[IrCl_6]^{2-}$. The strong bands are therefore assigned as $Cl^-\pi \rightarrow$ Ir(III)$d\sigma$ transitions. Full transition band assignments, peak maxima, and molar extinction coefficients are given in **Table 3.24**. The uv-vis spectroelectrochemical Ir(IV)/(III) reduction spectra show the species to be chemically reversible at 213 K.

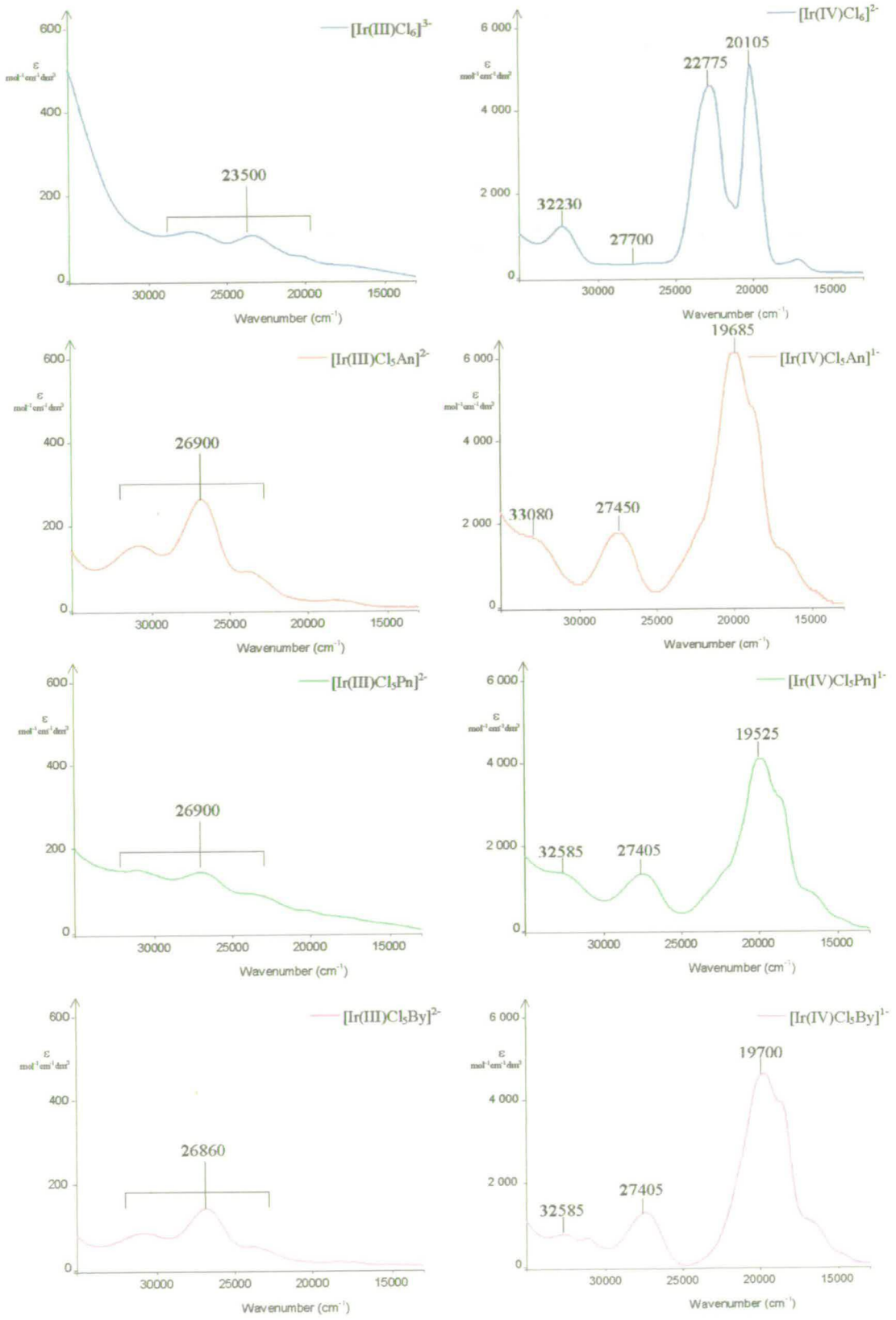

Figure 3.33 Uv-vis spectra of $[IrCl_6]^{z-}$ in 0.5 M $[N^nBu_4]BF_4$/dcm at 213 K, and $[IrCl_5L]^{z-}$, L = An, Pn, By, in 0.1 M $[N^nBu_4]BF_4$/L at 223 K

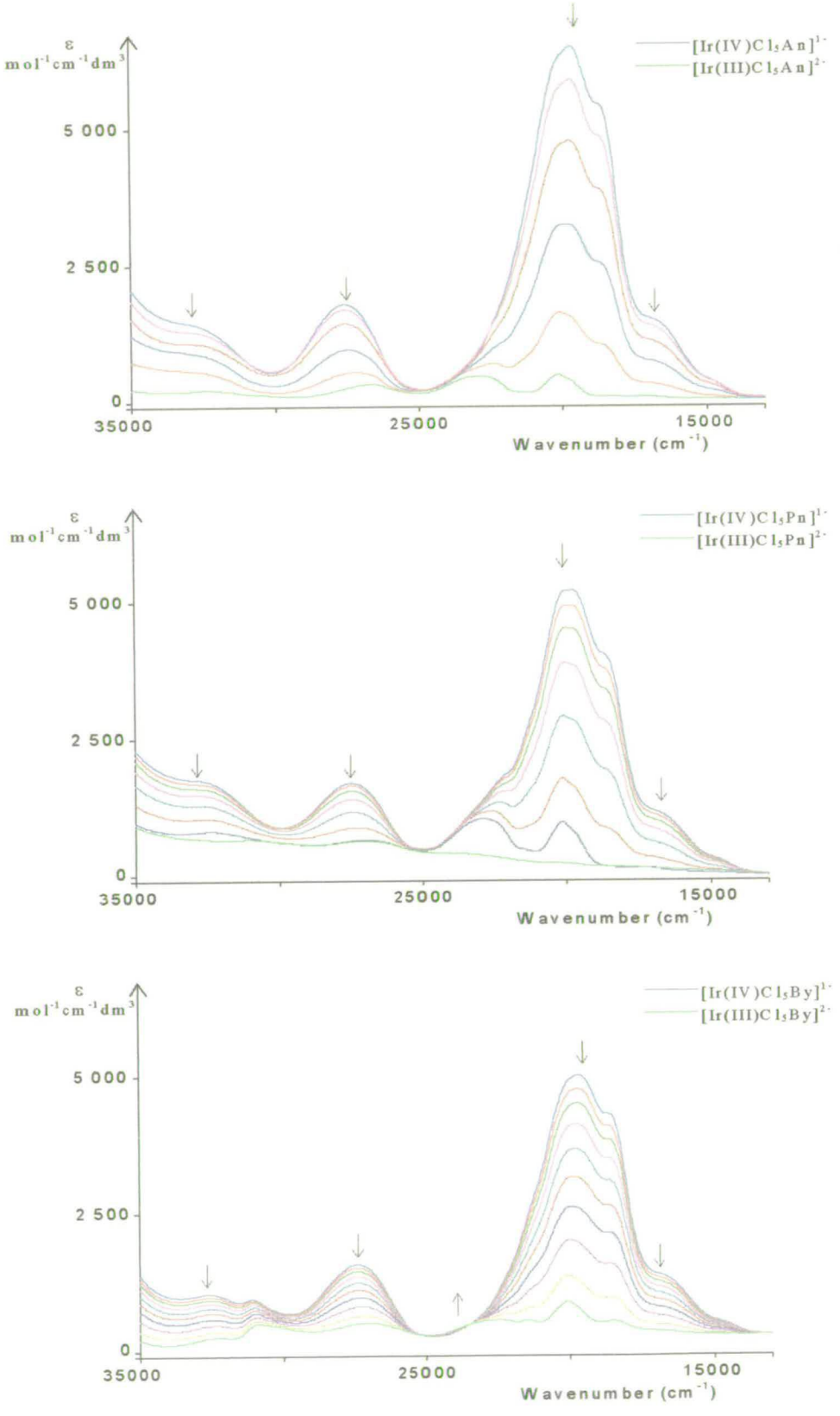

Figure 3.34 *In situ* uv-vis spectroelectrochemical reduction spectra of $[IrCl_5L]^{z-}$, L = An, Pn, By, in 0.1 M $[N^nBu_4]BF_4$/L at 213 K, electrogeneration potential –0.10 V

Complex	Peak max (cm^{-1})	ε / mol^{-1} cm^{-1} dm^3	Assignment
$[Ir(IV)Cl_6]^{2-}$	17 140	360	$Cl^-\pi \rightarrow Ir(IV)d\pi$
	19 800sh	4 000	$Cl^-\pi \rightarrow Ir(IV)d\pi$
	20 105	4 900	$Cl^-\pi \rightarrow Ir(IV)d\pi$
	22 775	4 500	$Cl^-\pi \rightarrow Ir(IV)d\pi$
	27 365	350	$d\pi \rightarrow d\sigma$
	32 230	1 100	$d\pi \rightarrow d\sigma$
	41 800	23 500	$Cl^-\pi \rightarrow Ir(IV)d\pi$
$[Ir(III)Cl_6]^{3-}$	20 385	60	$d\pi \rightarrow d\sigma$
	23 500	100	$d\pi \rightarrow d\sigma$
	27 365	100	$d\pi \rightarrow d\sigma$
	48 600	22 000	$Cl^-\pi \rightarrow Ir(III)d\sigma$
$[Ir(IV)Cl_5An]^{1-}$	14 730sh	500	$Cl^-\pi \rightarrow Ir(IV)d\pi$
	16 690sh	1 600	$Cl^-\pi \rightarrow Ir(IV)d\pi$
	18 640sh	5 400	$Cl^-\pi \rightarrow Ir(IV)d\pi$
	19 685	6 100	$Cl^-\pi \rightarrow Ir(IV)d\pi$
	27 450	1 700	$d\pi \rightarrow d\sigma$
	33 080sh	1 200	$d\pi \rightarrow d\sigma$
	42 730	14 000	$Cl^-\pi \rightarrow Ir(IV)d\pi$
$[Ir(III)Cl_5An]^{2-}$	23 880	110	$d\pi \rightarrow d\sigma$
	26 900	270	$d\pi \rightarrow d\sigma$
	30 780	160	$d\pi \rightarrow d\sigma$
$[Ir(IV)Cl_5Pn]^{1-}$	14 735sh	300	$Cl^-\pi \rightarrow Ir(IV)d\pi$
	16 505sh	1 000	$Cl^-\pi \rightarrow Ir(IV)d\pi$
	18 685sh	2 400	$Cl^-\pi \rightarrow Ir(IV)d\pi$
	19 525	4 100	$Cl^-\pi \rightarrow Ir(IV)d\pi$
	27 625	1 000	$d\pi \rightarrow d\sigma$
	32 720sh	800	$d\pi \rightarrow d\sigma$
	42 670	11 400	$Cl^-\pi \rightarrow Ir(IV)d\pi$
$[Ir(III)Cl_5Pn]^{2-}$	23 640	90	$d\pi \rightarrow d\sigma$
	26 900	160	$d\pi \rightarrow d\sigma$
	31 145	160	$d\pi \rightarrow d\sigma$
	43 700sh	14 000	$Cl^-\pi \rightarrow Ir(III)d\sigma$
$[Ir(IV)Cl_5By]^{1-}$	14 745	300	$Cl^-\pi \rightarrow Ir(IV)d\pi$
	16 715sh	1 000	$Cl^-\pi \rightarrow Ir(IV)d\pi$
	18 615sh	2 400	$Cl^-\pi \rightarrow Ir(IV)d\pi$
	19 700	4 600	$Cl^-\pi \rightarrow Ir(IV)d\pi$
	27 405	1 100	$d\pi \rightarrow d\sigma$
	31 130	500	$d\pi \rightarrow d\sigma$
	32 585	900	$d\pi \rightarrow d\sigma$
	48 100	12 000	$Cl^-\pi \rightarrow Ir(IV)d\pi$
$[Ir(III)Cl_5By]^{2-}$	23 380	50	$d\pi \rightarrow d\sigma$

Complex	Peak max (cm^{-1})	ε / mol^{-1} cm^{-1} dm^3	Assignment
$[Ir(III)Cl_5By]^{2-}$ (cont.)	26 860	140	$d\pi \rightarrow d\sigma$
	31 090	70	$d\pi \rightarrow d\sigma$
	43 555sh	14 800	$Cl^-\pi \rightarrow Ir(III)d\sigma$

Table 3.24 Transition bands, molar extinction coefficients, and assignments for $[IrCl_5L]^{z-}$

3.3.3.2 Rate constants, activation energies, and activation parameters for the substitution reactions of $[IrCl_6]^{3-}$

The pseudo first order rate constants, k, for the substitution reactions of electrochemically generated $[IrCl_6]^{3-}$ with L, have been studied using double-step chronoamperometry in 0.1 M $[N^nBu_4]BF_4$/L. The rate constants were determined from data over the range 278-348 K. The rate constant at 298 K, the activation energy, E_a, and the activation parameters, $\Delta H^{\ddagger}$, $\Delta G^{\ddagger}_{298K}$, $\Delta S^{\ddagger}_{298K}$, for the reactions are presented in **Table 3.25**. The activation energies, E_a, were calculated from the Arrhenius relationship (**Figure 3.35**) and the activation parameters, $\Delta H^{\ddagger}$, $\Delta G^{\ddagger}$, $\Delta S^{\ddagger}$, from the Eyring relationship without modification (Equation 1.10). The rate constants at 298 K were determined from the linear regression fit from the Arrhenius plots of lnk against 1/T. Errors in k were calculated from the average error for each point determined from the average measured value for each experiment and the statistical errors involved in their calculation. The errors given for E_a and $\Delta H^{\ddagger}$ are the standard deviations from the linear regression fits. Errors given for $\Delta G^{\ddagger}$ and $\Delta S^{\ddagger}$ are calculated from the statistical errors involved in their calculation. Activation energies and activation parameters for $[IrCl_6]^{3-}$ in acetonitrile were unobtainable. The necessary warming of the reaction to achieve measurable rate constants over a range of temperatures caused the Ir(IV) species to react with acetonitrile. A new redox couple grew in at +0.80 V and is presumably that of the mono-substituted species. Furthermore, at higher temperatures, approaching the boiling point of acetonitrile (354 K), an evaporation/condensation cycle created perceptible convection

introducing convection as a mode of transport as well as diffusion. Non-linear results, out of character with previous results, were obtained and taken as invalid. The rate constant at 298 K, however, was still measurable.

Complex/L	k_{298} / s^{-1}	E_a kJ mol^{-1}	$\Delta H^{\ddagger}$ kJ mol^{-1}	$\Delta G^{\ddagger}_{298K}$ kJ mol^{-1}	$\Delta S^{\ddagger}_{298K}$ J K^{-1} mol^{-1}
$[IrCl_6]^{3-}$/An	1.38 ± 0.30	x	x	x	x
$[IrCl_6]^{3-}$/Pn	0.24 ± 0.03	57.0 ± 2.2	54.5 ± 2.2	76.5 ± 0.4	-74 ± 9
$[IrCl_6]^{3-}$/By	0.09 ± 0.02	57.7 ± 1.4	55.2 ± 1.4	78.9 ± 0.5	-80 ± 6

Table 3.25 Rate constants, activation energies, and activation parameters for $[IrCl_6]^{3-} \rightarrow [IrCl_5L]^{2-}$. x = values were not determined

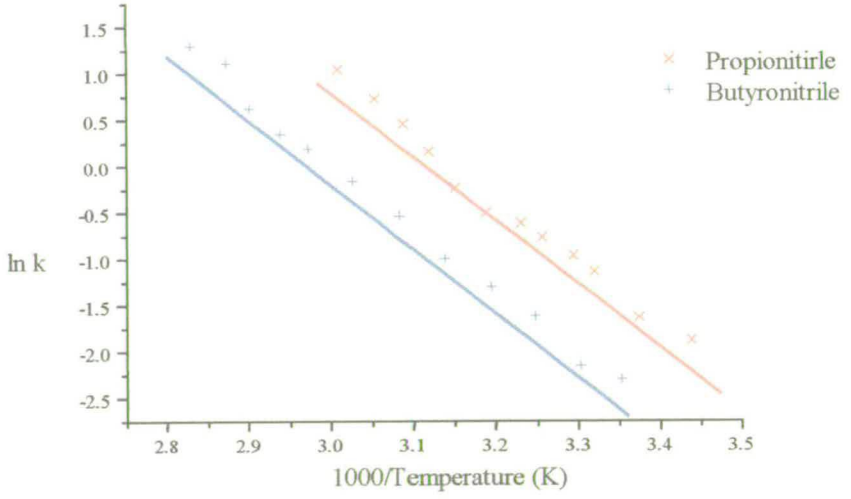

Figure 3.35 Arrhenius plot for the substitution reaction of $[IrCl_6]^{3-}$ with Pn and By

The rate constants at 298 K are from two to five times slower than their $[OsCl_6]^{3-}$ analogues and follow the same stepwise decrease, An > Pn > By. The activation energies for the Pn and By complex formation are the same within experimental error, on average 57.4 kJ mol^{-1} and are equivalent within experimental error to the analogous substitution reaction of $[OsCl_6]^{3-}$ with Pn and By. The activation parameters are incompatible with the EXAFS results which indicate the presence of the five co-ordinate intermediate $[IrCl_5]^{2-}$.[42] No solvent molecule or free chloride was observed close enough to be evidence of even a weak bond. The entropy of activation energies are large and negative indicating an increase in order: a situation very difficult to imagine for a five co-ordinate intermediate. These results support the

summation made in 3.3.2.5, that no clear information can be obtained from the direct interpretation of the Eyring relationship without modification for ionic reactions in electrolyte solutions.

3.3.3.3 Iridium hexabromide, $[IrBr_6]^{2-}$

The cyclic voltammogram of $[IrBr_6]^{2-}$ in 0.5 M $[N^nBu_4]BF_4$/dcm at 293 K is shown in **Figure 3.36**. The oxidation at $E_p^{ox} = +1.65$ V is electrochemically reversible and clearly chemically irreversible at 293 K. At 203 K the oxidation still shows no chemical reversibility. The reduction at +0.18 V (ΔE = 87 mV), is both electrochemically and chemically reversible at 293 K, 0.1 V s^{-1}, in dichloromethane.

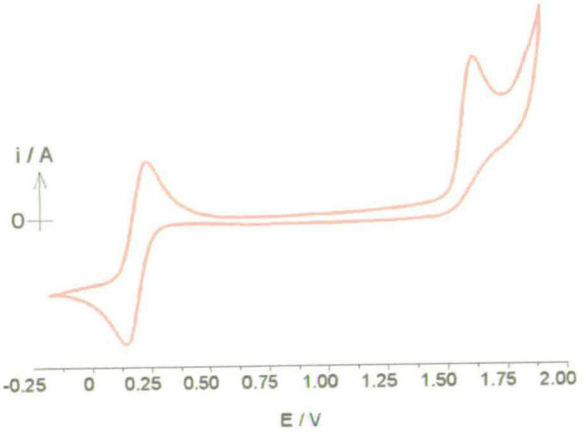

Figure 3.36 CV of $[IrBr_6]^{2-}$ in 0.5 M $[N^nBu_4]BF_4$/dcm at 0.1 V s^{-1}, 293 K

The reduction and oxidation are considered to be metal based, representing the Ir(IV/III) and Ir(V/IV) redox couples respectively. The reduction half-wave potential is only 0.06 V positive of $[IrCl_6]^{2-}$, compared to a difference of 0.18 V for the Os(IV) equivalents. This illustrates how the iridium species can accommodate the electron donation from the halides more efficiently than the osmium analogues.

The uv-vis spectra of the Ir(III) and Ir(IV) species and the *in situ* uv-vis spectroelectrochemical Ir(IV/III) reduction at 223 K in 0.5 M $[N^nBu_4]BF_4$/dcm is shown in **Figure 3.37**. The characteristic bands, A, centred around 16580 cm^{-1} have

been assigned as $Br^-\pi \rightarrow Ir(IV)d\pi(t_{2g})$ transitions involving different bromide based orbitals.[6] Jørgensen has assigned the transitions at higher energy (30865 cm^{-1} and 35610 cm^{-1}) as $Br^-\pi \rightarrow Ir(IV)d\sigma(e_g)$. The high energy transitions of the Ir(III) species are assigned as $Br^-\pi \rightarrow Ir(III)d\sigma(e_g)$. The lower energy bands were not recorded by Jørgensen, presumably because of their weak absorption. They are assigned as $d\pi \rightarrow d\sigma$ transitions. Full absorption maxima, molar extinction coefficients and transition band assignment are given in **Table 3.27**.

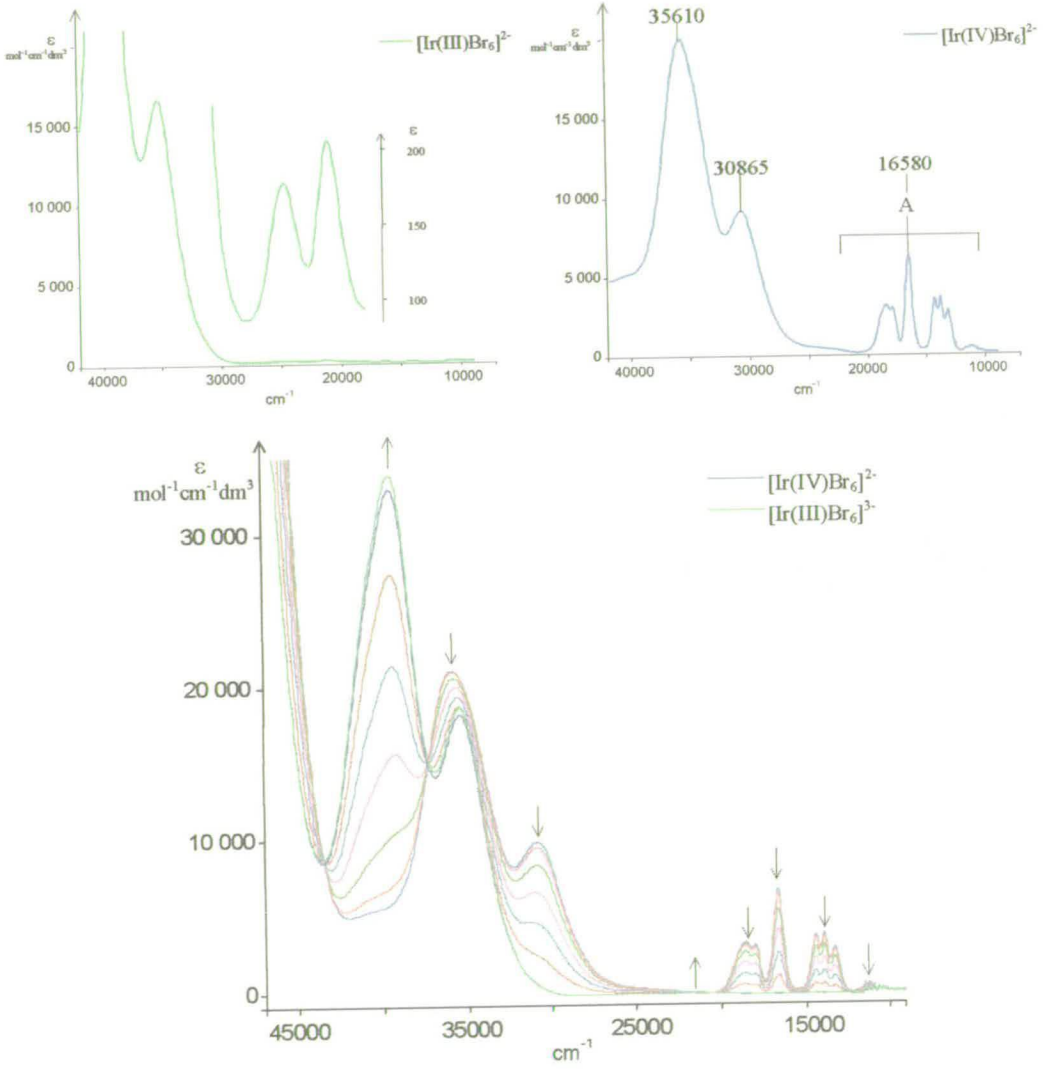

Figure 3.37 Uv-vis spectra of $[IrBr_6]^{3-}$ and $[IrBr_6]^{2-}$ and *in situ* spectroelectrochemical reduction spectra of $[IrBr_6]^{2-}$ in 0.5 M $[N^nBu_4]BF_4$/dcm at 223 K, electrogeneration potential –0.10 V

The energy of the d-d bands gives values of 21575 cm^{-1} and 200 cm^{-1} for Δ and B respectively, which supports the previous LMCT assignments. The value of B

(200 cm^{-1}) gives a very low value of β (0.30) for $[IrBr_6]^{3-}$ and indicates a greater amount of covalent character in the Ir-Br bond than in the Ir-Cl bond.

Electrogenerated $[IrBr_6]^{3-}$ in the presence of acetonitrile, propionitrile, and butyronitrile, reacts with a new redox couple growing in at approximately 0.6 V positive of the parent redox couple. The daughter redox couple is taken to be that of the metal based $[IrBr_5L]^{2-/1-}$ species. Half-wave potentials are shown in **Table 3.26**. The same stepwise stabilisation of the nitriles seen in $[OsCl_5L]^{2-/1-}$, $[OsBr_5L]^{2-/1-}$, and $[OsI_5L]^{2-/1-}$is observed. No intermediate species in the substitution reaction is observed either by cyclic voltammetry or spectroelectrochemically.

Complex	$E_{1/2}$ (IV/III) / V
$[IrBr_6]^{3-/2-}$	+0.18
$[IrBr_5An]^{2-/1-}$	+0.79
$[IrBr_5Pn]^{2-/1-}$	+0.77
$[IrBr_5By]^{2-/1-}$	+0.76

Table 3.26 Half-wave potentials for $[IrBr_5L]^{z-}$, L = Br^-, An, Pn, By

The uv-vis spectra of the substituted Ir(III) and Ir(IV) species are compared to the hexabromide Ir(III) and Ir(IV) anions in **Figure 3.38** and the *in situ* uv-vis spectroelectrochemical spectra at 223 K are shown in **Figure 3.39**. Full transition band maxima, molar extinction coefficients, and transition band assignment are given in **Table 3.27**. The transitions in the mono-substituted Ir(IV) species are of similar energy but the characteristic set of bands, A, loses definition as has been observed previously on the loss of symmetry of the metal centre. The transitions are also assigned as $Br^-\pi \rightarrow Ir(IV)d\pi$. The spectra of $[Ir(III)Br_5L]^{2-}$ show weak absorption bands at similar energies to the $d\pi \rightarrow d\sigma$ transition of $[IrBr_6]^{3-}$, and are also assigned as $d\pi \rightarrow d\sigma$ transitions giving rise to similar values of Δ and *B* for the mono-substitution complexes as for $[IrBr_6]^{3-}$. The high energy bands are again assigned as $Br^-\pi \rightarrow Ir(III)d\sigma$ transitions. The *in situ* uv-vis spectroelectrochemical spectra in particular demonstrate the very small effect each nitrile has on the electronic spectra. Only small changes in the energy and absorption of the bands are observed. Clear isosbestic points show chemical reversibility of the species at 223 K.

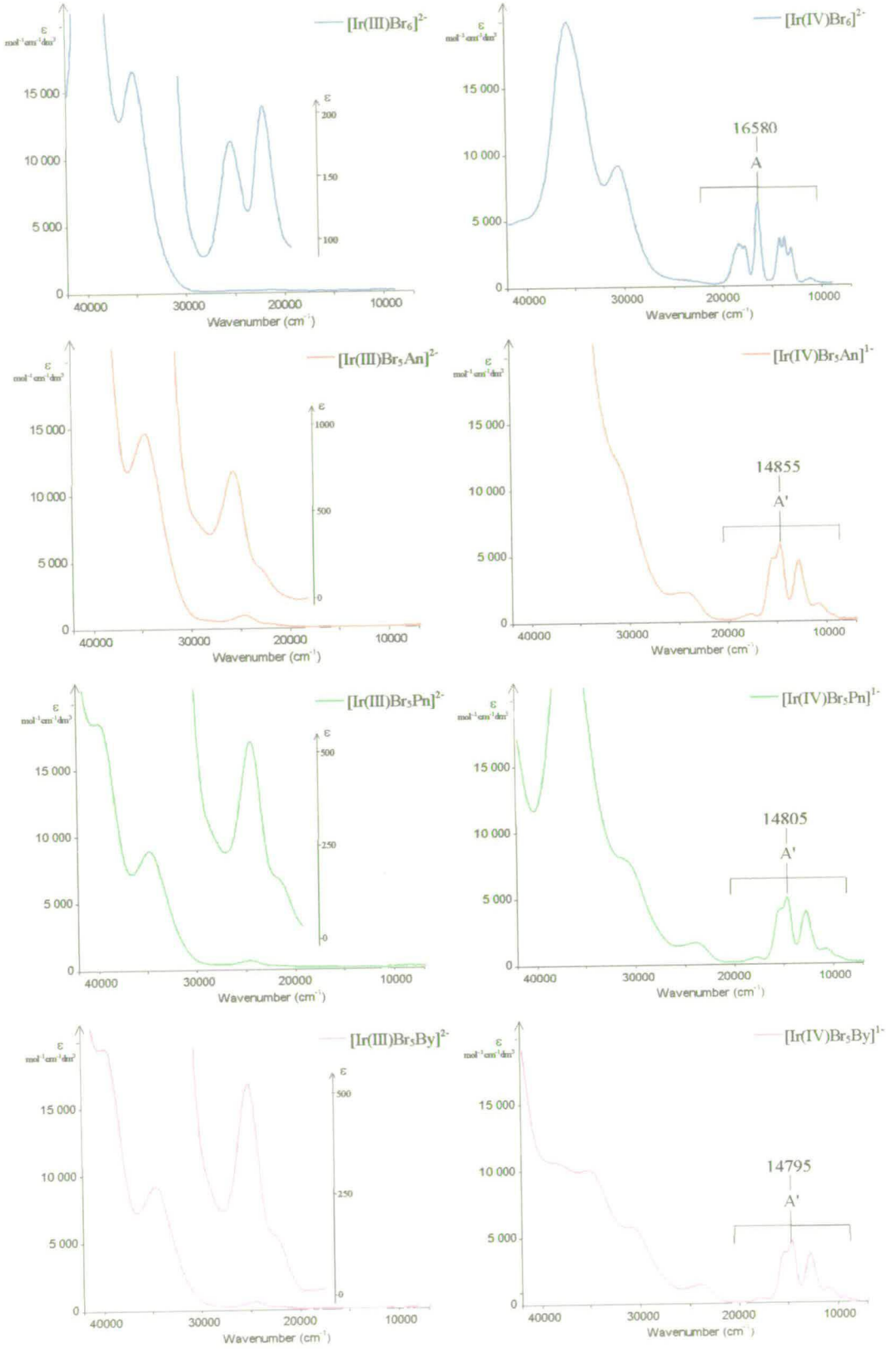

Figure 3.38 Uv-vis spectra of $[IrBr_6]^{z-}$ in 0.5 M $[N^nBu_4]BF_4$/dcm at 223 K, and $[IrBr_5L]^{z-}$, L = An, Pn, By, in 0.1 M $[N^nBu_4]BF_4$/L at 223 K

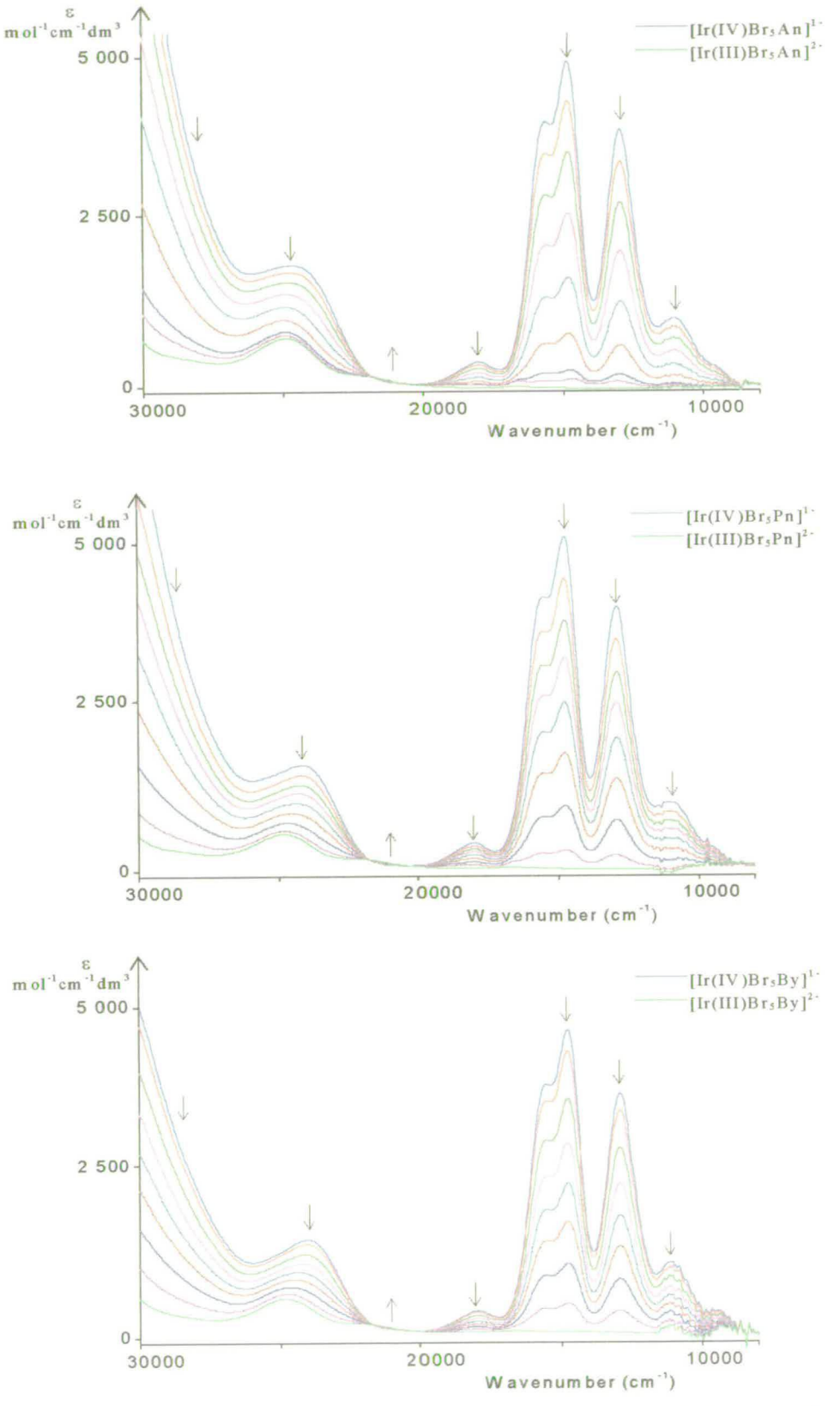

Figure 3.39 *In situ* uv-vis spectroelectrochemical reduction spectra of $[IrBr_5L]^{z-}$, L = An, Pn, By, in 0.1 M $[N^nBu_4BF_4]$/L at 223 K, electrogeneration potential –0.10 V

Complex	Peak max (cm^{-1})	ε / mol^{-1} cm^{-1} dm^3	Assignment
$[Ir(IV)Br_6]^{2-}$	11 545	400	$Br^-\pi \rightarrow Ir(IV)d\pi$
	13 255	2 500	$Br^-\pi \rightarrow Ir(IV)d\pi$
	13 975	3 700	$Br^-\pi \rightarrow Ir(IV)d\pi$
	14 505	4 000	$Br^-\pi \rightarrow Ir(IV)d\pi$
	16 580	6 200	$Br^-\pi \rightarrow Ir(IV)d\pi$
	18 010	3 500	$Br^-\pi \rightarrow Ir(IV)d\pi$
	18 600	3 200	$Br^-\pi \rightarrow Ir(IV)d\pi$
	30 865	9 300	$Br^-\pi \rightarrow Ir(IV)d\pi$
	35 610	20 000	$Br^-\pi \rightarrow Ir(IV)d\pi$
$[Ir(III)Br_6]^{3-}$	20 770	200	$d\pi \rightarrow d\sigma$
	24 775	100	$d\pi \rightarrow d\sigma$
	35 395	16 500	$Br^-\pi \rightarrow Ir(III)d\sigma$
	40 950	33 000	$Br^-\pi \rightarrow Ir(III)d\sigma$
$[Ir(IV)Br_5An]^{1-}$	11 125	4 700	$Br^-\pi \rightarrow Ir(IV)d\pi$
	14 855	6 000	$Br^-\pi \rightarrow Ir(IV)d\pi$
	15 635	4 900	$Br^-\pi \rightarrow Ir(IV)d\pi$
	18 030	500	$Br^-\pi \rightarrow Ir(IV)d\pi$
	24 640	2 300	$Br^-\pi \rightarrow Ir(IV)d\pi$
	31 100sh	12 000	$Br^-\pi \rightarrow Ir(IV)d\pi$
$[Ir(III)Br_5An]^{2-}$	21 765	200	$d\pi \rightarrow d\sigma$
	24 905	700	$d\pi \rightarrow d\sigma$
	34 740	15 200	$Br^-\pi \rightarrow Ir(III)d\sigma$
	39 830	38 300	$Br^-\pi \rightarrow Ir(III)d\sigma$
$[Ir(IV)Br_5Pn]^{1-}$	11 545	1 000	$Br^-\pi \rightarrow Ir(IV)d\pi$
	12 950	4 000	$Br^-\pi \rightarrow Ir(IV)d\pi$
	14 805	5 100	$Br^-\pi \rightarrow Ir(IV)d\pi$
	15 555	4 200	$Br^-\pi \rightarrow Ir(IV)d\pi$
	17 990	400	$Br^-\pi \rightarrow Ir(IV)d\pi$
	24 155	1 100	$Br^-\pi \rightarrow Ir(IV)d\pi$
	31 140sh	8 100	$Br^-\pi \rightarrow Ir(IV)d\pi$
	36 770	30 300	$Br^-\pi \rightarrow Ir(IV)d\pi$
$[Ir(III)Br_5Pn]^{2-}$	21 240	100	$d\pi \rightarrow d\sigma$
	24 790	500	$d\pi \rightarrow d\sigma$
	34 870	9 000	$Br^-\pi \rightarrow Ir(III)d\sigma$
	40 015	18 900	$Br^-\pi \rightarrow Ir(III)d\sigma$
$[Ir(IV)Br_5By]^{1-}$	11 065	1 100	$Br^-\pi \rightarrow Ir(IV)d\pi$
	12 935	3 700	$Br^-\pi \rightarrow Ir(IV)d\pi$
	14 795	4 700	$Br^-\pi \rightarrow Ir(IV)d\pi$
	15 550	3 900	$Br^-\pi \rightarrow Ir(IV)d\pi$
	17 965	400	$Br^-\pi \rightarrow Ir(IV)d\pi$
	24 105	1 600	$Br^-\pi \rightarrow Ir(IV)d\pi$
	31 125sh	5 700	$Br^-\pi \rightarrow Ir(IV)d\pi$

Complex	Peak max (cm^{-1})	ε / mol^{-1} cm^{-1} dm^3	Assignment
$[Ir(IV)Br_5By]^{1-}$ cont.	35 450	10 000	$Br^-\pi \rightarrow Ir(IV)d\pi$
	38 625sh	10 700	$Br^-\pi \rightarrow Ir(IV)d\pi$
$[Ir(III)Br_5By]^{2-}$	21 825sh	100	$d\pi \rightarrow d\sigma$
	24 805	500	$d\pi \rightarrow d\sigma$
	34 840	9 500	$Br^-\pi \rightarrow Ir(III)d\sigma$
	40 000	20 200	$Br^-\pi \rightarrow Ir(III)d\sigma$

Table 3.27 Transition bands, molar extinction coefficients, and assignments for $[IrBr_5L]^{z-}$

3.3.3.4 Rate constants and activation energies for the substitution reactions of $[IrBr_6]^{3-}$

The pseudo first order rate constants, k, for the substitution reactions of electrochemically generated $[IrBr_6]^{3-}$ with L, have been studied using double-step chronoamperometry in 0.1 M $[N^nBu_4]BF_4$/L. The rate constants were determined from data over the range 278-318 K. The rate constant at 298 K and the activation energy, E_a, for the reactions are presented in **Table 3.28**.

Complex/L	k_{298} / s^{-1}	E_a / kJ mol^{-1}
$[IrBr_6]^{3-}$/An	2.6 ± 0.6	x
$[IrBr_6]^{3-}$/Pn	0.64 ± 0.09	66.9 ± 2.0
$[IrBr_6]^{3-}$/By	0.37 ± 0.04	66.9 ± 1.0

Table 3.28 Rate constants, activation energies, and activation parameters for $[IrCl_6]^{3-} \rightarrow [IrCl_5L]^{2-}$

The activation energies, E_a, were calculated from the Arrhenius relationship. The rate constants at 298 K were determined from the linear regression fit from the Arrhenius plots of lnk against 1/T. Errors in k were calculated from the average error for each point determined from the average measured value for each experiment and the statistical errors involved in their calculation. The errors given for E_a are the standard deviations from the linear regression fits. Once again the activation energies for

$[IrBr_6]^{3-}$ in acetonitrile were unobtainable. Non-linear results, out of character with previous results, were obtained and taken as invalid. The rate constant at 298 K, however, was still measurable.

The rate constants are two to four times faster than for $[IrCl_6]^{3-}$/L at 298 K. They show the same stepwise decrease in rate An > Pn > By. The activation energies are approximately 5.5 kJ mol^{-1} more than $[IrCl_6]^{3-}$.

3.3.3.5 Rhenium hexachloride, $[ReCl_6]^{2-}$

The cyclic voltammogram of $[N^nBu_4]_2[ReCl_6]$ in 0.5 M $[N^nBu_4]BF_4$/dcm at 293 K is shown in **Figure 3.40**. The oxidation at +1.33 V (ΔE = 90 mV) is a one electron process both electrochemically and chemically reversible. The reduction process is clearly chemically irreversible. The high current amplitude has been found by to be a result of a rapid solvent related chemical reaction forming a catalytic process.[66]

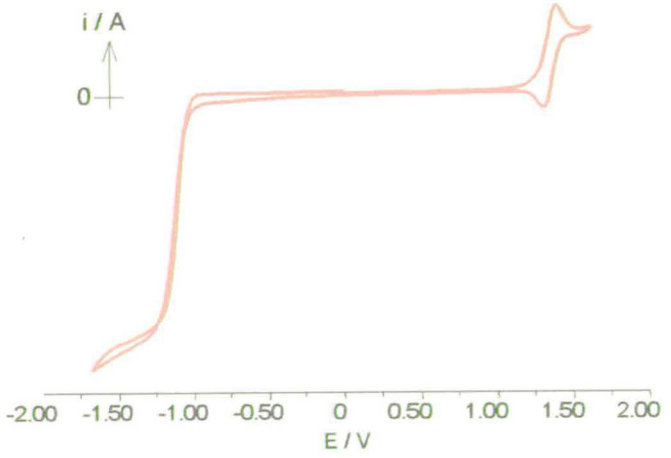

Figure 3.40 CV of $[ReCl_6]^{2-}$ in 0.5 M $[N^nBu_4]BF_4$/dcm at 0.1 V s^{-1}, 293 K

Upon reduction, the resulting $[ReCl_6]^{3-}$ species is highly unstable and rapidly forms the five co-ordinate intermediate, $[ReCl_5]^{2-}$. This extremely reactive intermediate abstracts one chlorine atom from any chlorinated solvent to yield the starting

complex $[ReCl_6]^{2-}$ and a solvent-related radical, e.g., $\cdot CH_2Cl$ from which $ClCH_2CH_2Cl$ molecules are formed in dichloromethane. Yellowlees *et al* showed that using an ionic liquid molten salt electrolyte in dichloromethane at 243 K, dissociation of the chloride was inhibited, and the reduction became a reversible one-electron process, $E_{1/2}$ = -1.17 V. This reversibility can also be achieved in 0.5 M $[N^nBu_4]BF_4$/dcm at 183 K. The ***in situ*** uv-vis spectroelectrochemical reduction spectrum of $[ReCl_6]^{2-}$ at 183 K is shown in **Figure 3.41**.

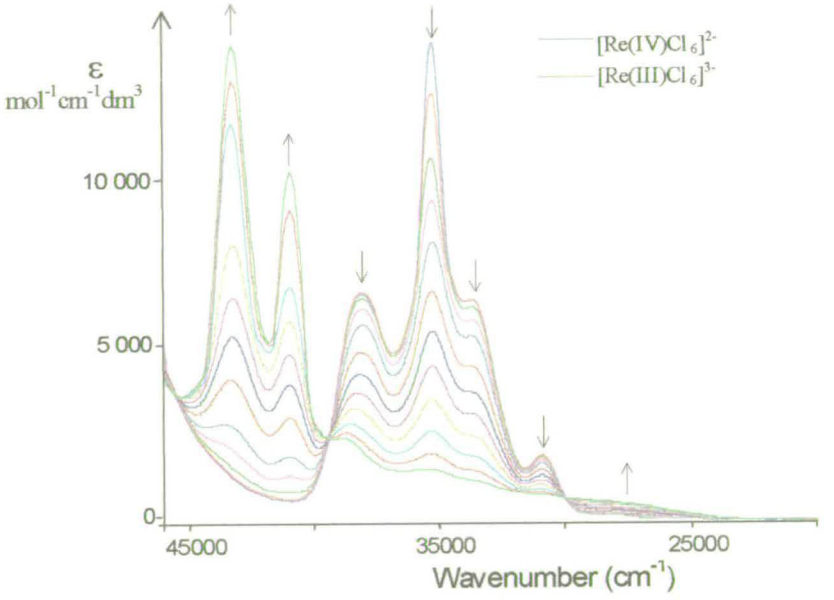

Figure 3.41 *In situ* uv-vis spectroelectrochemical reduction spectrum of $[ReCl_6]^{2-}$ in 0.5 M $[N^nBu_4]BF_4$/dcm at 183 K, electrogeneration potential –1.45 V

Clear isosbestic points are observed at *ca* 30000 cm^{-1} and 39500 cm^{-1}. The strong absorption bands have been assigned as $Cl^-\pi \rightarrow Re(IV)d\pi$ transitions from different chloride orbitals.[6,49] The weak absorption of the Re(III) species at *ca.* 28000 cm^{-1} has not been satisfactorily assigned. Liu suggests it to be from a Laporte forbidden transition, $Cl^-\pi \rightarrow Re(III)d\pi$. This seems unlikely since it is of higher energy than the Re(IV) transitions. The origins of this band could instead be a $Re(III)d\pi \rightarrow Cl^-\pi^*$ transition for Re(III). The transitions overall have moved to higher energy than for the analogous Os and Ir species as expected for a metal centre with a smaller effective nuclear charge.

Liu has shown that electrogenerated $[ReCl_6]^{3-}$ reacts in the presence of pyridine, acetonitrile, and benzonitrile forming the mono-substituted species $[ReCl_5L]^{2-}$.[49] Further reduction over time has generated the complete series $[ReCl_nPy_{6-n}]^{z-}$, where n = 0 to 6. In this work $[ReCl_5An]^{2-}$, $[ReCl_5Pn]^{2-}$ and $[ReCl_5By]^{2-}$ have been prepared and the half-wave potentials for the Re(IV/III) redox couple are shown in **Table 3.29**. The mono-substituted daughter species have an electrochemically and chemically reversible Re(IV/III) redox couple at room temperature at 0.1 V s^{-1}, the half-wave potential is *ca.* 0.7 V positive of the parent $[ReCl_6]^{3-/2-}$. The familiar stepwise stabilisation in the nitriles is observed.

Complex	$E_{1/2}$ (IV/III) / V
$[ReCl_6]^{3-/2-}$	-1.17
$[ReCl_5An]^{2-/1-}$	-0.43
$[ReCl_5Pn]^{2-/1-}$	-0.49
$[ReCl_5By]^{2-/1-}$	-0.50
$*[ReCl_5Py]^{2-/1-}$	-0.54
$*[ReCl_5Bn]^{2-/1-}$	-0.37

Table 3.29 Half-wave potentials for $[ReCl_5L]^{z-}$, L = Cl^-, An, Pn, By, Py, Bn. *Ref. 49

The uv-vis spectra and *in situ* spectroelectrochemical reduction of $[ReCl_5By]^{2-/1-}$ at 223 K are shown in **Figure 3.42**. The transitions, as may be expected, are of similar energy to $[ReCl_6]^{3-/2-}$ but are of a broader, less defined nature. On reduction, all bar one of the transitions shift to higher energy and are assigned as $Cl^-\pi \rightarrow Re(IV/III)d\pi$. An interesting observation is the small, broad absorption band growing in *ca.* 26000 cm^{-1}, illustrated most clearly in the spectroelectrochemical reduction. This band cannot be attributed to a LMCT since it would be expected to have shifted to higher energy. Liu has observed transitions at 24250 cm^{-1} and 18520 cm^{-1} in $[ReCl_5Py]^{2-}$ assigned as $Re(III)d\pi \rightarrow \pi^*$ transitions. No transition is observed below 20000 cm^{-1} for $[ReCl_5By]^{2-}$, however the transition at 26000 cm^{-1} is also tentatively assigned as $Re(III)d\pi \rightarrow \pi^*$. $[ReCl_5Py]^{2-}$ showed stronger absorption in the MLCT transitions than $[ReCl_5By]^{2-}$. The difference is perhaps a reflection of the π-accepting properties of the ligands as eluded to for $[OsCl_5L]^{2-/1-}$. However, an alternative

assignment would be to a $d\pi \rightarrow d\sigma$ transition. Full transition band maxima, molar extinction coefficients, and assignments are given in **Table 3.30**.

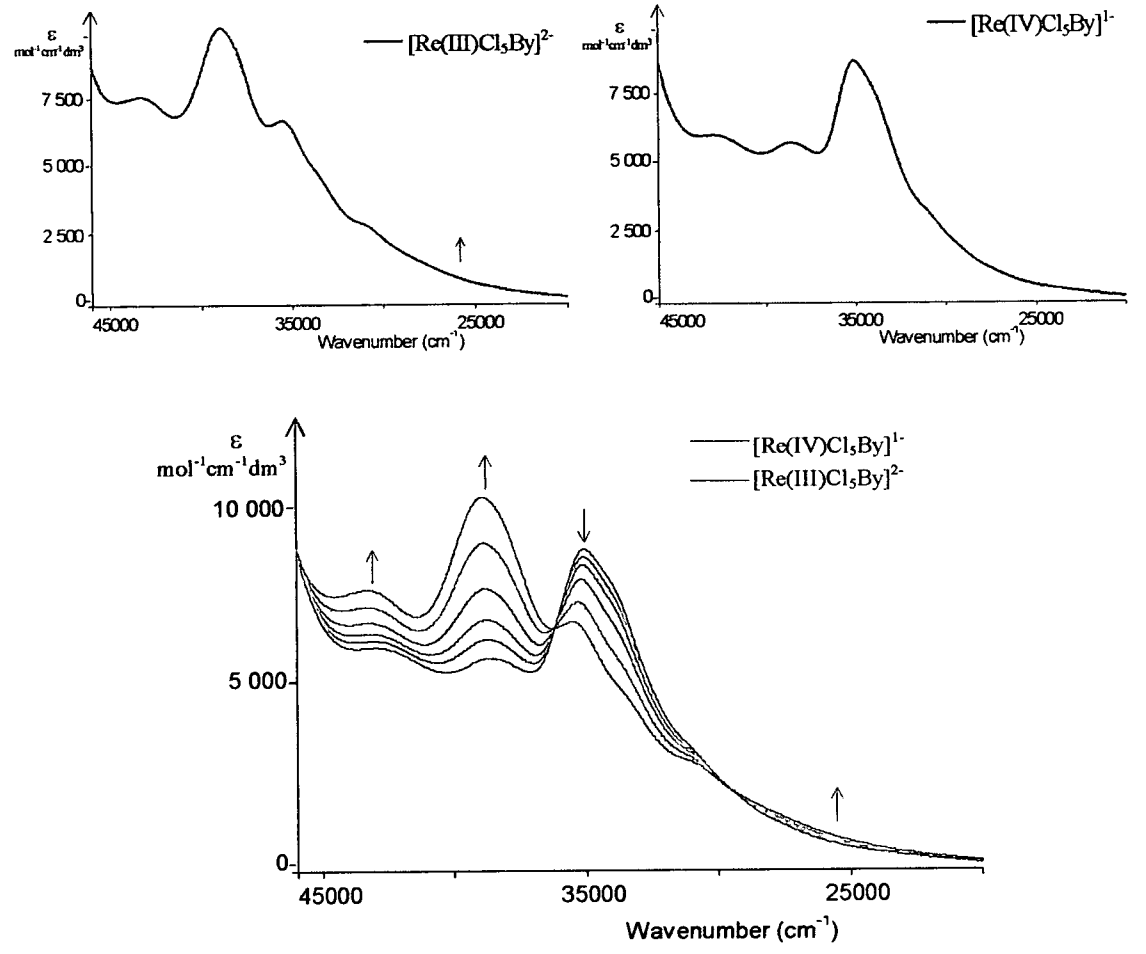

Figure 3.42 Uv-vis spectra and *in situ* spectroelectrochemical reduction of $[ReCl_5By]^{3-/2-}$ in 0.1 M $[N^nBu_4]BF_4$/By at 223 K, electrogeneration potential –1.45 V

Complex	Peak max (cm^{-1})	ε / mol^{-1} cm^{-1} dm^3	Assignment
$[Re(IV)Cl_6]^{2-}$	31 095	2 400	$Cl^-\pi \rightarrow Re(IV)d\pi$
	33 600sh	6 700	$Cl^-\pi \rightarrow Re(IV)d\pi$
	35 310	13 800	$Cl^-\pi \rightarrow Re(IV)d\pi$
	37 885	6 800	$Cl^-\pi \rightarrow Re(IV)d\pi$
$[Re(III)Cl_6]^{3-}$	28 000sh	1 000	$Re(III)d\pi \rightarrow Cl^-\pi^*$
	38 925	2 900	$Cl^-\pi \rightarrow Re(III)d\pi$
	40 990	10 300	$Cl^-\pi \rightarrow Re(III)d\pi$
	43 280	13 800	$Cl^-\pi \rightarrow Re(III)d\pi$
$[Re(IV)Cl_5By]^{1-}$	34 095sh	7 900	$Cl^-\pi \rightarrow Re(IV)d\pi$
	35 085	8 900	$Cl^-\pi \rightarrow Re(IV)d\pi$
	38 625	5 600	$Cl^-\pi \rightarrow Re(IV)d\pi$
	42 840	5 900	$Cl^-\pi \rightarrow Re(IV)d\pi$
$[Re(III)Cl_5By]^{2-}$	26 000sh	1 500	$Re(III)d\pi \rightarrow \pi^*$
	31 095	2 600	$Cl^-\pi \rightarrow Re(III)d\pi$
	35 085	6 700	$Cl^-\pi \rightarrow Re(III)d\pi$
	38 900	10 400	$Cl^-\pi \rightarrow Re(III)d\pi$
	43 305	7 700	$Cl^-\pi \rightarrow Re(III)d\pi$

Table 3.30 Transition maxima, molar extinction coefficients, and assignments for $[ReCl_5L]^{z-}$

3.3.3.6 Rate constants for the substitution reactions of $[ReCl_6]^{3-}$

Because of the very reactive nature of $[ReCl_6]^{3-}$ even at low temperatures rate constants over a suitable range of temperatures could not be measured in order to calculate the activation energy for this process. The rate constant has been measured at 244 ± 48 s^{-1} at 250 K in 0.1 M $[N^nBu_4]BF_4$/butyronitrile, cooled in a $N_{2(l)}$/iso-pentane bath. This is clearly a much faster reaction than for either $[OsCl_6]^{3-}$ or $[IrCl_6]^{3-}$.

3.4 Conclusions

The metal hexahalides of rhenium, osmium, and iridium display similar redox behaviours. Half-wave potentials for the complexes of the type $[MX_5Y]^{z-}$ (M = Re, Os, Ir; X = Cl^-, Br^-, I^-; Y = Cl^-, Br^-, I^-; An, Pn, By, Py, Bn, Bc) are given in **Table 3.31**. The half-wave potentials follow the same positive shift for all series studied on substitution of a halide for a nitrile which stabilises the metal(III) oxidation state. Stepwise stabilisation of the metal centre is observed within the nitriles depending on their σ-donor abilities. It is noted that the change in half-wave potential for the IV/V redox couple (when observed) on substitution of a nitrile for a halide is less significant (*ca.* 0.4 V positive) than for the IV/III redox couple (*ca.* 0.6 V). Clearly the metal centre is more capable of supporting the electron donation from the halide in the higher oxidation state.

Figure 3.43 shows the uv-vis spectra for the complexes $[MX_6]^{z-}$ in the metal (III) and (IV) oxidation states. The complexes show characteristic LMCT transitions from different halide π-orbitals in both oxidation states. The LMCT transitions shift to higher energy, M(III) > M(IV), Re > Os > Ir, and Cl^- > Br^- > I^-. $d\pi \rightarrow d\sigma$ transitions are observed in d^6 electronic configuration complexes in the range 20000 cm^{-1} to 30000 cm^{-1}; in the other complexes they are presumably masked by stronger absorption bands. The spectra become more complex going down the halide group which may be attributed to increased spin orbit coupling as the halide ligands become heavier.

Redox Couple	IV/III	V/IV		III/II	IV/III	V/IV		IV/III	V/IV
$[ReCl_6]^{z-}$	-1.17	1.33	$[OsCl_6]^{z-}$	x	-0.57	1.38	$[IrCl_6]^{z-}$	0.12	1.87
$[ReCl_5An]^{z-}$	-0.43	1.72	$[OsCl_5An]^{z-}$	x	0.10	1.89	$[IrCl_5An]^{z-}$	0.80	x
$[ReCl_5Pn]^{z-}$	-0.49	1.70	$[OsCl_5Pn]^{z-}$	x	-0.03	1.82	$[IrCl_5Pn]^{z-}$	0.79	x
$[ReCl_5By]^{z-}$	-0.50	1.69	$[OsCl_5By]^{z-}$	x	-0.08	1.80	$[IrCl_5By]^{z-}$	0.79	x
*$[ReCl_5Py]^{z-}$	-0.54	1.71	$[OsCl_5Vn]^{z-}$	x	-0.10				
*$[ReCl_5Bn]^{z-}$	-0.37	1.73	$[OsCl_5Py]^{z-}$	-1.53	-0.02	1.83	$^{f}[IrCl_5]^{z-}$	0.56	
			$[OsCl_5Bn]^{z-}$	$^{\$}$-1.24	0.04	1.85			
			$[OsCl_5Bc]^{z-}$	x	0.05	1.87			
			$[OsBr_6]^{z-}$	x	-0.39	1.38	$[IrBr_6]^{Z-}$	0.18	1.65i
			$[OsBr_5An]^{z-}$	x	0.16	x	$[IrBr_5An]^{z-}$	0.79	x
			$[OsBr_5Pn]^{z-}$	x	0.06	x	$[IrBr_5Pn]^{z-}$	0.77	x
			$[OsBr_5By]^{z-}$	x	0.02	x	$[IrBr_5By]^{z-}$	0.76	x
			$[OsBr_5Py]^{z-}$	x	0.10	1.72			
			$[OsI_6]^{z-}$		-0.31	0.90i			
			$[OsI_5An]^{z-}$		0.18				
			$[OsI_5Pn]^{z-}$		0.17				
			$[OsI_5By]^{z-}$		0.16				
			$^{\$}[OsI_5Py]^{z-}$		0.04				

Table 3.31 Half-wave potentials for the complexes of the type $[MX_5Y]^{z-}$ (M = Re, Os, Ir, X = Cl^-, Br^-, I^-; Y = Cl^-, Br^-, I^-; An, Pn, By, Py, Bn, Bc) in 0.5 M $[N^nBu_4]BF_4$/dichloromethane at 223 K. Reference electrode = Ag/AgCl. x = no redox couple observed in potential window of ± 1.9 V. i = irreversible: potential given as $E_p^{ox/red}$. *ref 49. $^{\$}$ref 21. ^{f}ref 42.

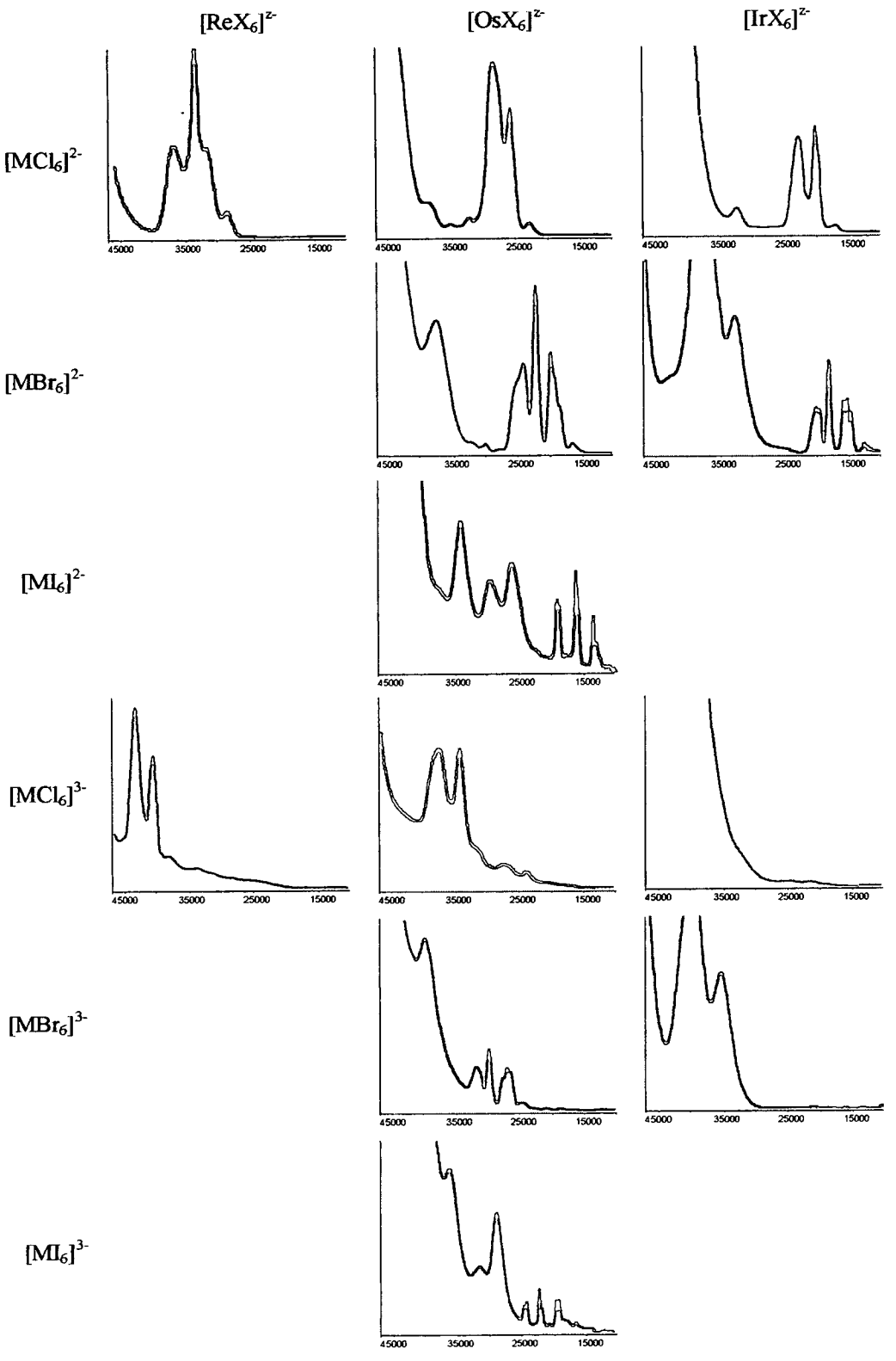

Figure 3.43 Uv-vis spectra of $[MX_6]^{z-}$, (M = Re, Os, Ir; X = Cl^-, Br^-, I^-) in 0.5 M $[N^nBu_4]BF_4$/dichloromethane. The x-axes are in wavenumbers (cm^{-1}) and Y-axes are the extinction coefficient, ε (mol^{-1} cm^{-1} dm^3); for exact values *vide supra*

The rate constants and activation energies of $[MX_6]^{3-}$ for the substitution reaction with butyronitrile are given in **Table 3.32** and illustrated in the Arrhenius plot, **Figure 3.44**. The iridium hexahalides exhibit similar activation energies to their osmium analogues. Ir(III) has a higher nuclear charge than Os(III) which is more able to balance the electron donation from the halides. In addition, Ir(II) has a d^6 electronic configuration which has a maximum ligand field stabilisation energy and therefore will be more inert than Os(III). The rate of reaction, taken to be the rate of halide loss from the six co-ordinate, metal(III) species, is slower for Ir(III) than for Os(III) reflecting the increase in stability of Ir(III). The five co-ordinate intermediate, $[IrCl_5]^{2-}$, may be observed electrochemically and by EXAFS. Although the five co-ordinate intermediate $[OsCl_5]^{2-}$ has not been directly observed, the very similar behaviour of the Ir and Os hexahalide complexes indicate that such an intermediate is involved in the reduction-induced substitution reactions of $[OsX_6]^{2-}$.

	$^{1}[ReCl_6]^{z-}$	$[OsCl_6]^{z-}$	$[IrCl_6]^{z-}$
k_{298}	244 ± 48	0.51 ± 0.14	0.09 ± 0.02
E_a		55.1 ± 0.7	57.7 ± 1.4
		$[OsBr_6]^{z-}$	$[IrBr_6]^{z-}$
k_{298}		22.1 ± 0.9	0.37 ± 0.04
E_a		65.1 ± 1.0	66.9 ± 1.0
		$^{*}[OsI_6]^{z-}$	
k_{198}		134 ± 8	
E_a		4.0 ± 0.4	

Table 3.32 Rate constants and activation energies for the substitution reaction of $[MX_6]^{3-}$ and butyronitrile in 0.1M $[N^nBu_4]BF_4$/By. ^{1}170 K, *198 K.

The rate constants show a very small dependence on the incoming nucleophile. The activation energies for the substitution reaction of acetonitrile, propionitrile, and butyronitrile, however, are the same, within experimental error, for each individual complex, $[OsBr_6]^{3-}$, $[OsI_6]^{3-}$, $[IrCl_6]^{3-}$, and $[IrBr_6]^{3-}$. Evidence of a five co-ordinate intermediate describes a Dissociative mechanism, by its nature insensitive to the incoming nucleophile. The difference in rate constant between nitriles must therefore be attributed to the rate of solvation of the halide in dichloromethane.

Although only the rate constant at 170 K has been measured for $[ReCl_6]^{3-}$, it is clear it is considerably more reactive than the osmium and iridium analogues. It would appear the lower nuclear charge of rhenium is unable to support the electron density from the halides and loses a chloride very rapidly.

The activation energy is understood to be the energy required to cleave the metal-halide bond and the bond strength is understood to represent the extent of orbital overlap between the metal and halide. The Van der Waals radii of iridium(III) and osmium(III) are of similar size (1.35 Å and 1.36 Å respectively) and, as may be expected, both species have very similar activation energies; $[IrCl_6]^{3-}$ is 2.6 kJ mol^{-1} higher than $[OsCl_6]^{3-}$, while $[IrBr_6]^{3-}$ and $[OsBr_6]^{3-}$ are the same within experimental error. The nephelauxetic parameter, β, for $[IrCl_6]^{3-}$ and $[IrBr_6]^{3-}$ of 0.37 and 0.30 respectively indicates a very covalent character to the metal-halide bond reflecting a high overlap of the metal and halide orbitals (or from a molecular orbital view point; an orbital shared between both the metal and ligand). The lower value for the bromide complex than the chloride shows a better orbital overlap in the iridium-bromide bond mirrored by a higher activation energy for the reaction.

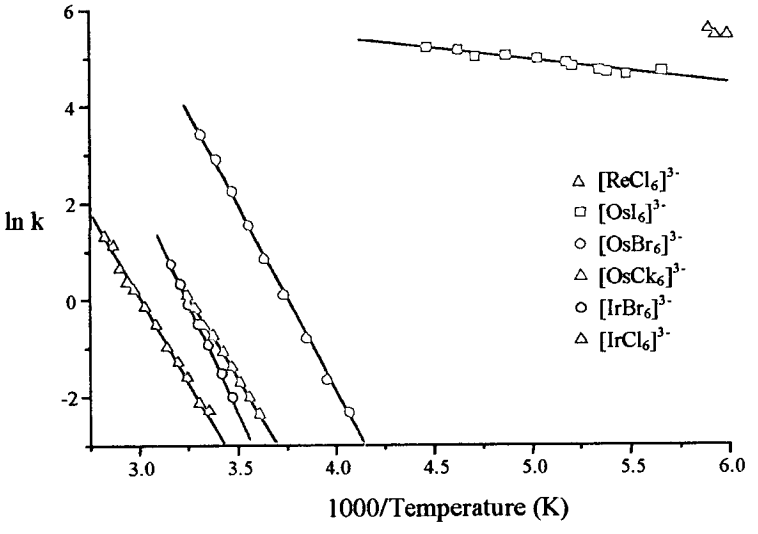

Figure 3.44 Arrhenius plots for the substitution reactions of $[MX_6]^{3-}$ with butyronitrile

Experimental evidence supports the claim that the substitution reaction proceeds by a Dissociative mechanism or dissociative Interchange mechanism. The rate constant and activation energy is largely independent of the incoming nucleophile. The small

difference in rate constant with L suggests a dependence on the solvation of halide or the formation of an outer-sphere association between the complex and entering ligand (the solvent). Only $[OsCl_6]^{3-}$ displays different activation energies (out with experimental error) for different incoming ligands L. Overall a Dissociative mechanism could be assigned to the reduction-induced substitution reaction of $[MX_6]^{2-}$ (**Scheme 3.3**).

$$[MX_6]^{2-} \xrightarrow{\text{fast}} [MX_6]^{3-} \underset{k_{-1}}{\overset{k_1}{\rightleftharpoons}} [MX_5]^{2-} + X^- \underset{k_{-2}}{\overset{k_2}{\rightleftharpoons}} [MX_5L]^{2-}$$

Scheme 3.3

The only exception would be for $[OsCl_6]^{2-}$ whose mechanism could be understood to take on more I_d character with the formation of an outer-sphere association with L.

3.5 References

[1] Wilkins, R. G.; *The Study of Kinetics and Mechanism of Reactions of Transition Metal Complexes*, Allyn and Bacon, Inc., Boston, 1974.
[2] Greenwood, N.N.; Earnshaw, A.; *Chemistry of the Elements*, 1st edition, Pergamon Press, 1984
[3] Campbell, N. J.; Davis, V. A.; Griffith, W. A.; Townend, T. J.; *J. Chem. Soc., Dalton Trans.*, 1985, 1673
[4] Heath, G. A.; Moock, K. A.; Sharp, D. W. A.; Yellowlees, L. J.; *J. Chem. Soc., Chem. Commun.*, 1985, 1503
[5] Robinson, P. D.; Hinckely, C. C.; Matusz, M.; Kibala, P. A.; *Acta. Cryst.*, 1988, **C44**, 619
[6] Jørgensen, C. K.; *Mol. Phys* 1959, **2**, 309
[7] Allen. G. C.; Al-Mobarak, R.; El-Sharkawy, A. M.; Warren, K. D.; *Inorg. Chem.*, 1972, **11(4)**, 787
[8] Robinson, P. D.; *Acta Cryst.*, 1988, **C44**, 619
[9] Kennedy, B. J.; Heath, G. A.; *Inorg. Chem.*, 1990, **29**, 1271
[10] a) Champness, N. R.; Levason, W.; Mould, R. A. S.; Pletcher, D.; Webster, M.; *J. Chem. Soc., Dalton Trans.*, 1991, 2777
b) Levinson, J. D.; Robinson, S. D.; *Inorg. Chem. Soc.*, 1970, **A**, 2947
[11] Harris, A. D.; Robinson, S. D.; *Inorg. Chim. Acta*, 1980, **35**, 25
[12] Preetz, W.; Semrau, M.; *Z. Anorg. Allg. Chem.*, 1995, **621(5)**, 725
[13] Pearson, J.; Cooke, J.; Takats, J.; Jordan, R.B.; *J.Am. Chem. Soc.* 1998, **120**, 1434
[14] Zerbe, H. D.; Preetz, W.; *Z. Anorg. Allg. Chem.*, 1983, **484**, 33
[15] Maiboroda, A.; Rheinwald, G.; Lang, H.; *Inorg. Chem.*, 2000, **39**, 5725
[16] Hasenpusch, W.; Preetz, W.; *Z. Anorg. Allg. Chem.*, 1977, **432**, 107
[17] Preetz, W.; Walter, H. J.; *Z. Anorg. Allg. Chem.*, 1973, **402**, 169
[18] Preetz W., Steinebach, H. J.; *Z. Anorg. Allg. Chem.*, 1985, **40(B)**, 745
[19] Komozin, P. N.; *Russ. J. Inorg. Chem.* 2000, **45**, 589
[20] a) Sun, I.W.; Ward, E.H.; Hussey, C.L.; *J. Electrochem. Soc.*, 1988, **135**, 3035
b) Heath, G. A.; Humphery, D. G.; *J. Chem. Soc., Chem. Comm.*, 1991, **23**, 1668
[21] Taylor, K.; *PhD Thesis, University of Edinburgh*, 1990
[22] Taylor, K. J.; Yellowlees, L. J.; *Molecular Electrochemistry of Inorganic, Bioinorganic and Organometallic Compounds*, Pombeiro, A.J.L. and McCleverty, J. A.(Eds.), Kluwer Academic Publishers, London, 1993, NATO ASI Series 385, 69
[23] Lever, A. B. P.; *Inorg. Chem.*, 1990, **29**, 1271
[24] Duff, C. M.; Heath, G. A.; *J. Chem. Soc., Dalton Trans.*, 1991, 2401
[25] Duff, C. M.; Heath, G. A.; *Inorg. Chem.*, 1991, **30**, 2528
[26] Commbe, V. T.; Heath, G. A.; Stevenson, T. A.; Whitelock, J. D.; Yellowlees, L. J.; *J. Chem. Soc., Dalton Trans.*, 1985, 2401
[27] Brown, A. R.; Elliot, M.; Macnamara, K. G.; Taylor, K. J.; Yellowlees, L. J.; *in press*
[28] Owen, J.; Stevens, K. W. H.; *Nature*, 1953, **171**, 836
[29] Cipriano, R. A.; Levason, W.; Mould, R. A. S.; Pletcher, D.; Powell, N. A.; *J. Chem. Soc., Dalton Trans.*, 1988, 2677
[30] Cecil, R.; Fear, A. J.; Littler, J. S.; *J. Chem. Soc.*, 1970, **B**, 632
[31] Sun, I.W.; Ward, E. H.; Hussey, C. L.; Seddon, K. R.; Turp, J. E.; *Inorg. Chem.*, 1987, **26**, 2140
[32] Bottger, G. L.; Salwin, E.A.; *Spectrochim. Acta*, 1972, **28(A)**, 925
[33] Fine, D. A.; *Inorg. Chem.*, 1969, **8**, 1014
[34] Fergusson, J. E.; Rankin, D. A.; *Aust. J. Chem.*, 1983, **36**, 863
[35] Delphine, M.; *Bull. Soc. Chim. Fr.*, 1911, 4SER, **9**, 711
[36] Sloth, E. N.; Garner, C. S.; *J. Chem. Phys.*, 1954, **22**, 2064
[37] Poulsen, I. A.; Garner, C. S.; *J. Am. Chem. Soc.*, 1962, **84**, 2032
[38] Chang, J. C.; Garner, C. S.; *Inorg. Chem.*, 1965, **4**, 209

[39] El-Awady, A. A.; Bounsall, E. J.; Garner, C. S.; *Inorg. Chem.*, 1967, **6**, 79
[40] Bauer, R. A.; Basolo, F.; *Inorg. Chem.*, 1969, **8**, 2237
[41] Campbell, N. J.; Davis, V. A.; Griffith, W. P.; Townend, T. J.; *J. Chem. Soc., Dalton Trans.*, 1985, 1673
[42] Brown, A. R.; Mosselmanns, W. F. J.; Taylor, K. J.; White, M.; Yellowlees, L. J.; *in press*
[43] Steinbach, H. J.; Preetz, W.; *Z. Anorg. Allg. Chem.*, 1985, **530**, 155
[44] a) Preetz, W.; Kelm, W.; *Z. Anorg. Allg. Chem.*; 1985, **531**,
b) Yao, O.; Maverick, A. W.; *Inorg. Chem.*; 1988, **27**, 1669
[45] Takazawa, H.; Ohba, S.; Saito, Yoshihiko; S.M.; *Acta Crystallogr.: Struct. Sci.;* 1990, **46 (B)**; 166
[46] Cotton, F. A.; *Chem. Soc. Rev.*, 1975, **4**, 27
[47] Barder, T. J.; Walton, R. A.; *Inorg. Chem.*; 1982, **21**, 2510
[48] Kelm, W.; Preetz, W.; *Z. Anorg. Allg. Chem.*, 1989, **568**, 117
[49] Liu, X.; PhD Thesis, University of Edinburgh, 1998.
[50] Fisher, A. C.; *Electrode Dynamics*, Oxford Chemistry Primers, Oxford University Press, 1996
[51] Magnuson, R. H.; *Inorg. Chem.*, 1984 **23**, 387
[52] Duff, C. M.; Heath, G. A.; *J. Chem. Soc. Dalton Trans.* 1991, **9**, 2401
[53] Murrel, J. N.; Kettle, S. F. A.; Tedder, J. M.; *The Chemical Bond*, John Wiley and Sons, New York, 1978
[54] Frost, A. A.; Pearson, R. G.; *Kinetics and Mechanism*, Second Edition, John Wiley and Sons, New York, 1961
[55] Shriver, D. F.; Atkins, P. W.; Langford, C. H.; *Inorganic Chemistry*, Oxford University Press, Oxford, 1990
[56] Kettle, S. F. A.; *Physical Inorganic Chemistry*, Spektrum, University Science Books, California, 1996
[57] Bond, A. M.; Coomber, D. C., Feldberg, S. W.; Oldham, K. B.; Vu, T.; *Anal. Chem.* 2001, **73**, 352
[58] Rudloph, M.; Reddy, D. P.; Feldberg, S. W.; *Anal. Chem.*, 1994, **66**, 589A
[59] Bond, A.; Feldberg, S. W.; *J. Phys. Chem. B*; 1998, **102**, 9966
[60] Lever, A. P. B.; *Inorganic Electronic Spectroscopy*, 2nd Edition, 1984, Elsevier
[61] Bowyer, W. J.; Enelman, E. E.; Evans, D. H.; *J. Electroanal. Chem.*, 1989, **262**, 67
[62] Tobe, M. L.; *Inorganic Reaction Mechanisms*, Thomas Nelson and Sons Ltd, London, 1972
[63] Weast, R. C.; *Handbook of Chemistry and Physics*, CRC Press, Cleveland, Ohio, 55th Edition, 1974
[64] Preetz, W.; Krull, A.; *Z. Naturforschung*, 1997, **52(3)**, 315
[65] Bard, A. J.; Faulkner, L. R.; *Electrochemical Methods, Fundamentals and Applications*, John Wiley & Sons, New York, 1980
[66] Brown, A. R; Taylor, K. J.; Yellowlees, L. J.; *J. Chem. Soc., Dalton Trans.*, 1998, **14**, 2401

CHAPTER FOUR:

The Influence of Electrolyte on Substitution Reactions of Osmium(III) Hexachloride

4 The Influence of Electrolyte on the Substitution Reactions of Osmium(III) Hexachloride

4.1 Introduction

The literature contains a number of examples where the rate of homogeneous electrochemical reactions affected by the concentration and the type of supporting electrolyte.[1,2,3] However, the current understanding of the effects of supporting electrolyte on a homogeneous chemical reaction following an electrochemical reaction is poor. In this chapter the rate constant for the reduction-induced reaction of $[OsCl_6]^{2-}$ with L is investigated with a variety of different concentrations and types of supporting electrolyte.

Electrochemical reactions with little, or without, deliberate excess of inert supporting electrolyte have recently come under some study.[4,5,6] The addition of electrolyte (usually in a 50 to 100 fold excess to electroactive species) increases electrical conductivity of the solvent, suppresses migration currents, and establishes a well defined double layer.[7] There are, however, a number of reasons why experiments with little or no added electrolyte are desirable, 1) to obtain data that may be validly compared with those obtained from non-electrochemical analysis where no electrolyte was added, and 2) to minimise complications associated with electrolyte including ion pairing and ionic strength effects.

It is now well documented, both experimentally and theoretically, that problems involved with high resistance and migration can be tolerated under steady state conditions at microelectrodes and even macroelectrodes.[5] When the electroactive species is charged, i.e., an ion, there is no inherent reason why supporting electrolyte is required in voltammetric experiments.[8] The electro-active ion and its counter ion

can provide the means whereby current may be carried through the cell. Ionic strength is defined by,

$$\mu = \frac{1}{2}\sum_i z_i^2 c_i$$

where z_i is the charge and c_i is the concentration of the i^{th} ion. It clearly follows that a charged ionic species can have appreciable ionic strength although some resistance in solution and mass transport by migration and convection arising from density gradients can still remain. Providing the complexities associated with enhanced resistance and mass transport are considered, however, electrochemistry is a viable technique for studies of multiply charged electroactive species without added electrolyte. Some analysis can be simplified by invoking the principle that for any electrochemical experiment, where diffusion coefficients of all the solute species do not differ significantly from a common value, the total solute concentration remains uniform and constant. This principle applies to both transient and steady state regimes and is independent of the cell and electrode geometry and is not compromised by mass transport.

In this chapter double-step chronoamperometry has been used to study the reduction-induced substitution reaction of $[N^nBu_4]_2[OsCl_6]$ with benzyl cyanide. The concentration of supporting electrolyte, $[N^nBu_4]BF_4$, has been varied from as much as 0.4 M to no electrolyte. The $[OsCl]^{z-}$ species is charged so that the problem of mass transport in the form of migration and convection from density gradients is negated in little or no electrolyte. The overall ionic strength of the solution is constant throughout the substitution process. Although resistance encountered in cyclic voltammetry is higher in low concentrations of electrolyte, the chronoamperometric technique is unaffected, as it is independent of internal resistance (see 2.2). Jaworski *et al* have simulated experimental chronoamperometric responses under little and no electrolyte conditions.[6] The results obtained showed the measured current continues to be diffusion controlled under these conditions. The time scale of the chronoamperometric experiment, at fastest 0.01 seconds, is much

slower than the time necessary to reach an equilibrium so that a steady state regime can be accepted.

The effect of various types of supporting electrolyte has come under some scrutiny in respect to modified electrodes. Catalytic activity of Ti/RuO_2 and Ti/IrO_2 electrodes was found to be independent of the size of the supporting electrode cation.[9] Electrochemical behaviours, such as redox potential, wave shape and peak current were found to change for osmium polymer electrodes with different electrolytes depending on the electrolyte anions and their hydrophobicity.[10] A report of the electrochemical reduction behaviour of TCNQ and TCNE to their anions and dianions reveals some dependence on the supporting electrolyte for the second reduction of TCNE.[11] The reversibility of the $TCNE^{2-/1-}$ redox couple is dependent upon the electrolyte. The rate constant decreases for the reduction as the size of cation increases.

Overall, however, there has been very little attention paid in the literature to the role of what have been thought of as "inert" electrolytes, especially for chemical reactions following an electrochemical redox process (an EC process). For this reason, a study of the reduction-induced substitution reaction of $[N^nBu_4]_2[OsCl_6]$ with acetonitrile with a number of supporting electrolytes, $[N^nBu_4]BF_4$, $[N^nBu_4]Cl$, $NaBF_4$, and Adogen 464, has been made using the double-step chronoamperometry technique.

4.2 Experimental

All solvents were purified and dried as outlined in 3.2.1. $[N^nBu_4]_2[OsCl_6]$ and $[N^nBu_4]BF_4$ were prepared as outlined in 3.2.2. Tetrabutylammonium chloride (Fluka, >99 %) and sodium tetrafluoroborate (Acros, 98 %) were dried under vacuum for at least 48 hours. Adogen 464 (methyltrialkyl(C_8-C_{10})ammonium chloride) (Acros) was found to be very hygroscopic and dried for 7 days under vacuum. A strictly water-free environment was maintained throughout the experimental procedure.

4.3 Results and Discussion

4.3.1 Electrolyte Concentration

The rate constants for the pseudo first order reduction-induced substitution reaction of $[OsCl_6]^{2-}$ in benzyl cyanide with concentrations of 0.4 M, 0.1 M, 0.05 M, 0.01 M, 0.001 M and zero $[N^nBu_4]BF_4$ as supporting electrolyte have been measured by double-step chronoamperometry. The concentration of $[N^nBu_4]_2[OsCl_6]$ was kept at 0.0020 M ± 0.0002. The activation energy, E_a, for the reaction for each concentration has been calculated from the Arrhenius plots of rate constants over a range of temperatures (290 K to 320 K) (**Figure 4.1**). The activation energies are tabulated along with the rate constant at 298 K in **Table 4.1**. The rate constants at 298 K were read from the linear regression fit from the Arrhenius plots of lnk against 1/temperature. Errors in rate constant, k, were calculated from the average error for each point determined from the average measured value for each experiment and the statistical errors involved in their calculation. The errors given for E_a are the standard deviations from the linear regression fits. Note that these results were obtained under a strictly water-free environment.

Conc. $[N^nBu_4]BF_4$	k_{298K} / s^{-1}	E_a kJ mol^{-1}
0	0.20 ± 0.03	68.0 ± 2.4
0.001M	0.17 ± 0.03	68.1 ± 2.4
0.01M	0.16 ± 0.02	69.5 ± 1.8
0.05M	0.13 ± 0.02	70.2 ± 2.2
0.1M	0.12 ± 0.01	65.3 ± 2.5
0.4M	0.11 ± 0.01	66.7 ± 1.5

Table 4.1 Rate constant at 298 K and activation energy for the reduction-induced substitution reaction of $[OsCl_6]^{2-}$ in benzyl cyanide for various concentrations of supporting electrolyte $[N^nBu_4]BF_4$

An increase in the concentration of supporting electrolyte decreases the rate constant from 0.20 s^{-1} to 0.11 s^{-1} for zero added electrolyte and 0.4 M electrolyte respectively.

The activation energy remains constant for the reaction within experimental error, on average 68.0 kJ mol^{-1}.

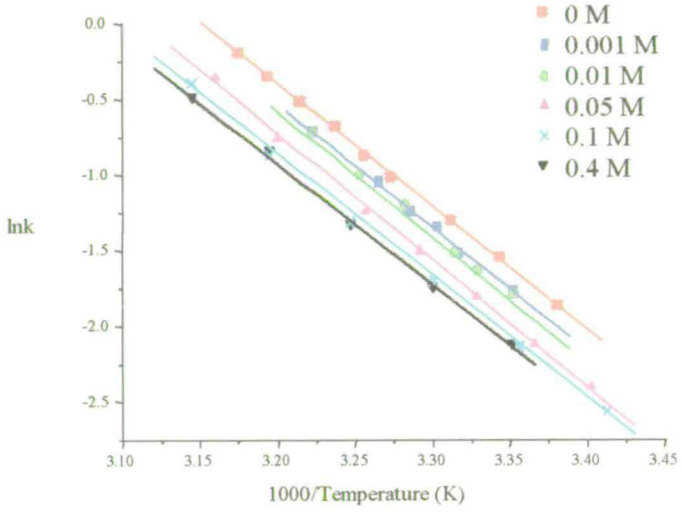

Figure 4.1 Arrhenius plots for the reduction-induced substitution reaction of $[OsCl_6]^{2-}$ in benzyl cyanide with various concentrations of supporting electrolyte $[N^nBu_4]BF_4$

The rate limiting step for the reduction-induced substitution reaction of $[OsCl_6]^{2-}$ where one chloride is replaced by a ligand, L, of less electron donating ability has been previously established as the rate of chloride dissociation (see chapter 3). The activation energy for the process is that required to cleave the Os-Cl bond and the mechanism is predominantly dissociative in nature. As the activation energy stays constant for the reaction it is surmised that the reaction mechanism is unchanged by the change of supporting electrolyte concentration. The rate has been shown in 3.3.1.3 to have a slight influence on the rate at which the free chloride can solvate in different solvents. In this case the rate constant decreases with increasing ionic strength of the solution as the supporting electrolyte concentration is increased from zero to 0.4 M although 0.20 s^{-1}, with an experimental error of ± 0.03, by three standard deviation is the same as 0.11 s^{-1}. Therefore, it is concluded that the rate constant is also little affected by the concentration of supporting electrolyte present.

The activation energy remains constant for the reaction within experimental error, on average 68.0 kJ mol^{-1}.

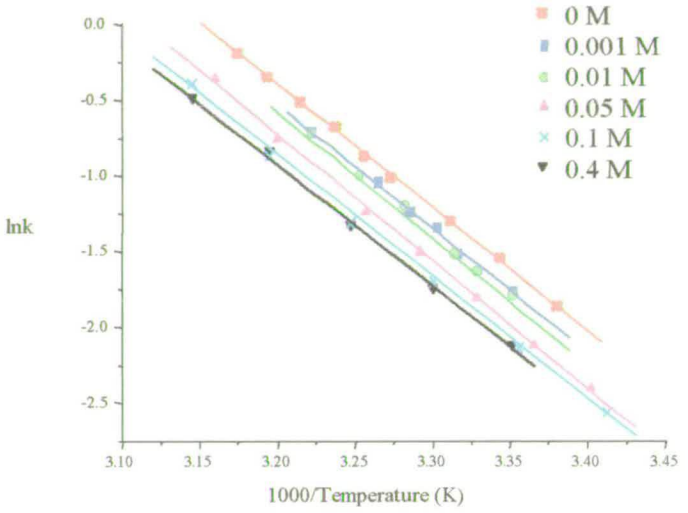

Figure 4.1 Arrhenius plots for the reduction-induced substitution reaction of $[OsCl_6]^{2-}$ in benzyl cyanide with various concentrations of supporting electrolyte $[N^nBu_4]BF_4$

The rate limiting step for the reduction-induced substitution reaction of $[OsCl_6]^{2-}$ where one chloride is replaced by a ligand, L, of less electron donating ability has been previously established as the rate of chloride dissociation (see chapter 3). The activation energy for the process is that required to cleave the Os-Cl bond and the mechanism is predominantly dissociative in nature. As the activation energy stays constant for the reaction it is surmised that the reaction mechanism is unchanged by the change of supporting electrolyte concentration. The rate has been shown in 3.3.1.3 to have a slight influence on the rate at which the free chloride can solvate in different solvents. In this case the rate constant decreases with increasing ionic strength of the solution as the supporting electrolyte concentration is increased from zero to 0.4 M although 0.20 s^{-1}, with an experimental error of ± 0.03, by three standard deviation is the same as 0.11 s^{-1}. Therefore, it is concluded that the rate constant is also little affected by the concentration of supporting electrolyte present.

4.3.2 Electrolyte Type

The rate constants for the reduction-induced substitution reaction of $[OsCl_6]^{2-}$ with 0.05 M Y/acetonitrile, where Y = $NaBF_4$, $[N^nBu_4]BF_4$, $[N^nBu_4]Cl$, and Adogen 464, as supporting electrolyte have been measured by double-step chronoamperometry. The activation energy, E_a, for the reaction with each electrolyte has been calculated from the Arrhenius plots of rate constants over a range of temperatures (240 K to 300 K) (**Figure 4.2**). The activation energies are tabulated along with the rate constant at 298K in **Table 4.2**. The rate constants at 298 K were determined from the linear regression fit from the Arrhenius plots of lnk against 1/T. Errors in rate constant, k, were calculated from the average error for each point determined from the average measured value for each experiment and the statistical errors involved in their calculation. The errors given for E_a are the standard deviations from the linear regression fits. Note that these results were measured under a strictly water-free environment. A concentration of 0.05 M supporting electrolyte was used to ensure a high as possible solvation of each electrolyte in solution and therefore maintaining an almost constant ionic strength, μ ($\mu = \frac{1}{2}\sum_i z_i^2 c_i$, where z_i is the charge and c_i is the concentration of the i^{th} ion).

Electrolyte, Y	k_{298K} / s^{-1}	E_a kJ mol^{-1}
$NaBF_4$	42.7 ± 1.2	56.8 ± 2.2
$[N^nBu_4]BF_4$	2.01 ± 0.21	51.9 ± 2.0
$[N^nBu_4]Cl$	0.82 ± 0.10	53.9 ± 0.9
Adogen-464	0.30 ± 0.12	52.1 ± 1.6

Table 4.2 Rate constant at 298 K and activation energy for the reduction-induced substitution reaction of $[OsCl_6]^{2-}$ in 0.05 M Y/An, where Y = $NaBF_4$, $[N^nBu_4]BF_4$, $[N^nBu_4]Cl$, and Adogen 464, as supporting electrolyte

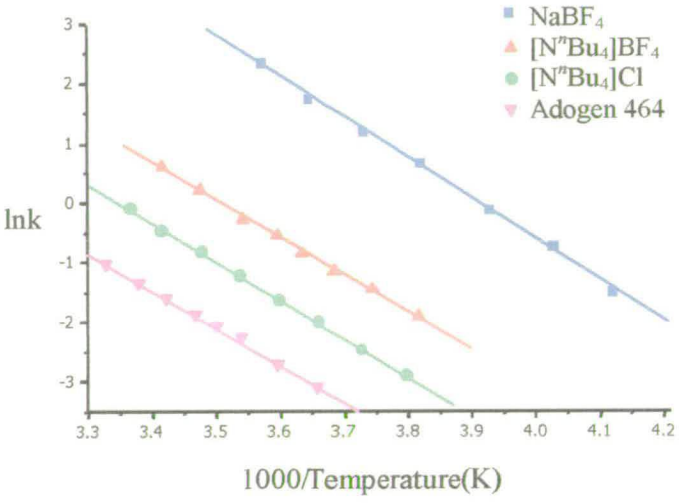

Figure 4.2 Arrhenius plots for the reduction-induced substitution reaction of $[OsCl_6]^{2-}$ in 0.05 M Y/An, where Y = $NaBF_4$, $[N^nBu_4]BF_4$, $[N^nBu_4]Cl$, and Adogen 464, as supporting electrolyte

There is a considerable change in the rate constant for the reaction from 42.7 s^{-1} to 0.30 s^{-1} for $NaBF_4$ and Adogen 464 respectively. The activation energy for the process remains constant within experimental error, on average 53.7 $kJmol^{-1}$. Once again, as the activation energy stays constant for the reaction it is surmised that the reaction mechanism is unchanged by the change of supporting electrolyte. Rather, the change in the rate constant is considered to reflect the ability of the free chloride to form an ion pair with the electrolyte. Free chloride will form a strong ion pair with the sodium cation of $NaBF_4$ augmenting the dissociation of the chloride from $[OsCl_6]^{3-}$ (the rate limiting step). Where the cation is unchanged, i.e. in $[N^nBu_4]BF_4$ and $[N^nBu_4]Cl$, the anion can be seen to play a role; Cl^- inhibits the reaction more than BF_4^-. Where the anion is the same in each electrolyte, i.e. in $[N^nBu_4]Cl$ and Adogen 464 (methyltrialkyl(C_8-C_{10})ammonium chloride) and in $NaBF_4$ and $[N^nBu_4]BF_4$, the localised strength of the single positive charge on the cation controls the ability of the cation to form a strong ion pair and hence effect the rate of chloride dissociation. In Adogen 464 the positive charge is delocalised over a larger alkyl group than the tetrabutyl ammonia cation of $[N^nBu_4]Cl$ and forms a weaker ion pair reflected in the rate constants of 0.30 s^{-1} and 0.82 s^{-1} respectively. In the same regard, a tighter ion pair is formed between the sodium cation of $NaBF_4$ than the more delocalised positive charge of $[N^nBu_4]^+$ of $[N^nBu_4]BF_4$.

4.4 Conclusions

The rate of the reduction-induced substitution reaction of $[OsCl_6]^{2-}$ where one chloride is replaced by a ligand, L, of less electron donating ability has been shown previously to be dependent on the dissociation of chloride and the activation energy is the cleavage of the Os-Cl bond (chapter 3). The rate is facilitated by the ability of the solvent to solvate free chloride and inhibited by the prior presence of $[N^nBu_4]Cl$ in solution.

It has now been shown that "inert" supporting electrolyte can play a significant role in the reaction rate. The supporting electrolyte does not effect the activation energy of the reaction in either of the two cases studied; electrolyte concentration and electrolyte type. Presumably therefore the pathway by which the substitution proceeds is unaffected, and the change in rate constant is a measure of how the inert electrolyte interacts with the chloride on dissociation from $[OsCl_6]^{3-}$.

The increasing concentration of supporting electrolyte and by association the increasing ionic strength of the solution has little affect on the rate constant.

The type of electrolyte has a larger effect on the rate constant than the concentration of electrolyte. The different electrolytes span the range of rate constants of 0.30 s^{-1} to 42.7 s^{-1}, for Adogen 464 and $NaBF_4$ respectively, compared to a range of 0.11 s^{-1} to 0.20 s^{-1} for 0.4 M and zero $[N^nBu_4]BF_4$. The rate appears to be increased by the ability of the free chloride to form an ion pair with the cation of the electrolyte and inhibited by the anion. The relative abilities of cations to form ion pairs and anions to inhibit the reaction are determined by the strength of the localised 1+ or 1- charge.

4.5 References

[1] Nielson, R. M.; McManis, G. E.; Stafford, L. K.; Weaver, M. J.; *J. Phys. Chem.*, 1989, **93**, 2152
[2] Triegaardt D. M.; Wahl, A. C.; *J. Phys. Chem.*, 1986, **90**, 1957
[3] Thompson, P. A.; Simon, J. D.; *J. Am. Chem. Soc.*, 1993, **115**, 5657
[4] Bond, A. M.; Feldberg, S. W.; *J. Phys. Chem. B*; 1998, **102**, 9966
[5] Bond, A. M.; Coomber, D. C.; Feldberg, S. W.; Oldam, K. B.; Vu, T.; *Anal. Chem.*; 2001, **73**, 352, and references therein
[6] a) Jaworski, A.; Donten, M.; Tojek, Z.; *J. Electroanal. Chem.*; 1996, **407**, 75. b) Jaworski, A.; Donten, M.; Tojek, Z.; *J. Electroanal. Chem.*; 1997, **420**, 307 (correction to 6a)
[7] Bard, A. J.; Faulkner, L. R.; *Electrochemical Methods: Fundamentals and Applications, 2nd ed.* John Wiley & Sons, New York, 2001
[8] Oldham, K. B.; Feldberg, S. W.; *J. Phys. Chem. B.;* 1999, **103**, 1699
[9] Zanta, C. L. P. S.; Andrare, A. R.; Boodts, J. F. C.; *Electrochimica Acta*, 1999, **44**, 3333
[10] Ju, H.; Gong, Y.; Zhu, H.; *Analytical Sciences*, 2001, **17**, 59
[11] Khoo, S. B.; Foley, J.K.; Pons, S.; *J. Electroanal. Chem.*; 1986, **215**, 273

CHAPTER FIVE:

Reactions of Osmium(II)-Halide-Group 15 Ligand Complexes

5 Reactions of Osmium(II)-Halide-Group 15 Ligand Complexes

5.1 Introduction

This chapter presents a study of the redox-induced reactions of a series of osmium halide-phosphine/arsine complexes of the type, $[OsX_3Y_3]$, where X = Cl^-, Br^-; and Y is a tertiary alkyl phosphine or arsine. On reduction, a halide, X, is substituted by a ligand of less electron donor strength. The rate of the reaction can be calculated using the double-step chronoamperometry technique (2.2.1.3) and the activation energy for the process evaluated by the Arrhenius relationship (Equation 1.1). The rate of dissociation of X and the activation energy for the process for each osmium-halide-phosphine/arsine complex are rationalised with reference to their electrochemical reduction and oxidation potentials and Tolman's electronic parameter, χ_i, and cone angle, θ.

By way of introduction, a variety of osmium-halide-phosphine/arsine complexes from the literature are described and the affects of the group 15 ligands on redox potentials and reaction rates are discussed with respect to their electronic and steric properties.

Osmium-halide-group 15 complexes

For more than fifty years there has been a great interest in the chemistry of phosphorus and other group 15 ligands and their interaction with transition metals. Their involvement in catalytic processes has had a major impact on the growth of organometallic chemistry. The steric and electronic characters of the phosphine ligand plays an extremely important role in such processes. There is a need to learn

how to control catalytic reactions which give high yields of desired products under mild conditions.

Co-ordination compounds of osmium with mixed halide and group 15 ligands were first prepared in the 1940's.[1] Over the next two decades a number of groups, most notably Chatt *et al,* synthesised a range of phosphine and arsine donor ligand complexes of the type, $[OsX_4Y_2]$, $[OsX_3Y_3]$, and $[OsX_2Y_4]$, where X = Cl^-, Br^-; Y = a tertiary alkyl phosphine or arsine.[2,3,4] Studies in the far IR showed the first compounds of the type $[OsX_3Y_3]$ were of the *mer* configuration and it was some years before the less stable *fac* isomers were synthesised.[5,6] The osmium halide-group 15 complexes, as well as rhenium, iridium, and ruthenium analogues, have been well characterised by other techniques including, EPR and uv-vis spectroscopy, and X–ray crystallography.[7,8,9]

The general synthesis for the complexes $[OsX_nY_{6-n}]$ is from osmium tetroxide, OsO_4, dissolved in the reducing solvent ethanol containing hydrohalic acid in order to convert the oxide to $H_2[OsX_6]$ which is then reacted with tertiary phosphines or arsines. Five co-ordinate complexes, $[OsX_2(PPh_3)_3]$, have also been synthesised by changing the solvent from ethanol to a tertiary butanol/water mixture.[10,11] X-ray crystallography showed the structure of $[OsCl_2(PPh_3)_3]$ to be a distorted square-based pyramid suggesting that the bulk of the phenyl groups prevented the occupation of the sixth co-ordination site.[12] The structure for the analogous $[RuCl_2(PPh_3)_3]$ showed the same square-based pyramidal geometry.[13] The stability of the system was understood to originate from either intramolecular blocking of the vacant sixth site by a phenyl group or an "agostic" bonding interaction between an *ortho*-hydrogen on the phenyl group and the metal centre.[14]

The transition metal-phosphine bond

Chatt described the phosphine-transition metal bond as a σ-bond formed from the donation of the lone pair on the phosphorus to the metal and a π-bond formed from the back-donation of electron density from the filled metal d-orbitals (of suitable

symmetry) to the empty phosphorus 3d orbitals.[15] In this way, the phosphorus is seen as a π-acceptor and the bond is mutually reinforcing (synergic). There has been considerable debate, however, on whether π-backbonding is actually involved and, if so, whether the metal donates electron density to the phosphorus d-orbitals or p-orbitals.[16,17,18,19,20] It is now generally accepted that the π-bonding effect varies from ligand to ligand.[21,22] Certainly it is well recognised that changing the substituents, R, on phosphine ligands, PR_3, can cause marked changes in the behaviour of the free ligands and of their transition metal complexes.[23]

Electronic properties

Perhaps the most definitive work on defining the electronic properties of phosphine ligands was carried out by Tolman.[21] He studied the A_1 ν(CO) stretching vibration of $[Ni(CO)_3Y]$ with a set of 70 different phosphine ligands, Y, as a measure of their electronic influence on the complex. Tolman introduced the more general term "electron donor acceptor property" rather than trying to describe the bonding of the phosphine-transition metal bond in terms of σ-donor strength and π-acceptor strength circumventing problems encountered by previous groups. The contribution to the ν(CO) stretching vibration for each substituent, R, to a phosphine ligand, PR_3, can be designated a value, χ_i, with a magnitude in cm^{-1}. Of all the phosphorus ligands studied the lowest frequency found was that of PBu^t_3 at 2056.1 cm^{-1}. This was taken as the origin, i.e. χ_i for Bu^t = 0 cm^{-1}. Thus, for any complex of the type $[Ni(CO)_3(PR_1R_2R_3)]$, the A_1 ν(CO) stretching frequency can be calculated using the equation:

$$\nu(CO) = 2056.1 + \sum_{i=1}^{3} \chi_i$$

The calculated χ_i values for a number of substituent groups, R, are given in **Table 5.1**.

Substituent, R	χ_i / cm^{-1}	Substituent, R	χ_i / cm^{-1}
-Bu^t	0.0	-OEt	6.8
-Pr^i	1.0	-CH_2CH_2CN	7.3
-Bu	1.4	-OMe	7.7
-Et	1.8	-H	8.3
-Me	2.6	-OPh	9.7
-CH_2Ph	3.5	-C_6F_5	11.2
-Ph	4.3	-Cl	14.8
-$CH{=}CH_2$	4.5	-F	18.2
-OBu	6.5	-CF_3	19.6

Table 5.1 Tolman's electronic parameter, χ_i, for selected substituents, R, on phosphorus ligands[23]

Since this pioneering work the electronic parameters for a number of tertiary phosphorus ligands using ^{13}C NMR have been determined and are in good agreement to those of Tolman's.[22]

Attempts to separate σ-donor and π-acceptor properties have been carried out by many groups using a variety of techniques including uv-vis,[24] IR,[25] Mössbauer,[26] and photoelectron[27] spectroscopies as well as theoretical[28] and electrochemical[29] methods and X-ray crystallography[30]. The success of these early attempts at separating the components was mixed. It wasn't until 1985 when Giering *et al* presented work on a series of compounds [μ-$MeCp(CO)_2MnY$], where Y was a tertiary phosphine ligand, that the first satisfactory account of the σ- and π-components of the phosphine-transition metal bond was given.[31] Series of compounds were shown to have linear relationships between the redox potentials of the complexes and Tolman's electronic potentials of the phosphine ligands and between the redox potentials of the complexes and the pK_a of the protonated phosphine ligands. The phosphine ligands were separated into 3 classes:

Class I	σ-donor/π-donor
	PEt_3, PBu_3, PCy_3
Class II	σ-donor
	PMe_3, PMe_2Ph, PEt_2Ph, PBu_2Ph, $PMePh_2$, $PEtPh_2$, $P(p\text{-}OPhMe)_3$, $P(p\text{-}PhMe)_3$, PPh_3
Class III	σ-donor/π-acceptor
	$P(p\text{-}PhCl)_3$, $P(OMe)Ph_2$, $P(OPr^i)_3$, $P(OEt)_3$, $P(OMe)_3$, $P(OPh)_3$

An excellent linear correlation of the redox potentials against the pK_a for complexes of Class II ligands showed that the ease of oxidation must be dependent on the σ-donor ability of the ligand only. Complexes with Class I ligands lie off the linear fit for Class II ligands and are easier to oxidise than might otherwise be expected. This was accounted for by an increased electron richness of the Class I ligands due to their π-basicities. Complexes with Class III ligands are harder to reduce than expected due to the removal of electron density from the metal by the π-acceptor abilities of the ligands. It is noted in this work, however, that the boundaries of the three classes of ligands will be dependent on the π-basicity of the metal to which they are co-ordinated. The more π-basic metals will accentuate the metal-ligand π-interactions. Caution should therefore be taken in the strict definition of each class when evaluating the relationship between pK_a values and electronic components because the pK_a values are dependent on the interactions between phosphorus and a hard acid, H^+, rather than a soft acid such as a low valent metal centre.

Steric properties

Tolman continued his work with phosphine ligands to take account of their steric properties.[23] The steric effects of a phosphine ligand were quantified by the definition of a ligand cone angle, θ. The cone angle is defined as, "The angle of the cone with the apex at the metal which just encloses the Van der Waals surface of all the substituent atoms on the phosphorus ligands, assuming the bond length TM-P = 2.228 Å". This is represented schematically in **Figure 5.1a**. For unsymmetrical ligands Tolman introduced the concept of half cone angles, θ/2.[32] These are defined

as the angles between the metal-phosphorus bond and the vector that just touches the Van der Waals radii of the outer most atoms (**Figure 5.1b**). The final value of θ is defined as two times the average of the maximum θ/2 values for the three substituents, R. Tolman's cone angles for some phosphines are given in **Table 5.2**.

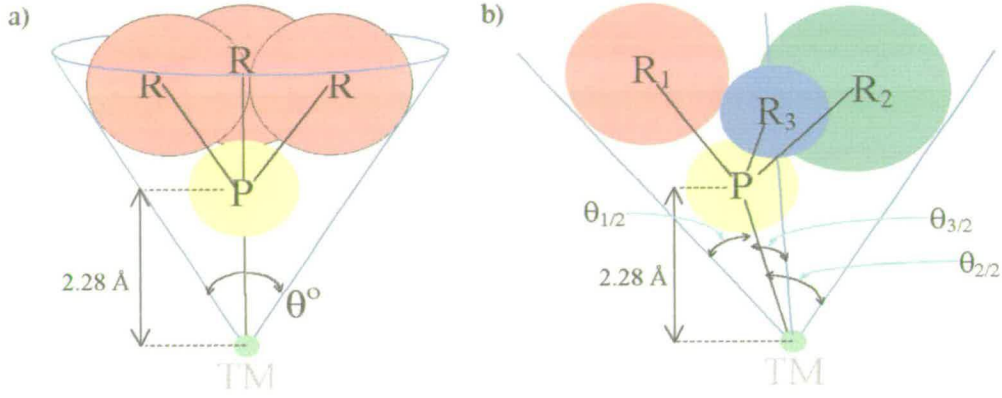

Figure 5.1 Representation of Tolman's cone angle for a transition metal-phosphine bond, a) symmetric ligands, b) unsymmetrical ligands

Phosphine ligand	θ /°
-PMe_3	116
-PMe_2Ph	121
-PEt_3, -PBu_3, -$P(CH_2CH_2CN)_3$	132
-$PMePh_2$, -PEt_2Ph	136
-$P(CF_3)_3$	137
-$PEtPh_2$	140
-PPh_3	145
-PBu^t_3	182

Table 5.2 Tolman's cone angles for selected phosphine ligands[23]

There are numerous cases where steric effects have been related to NMR chemical shifts and coupling constants, infrared frequencies and intensities, electronic spectra, dipole moments, electrochemistry, ionisation potentials, rates of reactions, equilibrium constants and the structure of molecules.[23]

Rates of reaction

Ligand size can have a marked influence on reaction rates.[23] Dissociation of a phosphine ligand, Y, in the complex PdY_4, has been shown to be dominated by steric effects rather than their electronic properties.[33] Furthermore the rate of dissociation of Y will depend on the size of Y itself and the steric requirements of the other ligands.[34,35]

For the dissociation reaction of CO from the complex *cis*-$[MnBr(CO)_4Y]$, the rate limiting step is the loss of CO. The rates of dissociation are seen to increase with the size of the phosphorus ligand, Y, i.e. steric strain within the complex augments the rate of dissociation.[32] The same increase in reaction rate is seen in the CO dissociation from the complex $[CpMo(CO)_2YCOMe]$ although considerable variance from a straight line for the plot of reaction rate against cone angle, θ, shows an electronic effect on the reaction rate must also be considered.[36]

Geiring *et al* have attempted to quantify the contributions to the reaction rate for steric and electronic effects using plots of k and log k against, χ_i, θ, and pK_a, from which the electronic and steric components to the overall rate can be evaluated.[31,37] The plots were applied to a number of reactions from the literature with some success.[36,38,39]

Electrochemical studies

Electrochemical studies have been reported in a series of papers by Levason *et al* for only the first oxidation process for the complexes, *trans*-$[OsX_4Y_2]$, *mer/fac*-$[OsX_3Y_3]$, and *trans*-$[OsX_2Y_4]$, where X = Cl^-, Br^-; Y = tertiary alkyl phosphine, arsine, or stibine.[40,41,42] Electrochemical, spectroelectrochemical, and structural studies of the complexes *mer/fac*-$[OsX_3Y_3]$ have been carried out in this laboratory.[43,44,45,46] The *mer*-$[OsX_3Y_3]$ complexes at 233 K undergo reversible one-electron oxidation and reduction processes between +0.89 and +1.13 V and –0.11 and –0.61 V respectively. The half-wave potentials are primarily metal based and

depend on the halide, X, and vary linearly with Tolman's electronic parameter for L. The *fac*-$[OsX_3Y_3]$ isomers undergo an irreversible oxidation to form the *mer* isomer. Electrochemical reduction of $[OsCl_3(PMe_2Ph)_3]$ produces the five co-ordinate neutral species $[OsCl_2(Me_2Ph)_3]$ characterised by ^{31}P-$\{^1H\}$ NMR.[45,46] This reactive species readily reacts with a donor solvent or available ligand to produce $[OsCl_2(PMe_2Ph)_3L]$, where L = MeCN, dimethylformamide, dimethyl sulphoxide, benzonitrile, CO, N_2, or C_2H_4, initially as the *trans* isomer. This series of electro-initiated reactions of $[OsCl_3(PMe_2Ph)_3]$ has so far yielded over 20 separate complexes including doubly and triply bridged binuclear complexes.

5.2 Experimental

Dichloromethane and acetonitrile were purified and dried as outlined in 3.2.1. Dichloroethane (99 %+, spectrophotometric grade, Aldrich) was distilled three times from phosphorus pentoxide (Lancaster). $[N^nBu_4]BF_4$ was prepared as outlined in 3.2.2.

5.2.1 Chemical Synthesis

All complexes studied were prepared by Dr Nicholas Payne, University of Edinburgh. Complexes of the type *mer*-$[OsCl_3Y_3]$, where Y = PMe_3, PMe_2Ph, $PMePh_2$, PEt_2Ph, and $PEtPh_2$, were made by the method of Chatt *et al.*[5] OsO_4 was reacted with concentrated HCl in ethanol forming $H_2[OsCl_6]$. After addition of excess phosphine the solution was heated at reflux under nitrogen. The time the solution was heated differed for the various phosphine ligands. On cooling to 0 °C the red/orange product formed as microcrystals. The crystals were isolated and washed with diethyl ether and dried under vacuum.

Complexes of the type *mer*-$[OsBr_3Y_3]$, where Y = PMe_3, PMe_2Ph, PEt_2Ph, $AsMe_2Ph$, and $AsEt_2Ph$, were obtained by the same route as the analogous chloro compounds using hydrobromic acid.

The complexes were characterised by Payne by a combination of CHN microanalysis, mass spectroscopy, uv-vis spectroscopy, and electrochemical half-wave potentials. Crystal structures for the complexes, *mer*-$[OsCl_3(PMe_2Ph)_3]$, *mer*-$[OsCl_3(PEt_2Ph)_3]$, and, *mer*-$[OsCl_3(AsMe_2Ph)_3]$ were obtained.

5.2.2 Electrochemistry

In this work the reduction and oxidation potentials were re-measured using a standard three electrode electrochemical cell with a Ag/AgCl reference electrode where the ferrocenium/ferrocene oxidation is at +0.55 V.

All electrochemical experiments for the osmium-halide-phosphine complexes were carried out in 0.5 M $[N^nBu_4]BF_4$/dichloromethane. Electrochemical experiments for the osmium-halide-arsine complexes were carried out in 0.5 M $[N^nBu_4]BF_4$/dichloroethane because of the higher temperatures required for the double-step chronoamperometry experiments, causing dichloromethane to be unsuitable. The concentration of the osmium-halide-group 15 ligand complexes was 0.0020 M ± 0.0002 for each double-step chronoamperometric experiment. All experiments were carried out under a strictly water-free environment.

5.2.3 Simulation

Experimental cyclic voltammograms of *fac*-$[OsCl_3(Me_2Ph)_3]$ in 0.5 M $[N^nBu_4]BF_4$/dicholomethane have been simulated using the software, Digisim 2.1©. The accuracy of the simulations was tested by comparison of the fit over a number of scan rates. The full input data for the simulated isomerisation reaction are given in **Table 5.3**. The electron transfer rates, diffusion coefficients, and transfer coefficient (α) for each process were not measured and were left as the Digisim default, 1 x10^4 cm^{-1}, 1 x10^{-5} cm^2s^{-1}, and 0.5, respectively. There is no reason to believe they should be significantly different from these figures.

Known parameters		Diffusion	Semi-infinite
Electrode area	0.020 cm^2	Start potential	0.30 V
Electrode Geometry	planar	End potential	1.30 V
Temperature	297 K	Concentration [A]	0.0028 M
		Resistance	2000 Ω
Charge transfer reactions		Charge transfer parameters	
Reaction 1	B + e = A	$E_{1/2}$ 1	1.25 V
Reaction 2	C + e = D	$E_{1/2}$ 2	1.07 V
		α 1 and 2	0.5
		Rate 1	10000 cm s^{-1}
		Rate 2	10000 cm s^{-1}
Homogeneous chemical reactions		Chemical reaction parameters	
		K_B	k_f	k_b
Reaction	B = C	50	1900	38
Diffusion coefficients			
A	1.00x10^{-5} cm^2 s^{-1}	C	1.00x10^{-5} cm^2 s^{-1}
B	1.00x10^{-5} cm^2 s^{-1}	D	1.00x10^{-5} cm^2 s^{-1}

Table 5.3 Input parameters for simulated cyclic voltammetry for a Dissociative mechanism on Digisim 2.1

5.3 Results and Discussion

5.3.1 Electrochemistry of *mer*-$[OsX_3L_3]$

The cyclic voltammogram of *mer*-$[OsCl_3(PMe_2Ph)_3]$ in 0.5 M $[N^nBu_4]BF_4$/ dichloromethane at 295 K (**Figure 5.2**) shows an oxidation at +1.09 V and a reduction at –0.34 V; both are one electron process as determined by coulometry and electron transfer rates are diffusion limited, $i_p \propto \nu^{1/2}$. Both the oxidation and reduction are assigned to metal-based electron transfer processes.

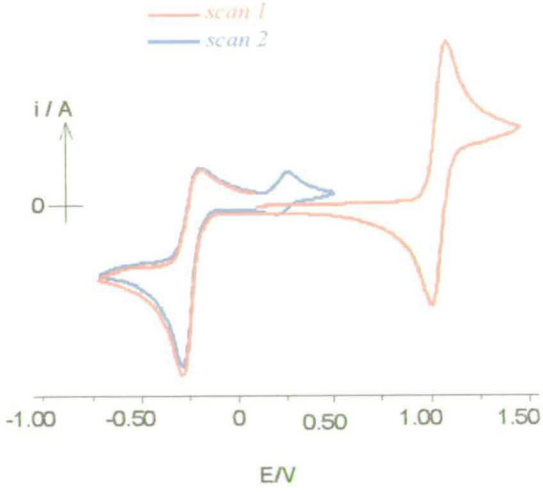

Figure 5.2 CV of *mer*-$[OsCl_3(PMe_2Ph)_3]$ in 0.5 M $[N^nBu_4]BF_4$/dichoromethane at 0.1 V s^{-1}, 295 K

The reduction process is not chemically reversible at 0.1 V s^{-1}, 295 K, since $i_p^{red} > i_p^{ox}$. The new couple at ~0.20 V is generated on reduction, Os(III) → Os(II), and has been identified by $^{31}P\text{-}\{^1H\}$ NMR as the five co-ordinated species $[OsCl_2(PMe_2Ph)_3]$.[46] In a co-ordinating solvent, L, the five co-ordinated species reacts to give $[OsCl_2(PMe_2Ph)_3L]$, where L = MeCN, dimethylformamide, dimethyl sulphoxide, benzonitrile, CO, N_2, or C_2H_4 initially as the *trans* isomer.[46] This electrochemical response in $[N^nBu_4]BF_4$/dichloromethane has been found to be typical for a range of the complexes of the type *mer*-$[OsX_3Y_3]$ with the daughter five

co-ordinate species showing a redox couple *ca.* 0.55 V positive of the parent couple. Reduction of the complexes, *mer*-$[OsX_3Y_3]$, each time results in the dissociation of a halide. Reaction of the five co-ordinate species, $[OsX_2Y_3]$, with acetonitrile gives $[OsX_2Y_3An]$ which shows a redox couple a further *ca.* 0.10 V positive of the five co-ordinate species.

The half wave potentials for the species of the type *mer*-$[OsX_3Y_3]$, where X = Cl^-, Br^-; Y = a tertiary phosphine/arsine, in 0.5 M $[N^nBu_4]BF_4$/dichloromethane for the oxidation and reduction process at 223 K along with Tolman's electronic parameter, χ_i, and cone angle, θ are given in **Table 5.4**.

Inspection of the table shows that exchanging chloride ligands with bromide ligands makes very little difference to the Os(IV/III) redox couple; the half-wave potential for *mer*-$[OsX_3(PMe_3)_3]^{1+/0}$ is +1.02 V and +1.03 V for X = Cl^- and Br^- respectively. Thus the halide ligands stabilise the higher oxidation states of Os to approximately the same degree. However, the Os(III/II) couple does depend on the ligated halide. For the phosphine complexes the bromide analogues' half-wave potentials are 120 mV to 170 mV positive relative to those of the chloride complexes. For example, the half-wave potential for *mer*-$[OsX_3(PEt_3)_3]^{0/1-}$ is –0.40 V and –0.25 V for X = Cl^- and Br^- respectively.

It is clear from **Table 5.4** that variation of R, where R is an alkyl group of the tertiary Group 15 ligand, has a marked effect on the observed metal based oxidation and reduction potentials. The potential of the oxidation for *mer*-$[OsCl_3Y_3]$, where Y = $PMePh_2$ is 180 mV positive relative of those where Y = PEt_3. For the corresponding reduction $PMePh_2$ is 220 mV positive of that of PEt_3.

The redox potentials of complexes of the tertiary Group 15 ligands, PR_3 and AsR_3, show a considerable difference. For example, the reduction of *mer*-$[OsBr_3(AsEt_2Ph)_3]$ at –0.45 V is 240 mV more negative than *mer*-$[OsBr_3(PEt_2Ph)_3]$ at –0.21 V. Overall the reduction half-wave potentials for arsine complexes exhibit potentials between 80 mV and 250 mV more negative than their phosphine

analogues. The oxidation half-wave potentials for arsine complexes do not exhibit such a large difference but are all between 20 mV and 70 mV more negative than their phosphine analogues. Arsenic is below phosphorus in the periodic table and hence the orbital containing the lone pair of electrons in the arsine ligand will be more diffuse than the corresponding orbital in the analogous phosphine ligand. A more diffuse orbital will make arsine a poorer σ-donor. The more negative reduction potential of the arsine containing compounds must therefore be due to either arsine orbitals with stronger π-donor character or to better π-accepting properties of phosphine ligands.

Group 15 Ligand, Y*	Os(III/II) Reduction/V	ΔE /mV	Os(IV/III) Oxidation/V	ΔE /mV	χ_i/cm^{-1}	Cone angle/°
$Cl_3(PMePh_2)_3$	-0.18	73	+1.13	68	11.2	136
$Cl_3(PMe_2Ph)_3$	-0.25	73	+1.08	69	9.5	122
$Cl_3(PMe_3)_3$	-0.32	74	+1.02	73	7.8	118
$Cl_3(PEtPh_2)_3$	-0.23	71	+1.06	65	10.4	140
$Cl_3(PEt_2Ph)_3$	-0.34	71	+1.03	66	7.9	136
$Cl_3(PEt_3)_3$	-0.40	72	+0.95	66	5.4	132
$Cl_3(AsMe_2Ph)_3$	-0.33	72	+1.05	65		
$Cl_3(AsEt_2Ph)_3$	-0.46	70	+0.96	69		
$Br_3(PMePh_2)_3$	-0.04	73	+1.11	60	11.2	136
$Br_3(PMe_2Ph)_3$	-0.12	75	+1.09	66	9.5	122
$Br_3(PMe_3)_3$	-0.15	76	+1.03	66	7.8	118
$Br_3(PEtPh_2)_3$	-0.11	78	+1.05	71	10.4	140
$Br_3(PEt_2Ph)_3$	-0.21	78	+1.00	72	7.9	136
$Br_3(PEt_3)_3$	-0.25	79	+0.98	72	5.4	132
$Br_3(AsMe_2Ph)_3$	-0.37	70	+1.05	68		
$Br_3(AsEt_2Ph)_3$	-0.45	71	+0.98	69		

Table 5.4 Half-wave potentials for the reduction and oxidation processes of *mer*-$[OsX_3Y_3]$ (where X = Cl^- or Br^- and Y = a tertiary phosphine/arsine in 0.5 M $[N^nBu_4]BF_4$/dcm, at 0.1 V s^{-1}, 223 K) and Tolman's electronic parameter, χ_i, and cone angle, θ. *All complexes were prepared by Dr Nicholas Payne, University of Edinburgh

5.3.2 Comparison of half-wave potentials with Tolman's electronic parameter, χ_i, and cone angle, θ, and pK_a

A linear relationship is obtained from a plot of Tolman's electronic parameters, χ_i, against the reduction and oxidation half-wave potentials for the tertiary phosphine complexes (**Figure 5.3**). Thus the redox chemistry of *mer*-$[OsX_3Y_3]$ can be understood to be dependent on the electronic properties of the tertiary phosphine ligands. The gradients of the linear regression fit in plots **Figure 5.3a** and **Figure 5.3c** are almost identical indicating that the electronic effect of the tertiary phosphine on the Os-based reduction is independent of the ligated halide. Likewise the gradients of the linear regression fit in the plots **Figure 5.3b** and **Figure 5.3d** are very similar but are different from the gradients in **Figures 5.3a** and **Figures 5.3c** indicating the electronic effect of the metal centre is different for the oxidation and reduction processes as might be expected.

A plot of redox potentials against cone angle, θ, for the reduction and oxidation processes in the chloride and bromide analogues (**Figure 5.4**) show no clear relationship like that for χ_i against redox potentials (although it is perhaps noteworthy that within the methyl and ethyl phosphines sets there is a stepwise increase in potential with increasing cone angle). This suggests that the redox chemistry is chiefly dependent on the electronic parameters. Any scatter of points away from linearity on the χ_i plot (**Figure 5.3**) is likely to be due to the minimal steric effects of the ligands. The deviation from linearity is most pronounced for the Os(IV/III) redox couple for Y = $PEtPh_2$. This ligand has the largest cone angle of 140°, of all the phosphine ligands studied here. Since oxidation results in a loss of an electron from the metal centre and an increase in effective nuclear charge then this will create a smaller metal centre and a more sterically hindered. Hence we must conclude that for large bulky ligands steric as well as electronic considerations are involved in determining half-wave potential values.

Giering proposed that these Class II ligands were σ-donors only and that a plot of pK_a against reduction and oxidation potentials would give a straight line correlation.[31] In practise, the complexes studied were shown to have no complete correlation between redox potentials and pK_a (**Figure 5.5**). There is, however, there is a good correlation between the methyl phosphines and a less good fit between the ethyl phosphines particularly for the chloride complexes (**Figure 5.5a** and **Figure 5.5b**).

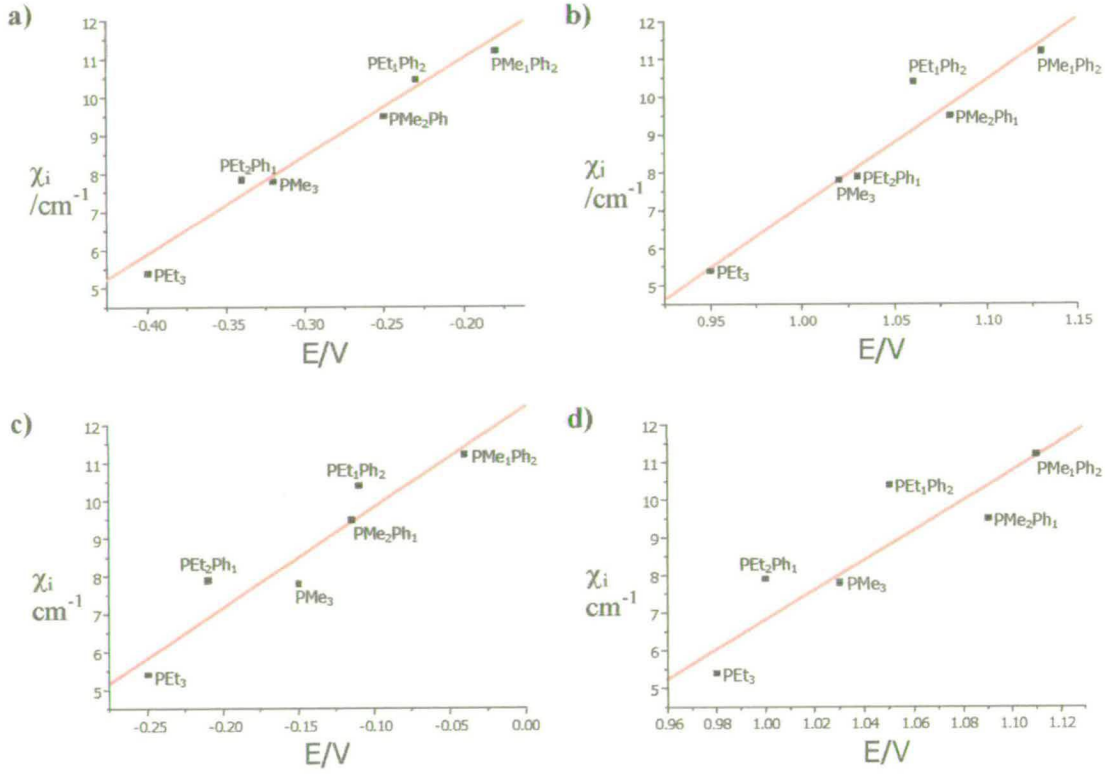

Figure 5.3 Plots of half-wave potentials against Tolman's electronic parameter, χ_i. a) Reduction potentials of *mer*-$[OsCl_3Y_3]$ b) Oxidation potentials of *mer*-$[OsCl_3Y_3]$ c) Reduction potentials of *mer*-$[OsBr_3Y_3]$ d) Oxidation potentials of *mer*-$[OsBr_3Y_3]$

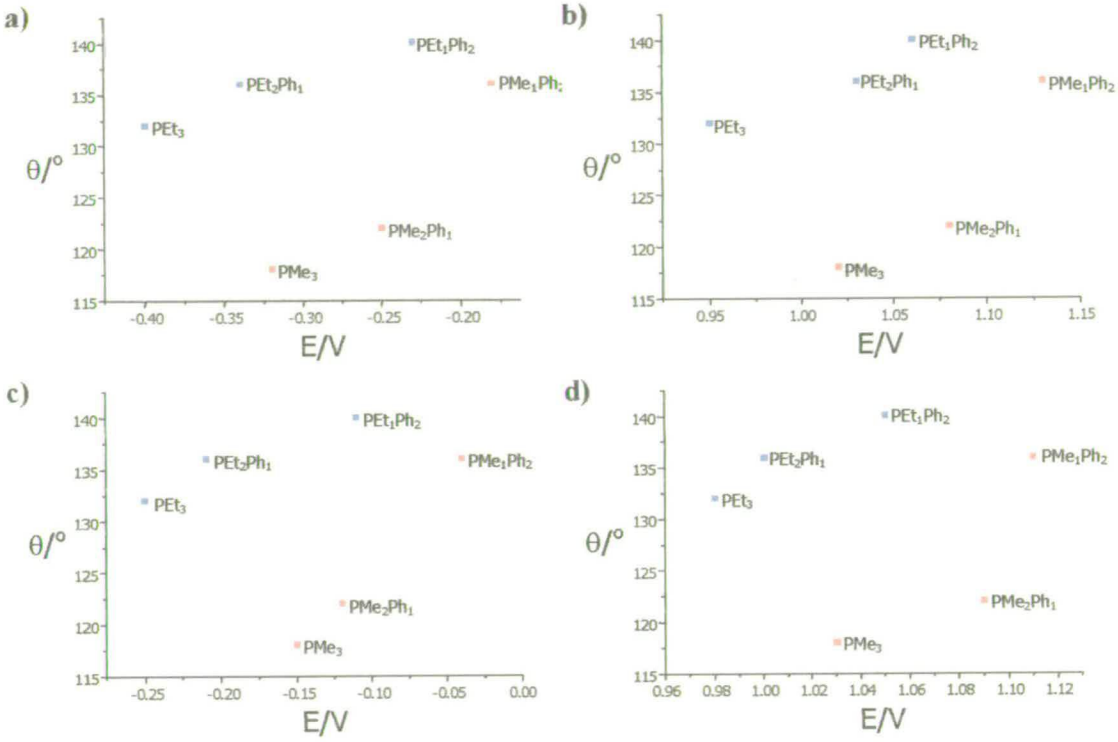

Figure 5.4 Plots of half-wave potentials against Tolman's cone angle, θ. a) Reduction potentials of *mer*-$[OsCl_3Y_3]$ b) Oxidation potentials of *mer*-$[OsCl_3Y_3]$ c) Reduction potentials of *mer*-$[OsBr_3Y_3]$ d) Oxidation potentials of *mer*-$[OsBr_3Y_3]$

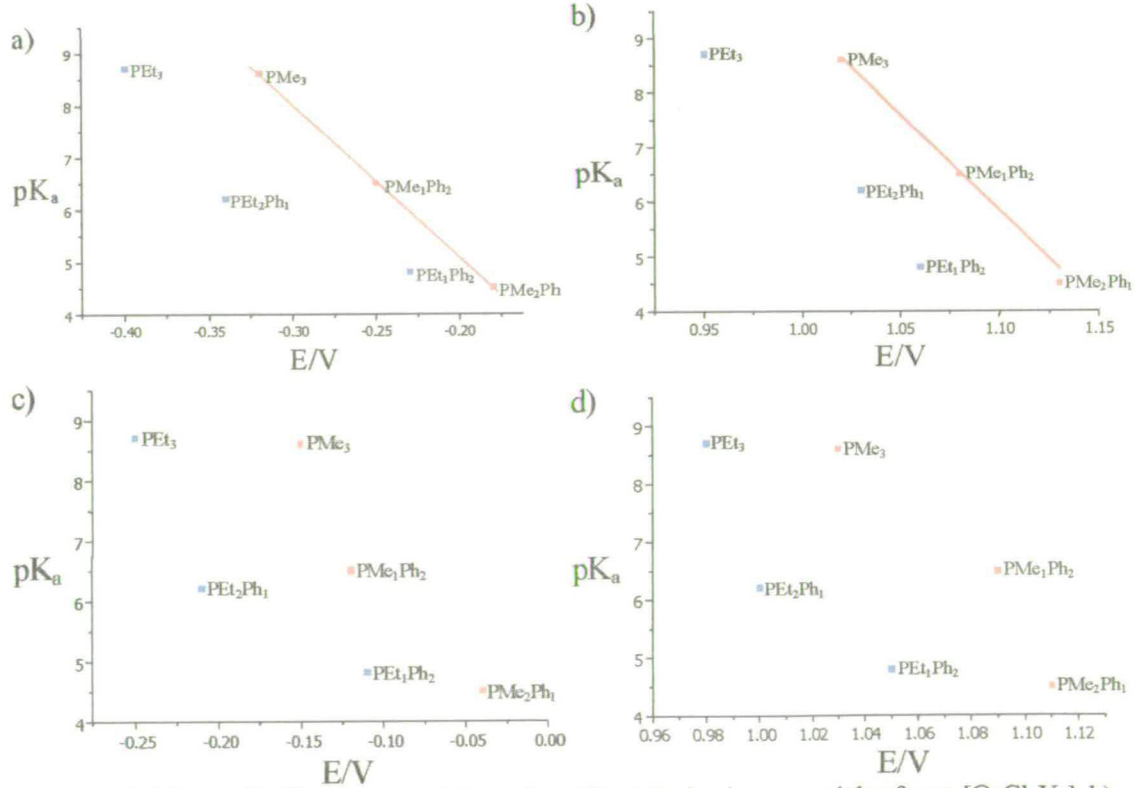

Figure 5.5 Plots of half-wave potentials against pK_a a) Reduction potentials of *mer*-$[OsCl_3Y_3]$ b) Oxidation potentials of *mer*-$[OsCl_3Y_3]$ c) Reduction potentials of *mer*-$[OsBr_3Y_3]$ d) Oxidation potentials of *mer*-$[OsBr_3Y_3]$

We therefore conclude that for $[OsX_3Y_3]$ compounds the redox potentials may be correlated with Tolman's electronic parameter. We also suggest that the phosphine ligands studied here should not be considered as strictly Class II, i.e., they are not solely σ-donor ligands.

5.3.3 Rate constants and activation energies for the dissociation reaction of *mer*-$[OsX_3L_3]$

The rate constants, k, for the dissociation of a halide, X, from the electrochemically generated anion, *mer*-$[OsX_3Y_3]^{1-}$, have been studied using double-step chronoamperometry in 0.1 M $[N^nBu_4]BF_4$/dichloromethane or 0.1 M $[N^nBu_4]BF_4$/ dichloroethane.

The rate constants were measured over a temperature range of at least 30 °C and the activation energies were calculated from the Arrhenius relationship. The rate constants at 243 K for the phosphine complexes and 298 K for the arsine complexes were read from the linear regression fit from the Arrhenius plots of lnk against 1/temperature. Errors in k were calculated from the average error for each point determined from the average measured values for each experiment and the statistical errors involved in their calculation. The errors for E_a are the standard deviations from the linear regression fits.

The rate of dissociation and activation energies are first considered within smaller selections of similar complexes, *mer*-$[OsCl_3(PMe_nPh_{3-n})_3]^{1-}$, *mer*-$[OsBr_3(PMe_nPh_{3-n})_3]^{1-}$, *mer*-$[OsCl_3(PEt_nPh_{3-n})_3]^{1-}$, *mer*-$[OsBr_3(PEt_nPh_{3-n})_3]^{1-}$ and then as a whole.

5.3.3.1 *mer*-$[OsCl_3(PMe_nPh_{3-n})_3]^{1-}$

The rate of dissociation of Cl^- from the complexes, *mer*-$[OsX_3(PMe_nPh_{3-n})_3]^{1-}$ (where n = 1-3) and the activation energy for the process is given in **Table 5.5**. The dissociation of Cl^- shows a stepwise increase in both the rate constant, k, and activation energy, E_a, as n goes from 1 to 3 (illustrated in the Arrhenius plot, **Figure 5.6**).

The increase in the rate constant and activation energy, in order $PMePh_2 < PMe_2Ph < PMe_3$, is matched, although not in direct proportion, by increasingly negative reduction potentials, a lower value of χ_i, and a smaller cone angle.

From an electronic point of view the PMe_3 ligand is the best σ-donor creating the highest electron density on the metal centre and making it the most difficult to reduce. Consequently the reduced, Os(II) complex, can be regarded as the least stable complex and the dissociation of Cl^- is, as might be expected, the fastest. In terms of steric strain within the complexes, the rate would be anticipated to be the fastest for the complex with the largest cone angle. This is not the case, and electronic effects must be considered to be dominant in determining the rate of dissociation.

Y	k /s^{-1}	E_a /kJ mol^{-1}	Os(IV/III) reduction/ V	χ_i/ cm^{-1}	θ/°
PMe_3	26.2 ± 1.3	63.7 ± 1.1	-0.32	7.8	118
PMe_2Ph	0.41 ± 0.05	51.0 ± 0.9	-0.25	9.5	122
$PMePh_2$	0.25 ± 0.05	45.7 ± 1.1	-0.18	11.2	136

Table 5.5 Rate constants, k, and activation energies, E_a, for the dissociation of Cl^- from *mer*-$[OsCl_3Y_3]^{1-}$ in 0.1 M $[N^nBu_4]BF_4$/dichloromethane

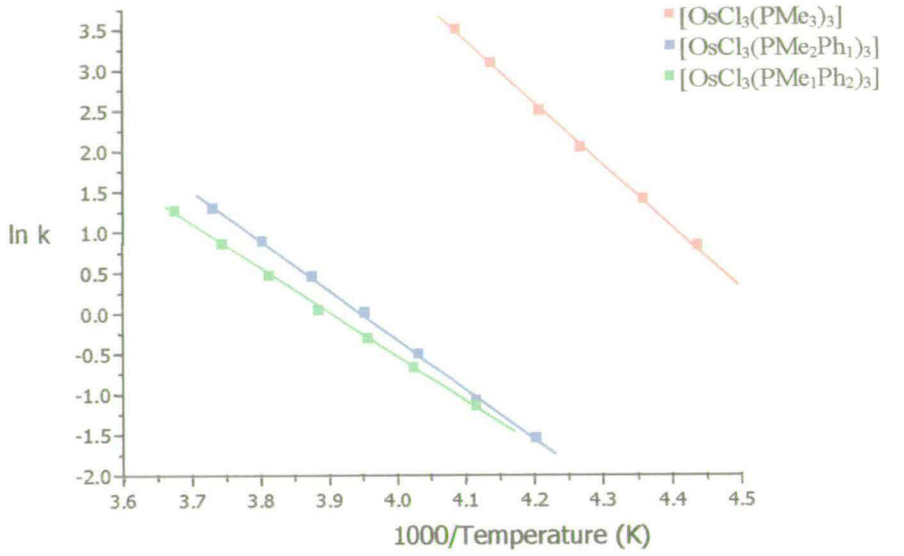

Figure 5.6 Arrhenius plot for the dissociation reaction of Cl^- from *mer*-$[OsCl_3(PMe_nPh_{3-n})_3]^{1-}$

As the Os(III/IV) half-wave potential becomes increasingly negative, -0.18, -0.25, and –0.32 V, for $PMePh_2$, PMe_2Ph, and PMe_3 respectively, the activation energy increases, 45.7, 51.0, and 63.7 kJ mol^{-1}. Perhaps more significantly, the activation energy decreases as the complexes become more sterically crowded. It has been observed that the dissociated halide is *trans* to a phosphine ligand in *mer*-$[OsCl_3(PMe_2Ph)_3]$.[46] The crystal structure of *mer*-$[OsCl_3(PMe_2Ph)]$ shows the chloride *trans* to the phosphine group to be longer than the *cis*-chlorides by on average 0.079 Å.[43] The angle of the two phosphine groups in the *cis* positions to the *trans*-chloride have an angle of 167.4°, P-Os-P': significantly less than the true octahedral angle of 180°. It could be that the bulkier phosphine groups weaken the Os-Cl bond and consequently lower the activation energy. The *trans influence* of the phosphine on the *trans*-chloride should increase as the σ-donor strength increases ($PMePh_2$ < PMe_2Ph < PMe_3) resulting in a corresponding decrease in the bond strength and activation energy. This is not the case. The *cis effect* of steric strain from the phosphine ligands seems to dominate. Interestingly, a lower activation energy does not appear to correspond to a faster rate of dissociation.

5.3.3.2 *mer*-$[OsBr_3(PMe_nPh_{3-n})_3]^{1-}$

The reaction rates and activation energies for the dissociation of the complexes *mer*-$[OsBr_3(PMe_3)_3]^{1-}$ and *mer*-$[OsBr_3(PMe_2Ph)_3]^{1-}$, are given in **Table 5.6**. The rates of reaction for the complex *mer*-$[OsBr_3(PMe_3)_3]^{1-}$ and *mer*-$[OsBr_3(PMe_2Ph)_3]^{1-}$ follow the same pattern as their chloride analogues. The rates increase from 1.1 s^{-1} to 114 s^{-1} for *mer*-$[OsBr_3(PMe_2Ph)_3]^{1-}$ and *mer*-$[OsBr_3(PMe_3)_3]^{1-}$ respectively as the complexes become increasingly more difficult to reduce (Os(III/II) $E_{1/2}$ = –0.15 V and -0.21 V respectively). The rate of dissociation again appears to be dominated by electronic effects.

Both bromo-complexes, $[OsBr_3(PMe_3)_3]^{1-}$ and $[OsBr_3(PMe_2Ph)_3]^{1-}$, exhibit faster rates of dissociation even though their reduction half-wave potentials are 130 to 140 mV more positive than their chloride analogues, $[OsCl_3(PMe_3)_3]^{1-}$ and $[OsCl_3(PMe_2Ph)_3]^{1-}$. The faster rate for the dissociation of bromide than chloride from the analogous complexes is likely to be due to the better leaving group ability of Br^- than Cl^- in organic solvents as seen in the case of the loss of halide in the complexes, $[MX_6]^{3-}$, where M = Os and Ir; X = Br^- and Cl^- (*vide supra*).

Y	k /s^{-1}	E_a /kJ mol^{-1}	Os(IV/III) reduction/ V	χ_i/ cm^{-1}	θ/°
PMe_3	114 ± 7	32.8 ± 2.2	-0.15	7.8	118
PMe_2Ph	1.1 ± 0.4	49.2 ± 1.1	-0.12	11.2	136

Table 5.6 Rates of reaction and activation for the dissociation of a halide, X^- from the complexes of the type, *mer*-$[OsBr_3Y_3]^{1-}$

The activation energy for the two complexes, *mer*-$[OsBr_3(PMe_3)_3]^{1-}$ and *mer*-$[OsBr_3(PMe_2Ph)_3]^{1-}$ do not increase in the same way as their chloride analogues. Because there are only two complexes to compare it is difficult to draw any convincing conclusions. In terms of steric strain experienced within the complex, *mer*-$[OsBr_3(PMe_3)_3]^{1-}$ will be under less steric constraint than

mer-$[OsBr_3(PMe_2Ph)_3]^{1-}$ and would therefore seem unlikely to be related to the lower activation energy. Rather, it may be that the stronger *trans influence* imposed by PMe_3 than PMe_2Ph plays a more important role.

5.3.3.3 *mer*-$[OsCl_3(PEt_nPh_{3-n})_3]^{1-}$

The rate constants and activation energies for the dissociation reactions of *mer*-$[OsCl_3(PEt_2Ph)_3]^{1-}$ and *mer*-$[OsCl_3(PEtPh_2)_3]^{1-}$ are given in **Table 5.7**.

The rates of reaction follow a different pattern in comparison to the analogous complexes, *mer*-$[OsX_3(PMe_nPh_{3-n})_3]^{1-}$. The rates for the dissociation reaction *increase* going from PEt_2Ph to $PEtPh_2$ although for the methyl phosphine analogues it has been observed that the rate *decreases* in the order PMe_2Ph to $PMePh_2$. For the methyl phosphines it appears that the electronic properties of the ligands dominate in determining the reaction rate. For the ethyl phosphines, although *mer*-$[OsCl_3(PEt_2Ph)_3]^{1-}$ is more difficult to reduce than *mer*-$[OsCl_3(PEtPh_2)_3]^{1-}$ (Os(III/II) $E_{1/2}$ = -0.34 V and –0.23 V respectively) sterically the strain within the complex is larger and may increase the reaction rate overshadowing the electronic σ-donor properties of the phosphine.

The activation energies for *mer*-$[OsCl_3(PEt_2Ph)_3]^{1-}$ and *mer*-$[OsCl_3(PEtPh_2)_3]^{1-}$ increase in energy, $PEtPh_2$ < PEt_2Ph, as do their direct methyl analogues. They are both larger in energy than their methyl phosphine analogues; E_a = 66.0 and 51.0 kJ mol^{-1} for *mer*-$[OsCl_3(PEt_2Ph)_3]^{1-}$ and *mer*-$[OsCl_3(PMe_2Ph)_3]^{1-}$ respectively and E_a = 53.2 and 45.7 kJ mol^{-1} for *mer*-$[OsCl_3(PEtPh_2)_3]^{1-}$ and *mer*-$[OsCl_3(PMePh_2)_3]^{1-}$ respectively. This may be surprising since the ethyl phosphines have higher cone angles and therefore a higher steric strain within the complex. The ethyl phosphines are also slightly better σ-donors and would therefore be expected to

deliver a slightly stronger *trans influence* and weaken the Os-Cl bond, hence lowering the activation energy compared to the methyl phosphines.

Y	k /s^{-1}	E_a /kJ mol^{-1}	Os(IV/III) reduction/ V	χ_i/ cm^{-1}	θ/°
PEt_2Ph	0.15 ± 0.02	66.0 ± 2.4	-0.34	9.5	122
$PEtPh_2$	3.2 ± 0.15	53.2 ± 1.0	-0.23	11.2	136

Table 5.7 Rates of reaction and activation for the dissociation of Cl^- from the complexes of the type, *mer*-$[OsCl_3(PEt_nPh_{3-n})_3]^{1-}$, where n = 1-2

5.3.3.4 *mer*-$[OsBr_3(PEt_2Ph)_3]^{1-}$

The rate of dissociation of Br^- from *mer*-$[OsBr_3(PEt_2Ph)_3]^{1-}$ is 7.4 ± 0.7 s^{-1} and has an activation energy of 55.6 ± 1.4 kJ mol^{-1}. Considering the different influences effecting the rates and activation energies of the other osmium-halide-phosphine complexes it is immediately obvious caution must be taken when evaluating only one complex of the immediate series, *mer*-$[OsBr_3(PEt_nPh_{3-n})_3]^{1-}$. However, it can be noted that the rate of reaction is, once more, faster and the activation energy lower than the direct chloride analogue, *mer*-$[OsCl_3(PEt_2Ph)_3]^{1-}$ (k = 0.15 s^{-1} E_a = 66.0 kJ mol^{-1}).

5.3.3.5 General comparison of *mer*-$[OsX_3(PZ_nPh_{3-n})_3]^{1-}$

Plots of rate constants against parameters including the electronic parameter, χ_i, or cone angle, θ, against the rate constant, k, or log k have been used previously as an aid to interpretation of numerous dissociative reactions, associative reactions, and

oxidative addition reactions of metal complexes containing tertiary phosphine ligands.[31,37] **Figure 5.7** shows graphs of χ_i and θ against the rate constants, k, log k, and activation energy, E_a, for the dissociation of a halide from the complexes *mer*-$[OsX_3(PZ_nPh_{3-n})_3]^{1-}$, where X = Cl^- or Br^-, and Z = Me or Et. Graphs of the rate constant against either the electronic parameter, χ_i (**Figure 5.7a**), or cone angle, θ (**Figure 5.7b**), show no clear correlation. Plotting the log of the rate constant against χ_i, however, does reveal some trend, particularly for the complexes 1, 2 and 3 (*mer*-$[OsCl_3(PMe_nPh_{3-n})_3]^{1-}$) (**Figure 5.7c**). The general trend is for the rate constant to increase as χ_i decreases. The notable exceptions are complexes, *mer*-$[OsCl_3(PEt_2Ph)_3]^{1-}$ and *mer*-$[OsCl_3(PEtPh_2)_3]^{1-}$. This spread of data is in contrast to that predicted by Giering *et al* for complexes of Class II ligands: a plot of χ_i against k should give a straight line for σ-donor only ligands. This is clearly not the case suggesting that these phosphine ligands are not acting as σ-only donors.

Although Giering *et al* have not used activation energy in their plots, the graph of χ_i against E_a (**Figure 5.7e**) shows a general trend where the activation increases as the χ_i decreases.

No plots of the cone angle, θ, show any fit indicating that the electronic properties of the phosphine ligands are the most important contribution to both the rate constant and activation energy.

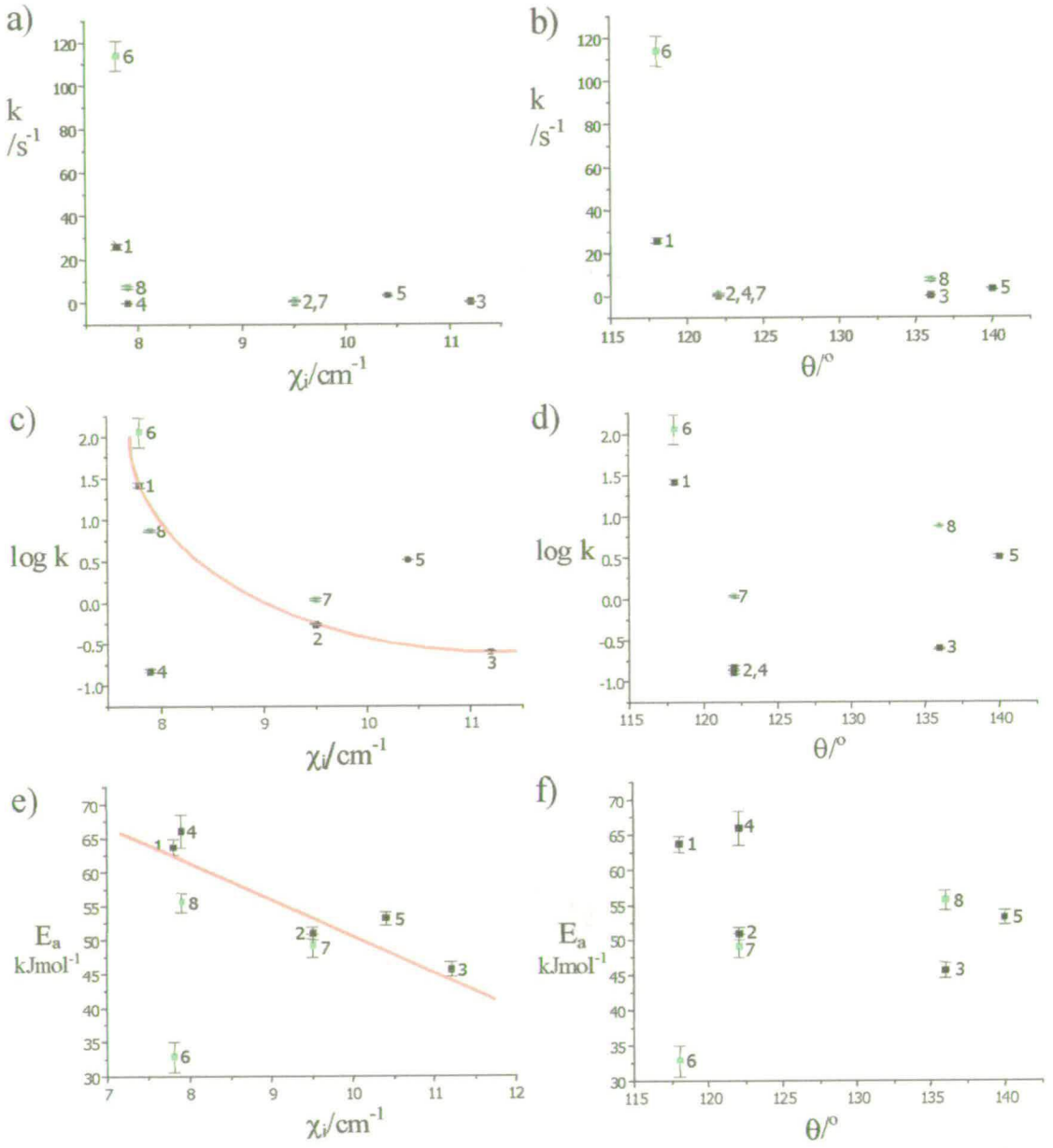

complex	No.
$[OsCl_3(PMe_3)_3]^{1-}$	1
$[OsCl_3(PMe_2Ph)_3]^{1-}$	2
$[OsCl_3(PMePh_2)_3]^{1-}$	3
$[OsCl_3(PEt_2Ph)_3]^{1-}$	4
$[OsCl_3(PEtPh_2)_3]^{1-}$	5
$[OsBr_3(PMe_3)_3]^{1-}$	6
$[OsBr_3(PMe_2Ph)_3]^{1-}$	7
$[OsBr_3(PEt_2Ph)_3]^{1-}$	8

Figure 5.7 For the dissociation of a halide, X^- from the complexes *mer*-$[OsX_3(PZ_nPh_{3-n})_3]^{1-}$, where X = Cl^- or Br^-, Z = Me or Et, and n = 1-3 a) Graph of rate constant, k, against χ_i b) Graph of k against θ c) Graph of log k against χ_i d) Graph of log k against θ e) Graph of activation energy, E_a, against χ_i f) Graph of E_a against θ

5.3.3.6 *mer*-$[OsBr_3(AsMe_2Ph)]^{3-}$ and $[OsBr_3(AsEt_2Ph)]^{1-}$

The rate of dissociation of Br^- from the complexes *mer*-$[OsBr_3(AsZ_2Ph)_3]^{1-}$, where Z = Me or Et, is slower than that of the analogous phosphine complexes. Dichloroethane, therefore, rather than dichloromethane was used as solvent for the double step chronoamperometry experiment because of the higher boiling point (83 °C compared to 40 °C for dichloroethane and dichloromethane respectively) which therefore makes higher temperatures available in order to increase the reaction rate to suitable rates for measurement.

The rate constants, k, and activation energies, E_a, for the arsine complexes, *mer*-$[OsBr_3(AsMe_2Ph)_3]^{1-}$ and *mer*-$[OsBr_3(AsEt_2Ph)_3]^{1-}$ are compared with their phosphine analogues in **Table 5.8**. The starred rate constants (*) have been calculated from the extrapolation of the Arrhenius plot, **Figure 5.8**. The rates of dissociation for the arsine complexes at 243 K are from 5 to 6 orders of magnitude slower than the analogous phosphine complexes.

Group 15 Ligand, Y	k_{243}/s^{-1}	k_{298}/s^{-1}	$E_a/kJ\ mol^{-1}$	Os(IV/III) reduction/ V
PMe_2Ph	1.1 ± 0.4	900*	49.2 ± 1.1	-0.37
PEt_2Ph	7.4 ± 0.7	110*	55.6 ± 1.4	-0.55
$AsMe_2Ph$	$7x10^{-5}$ *	0.18 ± 0.02	84.8 ± 2.0	-0.25
$AsEt_2Ph$	$5x10^{-6}$ *	0.53 ± 0.14	128 ± 5.7	-0.18

Table 5.8 Rate constants, k, and activation energies, E_a, for the dissociation of Br^- from the complexes *mer*-$[OsBr_3Y_3]^{1-}$ *extrapolated from the Arrhenius plot (Figure 5.8)

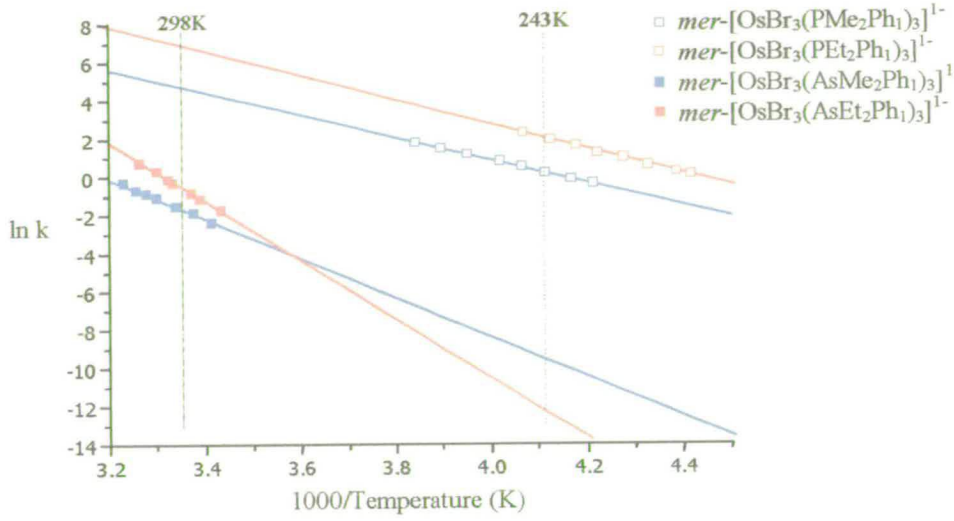

Figure 5.8 Arrhenius plot for the dissociation of Br^- from *mer*-$[OsBr_3Y_3]^{1-}$

The arsine complexes are more difficult to reduce than the phosphine complexes suggesting that either, they are better electron donors, or that these phosphine ligands should be considered as π-accepting ligands. This is contrary to the general trends of the phosphine complexes: the better electron donors generally have the faster rates of dissociation. This generates a number of points.

1) Such a significant change in the rate of dissociation suggests considerably different electronic interactions between the metal, the arsine ligand, and the halide.

2) The arsine and phosphine complexes can not be described in full as just σ-donors. Arsine ligands are expected to be poorer σ-donors than analogous phosphine ligands.

3) The activation energies for the reaction are approximately double that of their phosphine analogues. This would suggest a much stronger metal-halide bond.

Steric constraints within the complex are slightly decreased for the arsine ligands compared to the analogous phosphine ligands because the metal arsine bond is longer. Pictorially this can be represented by a smaller cone angle (**Figure 5.9**). In this way steric considerations are less important for the arsine complexes.

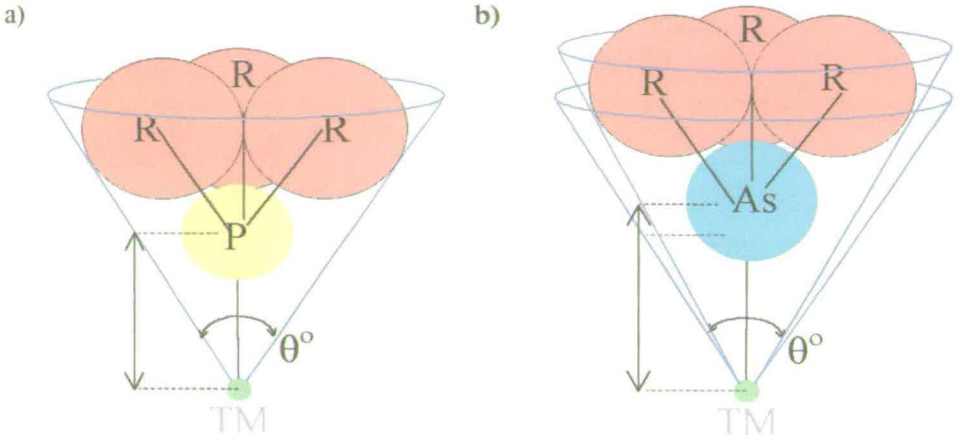

Figure 5.9 Cone angles for a) PR_3 and b) AsR_3

5.3.3.7 Solvent dependence of *mer*-$[OsCl_3(PMe_3)_3]^{1-}$ and *mer*-$[OsCl_3(PEt_2Ph)_3]^{1-}$

The rate constant at 243 K and activation energy for the dissociation of Cl^- from the complexes *mer*-$[OsCl_3Y_3]^{1-}$ in 0.5 M $[N^nBu_4]BF_4$/dichloromethane and 0.5 M $[N^nBu_4]BF_4$/acetonitrile are given in **Table 5.9**.

solvent	Ligand Set	k_{243} /s^{-1}	E_a /kJ mol^{-1}
dcm	$Cl_3(PEt_2Ph)_3$	0.15 ± 0.02	66.0 ±2.4
An	$Cl_3(PEt_2Ph)_3$	2.9 ± 0.40	64.9 ± 2.6
dcm	$Cl_3(PMe_3)_3$	26.2 ± 1.3	63.7 ± 1.1
An	$Cl_3(PMe_3)_3$	33.7 ± 2.0	58.6 ± 4.8

Table 5.9 Rate constants at 243 K and activation energy for the dissociation of Cl^- from *mer*-$[OsCl_3Y_3]^{1-}$

Complexes of the type, *mer*-$[OsCl_3Y_3]^{1-}$ are known to react with acetonitrile giving *mer*-$[OsCl_2An_1Y_3]$. In both cases the activation energies are the same within experimental error when dissolved in dichloromethane or acetonitrile. This indicates

that the mechanism involved in the substitution reaction is not solvent dependent and the activation energy probably involves the cleavage of the Os-Cl bond and the rate is the dissociation of Cl^-. The rates of reaction show a slight increase in acetonitrile rather than dichloromethane as observed previously for the rate determining loss of chloride in the reduction-induced substitution of $[OsCl_6]^{2-}$ (*vide supra*). In this instance, the rate of reaction is also understood to be augmented by the increased solubility of Cl^- in acetonitrile than in dichloromethane. This, and the fact that a five co-ordinate species can be observed in the non-co-ordinating solvent, dichloromethane, strongly suggests a Dissociative mechanism:

$$mer\text{-}[OsCl_3Y_3]^{1-} \xrightarrow{-Cl^-} mer\text{-}[OsCl_2Y_3] \xrightarrow{+An} mer\text{-}[OsCl_2An_1Y_3]$$

5.4 *fac*-[OsX_3Y_3]

The cyclic voltammogram for *fac*-[$OsCl_3(PMe_2Ph)_3$] in 0.5 M [N^nBu_4]BF_4/ dichloromethane at 297 K (**Figure 5.10**) shows a reduction at E_p^{red} 0.19 V and an oxidation at E_p^{ox} +1.20 V; both are one electron, metal based electron transfer processes.

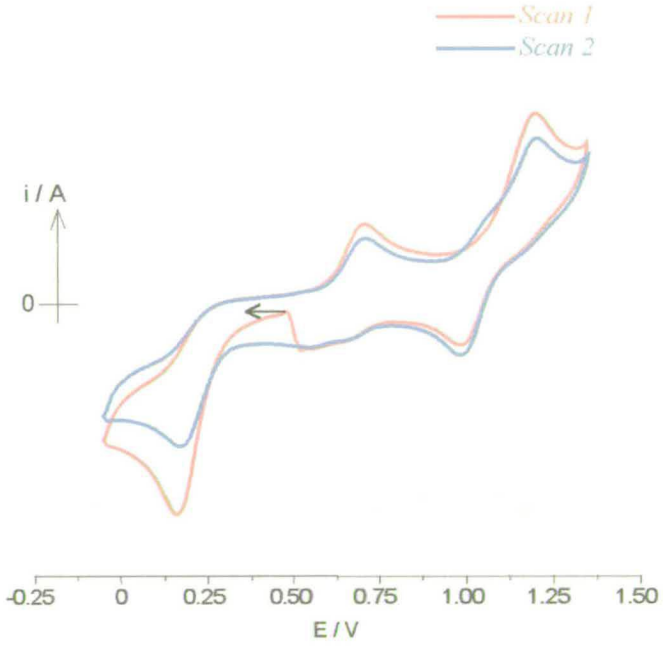

Figure 5.10 CV of *fac*-[$OsCL_3(PMe_2Ph)_3$] in 0.5 M [N^nBu_4]BF_4/dichloromethane at 0.1 V s^{-1}, 297 K

The *fac*-$[OsCl_3(PMe_2Ph)_3]^{0/-1}$ reduction potential is considerably more positive than that of the *mer* isomer. This can be rationalised by considering the π-interactions of each ligand with the Os t_{2g} orbitals (**Figure 5.11**). The *fac* isomer ligands will form three degenerate orbitals through the interaction with two chloride and two phosphine ligands. The *mer* isomer forms three non-degenerate orbitals interacting with three combinations of chlorides and phosphines. On reduction from Os(III) to Os(II), the sixth electron (*red*) fills the last site which is higher in energy in the case of *mer*-$[OsCl_3(PMe_2Ph)_3]$ than *fac*-$[OsCl_3(PMe_2Ph)_3]$.

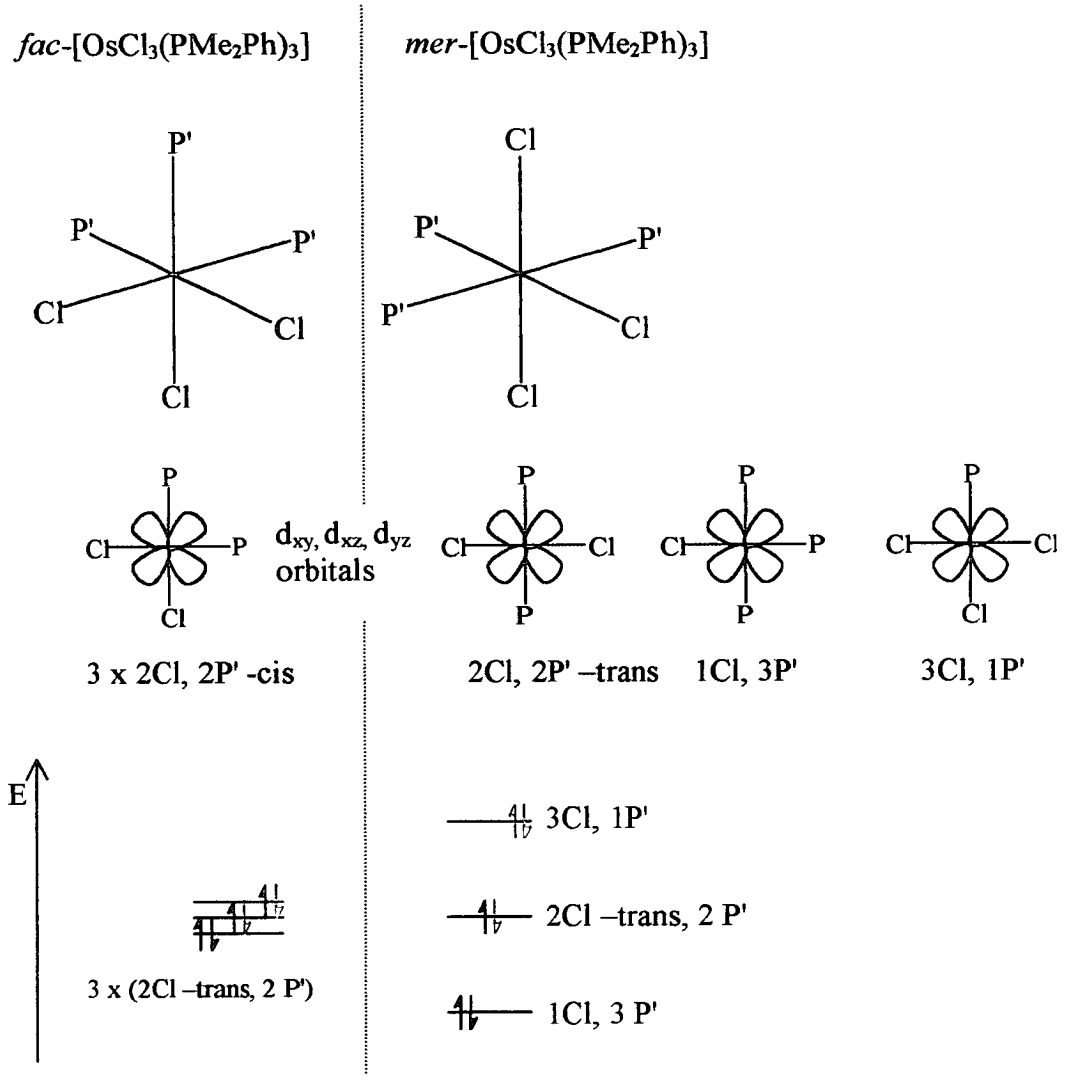

Figure 5.11 Electronic configuration of the Os t_{2g} orbitals for *fac*- and *mer*-$[OsCl_3(PMe_2Ph)_3]$

A daughter product is formed following the reduction process at E_p^{ox} +0.68 V. The EC mechanism involved in the reductive process is believed to be similar to that of the *mer* isomer with the loss of a halide ligand and the gain of a neutral co-ordinating ligand (vide supra). Bulk generation of the reduced species has shown the presence of free chloride in solution to support this mechanism. The daughter product is therefore expected to form one of the thermodynamically more stable complexes, either *cis* or *trans*-$[OsCl_2(PMe_2Ph)_3L]$, where L is a neutral co-ordinating ligand. The potential of the daughter product is not, however, the same potential as measured for the five co-ordinate species or mono-substituted species of *mer*-$[OsCl_3(Me_2Ph)_3]$. A

similar electronic configuration argument can be made for *cis*-$[OsCl_2(PMe_2Ph)_3L]$ as for *fac*-$[OsCl_3(PMe_2Ph)_3]$ and could explain this difference in half-wave potential of the daughter products where *cis*-$[OsCl_2(PMe_2Ph)_3L]$ exhibits a more positive half-wave potential than that of *trans*-$[OsCl_2(PMe_2Ph)_3L]$. Neither the *mer*- or *fac*- isomer of $[OsCl_3(Me_2Ph)_3]$ show a mixture of daughter products as evidenced by the single process in the electrochemical response, indicating that the five co-ordinate intermediate step maintains its original geometry, i.e., the substitution goes via a square based pyramid.

A comparative study of the rate and activation energy of the reduction-induced reaction for the *mer*- and *fac*- isomers of $[OsX_3Y_3]$ would be interesting but is beyond the scope of this thesis.

The oxidation step for *fac*-$[OsCl_3(PMe_2Ph)_3]$ warrants some discussion. On oxidation, a daughter product at *ca.* +1.05 V is formed. The half-wave potential of *mer*-$[OsCl_3(PMe_2Ph)_3]^{1+/0}$ is +1.08 V and therefore the product of oxidation of *fac*-$[OsCl_3(PMe_2Ph)_3]$ is considered to be the *mer*- isomer. Thus the *mer* isomer for the Os(IV) oxidation state is the more stable form. Further consideration of **Figure 5.11** indicates that removal of an electron (blue) from the *fac* isomer yields the electronic configuration at Os of $(d_{xy})^2(d_{xz})^1(d_{yz})^1$ or another such combination. Oxidation of the *mer* isomer results in removal of an electron from either the singly occupied $d\pi$ orbital or from the next energetically lower orbital. The electron which is removed will depend on the energy gap between these two orbitals. If the gap is large then a diamagnetic pairing of electrons occurs but if the gap is small then the paramagnetic case will result. The heavy Os(IV) metal centre will have a large energy gap which will favour formation of diamagnetic Os(IV). The overall energy of this configuration is lower than the energy of the *fac* isomer and hence Os(IV) will favour the *mer* geometry.

Two mechanism of isomerisation of octahedral complexes are generally considered; 1) a Dissociative mechanism, and 2) an intramolecular rearrangement mechanism. Many groups have shown that *cis/trans* and *fac/mer* isomerisation must follow an

intramolecular, non-dissociative course. Complexes studied include, $[M(CO)_4(ER_3)_2]$ (where M = Re, Ru, Os, and E = Si, Ge, Sn, Pb, and R = Me, Et, Pr^n, Bu^n, Ph, Cl^-), $[Cr(CO)_4(C(OMe)Me)(PR_3)]$ (where R = Et or Cy), $[Mo(CO)_4(PR_3)_2]$ (where R = Me, Et, or Bu) and $[Mn(CO)_4Ph(P(OPh)_3)]$.[47,48,49,50] A mechanism for this intramolecular rearrangement was proposed by Bailar – "the Bailar Twist".[51] The mechanism involves the twist of one face of an octahedral complex by 120° via a trigonal prism transition state (**Figure 5.12**) and hence converts a *trans* isomer to *cis* and *fac* to *mer*.

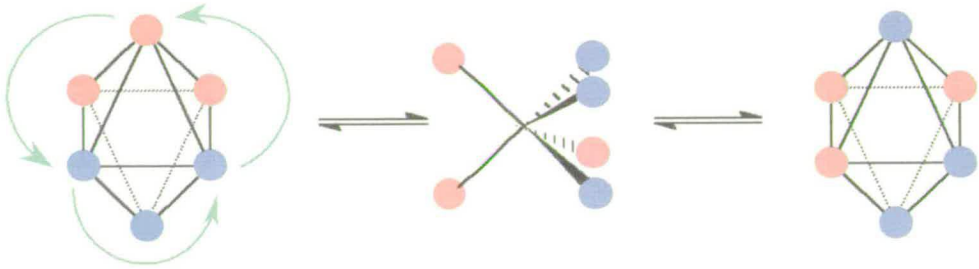

Figure 5.12 Mechanism for the "Bailar Twist"

Using the Nicholson and Shain approach (see 2.2.1.1), a study by Bond *et al* has shown the reduction–induced isomerisation of *fac*-$[Cr(CO)_3(P(OMe)_3)_3]^+$ to *mer*-$[Cr(CO)_3(P(OMe)_3)_3]^+$ to have an activation energy of 15.9 ± 0.7 kJ mol^{-1} and the rate of the reaction at 295 K to be 0.11 ± 0.01 s^{-1}.[52] This was in agreement with earlier studies on $[M(CO)_2(dppm)_2]$ (where, M = Cr, Mo, W and dppm = $Ph_2PCH_2PPh_2$) in which the mechanism was shown to occur via an intramolecular rearrangement.[53] It was noted that the rate of *fac/mer* isomerisation of $[Cr(CO)_3(P(OMe)_3)_3]$ could be greatly augmented by the chemical or electrochemical oxidation of *fac*-$[Cr(CO)_3(P(OMe)_3)_3]$.

The isomeric species *mer*-$[OsCl_3(PMe_2Ph)_3]$ and *fac*-$[OsCl_3(PMe_2Ph)_3]$ are both stable at 294 K in 0.5 M $[N^nBu_4]BF_4$/dichloromethane. However, an investigation of the oxidatively catalysed isomerisation by double-step chronoamperometry has shown the rate of isomerisation to be 2200 ± 160 s^{-1} and the activation energy for the process 26.0 ± 4 kJ mol^{-1}.* The isomerisation reaction of *fac*-$[OsCl_3(PMe_2Ph)_3]^+$ has

* The experiment was carried out by Dr Alan Brown, University of Edinburgh

been simulated in this study using Digisim 2.1. A good fit is obtained (**Figure 5.12**) for the parameters shown in **Table 5.10**. The rate for the forward reaction, $k_f = 1900 \pm 120\ s^{-1}$, is in good agreement with the experimentally observed rate.

homogeneous chemical reaction	chemical reaction parameters		
fac-$[OsCl_3(PMe_2Ph)_3]^+ \xrightarrow{k_f}$	K_E	k_f	k_b
mer-$[OsCl_3(PMe_2Ph)_3]^+$	50	1900	38

Table 5.10 Chemical reaction parameters for the simulated *fac/mer* isomerisation of $[OsCl_3(PMe_2Ph)_3]^+$. Full input data are given in Table 5.3.

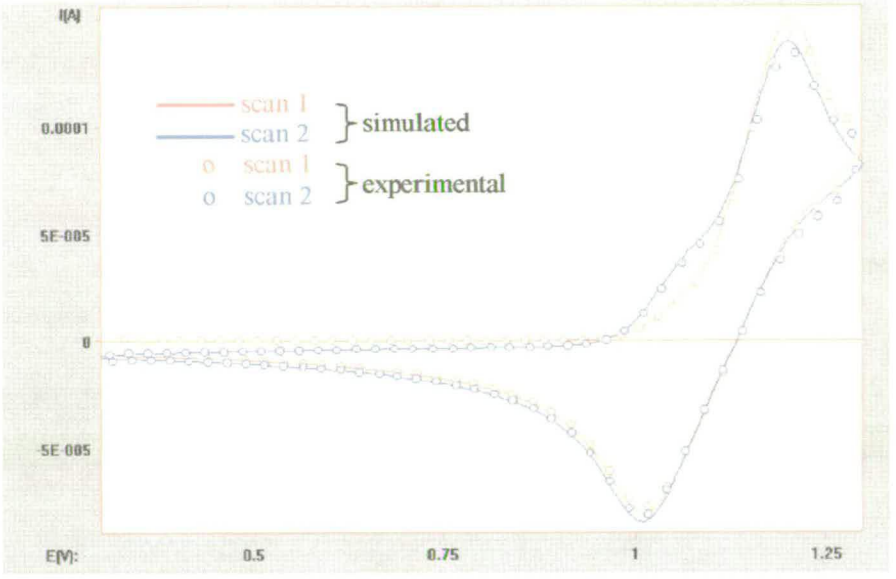

Figure 5.13 Simulated and experimental cyclic voltammograms for the oxidative isomerisation of *fac*-$[OsCl_3(PMe_2Ph)_3]$ to *mer*-$[OsCl_3(PMe_2Ph)_3]^+$ in 0.5 M $[N^nBu_4]BF_4$/dcm at 0.1 V s^{-1}, 297 K

The barrier of the Bailar twist mechanism is the steric hindrance in the intermediate trigonal prism. Analysis of the crystal structure of both the *fac* and *mer* isomers have shown that the structures are possible with only a small distortion of the methyl groups away from their ideal geometry.[43] The dissociation of a Os(II)-chloride bond for *mer*-$[OsCl_3(PMe_2Ph)_3]$ has been measured as 51.0 ± 0.9 kJ mol^{-1}. This is much larger than the activation energy for the *fac/mer* isomerisation, all be it in a different oxidation state. It does suggest, however, that the mechanism of isomerisation is by intramolecular rearrangement.

5.5 Conclusions

Small variations of the group 15 ligand in the complexes *mer*-$[OsX_3Y_3]^{1-}$, where X = Cl^- or Br^- and Y = a tertiary alkyl phosphine/arsine, have been shown to have an effect on the rate of reaction and activation energy for the reduction-induced dissociation reaction where one halide is liberated. The rate of dissociation of X and the activation energy for the process for the complexes of the type *mer*-$[OsX_3Y_3]^-$ are given in **Table 5.11**.

Group 15 Ligand, Y	Os(III/II) Reduction/V	k_{243} /s^{-1}	E_a /kJ mol^{-1}	χ_i /cm^{-1}	Cone angle/^{o}
$Cl_3(PMe_3)_3$	-0.32	26.15 ± 1.3	63.7 ± 1.1	7.8	118
$Cl_3(PMe_2Ph)_3$	-0.25	0.41 ± 0.05	51.0 ± 0.9	9.5	122
$Cl_3(PMePh_2)_3$	-0.18	0.25 ± 0.05	45.7 ± 1.1	11.2	136
$Cl_3(PEt_2Ph)_3$	-0.34	0.15 ± 0.05	66.0 ± 2.4	7.9	122
$Cl_3(PEtPh_2)_3$	-0.23	3.22 ± 0.15	53.2 ± 1.0	10.4	140
$Br_3(PMe_3)_3$	-0.15	114 ± 7	32.8 ± 2.2	7.8	118
$Br_3(PMe_2Ph)_3$	-0.12	1.07 ± 0.40	49.2 ± 1.07	9.5	122
$Br_3(PEt_2Ph)_3$	-0.21	7.4 ± 0.7	55.6 ± 1.4	7.9	136
		k_{298} /s^{-1}			
*$Br_3(AsMe_2Ph)_3$	-0.37	0.18 ± 0.02	84.8 ± 2.0		
*$Br_3(AsEt_2Ph)_3$	-0.45	0.53 ± 0.14	128 ± 5.7		

Table 5.11 Rate constants and activation energies for the dissociation of a halide from *mer*-$[OsX_3Y_3]^{1-}$ in 0.5M $[N^nBu_4]BF_4$/dichloromethane (*measured in 0.5 M $[N^nBu_4]BF_4$/dichloroethane)

An attempt has been made to rationalise the rate constants and activation energy by considering the electrochemical redox potentials and Tolman's electronic parameter,

χ_i, and cone angle, θ. A close examination of the data has generated more questions than the relatively small study can answer.

Linear regression fits for the plots of reduction and oxidation potentials against χ_i show the redox potentials to be dominated by the electron "donor/acceptor property" of the phosphine ligands. The plot of reduction and oxidation potentials against pK_a showed no clear trend suggesting that not only σ-donor properties but π-interactions were also involved in the osmium-phosphine bond despite Giering *et al*'s assignment of the ligands as Class II, σ-donors.

Within certain groups of complexes some trends in the rate of reaction and activation can be observed. The complexes *mer*-$[OsCl_3(PMe_nPh_{3-n})_3]^{1-}$, for example, increase in the rate of dissociation of Cl^- and activation energy as n goes from 1 to 3. The rate of reaction has been attributed to an electronic effect; PMe_3 is most difficult to reduce and has the lowest χ_i value and is understood, therefore, to destabilises the Os(II) metal centre to the greatest extent. The activation energy is the cleavage of the Os-Cl bond in the *trans* position to the phosphine. An increase in activation energy is experienced in order n = 1 to 3 as the cone angle decreases and steric strain is relieved within the complex.

The rate of dissociation of bromide is faster than that of chloride from the analogous complexes. This is attributed to the better leaving group ability of bromide than chloride in dichloromethane, i.e. Br^- is more soluble than Cl^- in dichloromethane.

In acetonitrile the rate of reaction for the complexes *mer*-$[OsCl_3(PMe_3)_3]^{1-}$ and *mer*-$[OsCl_3(PEt_2Ph)_3]^{1-}$ increased and the activation energy for the process was the same within experimental error compared to dichloromethane. This increase in rate is again attributed to the increased solubility of Cl^- in acetonitrile than in dichloromethane.

The arsine analogues of the phosphine complexes undergo the dissociation of a halide at a much slower rate and with a higher activation energy. This is not as might be expected as the reduction potentials are more negative which has previously led to

a faster rate of dissociation. To rationalise this it is considered that either the osmium-arsine bond has π-donor character or the osmium-phosphine bond has π-accepting properties.

Overall, however, no clear trend is immediately apparent in the rate of reaction or activation energy: both steric and electronic influences are closely involved without either ever being clearly dominant. There is a general trend that as Tolman's electronic parameter, χ_i, tends towards zero, the rate of reaction and activation energy for the process increase. Any *trans effect* or *trans influence* experienced within the complex appears to be less significant than the *cis effect* of the phosphine/arsine ligands. A larger study group would be necessary to make a more confident assignment of the effects that the electronic and steric properties have on the rate of reaction and activation energy and to further understand the π-interactions of osmium-phosphine and osmium-arsine bonds.

Oxidation of *fac*-$[OsCl_3(PMe_2Ph)_3]$ causes rapid isomerisation to *mer*-$[OsCl_3(PMe_2Ph)_3]^+$. The rate of reaction at 297 K has been simulated as 1900 ± 120 s^{-1} which compares well with experimentally measured data. A relatively low activation energy for the process, 26.0 kJ mol^{-1} compared to the activation energy required to break the Os(II)-chloride bond in *mer*-$[OsCl_3(PMe_2Ph)_3]$, 51.0 kJ mol^{-1} suggests the mechanism for the *fac/mer* isomerisation might be an intramolecular rearrangement, i.e., via the Bailar twist mechanism.

5.5 References

[1] Dwyer, F. P.; Nyholm, R. S.; Tyson, B. T.; *J. Proc. Roy. Soc. N.S.W.*, 1948, **81**, 272
[2] Nyholm, R. S.; Sutton, G. T.; *J. Chem. Soc.*, 1958, 572
[3] Vaska, L.; *Chem. Ind. (London)*, 1961, 1402
[4] a) Chatt, J.; Hayter, R. G.; *J. Chem. Soc.*, 1961, 896 b) Chatt, J.; Leigh, G. J.; Mingos, D. M. P.; Paske, R. J.; *J. Chem. Soc. (A).*, 1968, 2636
[5] Chatt, J.; Leigh, G. J.; Mingos, D. M.P.; *J. Chem. Soc. (A).*, 1969, 1674
[6] Douglas, P. G.; Shaw, B. L.; *J. Chem. Soc. (A)*, 1979, 334
[7] Hudson, A.; Kennedy, M. J.; *J. Chem. Soc. (A)*, 1969, 1116
[8] Leigh, G. J.; Mingos, D. M. P.; *J. Chem. Soc. (A)*, 1970, 587
[9] Aslanov, L.; Manson, R.; Wheeler, A. G.; Wimp, P. O.; *J. Chem. Soc., Chem. Commun.*, 1970, 30
[10] Hoffman, P. R.; Caulton, K. G.; *J. Am. Chem. Soc.*, 1975, **97**, 4221
[11] Moore, D. S.; Robinson, P. D.; *Inorg. Chem.*, 1979, **18**, 2307
[12] Chakravarty, A. R.; Cotton, F. A., Tocher, D. A.; *Acta Cryst.*, 1985, **C41**, 698
[13] La Placa, S. J.; Ibers, J. A.; *Inorg. Chem.*, 1965, **4**, 778
[14] Brookhart, M.; Gran, M. L. H.; *J. Organomet. Chem.*, 1983, **250**, 395
[15] Chatt, J.; *Nature*, 1950, 637
[16] Abel, E. W.; Bennett, A.; Wilkinson, G.; *J.Chem. Soc.*, 1959, 2323
[17] Cotton, F. A.; *Inorg. Chem.*, 1964, **5**, 702
[18] Cotton, F. A.; Kraihanzel, C. S.; *J. Am. Chem. Soc.*, 1962, **84**, 4432
[19] Bigorgne, M.; *C. R. Acad. Sci. Paris*, 1960, **250**, 3484
[20] Bigorgne, M.; *J. Inorg. Nucl. Chem.*, 1964, **26**, 107
[21] Tolman, C. A.; *J. Am. Chem. Soc.*, 1970 , **92**, 2953
[22] Bodner, G. M.; Gogan, C.; Whittern, D. N.; *J. Organomet. Chem.*, 1983, **243**, 305
[23] Tolman, C. A.; *Chem. Rev.*, 1977, **77**, 313
[24] a) Honeychuck, R. V.; Hersh, W. H.; *Inorg. Chem.*, 1987, **26**, 1826 b) Blau, R. J.; Espenson, J. H.; *Inorg. Chem.*, 1986, **25**, 878 c) Masters, F. A.; Bossard, G. E.; George, T. A.; Brownlee, R. T. C.; O'Connor, M. J.; Wedd, A. G.; *Inorg. Chem.*, 1983, **22**, 908
[25] a) Ihmels, K.; Redher, D.; *Organometallics*, 1985, **4**, 1334 b) Bartik, T.; Himmler, T.; Schulte, H. G.; Seevogel, K. J.; *J. Organomet. Chem.*, 1984, **272**, 29 c) Gray, G. M.; Kraihanzel, C. S.; *J. Organomet. Chem.*, 1983, **241**, 201
[26] a) Carrol, W. E.; Deeney, F. A.; Delaney, F. A.; Lalor, F. J.; *J. Chem. Soc. Dalton Trans.*, 1973, 718 b) Inoue, H.; Sasagawa, M.; Fluck, E.; *Z. Naturforsch., B: Anorg. Chem., Org. Chem.*, 1985, **40B**, 22 c) Johnson, B. V.; Steinmetz, A. L.; Ouseph, P. J.; *J. Coord. Chem.*, 1985, **14**, 103
[27] a) Puddephatt, R. J.; Dignard-Bailey, L.; Bancroft, G. M.; *Inorg. Chim. Acta*, 1985, **96**, 91 b) Bursten, B. E.; Darensbourg, D. J.; Kellog, G. E.; Lichtenberger, D. L.; *Inorg. Chem.*, 1984, **23**, 4361 c) Ikuta, S.; Kebarle, P.; Bancroft, G. M.; Chain, T.; Puddlephatt, R. J.; *J. Am. Chem. Soc.*, 1982, **104**, 5899
[28] Whangbo, M. H.; Steward, K. R.; *Inorg. Chem.*, 1982, **21**, 1720 b) Xiaxi, S., Trogle, W. C; Ellis, D. E.; Berkovitch-Yellin, Z.; *J. Am. Chem. Soc.*, 1983, **105**, 7033 c) Marynick, D. S.; *J. Am. Chem. Soc.*, 1984, **106**, 4064
[29] a) Kuchynka, D. J.; Amatore, C.; Kochi, J. K.; *Inorg. Chem.*, 1986, **25**, 4087 b) Hershberger, J. W.; Kochi, J. K.; *Polyhedron, Chem.*, 1983, **2**, 929 c) Bond, A. M.; Carr, S. W.; Colton, R.; Kelly, D. P.; *Inorg. Chem.*, 1983, **22**, 989
[30] a) Orpen, A. G.; Connelly, N. G.; *J. Chem. Soc., Chem. Commun.*, 1985, 1310 b) Wovkulich, M. J.; Atwood, J. L.; Canada, L.; Atwood, J. D.; *Organometallics*, 1985, **4**, 867 c) Bresciani-Pahor, N.; Forcolin, M.; Marzilli, L. G.; Randaccio, L.; Summers, M. F.; Toscano, P. J.; *Coord. Chem. Rev.*, 1985, **63**, 1
[31] Golvin, N. M.; Rahman, M.; Belmonte, J. E.; Giering, W. P.; *Organometallics*, 1985, **4**, 1981

[32] Tolman, C. A., Seidel, W. C.; Gosser, L. W.; *J. Am. Chem. Soc.*, 1974, **96**, 2329
[33] a) Musco, A.; Kuran, W.; Silvani, A.; Anker, M.; *J. Chem. Soc., Chem. Commun.*, 1973, 938 b) Kuran, W.; Musco, A.; *Inorg. Chim. Acta.*, 1975, **12**, 187 c) Mann, B. E.; Musco, A.; *J. Chem. Soc., Dalton Trans.*, 1975, 1673
[34] Druliner, J. D.; English, A. D.; Jesson, J. P.; Meakin, P.; Tloman, C. A.; *J. Am. Chem. Soc.*, 1976, **98**, 2156
[35] Hoffman, P. R.; Caulton, K. G.; *J. Am. Chem. Soc.*, 1975, **97**, 4221
[36] Barnett, K. W.; Pollmann, T. G.; *J. Organomet. Chem.*, 1974, **69**, 413
[37] Rahmann, M.; Liu, H.; Eriks, K.; Prock, A.; Giering, W. P.; *Organometallics*, 1989, **8**, 1
[38] Chang, C. Y.; Johnson, C. E.; Richmond, T. G.; Chen, Y. T.; Trogler, W. C.; Basolo, F.; *Inorg. Chem.*, 1981, **20**, 3167
[39] Halpern, J.; Phelen, P. F.; *J. Am. Chem. Soc.*; 1972, **94**, 1881
[40] Cipriano, R. A.; Levason, W.; Mould, R. A. S; Pletcher, D.; Webster, M.; *J. Chem. Soc. Dalton Trans.*, 1990, 339
[41] Cipriano, R. A.; Levason, W.; Mould, R. A. S; Pletcher, D.; Webster, M.; *J. Chem. Soc. Dalton Trans.*, 1990, 2609
[42] Champness, N. A.; Levason, W.; Mould, R. A. S; Pletcher, D.; Webster, M.; *J. Chem. Soc. Dalton Trans.*, 1991, 2777
[43] Nicholas Payne, *PhD Thesis, University of Edinburgh*, 1997
[44] Macnamara, K. G.; Parsons, S.; Payne, N. N.; Yellowlees, L. J.; *in press*
[45] Vyvyan Coombe, *PhD Thesis, University of Edinburgh*, 1985
[46] Coombe, V. T.; Heath, G. A.; Stephenson, T. A., Whitelock, J. D., Yellowlees, L. J.; *Chem. Soc. Dalton Trans.*, 1985, 947
[47] a) Graham, W. A. G.; Pomeroy, R. K.; Vancea, L.; *J. Am. Chem. Soc.*, 1976, **98**, 1407. b) Calhoun, H. P.; Graham, W. A. G.; Pomeroy, R. K.; Vancea, L.; *Inorg. Chem.*, 1977, **16**, 1508
[48] Fischer, H.; Fischer, E. O.; Werner, H.; *J. Organomet. Chem.*, 1974, **73**, 331
[49] a) Darensbourg, D. J.; Kump, R. L.; *Inorg. Chem.*, 1978, **17**, 2680. b) Darensbourg, D. J.; *Inorg. Chem.*, 1979, **18**, 14. c) Cotton, F. A.;Darensbourg, D. J.; Klein, S.; Kolthammer, B. W. S.; *Inorg. Chem.*, 1982, **21**, 2661.
[50] Stewart, R. P.; *Inorg. Chem.*, 1979, **18**, 2083
[51] Bailer, J. C.; *J. Inorg. Nucl. Chem.*, 1958, **8**, 165
[52] Bond, A. M.; Colton, R.; Kevekordes, J. E.; *Inorg. Chem.*, 1986, **25**, 749
[53] Bond, A. M.; Grabaric, B. S.; Jockowski, J. J.; *Inorg. Chem.*, 1978, **17**, 2153

CHAPTER SIX:

Substitution Reactions of Osmium(II) Hexathiocyanate Isomers

Substitution Reactions of Osmium (II) Hexathiocyanate Isomers

6.1 Introduction

This chapter presents a study of the isomeric series of complexes, *cis*-$[Os(NCS)_2(SCN)_4]^{z-}$, *fac*-$[Os(NCS)_3(SCN)_3]^{z-}$, and $[Os(NCS)_6]^{z-}$. By way of introduction, the nature of the thiocyanate ligand is considered and the variety of complexes formed with this ligand.

The thiocyanate ion is the most common and most comprehensively investigated ambidentate ligand. It is readily available, stable, and forms many complexes of both N- and S-bound isomers which can be distinctly different in their behaviour. The ambidentate thiocyanate ion should co-ordinate to hard Lewis acids with its N atom as a hard Lewis base and to soft Lewis acids with its S atom as a soft Lewis base.[1,2,3] In this way, the thiocyanate ion is a useful ligand in characterising the Lewis acid character of the central metal atoms, especially if no other ligands participate in the co-ordination sphere, since these may influence the bonding of the thiocyanate by electronic or steric effects.[4,5]

In 1987 Preetz *et al* prepared for the first time all 10 possible isomers $[Os(NCS)_n(SCN)_{6-n}]^{z-}$ of both Os(III) and Os(IV).[6] The series is well characterised by well-resolved IR, Raman, and uv-vis spectra and recently published X-ray crystal structures of $[N^nBu_4]_2[Os(NCS)_6]$, $[N^nBu_4]_3[Os(NCS)_6]$, and $[Co(NH_3)_6][Os(SCN)_6]$.[7,8,9] Analogous series include, $[Ru(NCS)_n(SCN)_{6-n}]^{3-}$ (9 isomers, n = 1-6), $[Rh(NCS)_n(SCN)_{6-n}]^{3-}$ (5 isomers, n = 0-4), $[Ir(NCS)_n(SCN)_{6-n}]^{3-}$ (8 isomers, n = 0-5), and have been isolated and characterised using a variety of physical methods.[10,11,12,13,14] A feature of these complexes is that the –NCS ligand

tends to be almost linear (*ca.* 173° for the complex $[N^nBu_4]_3[Os(NCS)_6]$) whereas the –SCN ligand is bent with a metal-sulphur-carbon angle of *ca.* 109° for the complex $[Co(NH_3)_6][Os(SCN)_6]$.[8,9] It is generally believed that this difference in geometry causes greater steric strain in the –SCN ligand set and makes the –NCS ligand set more stable.[15]

Complexes of the type, $[M(NCS)_n(SCN)_{6-n}]^{4-/3-}$, where M = Ru, Os, Ir, and Rh, are all thought of as boarder line hard/soft metal centres likely to bond to either end of the ambidentate ligand. Preetz gave the order:

$$Rh^{3+} < Ir^{3+} << Ru^{3+} < Os^{3+} < Os^{4+}$$

where Rh^{3+} is the softest and Os^{4+} the hardest Lewis acid.[6] Harder metals have been shown to prefer the harder –NCS linkage and the softer metals the softer –SCN option.

Cyclic voltammetry of the isomeric series $[Os(NCS)_n(SCN)_{6-n}]^{3-}$, where n = 0 to 6, showed two metal based redox couples; Os(IV/III) between +0.38 V and +0.49 V and Os(III/II) between –1.11 V and –0.78 V against a Ag/AgCl reference electrode where the ferrocenium/ferrocene redox couple was at +0.55 V (**Table 6.1**).[6] For Os(III)/(IV) $|i_p^{ox}/i_p^{red}|$ for n = 2-6 are approximately equal to one: a chemically reversible process within the limits of detection. For n = 0 and 1, the couple is not fully chemically reversible. The Os(II)/(III) redox couple is not chemically reversible at room temperature and 0.1 V s^{-1} for any value of n. The peak-to-peak separation, ΔE_p, gets larger with increasing number of S-bound isomers. For both the oxidation and reduction, the more S-bound ligands present in the isomer, the more negative the half-wave potential, illustrating the increased electron density on the metal centre and, by association, the more electron donating character of the –SCN linkage. Back bonding in the -NCS ligand relieves electron density at the metal centre making the complex harder to oxidise and conversely easier to reduce. The increase in potential is not stepwise. In all cases the *trans-* and *mer-* isomers have a more negative half-wave potential than the *cis* and *fac* isomers. The special stability of the unsymmetrical *fac* and *cis* isomers is accounted for by Preetz as a synergic

relationship between π-donation of –SCN and π-back donation to –NCS creating a dipole which is most obvious in the *fac* isomer.[10,16]

	Os(II)/(III)			Os(III)/(IV)		
n	$E_{1/2}$ / V	ΔE / mV	$\lvert i_p^{ox}/i_p^{red}\rvert$	$E_{1/2}$ / V	ΔE / mV	$\lvert i_p^{ox}/i_p^{red}\rvert$
0	-1.109	162	<<1	0.413	80	~1
1	-1.037	144		0.415	72	~1
2 *cis*	-0.987	119		0.434	60	~1
2 *trans*	-1.003	129		0.378	75	~1
3 *fac*	-0.937	147		0.457	60	~1
3 *mer*	-0.946	127		0.414	59	~1
4 *cis*	-0.886	120		0.450	59	~1
4 *trans*	-0.890	119		0.440	65	~1
5	-0.834	108		0.467	71	~1
6	-0.782	94	~1	0.485	71	~1

Table 6.1 Half-wave potentials, ΔE, and $\lvert i_p^{ox}/i_p^{red}\rvert$, for the reduction and oxidation of the series of complexes $[Os(NCS)_n(SCN)_{6-n}]^{3-}$ in ethanol.[6] Note that values are adjusted from the original paper so that the ferrocenium/ferrocene redox couple is at +0.55 V

The differing electronic character of the isomers is also displayed in the procedure used to separate the isomers, n = 1 to 6. Increasing the number of N-bound ligands gives the complex a greater electron density at the surface of the complex which were, therefore, slower to elute from a diethylaminoethyl (DEAE) cellulose ion exchange column due to the increased interaction with the stationary phase. The isomer, $[Os(SCN)_6]^{3-}$, was the most mobile in 1.5 M KSCN/methanol; 116 times faster than $[Os(NCS)_6]^{3-}$.[6]

All isomers can undergo oxidation to Os(IV) without change in the co-ordination sphere except $[Os(SCN)_6]^{2-}$ which rearranges to 25-40 % $[Os(NCS)(SCN)_5]^{2-}$.[6] In fact, $[Os(SCN)_6]^{3-}$ has been shown to undergo oxidation in most organic solvents (especially acetone) in air with an accompanying colour change from a red to a blue solution.[17] The isomerism shows Os(IV) prefers the –NCS linkage, indicating that it is a harder Lewis base than –SCN.

6.2 Experimental

6.2.1 Chemical Synthesis

The complexes *cis*-$[Os(NCS)_2(SCN)_4]^{3-}$, *fac*-$[Os(NCS)_3(SCN)_3]^{3-}$, and $[Os(NCS)_6]^{3-}$ were prepared by the method of Preetz *et al.*[6] The preparations gave mixtures of the isomers $[Os(NCS)_n(SCN)_{6-n}]^{3-}$ (n = 0 to 6), each preparation giving favourable amounts of the desired isomer. Higher reaction times and temperatures favour the more thermodynamically stable N-bound isomers. The approximate ratios of isomers from each preparation are given in the original paper.

cis-$[Os(NCS)_2(SCN)_4]^{3-}$

300 mg (0.4 mmol) $K_2[OsBr_6]$ (Johnson Matthey) was dissolved in 16 ml aqueous 1.5 M KSCN solution and stirred for three days at 313 K. The solution was then filtered and the water evaporated and the solid re-dissolved in the minimum of methanol.

fac-$[Os(NCS)_3(SCN)_3]^{3-}$

300 mg (0.62 mmol) $K_2[OsCl_6]$ was dissolved in 25 ml aqueous 1.5 M KSCN solution and stirred for seven days at 333 K. The solution was then filtered and the water evaporated and the solid re-dissolved in the minimum of methanol.

The non-trivial separation of isomers was achieved using diethylaminoethyl (DEAE) cellulose anion exchange resin (Sigma) with a concentration gradient of 0 to 1.5 M KSCN/methanol solution as the mobile phase at 278 K. The greater the number of N-bound ligands the slower the passage through the column and hence a greater concentration of KSCN/methanol solution was required to separate the isomers. The separated red/orange solutions were concentrated precipitating KSCN. The solution was filtered and excess $[N^nBu_4]SCN$ added for the metathesis exchange of counter ions. Addition of acetone precipitated microfine crystals of $[N^nBu_4]_2K[Os(NCS)_3(SCN)_3]$. The complexes were recrystallised at least twice from acetone/ether.

$[N^nBu_4]_3[Os(NCS)_6]$

280 mg (0.22 mmol) *cis*-$[N^nBu_4]_3[Os(NCS)_2(SCN)_4]$ was heated to 413 K over one week in a sealed glass vial and heated at 413 K for a further two weeks. The resulting solid was recrystallised from acetone ether.

The isomers were characterised by a combination of uv-vis and IR spectroscopy, electrochemical redox potentials, and X-ray crystallography.

Crystal structure of cis-$[N^nBu_4]_3[Os(NCS)_2(SCN)_4]$

X-ray diffraction data was collected on a Bruker AXS SMART diffractometer equipped with a CCD area detector, Oxford Cyrosystems cryostream and graphite monochromated Mo-K_α radiation using ω-θ scans in the range $1.29 \leq \theta \leq 26.45^\circ$. The crystal was a red plate of dimensions 0.20 mm x 0.15 mm x 0.08 mm. Of a total 38458 reflection collected, 21029 were independent. The final difference map extrema were 3.659 and –0.705 e.Å^{-3} with a final R of 7.93 % of 13467 strong data.

An optimised numerical absorption correction based on face indices was applied (T_{min} = 0.729, T_{max} = 0.928). The space group is a non-centrosymmetric Cc with two *cis*-$[N^nBu_4]_3[Os(NCS)_2(SCN)_4]$ groups per asymmetric unit. Due to high thermal motion it was necessary to use distance restraints (obtained from International Tables) on all the -SCN ligand distances.

Empirical formula	$C_{108}H_{216}N_{18}Os_2S_{12}$	a / Å	48.132(3)
Formula weight	2532.11	b / Å	16.8015(10)
Crystal system	monoclinic	c / Å	17.1893(10)
Space group	Cc	α / °	90
Volume / Å^3	13626(14)	β / °	101.4
Z	4	γ / °	90
Temperature / K	150(2)	μ(Mo-K_α) / mm^{-1}	2.093
Wavelength / Å	0.71073	R_1[F>4σF]	0.0793
Density calc. / Mg m^{-3}	1.234	wR_2 (all data)	0.2108

Table 6.2 Crystallographic data for $[N^nBu_4]_3[Os(NCS)_2(SCN)_4]$

Crystal structure of fac-$[N^nBu_4]_2K[Os(NCS)_3(SCN)_3]$

X-ray diffraction data was collected on a Bruker AXS SMART diffractometer equipped with a CCD area detector, Oxford Cyrosystems cryostream and graphite monochromated Mo-K_α radiation using ω-θ scans in the range $1.29 \leq \theta \leq 26.44°$. The crystal was a red shard of dimensions 0.30 mm x 0.08 mm x 0.05 mm. Of a total 13124 reflection collected, 8753 were independent. The final difference map extrema were 1.712 and –0.507 e.Å^{-3} with a final R of 6.61 % of 4857 strong data. An optimised numerical absorption correction based on face indices was applied (T_{min} = 0.928, T_{max} = 0.592).

Empirical formula	$C_{38}H_{72}KN_8OsS_6$	a / Å	10.5101(17)
Formula weight	1062.7	b / Å	31.466(5)
Crystal system	monoclinic	c / Å	15.899(3)
Space group	Cc	α / °	90
Volume / Å^3	5184.9(14)	β / °	99.565(3)
Z	4	γ / °	90
Temperature / K	150(2)	μ(Mo-K_α) / mm^{-1}	2.814
Wavelength / Å	0.71073	R_1[F>4σF]	0.0661
Density calc. / Mg m^{-3}	1.361	wR_2 (all data)	0.1545

Table 6.3 Crystallographic data for $[N^nBu_4]_2K[Os(NCS)_3(SCN)_3]$

$[N^nBu_4]_3[Os(NCS)_6]$ crystal structure

X-ray diffraction data was collected on a Bruker AXS SMART diffractometer equipped with a CCD area detector, Oxford Cyrosystems cryostream and graphite monochromated Mo-K_α radiation using ω-θ scans in the range $1.46 \leq \theta \leq 28.82°$. The crystal was an orange block of dimensions 0.27 mm x 0.27 mm x 0.36 mm. Of a total 88308 reflection collected, 6153 were independent. The final difference map extrema were 2.10 and –2.26 e.Å^{-3} with a final R of 5.74 % of 212 strong data. An optimised numerical absorption correction based on face indices was applied (T_{min} = 0.656, T_{max} = 1.000).

Empirical formula	$C_{54}H_{208}KN_9OsS_6$	a / Å	24.195(2)
Formula weight	1265.91	b / Å	24.195(2)
Crystal system	cubic	c / Å	24.195(2)
Space group	Pa-3	α / °	90
Volume / Å^3	14163.7	β / °	90
Z	8	γ / °	90
Temperature / K	150(2)	μ(Mo-K_α) / mm^{-1}	2.012
Wavelength / Å	0.71073	$R_1[F>4\sigma F]$	0.0574
Density calc. / Mg m^{-3}	1.187	wR_2 (all data)	0.0458

Table 6.4 Crystallographic data for $[N^nBu_4]_3[Os(NCS)_6]$

6.2.2 Electrochemistry

All solvents were purified and dried as outlined in 3.2.1. $[N^nBu_4]BF_4$ was prepared as outlined in 3.2.2.

All half-wave potentials were measured in a 0.5 M $[N^nBu_4]BF_4$/dichloromethane solution using a standard three electrode electrochemical system and are quoted against a Ag/AgCl reference electrode for which the ferrocenium/ferrocene redox couple was measured at +0.55 V.

Rate constants for the reduction induced substitution reaction of a thiocyanate ligand for pyridine or acetonitrile on the Os(II) complex were measured by the double-step chronoamperometry technique in 0.2 M $[N^nBu_4]BF_4$/(pyridine or acetonitrile) solutions. The concentrations of the complexes $[Os(NCS)_n(SCN)_{6-n}]^{3-}$ (n = 0 to 6) were 0.0020 M ± 0.0002. All experiments were carried out under a strictly water-free environment.

The rate constant for the reaction of acetonitrile with *cis*-$[Os(NCS)_2(SCN)_4]^{3-}$ and *fac*-$[Os(NCS)_3(SCN)_3]^{3-}$ at 323 K were calculated by the plot of $\ln[A]/[A_0]$ against time giving a straight line with gradient k (See introduction for integrated rate law of first order reaction). The concentration, A, and starting concentration, A_0, of the complex were calculated by the area under the differential pulse peak for the Os(III)/(II) reduction.

6.2.3 *In situ* spectroelectrochemical uv-vis

In situ spectroelectrochemical uv-vis experiments were carried out using the optically transparent thin layer electrode (OTTLE) as described in chapter two.

A 0.5 M $[N^nBu_4]BF_4$/dichloromethane solution was used after being previously bubbled with argon to displace any dissolved dioxygen. 2 to 3 mg of the complexes, $[Os(NCS)_n(SCN)_{6-n}]^{3-}$ (n = 6, 3, and 2), were weighed into a 1ml standard flask and dissolved in the 0.5 M $[N^nBu_4]BF_4$/dichloromethane solution. The cell was assembled and placed in the cavity and cooled to 223K. The potential was set to reduce at –1.20 V and oxidise at +0.60 V and the process followed by uv-visible spectroscopy every five minutes.

6.2.4 IR spectroelectrochemistry

In situ experiments were carried out as described in 2.3.3 at 293 K ± 2 under nitrogen.

Ex situ experiments were carried out in the H-cell (see 2.1) at 243 K and the solution IR spectra were measured in the micro-cavity KBr cell (see 2.3.2) under nitrogen.

6.3 Results and Discussion

6.3.1 Crystal Structures for cis-$[N^nBu_4]_3[Os(NCS)_2(SCN)_4]$, fac-$[N^nBu_4]_2K[Os(NCS)_3(SCN)_3]$, and $[N^nBu_4]_3[Os(NCS)_6]$

The molecular crystal structure of $[N^nBu_4]_3[Os(NCS)_2(SCN)_4]$ is shown in **Figure 6.1**. The space group is non-centrosymmetric Cc with two $[N^nBu_4]_3[Os(NCS)_2(SCN)_4]$ groups per asymmetric unit (for clarity, only one $[Os(NCS)_2(scn)_4]^{2-}$ dianion is shown without the counter ions). Each $[Os(NCS)_2(SCN)_4]^{3-}$ trianion is boxed in a cube by a counter ion on all six faces and each counter ion is shared between two $[Os(NCS)_2(SCN)_4]^{3-}$ trianions. Selected bond lengths and angles are given for both $[Os(NCS)_2(SCN)_4]^{3-}$ trianions in **Table 6.5**.

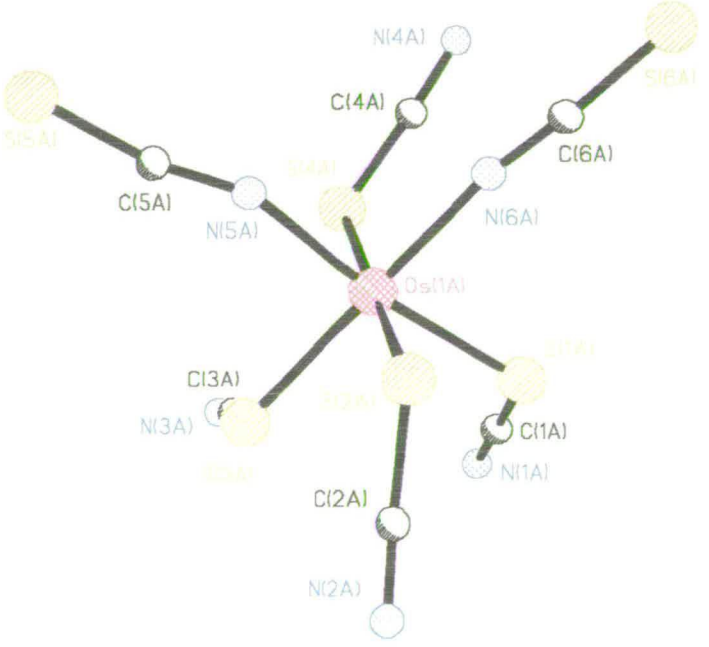

Figure 6.1 Crystal structure for *cis*-$[N^nBu_4]_3[Os(NCS)_2(SCN)_4]$

Bond Lengths / Å		Bond Angles / °	
Os(1A)-S(1A)	2.325(4)	C(1A)-S(1A)-Os(1A)	113.8(6)
Os(1A)-S(2A)	2.357(4)	C(2A)-S(2A)-Os(1A)	108.2(7)
Os(1A)-S(3A)	2.377(4)	C(3A)-S(3A)-Os(1A)	109.2(5)
Os(1A)-S(4A)	2.405(4)	C(4A)-S(4A)-Os(1A)	105.1(6)
Os(1A)-N(5A)	2.091(10)	C(5A)-N(5A)-Os(1A)	152.5(12)
Os(1A)-N(6A)	2.095(9)	C(6A)-N(6A)-Os(1A)	169.8(12)
Os(1B)-S(1B)	2.405(4)	C(1B)-S(1B)-Os(1B)	112.3(6)
Os(1B)-S(2B)	2.373(4)	C(2B)-S(2B)-Os(1B)	110.4(5)
Os(1B)-S(3B)	2.288(6)	C(3B)-S(3B)-Os(1B)	110.1(12)
Os(1B)-S(4B)	2.348(5)	C(4B)-S(4B)-Os(1B)	110.8(6)
Os(1B)-N(5B)	2.146(13)	C(5B)-N(5B)-Os(1B)	152.5(16)
Os(1B)-N(6B)	2.066(11)	C(6B)-N(6B)-Os(1B)	171(2)

Table 6.5 Selected bond lengths and angles for *cis*-$[N^nBu_4]_3[Os(NCS)_2(SCN)_4]$

It is clear that the –SCN ligand is bent. On average, the C-S-Os bond angle is 109°. The –NCS ligand is more linear; the two N-C-Os bond angles are 152.5° and 169.8°, slightly less than the average of 173° in the complex $[N^nBu_4]_3[Os(NCS)_6]$.[9] The Os-N bond lengths are as expected for an Os(III) complex.[9]

The crystal structure for *fac*-$[N^nBu_4]_2K[Os(NCS)_3(SCN)_3]$ is shown in **Figure 6.2**. The $[N^nBu_4]^+$ counter ions are not shown. Each $[Os(NCS)_3(SCN)_3]^{3-}$ trianion is linked by a K^+ counter ion forming a chain. Two $[N^nBu_4]^+$ counter ions surround each $[Os(NCS)_3(SCN)_3]^{3-}$ trianion. Selected bond lengths and angles are given in **Table 6.6**.

The Os-N and Os-S bond lengths are as expected for an Os(III) complex.[8,9] Interestingly, two of the C-N-Os bond angles, 131.4° and 138.9°, are much more acute than the average of 173° for the complex $[N^nBu_4]_3[Os(NCS)_6]$. Presumably the

difference in bond angle is due to the geometry imposed by the potassium counter ion in forming the polymeric chain.

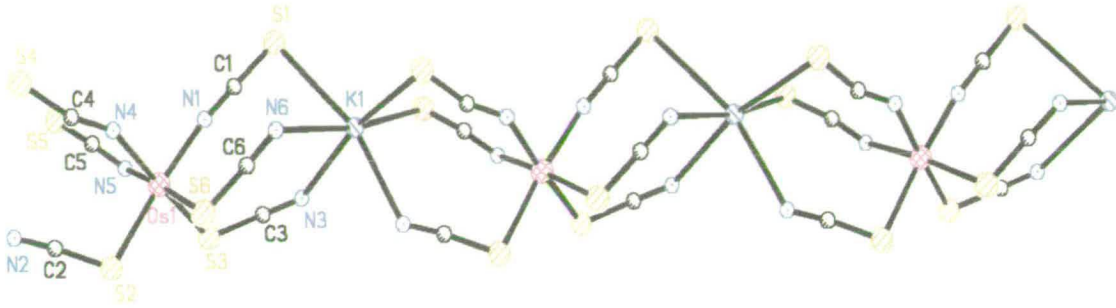

Figure 6.2 Crystal structure for *fac*-$[N^nBu_4]_2K[Os(NCS)_3(SCN)_3]$

Bond Lengths / Å		Bond Angles / °	
Os(1)-N(1)	2.047(8)	C(1)-N(1)-Os(1)	172.9(10)
Os(1)-S(2)	2.415(4)	C(2)-S(2)-Os(1)	102.9(4)
Os(1)-S(3)	2.382(5)	C(3)-S(3)-Os(1)	105.7(5)
Os(1)-N(4)	2.198(14)	C(4)-N(4)-Os(1)	138.9(16)
Os(1)-N(5)	2.251(13)	C(5)-N(5)-Os(1)	131.4(15)
Os(1)-S(6)	2.385(5)	C(6)-S(6)-Os(1)	106.8(7)

Table 6.6 Selected bond lengths and angles for *fac*-$[N^nBu_4]_2K[Os(NCS)_3(SCN)_3]$

The crystal structure of $[N^nBu_4]_3[Os(NCS)_6]$ is shown in **Figure 6.3**. The counter ions are not shown but form faces of the unit cell; each counter ion is shared between two $[Os(NCS)_6]^{3-}$ trianions. Selected bond lengths and angles are given in **Table 6.7**. All bond lengths are as expected for the Os(III) complex.[9] The C-N-Os bond angle is almost linear.

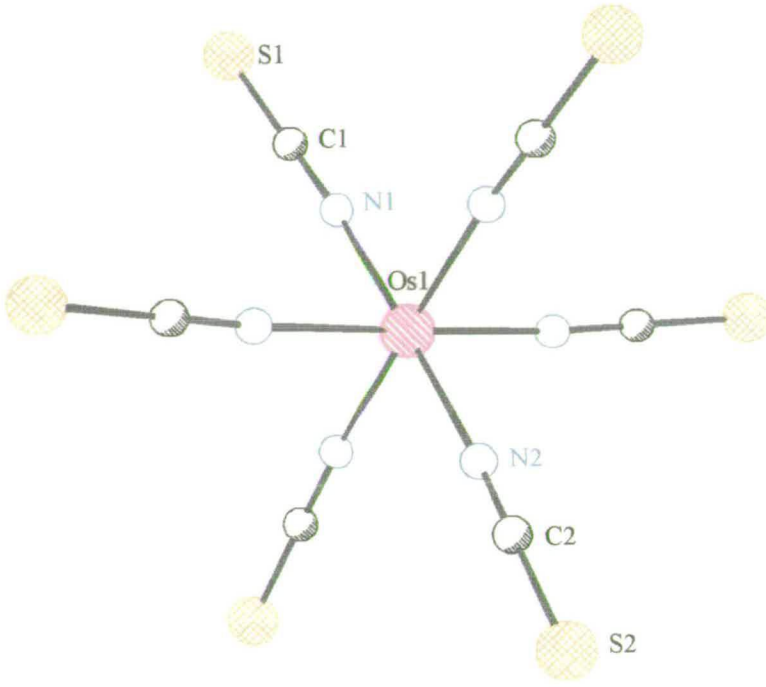

Figure 6.3 Crystal structure for $[N^nBu_4]_3[Os(NCS)_6]$

Bond Lengths / Å		Bond Angles / °	
Os(1)-N(1)	2.016(4)	C(1)-N(1)-Os(1)	173.7(4)
Os(1)-N(1)#1	2.016(4)	C(1)#1-N(1)#1-Os(1)	173.7(4)
Os(1)-N(1)#2	2.016(4)	C(1)#2-N(1)#2-Os(1)	173.7(4)
Os(1)-N(2)	2.023(4)	C(2)-N(2)-Os(1)	171.7(4)
Os(1)-N(2)#1	2.023(4)	C(2)#1-N(2)#1-Os(1)	171.7(4)
Os(1)-S(2)#2	2.023(4)	C(2)#2-N(2)#2-Os(1)	171.7(4)

Table 6.7 Selected bond lengths and angles for $[N^nBu_4]_3[Os(NCS)_6]$ (Symmetry transformations used to generate equivalent atoms: #1 y,z,x and #2 z, x, y)

6.3.2 Electrochemistry of cis- $[Os(NCS)_2(SCN)_4]^{3-}$, fac-$[Os(NCS)_3(SCN)_3]^{3-}$, and $[Os(NCS)_6]^{3-}$

The CV of *cis*-$[Os(NCS)_2(SCN)_4]^{3-}$ in 0.5 M $[N^nBu_4]BF_4$/dichloromethane at 293 K (**Figure 6.4**) shows a reduction at –0.99 V (ΔE = 155 mV) and an oxidation at +0.43 V (ΔE = 60 mV); both are one electron processes as determined by coulometry and the electron transfer rates are diffusion limited, $i_p \alpha \nu^{1/2}$. The reduction process is not chemically reversible at 0.1 V s^{-1}, 293 K since $i_p^{red} > i_p^{ox}$.

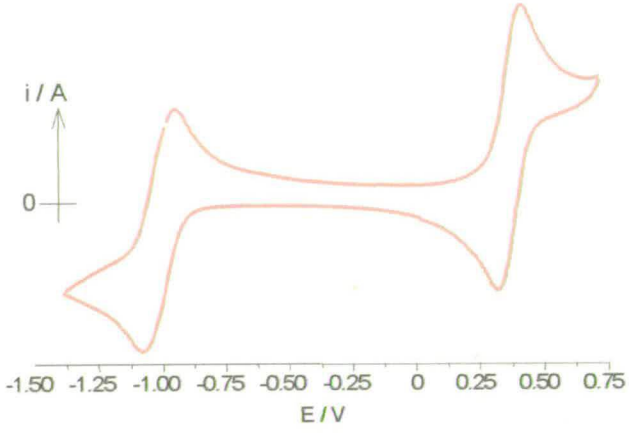

Figure 6.4 CV of *cis*-$[Os(NCS)_2(SCN)_4]^{3-}$ in 0.5 M $[N^nBu_4]BF_4$/dcm at 0.1 V s^{-1}, 293 K

The cyclic voltammograms of *fac*-$[Os(NCS)_3(SCN)_3]^{3-}$ and $[Os(NCS)_6]^{3-}$ show similar behaviour to *cis*-$[Os(NCS)_2(SCN)_4]^{3-}$. The half-wave potentials for the reduction and oxidation processes, the peak to peak separation (ΔE), and the ratio $|i_p^{ox}/i_p^{red}|$ for the isomers *cis*-$[Os(NCS)_2(SCN)_4]^{z-}$, *fac*-$[Os(NCS)_3(SCN)_3]^{z-}$, and $[Os(NCS)_6]^{z-}$ are given in **Table 6.8**.

The values compare well with those of Preetz *et al.*[6] For the reduction process, as the number of N-bound ligands increases, $|i_p^{ox}/i_p^{red}|$ tends towards unity and ΔE decreases towards 59 mV (the Nernst ideal for a fully reversible, diffusion controlled electron transfer process at 298 K) indicating that the redox processes become increasingly chemically reversible and that the $[Os(NCS)_6]^{3-}$ isomer undergoes very little, if any, geometrical change on reduction.

An interesting comparison of the $[Os(NCS)_n(SCN)_{6-n}]^{z-}$ complexes can be made to $[OsX_6]^{z-}$, where X = Cl^-, Br^- and I^-. Although two redox processes are observed in the thiocyanate case, they are assigned to the Os(III)/(II) and Os(IV)/(III) couples, whereas for $[OsX_6]^{z-}$, they are Os(IV)/(III) and Os(V)/(IV) couples. Thus the Os(IV)/(III) couple is significantly more positive for the thiocyanate ligands than for the halides to the extent that the hexahalide complexes are isolated in the Os(IV) oxidation state whereas the hexathiocyanate complexes are stable in the Os(III) oxidation state. The -NCS ligand is commonly referred to as a pseudo-halide however these results indicate that it does not stabilise high oxidation state metals to nearly the same extent as halide ligands. The thiocyanate ligand is probably not as good a π-donor as a halide ligand, in fact the –NCS linkage can be considered to be a weak π-acceptor.

	Os(III/II) Reduction			Os(IV/III) Oxidation		
Complex	$E_{1/2}$/V	ΔE/mV	$\lvert i_p^{ox}/i_p^{red} \rvert$	$E_{1/2}$/V	ΔE/mV	$\lvert i_p^{ox}/i_p^{red} \rvert$
cis-$[Os(NCS)_2(SCN)_4]^{3-}$	-0.99	155	0.69	+0.43	60	~1
fac-$[Os(NCS)_3(SCN)_3]^{3-}$	-0.94	135	0.83	+0.46	60	~1
$[Os(NCS)_6]^{3-}$	-0.78	85	0.95	+0.49	65	~1
$[OsCl_6]^{2-}$	-0.57	80	~1	+1.38	75	~1

Table 6.8 Half-wave potentials, ΔE, and $\lvert i_p^{ox}/i_p^{red} \rvert$ for the reduction and oxidation processes for the isomers $[Os(NCS)_n(SCN)_{6-n}]^{z-}$ in 0.5 M $[N^nBu_4]BF_4$/dcm at 0.1 V s^{-1}, 294 K

In the presence of a co-ordinating solvent such as acetonitrile or pyridine the cyclic voltammogram shows a daughter product is formed following the reduction of the Os(III) complex to Os(II) (**Figure 6.5**). The daughter product (B) has a half-wave potential approximately 0.35 V positive of the parent reduction (A).

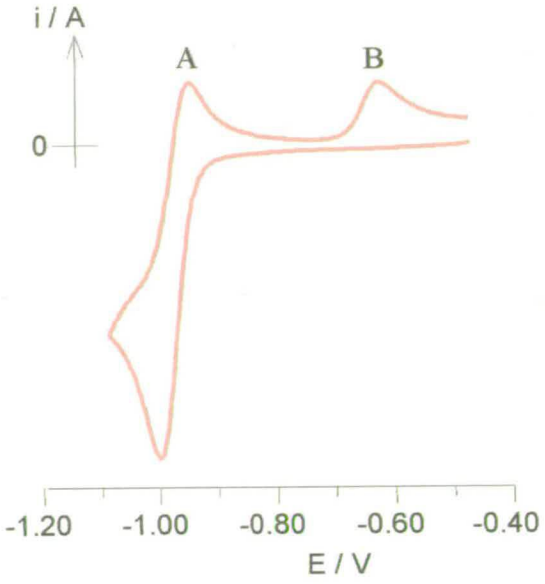

Figure 6.5 CV of *fac*-$[Os(NCS)_3(SCN)_3]^{3-}$ in 0.2 M $[N^nBu_4]BF_4$/pyridine at 0.1 V s^{-1}, 294 K

Reduction in bulk of the Os(III) complex results in almost complete conversion to the daughter species with two more redox couples at a further 0.65 V (C) and 0.95 V (D) positive of the original Os(III)/(II) parent reduction (**Figure 6.6**).

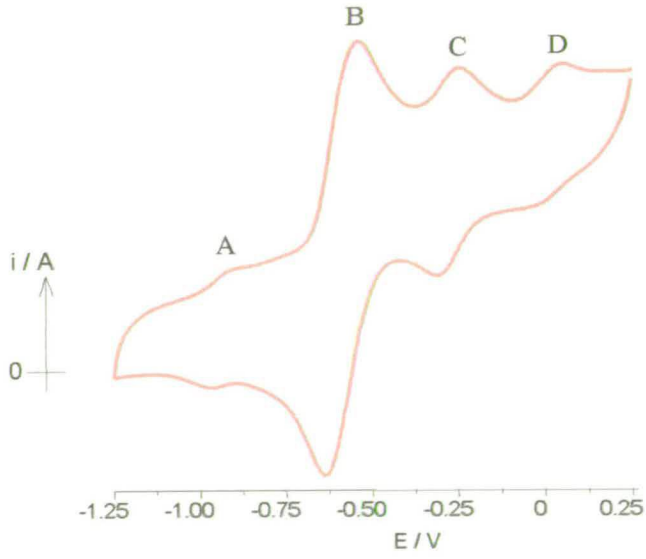

Figure 6.6 CV following the one electron reduction at –1.20 V of *fac*-$[Os(NCS)_3(SCN)_3]^{3-}$ in 0.2 M $[N^nBu_4]BF_4$/pyridine at 0.1 V s^{-1}, 294 K

Re-oxidation of the species at –0.50 V resulted in a partial re-forming of the original complex *fac*-$[Os(NCS)_3(SCN)_3]^{3-}$. The daughter species, of the reduced complex (B, C, and D) were isolated from the supporting electrolyte on a silica gel 60 (Merck)

column. However, complete isolation of a pure product species has proved elusive to date and all efforts at crystallisation have been unsuccessful. The cyclic voltammogram of the electrogenerated solution, in the region 0 to +1.5 V, reveals an absorption peak at *ca.* +0.7 V corresponding to the oxidation of free thiocyanate.

Importantly, the reduction of *fac*-$[Os(NCS)_3(SCN)_3]^{3-}$ in non co-ordinating 0.5 M $[N^nBu_4]BF_4$/dichloromethane at 294 K results in the decomposition of the starting complex. The cyclic voltammogram reveals an oxidation at *ca.* 0.7 V corresponding to the oxidation of free thiocyanate but no other clear electroactive species. The bulk reduction/oxidation can be carried out with complete reversibility at 223 K yielding 100% conversion to *fac*-$[Os(NCS)_3(SCN)_3]^{4-}$ and then total regeneration of *fac*-$[Os(NCS)_3(SCN)_3]^{3-}$.

From this, and previous examples of reduction induced substitution reactions of $[MX_6]^{3-}$ (where M = Os, Ir, or Re, and X = Cl^-, Br^-, I^-) and $[OsX_3Y_3]$ (where X = Cl^- or Br^- and Y is a tertiary alkyl phosphine or arsine), the first daughter species at –0.60 V is confidently expected to be the mono-substitution reaction of one thiocyanate ligand for pyridine or acetonitrile. The shift in half-wave potential from –0.94 V to –0.60 V is as expected when replacing a strong electron donor for a weak electron donor. The further daughter products, C and D, are presumed to be further substitutions of the thiocyanate ligands for pyridine or acetonitrile. The decomposition of *fac*-$[Os(NCS)_3(SCN)_3]^{3-}$ in 0.5 M $[N^nBu_4]BF_4$/dichloromethane at 294 K could suggest that a highly reactive five co-ordinate intermediate is formed which then reacts further.

6.3.3 In situ uv-vis spectroelectrochemistry of $[Os(NCS)_n(SCN)_{6-n}]^{3-}$

The *in situ* spectroelectrochemical uv-vis spectra of the complexes *cis*-$[Os(NCS)_2(SCN)_4]^{z-}$, *fac*-$[Os(NCS)_3(SCN)_3]^{z-}$, and $[Os(NCS)_6]^{z-}$ are shown in **Figure 6.7**. The electronic transitions for the Os(III) and Os(IV) complexes have been well characterised by Preetz *et al.*[7] The main transition band for the Os(III) complexes lies between 20000 cm^{-1} and 22700 cm^{-1} for all the isomers $[Os(NCS)_n(SCN)_{6-n}]^{3-}$, n = 0-6, and has been assigned as a $(\pi + \sigma)t_{1u} \rightarrow dt_{2g}$ charge transfer. As expected for a ligand to metal charge transfer (LMCT), the transition moves to lower energy on oxidation from Os(III) to Os(IV). Reduction of the Os(III) species to Os(II) shows a featureless spectrum; as the t_{2g} orbitals are fully occupied, there are no possible LMCT transitions. There are also no metal to ligand charge transfer (MLCT) transitions observed indicating that the thiocyanate ligands can not have low energy π^* orbitals. The transition band positions and molar extinction coefficients for the $(\pi + \sigma)t_{1u} \rightarrow dt_{2g}$ transition for the Os(III) and Os(IV) species are given in **Table 6.7** and match very well with those of Preetz *et al.*[7] Interestingly, values for the molar extinction coefficient, ε, increase as n increases. This would suggest the LMCT must primarily involve the N-bound thiocyanate ligand.

n	Os(III)		Os(IV)	
	peak max / cm^{-1}	ε / mol^{-1} cm^{-1} dm^3	peak max / cm^{-1}	ε / mol^{-1} cm^{-1} dm^3
2 *cis*	21500	8800	16000	22000
3 *fac*	22025	12400	16300	28000
6	22525	24800	17125	57000

Table 6.9 Transition band positions and molar extinction coefficients for the transition $(\pi + \sigma)t_{1u} \rightarrow dt_{2g}$ for the Os(III) and Os(IV) species of $[Os(NCS)_n(SCN)_{6-n}]^{z-}$

Importantly, the spectra all show precise isosbestic points. This shows two points; (i) that there is no detectable intermediate step in the oxidation or reduction of the isomers, and (ii) that each isomer has been successfully isolated from the other products of the synthesis.

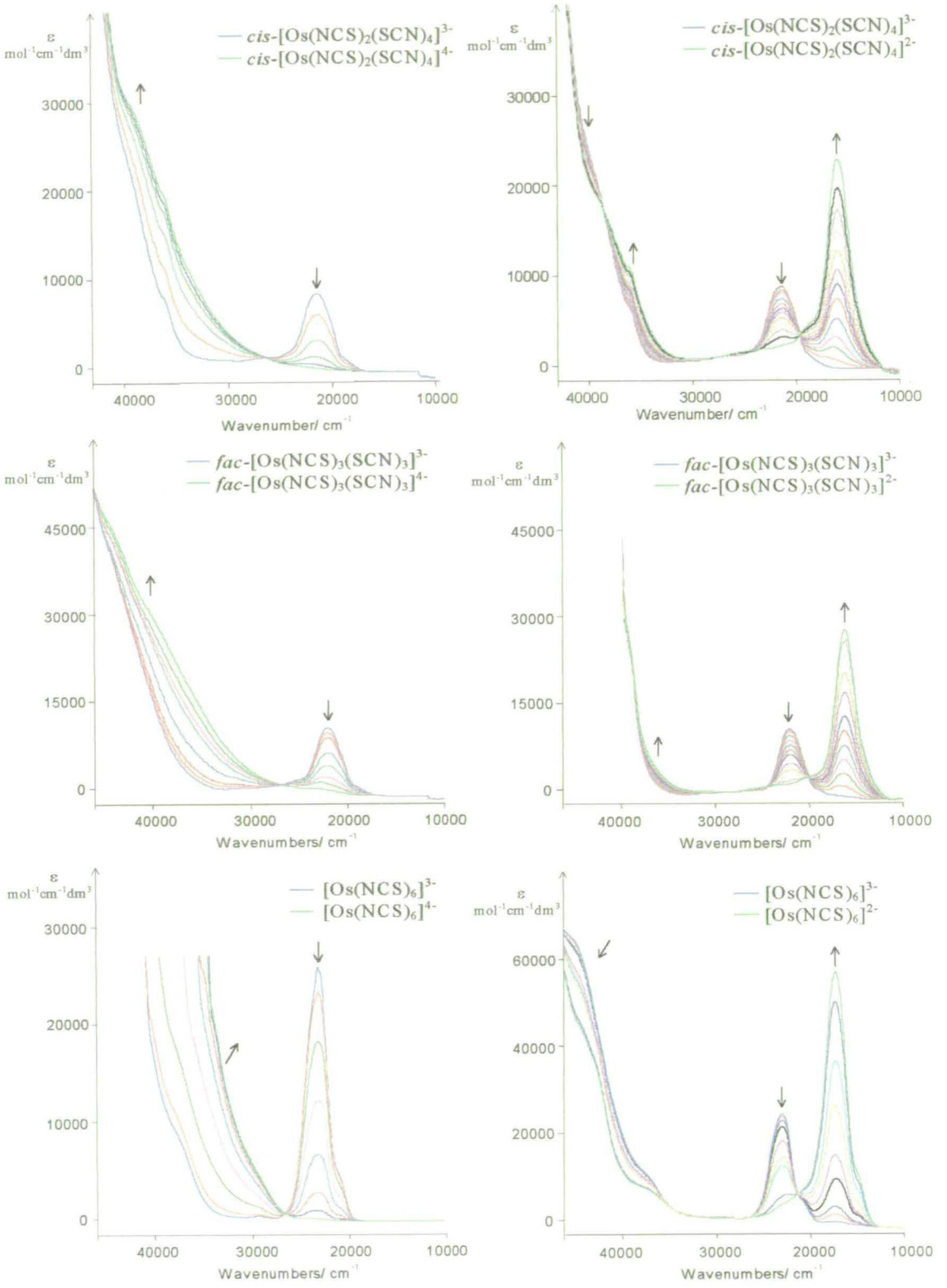

Figure 6.7 *In situ* spectroelectrochemical uv-vis spectra of the complexes *cis*-$[Os(NCS)_2(SCN)_4]^{z-}$, *fac*-$[Os(NCS)_3(SCN)_3]^{z-}$, and $[Os(NCS)_6]^{z-}$ in 0.5M $[N^nBu_4]BF_4$/dcm at 223K, reduced at –1.20V and oxidised at +0.60V

6.3.4 Rates and Activation Energies for the reaction of $[Os(NCS)_n(SCN)_{6-n}]^{z-}$ with L, where L = acetonitrile or pyridine

The pseudo first order rate constants, k, for the substitution reactions of electrochemically generated Os(II) species with L, have been studied using double-step chronoamperometry in 0.2 M $[N^nBu_4]BF_4$/L. The rate constants were measured over the range 298-356 K. The rate constant at 323 K and the activation energy, E_a, for the reactions are presented in **Table 6.10**. The activation energies, E_a, were calculated from the Arrhenius relationship (**Figure 6.8**). The rate constants at 323 K were read from the linear regression fit from the Arrhenius plots of lnk against 1/temperature. Errors in k were calculated from the average error for each point determined from the average measured value for each experiment and the statistical errors involved in their calculation. The errors given for E_a are the standard deviations from the linear regression fits. No activation energy for the reaction of acetonitrile with $[Os(NCS)_6]^{2-}$ was obtainable because the high temperatures required to increase the rate of reaction to a suitable level for measurement were too close to the boiling point of the solution (boiling point of neat acetonitrile = 354 K). The smaller number of data available are also reflected in the relatively large error given in **Table 6.10** (calculated from the average of 3 measurements, each measurement being the average of five recorded values).

n	Os(II) k_{323K} /s^{-1}		Os(II) E_a / kJ mol^{-1}	
	An	Py	An	Py
2 *cis*	1.59 ± 0.10	2.05 ± 0.15	64.5 ± 1.9	67.9 ± 2.0
3 *fac*	0.63 ± 0.06	1.05 ± 0.09	78.1 ± 2.3	79.0 ± 2.3
6	0.07 ± 0.04	0.15 ± 0.05		86.4 ± 1.7

Table 6.10 Rate constants, k, at 323 K and activation energies, E_a, for the reaction of *cis*-$[Os(NCS)_2(SCN)_4]^{4-}$, *fac*-$[Os(NCS)_3(SCN)_3]^{4-}$, and $[Os(NCS)_6]^{4-}$ in 0.2 M $[N^nBu_4]BF_4$/L

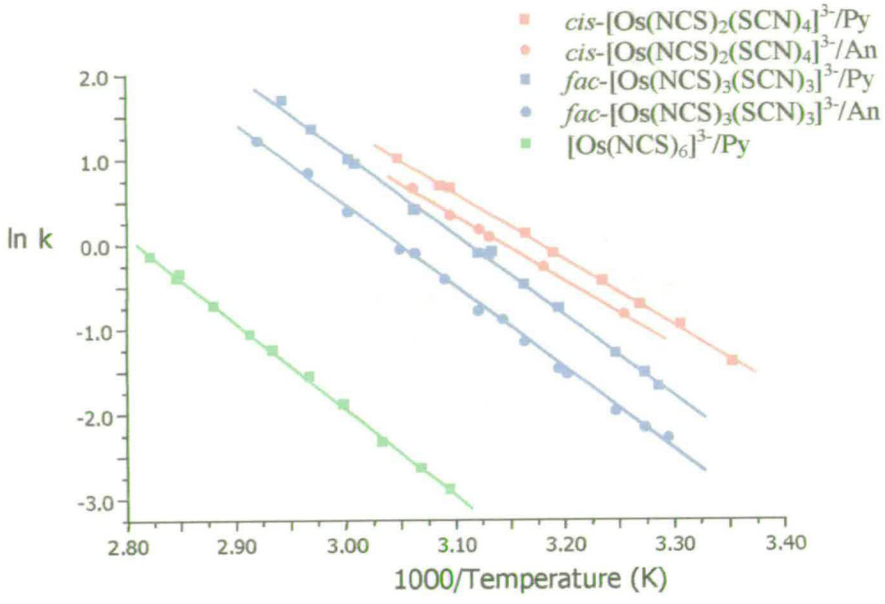

Figure 6.8 Arrhenius plot for the reactions of *cis*-$[Os(NCS)_2(SCN)_4]^{4-}$, *fac*-$[Os(NCS)_3(SCN)_3]^{4-}$, and $[Os(NCS)_6]^{4-}$ in 0.2 M $[N^nBu_4]BF_4$/L (L = acetonitrile or pyridine)

The activation energy for the reaction with acetonitrile and pyridine are the same within experimental error for both *cis*-$[Os(NCS)_2(SCN)_4]^{4-}$ (on average 66.2 kJ mol^{-1}) and *fac*-$[Os(NCS)_3(SCN)_3]^{4-}$ (on average 78.6 kJ mol^{-1}). The rate constants are also very similar. For the reaction of *cis*-$[Os(NCS)_2(SCN)_4]^{4-}$ the rate constant is 1.59 ± 0.10 s^{-1} and 2.05 ± 0.15 s^{-1} in acetonitrile and pyridine respectively.

On the basis that the rate constant and activation energies are largely independent of the nature of the entering ligand the most likely mechanisms for the reduction induced reaction are the Dissociative mechanism and the dissociative Interchange mechanism. Either of these mechanisms would be consistent with the similar complexes, $[MX_6]^{3-}$ (where M = Ir, Os, Re, and X = Cl^-, Br^-, I^-) and $[OsX_3Y_3]^{1-}$ (where X = Cl^- or Br^- and Y = a tertiary alkyl phosphine or arsine). The activation energy would, therefore, be expected to be the cleavage of the osmium-thiocyanate bond and the rate constant the rate of thiocyanate loss.

As the number of N-bound ligands decreases the rate constant increases from 0.1 s^{-1} to 2.0 s^{-1} and the activation energy decreases from 86.4 kJ mol^{-1} to 67.9 kJ mol^{-1} for

n = 6 and 2 respectively. The –NCS ligand is a weak π-acceptor and is more capable of stabilising the Os(II) centre than the σ-only donor –SCN ligand. Furthermore, the –NCS linkage is recognised as the more thermodynamically stable arrangement.[6,15] It would seem reasonable, therefore, if the rate limiting step was the loss of the thiocyanate ligand, that the reduction induced reaction should be slower for $[Os(NCS)_6]^{4-}$ than *cis*-$[Os(NCS)_2(SCN)_4]^{4-}$. If the activation energy is taken to be the energy required to cleave the osmium-thiocyanate bond, the decrease in activation energy may be expected because of the greater steric strain experienced in *cis*-$[Os(NCS)_2(SCN)_4]^{2-}$ and *fac*-$[Os(NCS)_3(SCN)_3]^{4-}$ due to the non-linear –SCN ligands thereby encouraging formation of the five coo-ordinate intermediate.

In the cases of *cis*-$[Os(NCS)_2(SCN)_4]^{4-}$ and *fac*-$[Os(NCS)_3(SCN)_3]^{4-}$ the rate constant is slightly faster in pyridine than in acetonitrile. The activation energies are the same within experimental error. As for previous examples of reduction induced reactions of $[MX_6]^{3-}$ (where M = Os, Ir, or Re, and X = Cl^-, Br^-, I^-) the slightly faster rate in pyridine than acetonitrile is attributed to the greater solubility of the thiocyanate ligand in pyridine than acetonitrile.

The Os(III) isomers, *cis*-$[Os(NCS)_2(SCN)_4]^{3-}$ and *fac*-$[Os(NCS)_3(SCN)_3]^{3-}$, react slowly with acetonitrile at 323 K giving a daughter product *ca.* 0.35 V positive of the parent Os(III)/(II) reduction as for the reduction induce reaction. The reaction of the Os(III) complexes with acetonitrile at 323 K was monitored electrochemically. The rate constant for the reaction in 0.2 M $[N^nBu_4]BF_4$/acetonitrile was calculated from the plot of $\ln[C]/[C_0]$ against time giving a straight line with gradient k, where the concentration, C, and starting concentration, C_0, of the complex were approximated by the area under the differential pulse peak for the Os(III)/(II) reduction. The rate was found to be 4 $x10^{-5}$ s^{-1} and 1 $x10^{-5}$ s^{-1} for *cis*-$[Os(NCS)_2(SCN)_4]^{3-}$ and *fac*-$[Os(NCS)_3(SCN)_3]^{3-}$ respectively. The rate constants are at least 10^4 s^{-1} faster for the Os(II) species than the Os(III) species illustrating that the reduction of the metal centre is an overwhelming driving force of the reaction. $[Os(NCS)_6]^{3-}$ in 0.2 M $[N^nBu_4]BF_4$/acetonitrile was heated at 323 K over a period of three days. No

daughter product was detectable by differential pulse voltammetry once again demonstrating the increased stability of the completely N-bound complex.

6.3.5 IR Spectroelectrochemistry of fac-$[Os(NCS)_3(SCN)_3]^{3-}$

In order to establish the identity of the leaving thiocyanate ligand, i.e., whether a N- or S-bound ligand is lost on substitution, an IR spectroelectrochemical study was undertaken. The IR spectra of the isomeric series of complexes $[Os(NCS)_n(SCN)_{6-n}]^{3-}$ have been well analysed by Preetz *et al.*[7] The frequency of the CS stretch is the surest band for assigning the co-ordination type. The region for the –N and –S bound ligands are well separated. The CS stretch for the –N bound ligand (measured between 820 cm^{-1} to 826 cm^{-1}) although only weak, is significantly stronger than for the –S bound ligand (measured at 688 cm^{-1} to 691 cm^{-1}). The intensities can be easily calibrated against a band for the $[N^nBu_4]^+$ counter ion at 880 cm^{-1}. Stronger bands for the CN stretch *ca.* 2100 cm^{-1} are not good for confirmation of binding type or degree because the region of -N and -S bound ligands overlap completely. A substitution reaction for acetonitrile would make little difference to the CN stretching band region of the spectrum.

Reduction of *fac*-$[Os(NCS)_3(SCN)_3]^{3-}$ in 0.2M $[N^nBu_4]BF_4$/acetonitrile at –1.0 V for both *in situ* and *ex situ* experiments gave similar results. The *in situ* IR spectroelectrochemical spectra of the reduction of *fac*-$[Os(NCS)_3(SCN)_3]^{3-}$ is shown in **Figure 6.9**. On reduction, the CS(N) stretch at 825 cm^{-1} shifts to 790 cm^{-1}. Reduction of the Os(III) to Os(II) will result in increased π-back donation of electron density from the Os(II) to the –NCS ligand. Electronic population of the antibonding π* orbital on the –NCS ligand will weaken the CS band and shift the IR stretching vibration to lower energy as observed. Such an explanation also applies to the CN stretching region where, on reduction, a new band at 2050 cm^{-1} grows in.

On re-oxidation at –0.5 V most bands go back to those of the original starting complex in the original proportions (**Figure 6.10**).

A notable exception is the CS(S) stretch at 692 cm^{-1}. Although it is a very weak band, it can be seen (**Figure 6.10**) that it has not grown back to the same degree following reduction and re-oxidation. The fact that the CS(N) stretch is of similar proportion to the starting complex could suggest that the substitution reaction involves a –S bound ligand. There is no observed shift of the CS(S) stretching band on reduction to Os(II). This is perhaps because the band is weak anyway and a shift in stretching vibration would be difficult to observe, or, in the –SCN linkage there is no π-accepting interaction and thus reduction to Os(II) will not give π-back donation into the –SCN linkage and therefore the band at 690 cm^{-1} will not shift significantly.

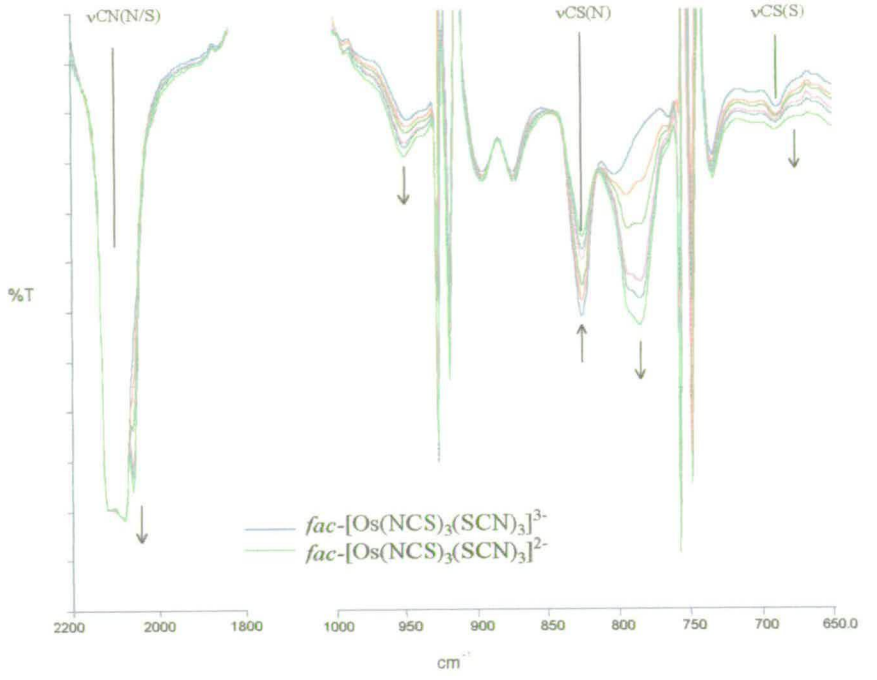

Figure 6.9 *In situ* IR spectroelectrochemical reduction spectra of *fac*-$[Os(NCS)_3(SCN)_3]^{3/4-}$ in 0.2 M $[N^nBu_4]BF_4$/acetonitrile at 293 K minus the background and $[N^nBu_4]^+$.
Electrogeneration potential –1.0 V

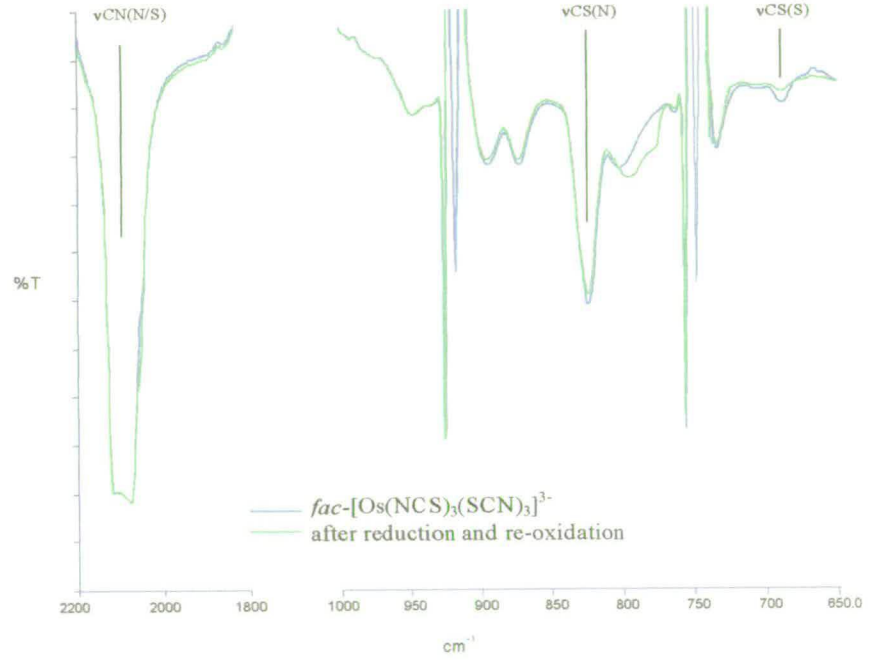

Figure 6.10 IR spectra of the complex *fac*-$[Os(NSC)_3(SCN)_3]^{3-}$ and the spectra following reduction and the corresponding re-oxidation in 0.2 M $[N^nBu_4]BF_4$/acetonitrile at 293 K minus the background and $[N^nBu_4]^+$

6.4 Conclusions

The isomeric complexes *cis*-$[Os(NCS)_2(SCN)_4]^{3-}$, *fac*-$[Os(NCS)_3(SCN)_3]^{3-}$, and $[Os(NCS)_6]^{3-}$ have been prepared, isolated, and characterised by electrochemistry, *in situ* uv-vis spectroelectrochemistry, and X-ray crystallography. They have been shown to react on reduction with a ligand, L, of less electron donating character than thiocyanate. Cyclic voltammetry investigations confidently predict the reaction to be the mono-substitution of one thiocyanate ligand for L.

On the basis that the rate constant and activation energies are largely independent of the nature of the entering ligand, the most likely mechanisms for the reduction induced reaction are the Dissociative mechanism and the dissociative Interchange mechanism. These mechanisms would be consistent with the similar complexes, $[MX_6]^{3-}$ (where M = Ir, Os, Re, and X = Cl^-, Br^-, I^-) and $[OsX_3Y_3]^{1-}$ (where X = Cl^- or Br^- and Y = a tertiary alkyl phosphine or arsine). The rate constant is understood therefore to be the rate of thiocyanate loss and the activation energy to be the cleavage of the osmium-thiocyanate bond.

A trend is observed where by the rate constant increases and the activation energy decreases for the series $[Os(NCS)_n(SCN)_{6-n}]^{2-}$ as the number of S-bound ligands increase, i.e., n tends to zero. The activation energy for the reaction of the isomeric complexes $[Os(NCS)_6]^{2-}$, *fac*-$[Os(NCS)_3(SCN)_3]^{2-}$, and *cis*-$[Os(NCS)_2(SCN)_4]^{2-}$ in 0.2 M $[N^nBu_4]BF_4$/pyridine decreases from 86.4 to 79.0 to 67.9 kJ mol^{-1} respectively. This is consistent with the understanding of the –NCS ligand as a weak π-acceptor, more capable of relieving the increased electron density experienced at the metal centre of the Os(II) species and forming a stronger Os-N bond than for the σ-only donor –SCN ligand.

An *in situ* IR spectroelectrochemical study suggests that a –SCN ligand is lost on substitution.

6.5 References

[1] Ahrland, S.; Chatt, J.; Davies, N. R.; *Q. Rev.* 1958, **12**, 265
[2] Pearson, R. G.; *J. Am. Chem. Soc.*, 1963, **85**, 3533
[3] Jørgensen, C. K.; *Inorg. Chem.*, 1964, **3**, 1201
[4] Preetz, W.; Peters G.; *Z. Naturforsch.* 1979, **34B**, 1243
[5] Basolo, F. Baddley, W. H., Burmeister, J. L.; *Inorg. Chem.*, 1964, **3**, 1202
[6] Bütje, K.; Preetz, W.; *Z. Naturforsch.* 1987, **43B**, 382
[7] Bütje, K.; Preetz, W.; *Z. Naturforsch.* 1988, **43B**, 371
[8] Stähler, O.; Preetz, W.; *Z Anorg. Allg. Chem.* 2001, **627**, 615
[9] Stähler, O.; Preetz, W.; *Z Anorg. Allg. Chem.* 2000, **626**, 2077
[10] Preetz, W.; Peters G.; *Z. Naturforsch.* 1980, **35B**, 994
[11] Preetz, W.; Frickle H.; *Fresenius Z. Anal.* Chem., 1981, **306**, 115
[12] Preetz, W.; Frickle H.; *Z Anorg. Allg. Chem.*, 1982, **486**, 49
[13] Frickle, H.; Preetz W.; *Z Naturforsch.*, 1983, **38B**, 917
[14] Frickle, H.; Preetz W.; *Z Anorg. Allg. Chem.* 1983, **507(12)**, 23
[15] Kettle, S. F. A.; *Physical Inorganic Chemistry: a co-ordination approach*, Spektrum, University Science Books, USA, 1996
[16] Preetz, W.; Peters, G.; Bulblitz, D.; *Chem. Rev.*, 1996, **96**, 977
[17] Schmidtke, H. H.; Garhoff, D.; *Helv. Chim. Acta*, 1967, **50**, 1631

Appendices

Crystal Data of $[N^nBu_4]_2[OsCl_5(C_5H_5N)_1]$

Table 1. Crystal data and structure refinement for osclpy.

A. CRYSTAL DATA

Empirical formula	C21 H41 Cl5 N2 Os
	[NBu4]+[OsCl5Py]-
Formula weight	689.01
Wavelength	0.71073 A
Temperature	220(2) K
Crystal system	Monoclinic
Space group	P21/n
Unit cell dimensions	a = 10.7663(16) A alpha = 90 deg. b = 19.013(4) A beta = 103.299(16) deg. c = 14.061(3) A gamma = 90 deg.
Volume	2801.0(10) A^3
Number of reflections for cell	42 (15 < theta < 16 deg.)
Z	4
Density (calculated)	1.634 Mg/m^3
Absorption coefficient	5.041 mm^-1
F(000)	1368

B. DATA COLLECTION

Crystal description	Yellow needle (mounted axially)
Crystal size	0.62 x 0.16 x 0.16 mm
Theta range for data collection	2.61 to 25.08 deg.
Index ranges 0<=l<=16	-12<=h<=12, 0<=k<=22,
Reflections collected	4973

Independent reflections	4969 [R(int) = 0.0627]
Scan type	Omega-theta
Absorption correction	Optimised numerical (Tmin= 0.570, Tmax=0.628)

C. SOLUTION AND REFINEMENT.

Solution	Patterson (DIRDIF)
Refinement type	Full-matrix least-squares on F^2
Program used for refinement	SHELXL-97
Hydrogen atom placement	geometric
Hydrogen atom treatment	riding
Data / restraints / parameters	4969/0/263
Goodness-of-fit on F^2	1.060
Conventional R [F>4sigma(F)]	R1 = 0.0363 [4034 data]
Weighted R (F^2 and all data)	wR2 = 0.0819
Extinction coefficient	0.00110(9)
Final maximum delta/sigma	0.002

Weighting scheme
calc w=1/[\s^2^(Fo^2^)+(0.0325P)^2^+4.1223P] where
P=(Fo^2^+2Fc^2^)/3

Largest diff. peak and hole	0.977 and -0.986 e.A^-3

Table 2. Atomic coordinates (x 10^4) and equivalent isotropic displacement parameters (A^2 x 10^3) for osclpy. U(eq) is defined as one third of the trace of the orthogonalized Uij tensor.

	x	y	z	U(eq)
Os(1)	1410(1)	1298(1)	1940(1)	31(1)
Cl(1)	2909(2)	1020(1)	3366(1)	53(1)
Cl(2)	2589(2)	2264(1)	1626(1)	50(1)
Cl(3)	2459(2)	605(1)	1017(1)	46(1)
Cl(4)	185(2)	339(1)	2179(1)	42(1)
Cl(5)	330(2)	2024(1)	2832(1)	40(1)
N(1)	5(5)	1541(2)	665(4)	32(1)
C(2)	-459(6)	1050(3)	-20(5)	40(2)
C(3)	-1384(7)	1191(4)	-847(5)	47(2)
C(4)	-1863(7)	1857(4)	-991(5)	47(2)
C(5)	-1418(7)	2365(4)	-304(5)	47(2)
C(6)	-483(6)	2198(3)	504(5)	39(2)
N(10)	2016(5)	3974(3)	8525(4)	35(1)
C(11)	1144(6)	4553(3)	8741(5)	46(2)
C(12)	1577(8)	5293(4)	8628(8)	80(3)
C(13)	631(8)	5828(4)	8845(7)	73(3)
C(14)	-627(9)	5857(4)	8136(7)	84(3)
C(21)	3339(6)	4032(3)	9177(5)	40(2)
C(22)	3435(7)	3982(4)	10264(5)	61(2)
C(23)	4840(8)	3945(5)	10821(6)	71(2)
C(24)	5481(9)	3268(5)	10673(6)	77(3)
C(31)	2189(6)	4042(4)	7480(5)	45(2)
C(32)	1011(7)	3958(5)	6666(5)	60(2)
C(33)	1402(9)	4038(7)	5696(6)	97(4)
C(34)	348(9)	3938(7)	4850(7)	122(5)
C(41)	1409(6)	3279(3)	8670(5)	41(2)
C(42)	2120(7)	2627(3)	8452(6)	50(2)
C(43)	1392(7)	1972(4)	8550(6)	56(2)
C(44)	2049(8)	1308(4)	8348(6)	61(2)

Table 3. Bond lengths [A] and angles [deg] for osclpy.

Os(1)-N(1)	2.115(5)
Os(1)-Cl(3)	2.3175(16)
Os(1)-Cl(4)	2.3204(15)
Os(1)-Cl(1)	2.3266(18)
Os(1)-Cl(2)	2.3308(16)
Os(1)-Cl(5)	2.3445(15)
N(1)-C(2)	1.352(8)
N(1)-C(6)	1.354(7)
C(2)-C(3)	1.372(9)
C(3)-C(4)	1.365(9)
C(4)-C(5)	1.373(9)
C(5)-C(6)	1.370(9)
N(10)-C(21)	1.510(8)
N(10)-C(41)	1.509(7)
N(10)-C(11)	1.521(8)
N(10)-C(31)	1.529(8)
C(11)-C(12)	1.503(10)
C(12)-C(13)	1.519(10)
C(13)-C(14)	1.486(11)
C(21)-C(22)	1.511(9)
C(22)-C(23)	1.537(10)
C(23)-C(24)	1.497(11)
C(31)-C(32)	1.509(9)
C(32)-C(33)	1.524(11)
C(33)-C(34)	1.455(12)
C(41)-C(42)	1.525(9)
C(42)-C(43)	1.494(9)
C(43)-C(44)	1.506(10)
N(1)-Os(1)-Cl(3)	89.71(14)
N(1)-Os(1)-Cl(4)	88.54(13)
Cl(3)-Os(1)-Cl(4)	90.04(6)
N(1)-Os(1)-Cl(1)	178.30(13)
Cl(3)-Os(1)-Cl(1)	91.29(7)
Cl(4)-Os(1)-Cl(1)	90.08(7)
N(1)-Os(1)-Cl(2)	88.96(13)
Cl(3)-Os(1)-Cl(2)	89.17(6)
Cl(4)-Os(1)-Cl(2)	177.38(6)
Cl(1)-Os(1)-Cl(2)	92.43(7)
N(1)-Os(1)-Cl(5)	88.79(14)
Cl(3)-Os(1)-Cl(5)	178.19(6)
Cl(4)-Os(1)-Cl(5)	90.93(6)
Cl(1)-Os(1)-Cl(5)	90.23(6)
Cl(2)-Os(1)-Cl(5)	89.80(6)
C(2)-N(1)-C(6)	116.9(5)
C(2)-N(1)-Os(1)	121.9(4)
C(6)-N(1)-Os(1)	121.2(4)
N(1)-C(2)-C(3)	123.0(6)
C(4)-C(3)-C(2)	118.9(6)
C(3)-C(4)-C(5)	119.3(6)
C(6)-C(5)-C(4)	119.4(6)
N(1)-C(6)-C(5)	122.4(6)
C(21)-N(10)-C(41)	111.1(5)
C(21)-N(10)-C(11)	111.5(5)

C(41)-N(10)-C(11)	107.4(4)
C(21)-N(10)-C(31)	105.7(5)
C(41)-N(10)-C(31)	110.8(5)
C(11)-N(10)-C(31)	110.4(5)
C(12)-C(11)-N(10)	115.8(6)
C(11)-C(12)-C(13)	111.6(7)
C(14)-C(13)-C(12)	116.1(8)
N(10)-C(21)-C(22)	116.4(5)
C(21)-C(22)-C(23)	110.4(7)
C(24)-C(23)-C(22)	113.5(7)
C(32)-C(31)-N(10)	117.0(5)
C(31)-C(32)-C(33)	108.1(6)
C(34)-C(33)-C(32)	113.2(8)
N(10)-C(41)-C(42)	115.6(5)
C(43)-C(42)-C(41)	111.2(5)
C(42)-C(43)-C(44)	113.7(6)

Table 4. Anisotropic displacement parameters (A^2 x 10^3) for osclpy. The anisotropic displacement factor exponent takes the form:
-2 pi^2 [h^2 a*^2 U11 + ... + 2 h k a* b* U12]

	U11	U22	U33	U23	U13	U12
Os(1)	22(1)	32(1)	42(1)	-2(1)	13(1)	-1(1)
Cl(1)	35(1)	64(1)	54(1)	-3(1)	0(1)	8(1)
Cl(2)	45(1)	46(1)	68(1)	-7(1)	30(1)	-16(1)
Cl(3)	37(1)	46(1)	62(1)	-8(1)	25(1)	4(1)
Cl(4)	37(1)	35(1)	60(1)	5(1)	20(1)	-3(1)
Cl(5)	33(1)	44(1)	48(1)	-8(1)	20(1)	-1(1)
N(1)	31(3)	28(3)	39(3)	2(2)	14(2)	-3(2)
C(2)	43(4)	25(3)	53(4)	1(3)	12(3)	-3(3)
C(3)	44(4)	50(4)	47(4)	-7(3)	8(3)	-6(3)
C(4)	40(4)	53(4)	45(4)	9(3)	8(3)	4(3)
C(5)	47(4)	48(4)	47(4)	7(3)	12(3)	14(3)
C(6)	48(4)	23(3)	49(4)	-4(3)	16(3)	0(3)
N(10)	26(3)	36(3)	49(3)	-4(2)	19(2)	-3(2)
C(11)	37(4)	45(4)	61(5)	-6(3)	21(3)	-3(3)
C(12)	40(5)	50(5)	151(9)	-3(5)	27(5)	2(4)
C(13)	75(6)	46(5)	96(7)	-8(4)	16(5)	10(4)
C(14)	73(7)	56(5)	119(8)	-2(5)	10(6)	20(5)
C(21)	29(3)	40(4)	52(4)	-4(3)	10(3)	-4(3)
C(22)	59(5)	67(5)	55(5)	-10(4)	12(4)	10(4)
C(23)	69(6)	71(6)	63(5)	-14(4)	-9(4)	8(5)
C(24)	71(6)	87(7)	66(6)	-12(5)	4(5)	22(5)
C(31)	30(4)	60(4)	50(4)	4(3)	21(3)	4(3)
C(32)	34(4)	89(6)	57(5)	1(4)	8(3)	6(4)
C(33)	63(6)	180(11)	47(5)	3(6)	11(5)	36(7)
C(34)	71(7)	232(14)	58(6)	-2(8)	6(5)	45(8)
C(41)	31(4)	40(4)	59(4)	-7(3)	25(3)	-10(3)
C(42)	41(4)	48(4)	68(5)	-3(4)	26(4)	-4(3)
C(43)	57(5)	49(4)	69(5)	-10(4)	31(4)	-8(4)
C(44)	59(5)	51(5)	69(5)	0(4)	7(4)	-3(4)

Table 5. Hydrogen coordinates (x 10^4) and isotropic displacement parameters (A^2 x 10^3) for osclpy.

	x	y	z	U(eq)
H(2)	-131	591	74	48
H(3)	-1684	835	-1306	57
H(4)	-2492	1967	-1556	56
H(5)	-1751	2824	-386	57
H(6)	-170	2552	962	47
H(11A)	298	4490	8306	55
H(11B)	1049	4493	9413	55
H(12A)	1677	5361	7959	96
H(12B)	2410	5369	9075	96
H(13A)	484	5727	9493	88
H(13B)	1024	6295	8874	88
H(14A)	-1174	6193	8361	127
H(14B)	-1020	5395	8084	127
H(14C)	-507	6001	7502	127
H(21A)	3705	4484	9044	48
H(21B)	3869	3660	8993	48
H(22A)	2985	3560	10405	73
H(22B)	3028	4393	10483	73
H(23A)	5306	4335	10608	86
H(23B)	4887	4007	11520	86
H(24A)	6360	3278	11043	115
H(24B)	5460	3209	9984	115
H(24C)	5036	2880	10895	115
H(31A)	2557	4506	7412	54
H(31B)	2814	3689	7387	54
H(32A)	378	4317	6723	72
H(32B)	630	3494	6704	72
H(33A)	1762	4508	5665	116
H(33B)	2071	3694	5670	116
H(34A)	623	4060	4261	182
H(34B)	-359	4239	4909	182
H(34C)	77	3451	4816	182
H(41A)	545	3270	8250	49
H(41B)	1327	3252	9348	49
H(42A)	2251	2658	7786	60
H(42B)	2960	2607	8905	60
H(43A)	553	1998	8097	67
H(43B)	1255	1949	9215	67
H(44A)	1563	904	8476	91
H(44B)	2900	1290	8768	91
H(44C)	2106	1303	7670	91

Crystal Data of $[N^nBu_4]_2[OsCl_5(NCCH_3)_1]$

Table 1. Crystal data and structure refinement for maybos.

A. CRYSTAL DATA

Empirical formula	C18 H39 Cl5 N2 Os [NBu4][OsCl5(MeCN)]
Formula weight	650.96
Wavelength	0.71073 A
Temperature	150(2) K
Crystal system	Orthorhombic
Space group	Fdd2
Unit cell dimensions	a = 28.116(5) A alpha = 90 deg. b = 36.205(7) A beta = 90 deg. c = 10.6385(19) A gamma = 90 deg.
Volume	10829(3) A^3
Number of reflections for cell	7044 (2 < theta < 29 deg.)
Z	16
Density (calculated)	1.597 Mg/m^3
Absorption coefficient	5.210 mm^-1
F(000)	5152

B. DATA COLLECTION

Crystal description	Yellow needle
Crystal size	0.29 x 0.04 x 0.04 mm
Instrument	CCD area detector
Theta range for data collection	1.83 to 26.40 deg.
Index ranges	-35<=h<=35, -45<=k<=44, -12<=l<=13
Reflections collected	17477
Independent reflections	5242 [R(int) = 0.0400]
Scan type	phi and omega scans
Absorption correction	Sadabs (Tmin= 0.652, Tmax=0.862)

C. SOLUTION AND REFINEMENT.

Solution	Patterson (DIRDIF)
Refinement type	Full-matrix least-squares on F^2
Program used for refinement	SHELXL-97
Hydrogen atom placement	geometric
Hydrogen atom treatment	riding/rotating group
Data / restraints / parameters	5242/5/255
Goodness-of-fit on F^2	0.904
Conventional R [F>4sigma(F)]	R1 = 0.0318 [4430 data]
Weighted R (F^2 and all data)	wR2 = 0.0636
Absolute structure parameter	-0.013(7)
Extinction coefficient	0
Final maximum delta/sigma	0.012

Weighting scheme
calc w=1/[\s^2^(Fo^2^)+(0.0317P)^2^+0.0000P] where P=(Fo^2^+2Fc^2^)/3

Largest diff. peak and hole	1.885 and -0.553 e.A^-3

Table 2. Atomic coordinates (x 10^4), equivalent isotropic displacement parameters (A^2 x 10^3) and site occupancies for maybos. U(eq) is defined as one third of the trace of the orthogonalized Uij tensor.

	x	y	z	U(eq)	Occ
Os(1)	229(1)	1739(1)	9821(1)	35(1)	1
N(1)	887(2)	1684(2)	10640(6)	43(2)	1
C(2)	1231(3)	1662(2)	11167(7)	46(2)	1
C(3)	1676(3)	1635(2)	11882(8)	65(2)	1
Cl(1)	-519(1)	1805(1)	8954(2)	51(1)	1
Cl(2)	-32(1)	1285(1)	11234(2)	44(1)	1
Cl(3)	549(1)	2176(1)	8477(2)	51(1)	1
Cl(4)	71(1)	2196(1)	11276(2)	45(1)	1
Cl(5)	421(1)	1278(1)	8366(2)	49(1)	1
N(1A)	-1904(2)	-823(1)	7352(7)	37(1)	1
C(1A)	-2375(2)	-709(2)	6759(7)	43(2)	1
C(2A)	-2790(2)	-658(2)	7648(6)	38(2)	1
C(3A)	-3217(2)	-520(2)	6953(7)	61(2)	1
C(4A)	-3665(3)	-501(2)	7746(8)	67(2)	1
C(5A)	-1956(3)	-1157(2)	8202(6)	45(2)	1
C(6A)	-2180(3)	-1493(2)	7619(8)	62(3)	1
C(7A)	-2310(5)	-1826(4)	8397(17)	46(5)	0.50
C(8A)	-1867(5)	-2047(5)	8557(18)	61(5)	0.50
C(7A')	-2060(8)	-1811(4)	8570(20)	74(7)	0.50
C(8A')	-2250(8)	-2184(4)	8240(20)	91(7)	0.50
C(9A)	-1558(2)	-925(2)	6295(6)	42(2)	1
C(10A)	-1406(2)	-617(2)	5410(7)	47(2)	1
C(11A)	-1089(3)	-791(2)	4393(8)	63(2)	1
C(12A)	-895(3)	-515(3)	3463(8)	74(3)	1
C(13A)	-1721(2)	-502(2)	8125(6)	38(2)	1
C(14A)	-1226(2)	-542(2)	8656(7)	47(2)	1
C(15A)	-1091(2)	-197(2)	9381(7)	56(2)	1
C(16A)	-591(2)	-221(2)	9905(10)	72(2)	1

Table 3. Bond lengths [A] and angles [deg] for maybos.

Os(1)-N(1)	2.054(6)
Os(1)-Cl(1)	2.3089(18)
Os(1)-Cl(4)	2.3102(17)
Os(1)-Cl(3)	2.3136(18)
Os(1)-Cl(5)	2.3388(18)
Os(1)-Cl(2)	2.3450(17)
N(1)-C(2)	1.121(8)
C(2)-C(3)	1.468(10)
N(1A)-C(13A)	1.513(8)
N(1A)-C(5A)	1.517(9)
N(1A)-C(1A)	1.524(8)
N(1A)-C(9A)	1.532(9)
C(1A)-C(2A)	1.513(9)
C(2A)-C(3A)	1.498(9)
C(3A)-C(4A)	1.516(10)
C(5A)-C(6A)	1.504(9)
C(6A)-C(7A)	1.508(14)
C(6A)-C(7A')	1.573(16)
C(7A)-C(8A)	1.491(14)
C(7A')-C(8A')	1.494(15)
C(9A)-C(10A)	1.521(9)
C(10A)-C(11A)	1.538(9)
C(11A)-C(12A)	1.507(11)
C(13A)-C(14A)	1.507(9)
C(14A)-C(15A)	1.516(9)
C(15A)-C(16A)	1.513(10)
N(1)-Os(1)-Cl(1)	178.39(19)
N(1)-Os(1)-Cl(4)	87.64(17)
Cl(1)-Os(1)-Cl(4)	91.01(7)
N(1)-Os(1)-Cl(3)	88.81(17)
Cl(1)-Os(1)-Cl(3)	92.07(7)
Cl(4)-Os(1)-Cl(3)	89.93(6)
N(1)-Os(1)-Cl(5)	90.19(17)
Cl(1)-Os(1)-Cl(5)	91.16(7)
Cl(4)-Os(1)-Cl(5)	177.74(7)
Cl(3)-Os(1)-Cl(5)	89.40(7)
N(1)-Os(1)-Cl(2)	86.62(17)
Cl(1)-Os(1)-Cl(2)	92.51(7)
Cl(4)-Os(1)-Cl(2)	90.69(7)
Cl(3)-Os(1)-Cl(2)	175.37(7)
Cl(5)-Os(1)-Cl(2)	89.81(6)
C(2)-N(1)-Os(1)	175.0(6)
N(1)-C(2)-C(3)	178.7(9)
C(13A)-N(1A)-C(5A)	108.7(6)
C(13A)-N(1A)-C(1A)	108.3(4)
C(5A)-N(1A)-C(1A)	112.1(5)
C(13A)-N(1A)-C(9A)	111.7(5)
C(5A)-N(1A)-C(9A)	107.8(4)
C(1A)-N(1A)-C(9A)	108.3(6)
C(2A)-C(1A)-N(1A)	116.4(6)
C(3A)-C(2A)-C(1A)	110.5(5)
C(2A)-C(3A)-C(4A)	114.0(6)
C(6A)-C(5A)-N(1A)	116.1(6)

C(5A)-C(6A)-C(7A)	121.5(9)
C(5A)-C(6A)-C(7A')	103.8(9)
C(7A)-C(6A)-C(7A')	27.3(7)
C(8A)-C(7A)-C(6A)	106.9(12)
C(8A')-C(7A')-C(6A)	115.5(15)
C(10A)-C(9A)-N(1A)	117.0(5)
C(9A)-C(10A)-C(11A)	107.3(6)
C(12A)-C(11A)-C(10A)	113.5(7)
C(14A)-C(13A)-N(1A)	116.3(5)
C(13A)-C(14A)-C(15A)	110.1(6)
C(16A)-C(15A)-C(14A)	112.0(6)

Table 4. Anisotropic displacement parameters (A^2 x 10^3) for maybos. The anisotropic displacement factor exponent takes the form:
-2 pi^2 [h^2 a*^2 U11 + ... + 2 h k a* b* U12]

	U11	U22	U33	U23	U13	U12
Os(1)	43(1)	39(1)	24(1)	0(1)	0(1)	3(1)
N(1)	32(3)	54(4)	42(4)	0(3)	-5(3)	2(3)
C(2)	51(4)	45(4)	42(4)	-3(3)	4(4)	7(3)
C(3)	56(5)	72(5)	66(6)	1(4)	-22(4)	18(4)
Cl(1)	49(1)	63(1)	40(1)	-3(1)	-9(1)	16(1)
Cl(2)	58(1)	41(1)	32(1)	4(1)	-3(1)	-7(1)
Cl(3)	75(1)	49(1)	29(1)	3(1)	10(1)	-4(1)
Cl(4)	66(1)	39(1)	29(1)	-2(1)	8(1)	-2(1)
Cl(5)	59(1)	49(1)	39(1)	-7(1)	2(1)	13(1)
N(1A)	40(3)	38(3)	32(3)	-12(3)	2(3)	3(2)
C(1A)	40(4)	53(4)	35(4)	-2(3)	-9(3)	5(3)
C(2A)	36(4)	45(4)	34(6)	0(3)	3(3)	1(3)
C(3A)	42(4)	94(6)	48(5)	-1(4)	-2(3)	14(4)
C(4A)	48(5)	96(6)	58(6)	-4(5)	1(4)	14(4)
C(5A)	59(4)	45(4)	32(4)	6(3)	6(3)	7(3)
C(6A)	91(6)	37(4)	58(7)	-2(4)	19(5)	-4(4)
C(7A)	33(9)	48(11)	56(11)	-8(8)	6(8)	-12(8)
C(8A)	66(11)	41(10)	76(13)	-4(9)	-15(10)	-4(9)
C(7A')	60(14)	36(11)	130(20)	2(11)	0(15)	-11(12)
C(8A')	123(17)	41(11)	109(18)	9(10)	-38(14)	-17(11)
C(9A)	40(4)	52(4)	32(4)	-5(3)	3(3)	8(3)
C(10A)	43(4)	61(5)	38(4)	0(4)	8(3)	4(4)
C(11A)	56(5)	80(6)	52(5)	2(4)	16(4)	1(4)
C(12A)	65(5)	113(8)	44(5)	6(5)	8(4)	-6(5)
C(13A)	40(4)	43(4)	32(4)	1(3)	0(3)	3(3)
C(14A)	46(4)	55(5)	40(4)	2(4)	-4(3)	8(3)
C(15A)	52(4)	59(5)	55(5)	-3(4)	-8(4)	-7(4)
C(16A)	54(4)	96(6)	64(6)	0(7)	-10(5)	-14(4)

Table 5. Hydrogen coordinates (x 10^4) and isotropic displacement parameters (A^2 x 10^3) for maybos.

	x	y	z	U(eq)
H(3A)	1946	1685	11324	97
H(3B)	1707	1387	12236	97
H(3C)	1673	1817	12565	97
H(1A1)	-2325	-474	6301	52
H(1A2)	-2464	-898	6130	52
H(2A1)	-2865	-897	8057	46
H(2A2)	-2702	-479	8313	46
H(3A1)	-3277	-685	6226	73
H(3A2)	-3148	-271	6621	73
H(4A1)	-3929	-409	7233	101
H(4A2)	-3612	-335	8458	101
H(4A3)	-3743	-749	8059	101
H(5A1)	-1637	-1226	8515	54
H(5A2)	-2149	-1084	8939	54
H(6A1)	-1961	-1579	6952	74
H(6A2)	-2474	-1409	7193	74
H(6A3)	-2041	-1544	6781	74
H(6A4)	-2528	-1461	7530	74
H(7A1)	-2435	-1748	9226	55
H(7A2)	-2557	-1974	7964	55
H(8A1)	-1934	-2263	9083	91
H(8A2)	-1623	-1895	8961	91
H(8A3)	-1753	-2129	7732	91
H(7A3)	-1710	-1830	8650	89
H(7A4)	-2186	-1742	9408	89
H(8A4)	-2159	-2363	8883	136
H(8A5)	-2120	-2260	7423	136
H(8A6)	-2598	-2172	8180	136
H(9A1)	-1268	-1031	6682	50
H(9A2)	-1706	-1123	5785	50
H(10A)	-1227	-425	5877	57
H(10B)	-1689	-501	5021	57
H(11A)	-819	-919	4806	75
H(11B)	-1275	-980	3933	75
H(12A)	-694	-643	2849	111
H(12B)	-706	-330	3909	111
H(12C)	-1160	-394	3027	111
H(13A)	-1728	-277	7594	46
H(13B)	-1943	-461	8832	46
H(14A)	-997	-582	7964	56
H(14B)	-1214	-759	9221	56
H(15A)	-1114	20	8818	67
H(15B)	-1318	-161	10081	67
H(16A)	-519	6	10375	107
H(16B)	-364	-248	9213	107
H(16C)	-567	-434	10468	107

Crystal Data of *cis*-$[N^nBu_4]_3[Os(NCS)_2(SCN)_4]$

Table 1. Crystal data and structure refinement for km3931.

A. CRYSTAL DATA

Empirical formula	C108 H216 N18 Os2 S12 (Os (SCN)4 (NCS)2)2 (NBu4)6
Formula weight	2532.11
Wavelength	0.71073 A
Temperature	150(2) K
Crystal system	Monoclinic
Space group	Cc
Unit cell dimensions	a = 48.132(3) A alpha = 90 deg. b = 16.8015(10) A beta = 101.4100(10) deg. c = 17.1893(10) A gamma = 90 deg.
Volume	13626.2(14) A^3
Number of reflections for cell	4715 (2 < theta < 22 deg.)
Z	4
Density (calculated)	1.234 Mg/m^3
Absorption coefficient	2.093 mm^-1
F(000)	5336

B. DATA COLLECTION

Crystal description	block red
Crystal size	0.20 x 0.15 x 0.08 mm
Theta range for data collection	1.29 to 26.45 deg.
Index ranges	-52<=h<=60, -21<=k<=16, -21<=l<=20
Reflections collected	38458
Independent reflections	21029 [R(int) = 0.0381]
Scan type	phi and omega scans
Absorption correction	Sadabs (Tmin= 0.729,Tmax=0.928)

C. SOLUTION AND REFINEMENT.

Solution	direct (sir92)
Refinement type	Full-matrix least-squares on F^2
Program used for refinement	SHELXL-97
Hydrogen atom placement	geometric
Hydrogen atom treatment	riding
Data / restraints / parameters	21029/711/902
Goodness-of-fit on F^2	0.965
Conventional R [F>4sigma(F)]	R1 = 0.0793 [13467 data]
Weighted R (F^2 and all data)	wR2 = 0.2108
Absolute structure parameter	0.00(3)
Extinction coefficient	0
Final maximum delta/sigma	0.229

Weighting scheme
calc w=1/[\s^2^(Fo^2^)+(0.1295P)^2^+0.0000P] where P=(Fo^2^+2Fc^2^)/3

Largest diff. peak and hole	3.659 and -0.705 e.A^-3

Table 2. Atomic coordinates (x 10^4) and equivalent isotropic displacement parameters (A^2 x 10^3) for km3931. U(eq) is defined as one third of the trace of the orthogonalized Uij tensor.

	x	y	z	U(eq)
Os(1A)	8697(1)	2330(1)	958(1)	60(1)
S(1A)	8400(1)	2242(3)	1871(2)	84(1)
C(1A)	8207(3)	3023(8)	1900(9)	83(4)
N(1A)	8076(3)	3614(8)	1926(9)	110(4)
S(2A)	9073(1)	1812(3)	1965(3)	86(1)
C(2A)	9135(4)	2466(9)	2718(9)	91(5)
N(2A)	9184(3)	2869(9)	3251(9)	112(5)
S(3A)	8850(1)	3647(2)	1261(2)	87(1)
C(3A)	8594(3)	4269(8)	876(9)	82(4)
N(3A)	8430(3)	4758(8)	616(8)	104(4)
S(4A)	8334(1)	2782(3)	-95(2)	80(1)
C(4A)	8185(3)	2003(8)	-481(9)	85(4)
N(4A)	8048(4)	1505(10)	-854(9)	131(6)
N(5A)	8968(3)	2204(8)	154(8)	92(4)
C(5A)	9104(3)	2461(8)	-285(8)	72(4)
S(5A)	9310(1)	2553(3)	-909(3)	100(1)
N(6A)	8597(3)	1128(5)	732(7)	77(3)
C(6A)	8514(3)	496(6)	679(8)	71(3)
S(6A)	8408(1)	-408(3)	551(3)	112(2)
N(1)	7404(3)	2775(8)	256(8)	73(3)
C(111)	7618(4)	2107(10)	560(10)	83(4)
C(112)	7479(3)	1338(9)	630(10)	83(4)
C(113)	7704(4)	726(10)	738(11)	103(5)
C(114)	7591(5)	-123(12)	890(12)	127(7)
C(121)	7584(4)	3548(10)	226(11)	94(4)
C(122)	7422(4)	4290(11)	-11(12)	119(6)
C(123)	7692(6)	4955(17)	185(17)	170(9)
C(124)	7592(11)	5530(30)	-80(30)	330(30)
C(131)	7198(3)	2890(10)	767(10)	83(4)
C(132)	7329(4)	3164(14)	1603(10)	115(6)
C(133)	7100(4)	3155(13)	2126(11)	115(6)
C(134)	7231(6)	3421(17)	3015(15)	173(10)
C(141)	7221(4)	2604(9)	-560(9)	79(4)
C(142)	7407(7)	2460(14)	-1191(13)	133(8)
C(143)	7231(5)	2198(14)	-1954(13)	122(6)
C(144)	7355(10)	1850(30)	-2440(30)	310(20)
N(2)	9924(3)	2789(9)	1597(8)	78(3)
C(211)	9753(4)	2058(11)	1197(11)	89(4)
C(212)	9918(4)	1372(12)	1071(11)	102(5)
C(213)	9734(5)	702(12)	744(12)	123(6)
C(214)	9877(7)	-47(18)	433(16)	194(11)
C(221)	10141(3)	3028(10)	1136(8)	76(3)
C(222)	10037(4)	3185(14)	267(9)	108(6)
C(223)	10275(4)	3413(11)	-149(10)	98(5)
C(224)	10186(5)	3469(14)	-980(12)	133(7)
C(231)	9713(3)	3426(11)	1624(9)	85(4)
C(232)	9833(4)	4225(11)	1886(11)	106(5)
C(233)	9605(4)	4776(11)	2129(11)	113(5)

C(234)	9712(6)	5582(15)	2361(15)	163(9)
C(241)	10081(4)	2579(12)	2412(10)	91(5)
C(242)	9901(6)	2312(17)	2940(14)	142(8)
C(243)	10051(5)	2155(14)	3768(13)	129(7)
C(244)	9963(8)	1410(20)	3950(20)	226(14)
N(3)	11404(3)	4458(6)	562(6)	61(2)
C(311)	11157(3)	4350(7)	970(7)	57(3)
C(312)	10948(3)	4997(10)	878(9)	78(4)
C(313)	10725(3)	4850(9)	1414(9)	84(4)
C(314)	10485(4)	5437(11)	1253(11)	114(6)
C(321)	11590(3)	3725(9)	691(8)	75(3)
C(322)	11841(4)	3684(11)	322(11)	101(5)
C(323)	11985(5)	2896(13)	445(13)	129(7)
C(324)	12249(6)	2899(16)	30(17)	173(10)
C(331)	11586(3)	5157(9)	899(7)	67(3)
C(332)	11669(3)	5155(11)	1773(8)	82(4)
C(333)	11905(4)	5760(10)	2089(10)	94(5)
C(334)	11946(4)	5961(12)	2963(10)	112(6)
C(341)	11309(3)	4547(9)	-316(7)	70(3)
C(342)	11119(4)	3903(10)	-744(8)	90(5)
C(343)	11108(4)	3980(10)	-1636(9)	93(4)
C(344)	10929(4)	3313(13)	-2069(12)	123(7)
N(4)	11008(3)	490(7)	6328(7)	66(2)
C(411)	11278(4)	502(10)	6000(10)	85(4)
C(412)	11471(4)	-183(13)	6249(14)	120(6)
C(413)	11760(7)	-170(20)	6007(19)	201(11)
C(414)	11951(7)	-860(20)	6265(19)	218(14)
C(421)	10860(3)	1258(8)	6066(8)	75(3)
C(422)	10586(4)	1377(10)	6360(12)	99(5)
C(423)	10465(5)	2176(13)	6052(14)	128(7)
C(424)	10182(7)	2380(15)	6435(17)	171(11)
C(431)	10831(3)	-246(8)	5984(9)	70(3)
C(432)	10737(4)	-276(10)	5085(9)	92(5)
C(433)	10565(4)	-989(11)	4861(10)	101(5)
C(434)	10445(6)	-1004(17)	3969(15)	175(11)
C(441)	11080(3)	385(8)	7209(7)	65(3)
C(442)	11258(3)	1020(9)	7653(8)	75(4)
C(443)	11277(4)	969(12)	8512(10)	97(5)
C(444)	11462(4)	1553(11)	9015(10)	100(5)
N(5)	8700(3)	5008(10)	-1508(7)	71(2)
C(511)	8445(3)	4499(9)	-1397(9)	81(4)
C(512)	8176(4)	4577(10)	-2051(9)	88(4)
C(513)	7935(4)	4178(11)	-1837(11)	107(5)
C(514)	7657(4)	4307(13)	-2367(12)	133(7)
C(521)	8622(3)	5899(9)	-1511(8)	78(3)
C(522)	8568(4)	6228(11)	-798(10)	101(5)
C(523)	8480(4)	7050(11)	-844(11)	108(5)
C(524)	8218(13)	7100(30)	-590(30)	370(30)
C(531)	8935(3)	4796(10)	-836(8)	81(4)
C(532)	9209(3)	5216(12)	-895(10)	93(5)
C(533)	9415(5)	5176(13)	-127(12)	126(6)
C(534)	9693(5)	5562(15)	-122(14)	156(9)
C(541)	8781(3)	4838(9)	-2307(8)	78(3)
C(542)	8867(4)	3977(9)	-2434(8)	90(4)
C(543)	8923(4)	3880(10)	-3292(10)	105(5)
C(544)	9032(5)	3072(13)	-3432(13)	136(7)
N(6)	8703(4)	272(10)	-1838(10)	118(4)
C(611)	8600(5)	1153(13)	-1855(14)	146(6)

C(612)	8432(6)	1382(14)	-2607(17)	168(8)
C(613)	8295(7)	2254(16)	-2583(17)	158(9)
C(614)	8169(10)	2592(18)	-3310(20)	223(16)
C(621)	8464(4)	-294(12)	-2146(10)	111(5)
C(622)	8229(5)	-323(13)	-1686(13)	126(6)
C(623)	8015(4)	-869(12)	-1948(12)	120(6)
C(624)	7769(5)	-885(15)	-1502(14)	160(9)
C(631)	8848(5)	87(19)	-1032(15)	146(6)
C(632)	8965(5)	-796(15)	-885(11)	139(6)
C(633)	9106(6)	-830(16)	-115(15)	162(9)
C(634)	9233(6)	-1609(16)	82(14)	162(9)
C(641)	8892(5)	223(13)	-2386(12)	126(6)
C(642)	9182(5)	642(15)	-2148(13)	146(7)
C(643)	9378(6)	544(17)	-2718(16)	177(10)
C(644)	9686(8)	1000(20)	-2480(20)	235(15)
Os(1B)	11125(1)	2511(1)	3422(1)	71(1)
S(1B)	10865(1)	2529(3)	2075(2)	87(1)
C(1B)	11056(3)	2277(8)	1455(8)	74(4)
N(1B)	11201(3)	2145(8)	1013(8)	98(4)
S(2B)	11371(1)	3628(3)	3053(2)	91(1)
C(2B)	11634(3)	3907(8)	3811(7)	67(3)
N(2B)	11804(3)	4083(7)	4318(7)	85(3)
S(5B)	11414(2)	2781(3)	6197(3)	128(2)
S(4B)	10867(2)	1447(4)	3811(3)	137(3)
C(4B)	10650(3)	1067(9)	3043(8)	77(4)
N(4B)	10504(3)	718(8)	2560(7)	87(4)
S(3B)	11463(1)	1688(3)	3091(4)	132(2)
N(6B)	10813(3)	3301(10)	3591(11)	135(6)
C(6B)	10664(4)	3796(10)	3632(11)	111(6)
S(6B)	10437(2)	4456(5)	3774(4)	186(4)
C(5B)	11313(3)	2710(8)	5274(7)	73(4)
N(5B)	11347(5)	2528(9)	4634(7)	126(7)
N(3B)	11646(9)	820(20)	4469(15)	315(18)
C(3B)	11591(7)	1121(16)	3828(13)	181(10)

Table 3. Bond lengths [A] and angles [deg] for km3931.

Os(1A)-N(5A)	2.091(10)
Os(1A)-N(6A)	2.095(9)
Os(1A)-S(1A)	2.325(4)
Os(1A)-S(3A)	2.357(4)
Os(1A)-S(4A)	2.377(4)
Os(1A)-S(2A)	2.405(4)
S(1A)-C(1A)	1.616(12)
C(1A)-N(1A)	1.181(13)
S(2A)-C(2A)	1.679(13)
C(2A)-N(2A)	1.126(14)
S(3A)-C(3A)	1.652(12)
C(3A)-N(3A)	1.166(13)
S(4A)-C(4A)	1.574(13)
C(4A)-N(4A)	1.175(14)
N(5A)-C(5A)	1.176(12)
C(5A)-S(5A)	1.606(12)
N(6A)-C(6A)	1.131(11)
C(6A)-S(6A)	1.604(11)
N(1)-C(131)	1.46(2)
N(1)-C(141)	1.53(2)
N(1)-C(111)	1.54(2)
N(1)-C(121)	1.57(2)
C(111)-C(112)	1.47(2)
C(112)-C(113)	1.48(2)
C(113)-C(114)	1.57(2)
C(121)-C(122)	1.48(2)
C(122)-C(123)	1.69(3)
C(123)-C(124)	1.14(5)
C(131)-C(132)	1.52(2)
C(132)-C(133)	1.56(2)
C(133)-C(134)	1.60(3)
C(141)-C(142)	1.55(3)
C(142)-C(143)	1.48(3)
C(143)-C(144)	1.26(4)
N(2)-C(221)	1.49(2)
N(2)-C(231)	1.48(2)
N(2)-C(241)	1.50(2)
N(2)-C(211)	1.56(2)
C(211)-C(212)	1.44(2)
C(212)-C(213)	1.47(2)
C(213)-C(214)	1.58(3)
C(221)-C(222)	1.50(2)
C(222)-C(223)	1.52(2)
C(223)-C(224)	1.41(2)
C(231)-C(232)	1.50(2)
C(232)-C(233)	1.55(2)
C(233)-C(234)	1.47(3)
C(241)-C(242)	1.44(3)
C(242)-C(243)	1.49(3)
C(243)-C(244)	1.37(4)
N(3)-C(341)	1.496(15)
N(3)-C(311)	1.505(17)
N(3)-C(331)	1.508(17)
N(3)-C(321)	1.513(18)

C(311)-C(312)	1.47(2)
C(312)-C(313)	1.57(2)
C(313)-C(314)	1.50(2)
C(321)-C(322)	1.47(2)
C(322)-C(323)	1.49(2)
C(323)-C(324)	1.58(3)
C(331)-C(332)	1.477(18)
C(332)-C(333)	1.54(2)
C(333)-C(334)	1.52(2)
C(341)-C(342)	1.51(2)
C(342)-C(343)	1.53(2)
C(343)-C(344)	1.52(2)
N(4)-C(441)	1.494(16)
N(4)-C(421)	1.498(18)
N(4)-C(411)	1.519(18)
N(4)-C(431)	1.551(16)
C(411)-C(412)	1.49(3)
C(412)-C(413)	1.53(3)
C(413)-C(414)	1.49(4)
C(421)-C(422)	1.52(2)
C(422)-C(423)	1.52(2)
C(423)-C(424)	1.66(4)
C(431)-C(432)	1.52(2)
C(432)-C(433)	1.46(2)
C(433)-C(434)	1.53(3)
C(441)-C(442)	1.483(18)
C(442)-C(443)	1.46(2)
C(443)-C(444)	1.48(2)
N(5)-C(531)	1.49(2)
N(5)-C(541)	1.529(18)
N(5)-C(511)	1.537(18)
N(5)-C(521)	1.54(2)
C(511)-C(512)	1.54(2)
C(512)-C(513)	1.45(2)
C(513)-C(514)	1.48(3)
C(521)-C(522)	1.416(19)
C(522)-C(523)	1.44(2)
C(523)-C(524)	1.41(5)
C(531)-C(532)	1.52(2)
C(532)-C(533)	1.49(2)
C(533)-C(534)	1.48(3)
C(541)-C(542)	1.53(2)
C(542)-C(543)	1.56(2)
C(543)-C(544)	1.49(2)
N(6)-C(641)	1.44(2)
N(6)-C(631)	1.46(3)
N(6)-C(621)	1.50(2)
N(6)-C(611)	1.56(3)
C(611)-C(612)	1.44(3)
C(612)-C(613)	1.61(3)
C(613)-C(614)	1.40(4)
C(621)-C(622)	1.50(2)
C(622)-C(623)	1.38(2)
C(623)-C(624)	1.53(3)
C(631)-C(632)	1.59(4)
C(632)-C(633)	1.36(3)
C(633)-C(634)	1.46(3)
C(641)-C(642)	1.54(3)

C(642)-C(643)	1.50(3)
C(643)-C(644)	1.64(4)
Os(1B)-N(6B)	2.066(11)
Os(1B)-N(5B)	2.146(13)
Os(1B)-S(3B)	2.288(6)
Os(1B)-S(4B)	2.348(5)
Os(1B)-S(2B)	2.373(4)
Os(1B)-S(1B)	2.405(4)
S(1B)-C(1B)	1.599(12)
C(1B)-N(1B)	1.150(13)
S(2B)-C(2B)	1.692(12)
C(2B)-N(2B)	1.111(12)
S(5B)-C(5B)	1.569(12)
S(4B)-C(4B)	1.641(12)
C(4B)-N(4B)	1.140(13)
S(3B)-C(3B)	1.609(16)
N(6B)-C(6B)	1.112(13)
C(6B)-S(6B)	1.609(13)
C(5B)-N(5B)	1.183(13)
N(3B)-C(3B)	1.191(16)

N(5A)-Os(1A)-N(6A)	86.0(5)
N(5A)-Os(1A)-S(1A)	170.5(4)
N(6A)-Os(1A)-S(1A)	85.1(3)
N(5A)-Os(1A)-S(3A)	91.8(4)
N(6A)-Os(1A)-S(3A)	175.0(3)
S(1A)-Os(1A)-S(3A)	96.78(16)
N(5A)-Os(1A)-S(4A)	89.4(4)
N(6A)-Os(1A)-S(4A)	93.4(3)
S(1A)-Os(1A)-S(4A)	94.47(15)
S(3A)-Os(1A)-S(4A)	91.13(15)
N(5A)-Os(1A)-S(2A)	87.7(4)
N(6A)-Os(1A)-S(2A)	84.1(3)
S(1A)-Os(1A)-S(2A)	88.07(15)
S(3A)-Os(1A)-S(2A)	91.29(15)
S(4A)-Os(1A)-S(2A)	176.27(16)
C(1A)-S(1A)-Os(1A)	113.8(6)
N(1A)-C(1A)-S(1A)	177.1(16)
C(2A)-S(2A)-Os(1A)	108.2(7)
N(2A)-C(2A)-S(2A)	175.9(18)
C(3A)-S(3A)-Os(1A)	109.2(5)
N(3A)-C(3A)-S(3A)	174.4(14)
C(4A)-S(4A)-Os(1A)	105.1(6)
N(4A)-C(4A)-S(4A)	169.2(17)
C(5A)-N(5A)-Os(1A)	152.5(12)
N(5A)-C(5A)-S(5A)	163.9(13)
C(6A)-N(6A)-Os(1A)	169.8(12)
N(6A)-C(6A)-S(6A)	175.9(14)
C(131)-N(1)-C(141)	104.0(13)
C(131)-N(1)-C(111)	112.3(14)
C(141)-N(1)-C(111)	113.5(12)
C(131)-N(1)-C(121)	110.7(12)
C(141)-N(1)-C(121)	110.3(13)
C(111)-N(1)-C(121)	106.2(13)
C(112)-C(111)-N(1)	112.5(14)
C(111)-C(112)-C(113)	106.8(14)
C(112)-C(113)-C(114)	112.7(16)
C(122)-C(121)-N(1)	116.3(14)

C(121)-C(122)-C(123)	99.2(17)
C(124)-C(123)-C(122)	104(3)
N(1)-C(131)-C(132)	113.9(14)
C(131)-C(132)-C(133)	109.5(16)
C(132)-C(133)-C(134)	111.2(18)
N(1)-C(141)-C(142)	111.3(17)
C(143)-C(142)-C(141)	111(2)
C(144)-C(143)-C(142)	118(3)
C(221)-N(2)-C(231)	112.4(14)
C(221)-N(2)-C(241)	106.7(13)
C(231)-N(2)-C(241)	111.3(13)
C(221)-N(2)-C(211)	109.9(13)
C(231)-N(2)-C(211)	106.0(14)
C(241)-N(2)-C(211)	110.5(14)
C(212)-C(211)-N(2)	116.1(15)
C(211)-C(212)-C(213)	111.3(16)
C(212)-C(213)-C(214)	118(2)
N(2)-C(221)-C(222)	116.6(12)
C(221)-C(222)-C(223)	112.3(14)
C(224)-C(223)-C(222)	112.8(16)
N(2)-C(231)-C(232)	115.4(14)
C(231)-C(232)-C(233)	111.3(16)
C(234)-C(233)-C(232)	113.2(19)
C(242)-C(241)-N(2)	114.1(18)
C(241)-C(242)-C(243)	115(2)
C(244)-C(243)-C(242)	106(3)
C(341)-N(3)-C(311)	111.6(10)
C(341)-N(3)-C(331)	110.4(10)
C(311)-N(3)-C(331)	111.5(10)
C(341)-N(3)-C(321)	106.5(11)
C(311)-N(3)-C(321)	109.4(10)
C(331)-N(3)-C(321)	107.3(11)
C(312)-C(311)-N(3)	116.6(11)
C(311)-C(312)-C(313)	110.7(13)
C(314)-C(313)-C(312)	112.3(14)
C(322)-C(321)-N(3)	119.1(12)
C(321)-C(322)-C(323)	112.2(16)
C(322)-C(323)-C(324)	109.0(19)
C(332)-C(331)-N(3)	114.1(11)
C(331)-C(332)-C(333)	112.9(12)
C(334)-C(333)-C(332)	116.1(14)
N(3)-C(341)-C(342)	117.1(11)
C(341)-C(342)-C(343)	109.0(13)
C(344)-C(343)-C(342)	109.5(14)
C(441)-N(4)-C(421)	114.0(11)
C(441)-N(4)-C(411)	109.5(12)
C(421)-N(4)-C(411)	105.5(11)
C(441)-N(4)-C(431)	107.0(10)
C(421)-N(4)-C(431)	112.3(11)
C(411)-N(4)-C(431)	108.4(11)
C(412)-C(411)-N(4)	114.5(14)
C(411)-C(412)-C(413)	117(2)
C(414)-C(413)-C(412)	117(3)
N(4)-C(421)-C(422)	114.0(12)
C(423)-C(422)-C(421)	107.4(15)
C(422)-C(423)-C(424)	109.3(18)
C(432)-C(431)-N(4)	116.3(12)
C(433)-C(432)-C(431)	109.4(13)

C(432)-C(433)-C(434)	111.1(17)
C(442)-C(441)-N(4)	115.6(11)
C(443)-C(442)-C(441)	113.1(12)
C(442)-C(443)-C(444)	117.4(16)
C(531)-N(5)-C(541)	111.1(13)
C(531)-N(5)-C(511)	105.9(11)
C(541)-N(5)-C(511)	111.0(13)
C(531)-N(5)-C(521)	112.4(13)
C(541)-N(5)-C(521)	106.4(11)
C(511)-N(5)-C(521)	110.1(13)
N(5)-C(511)-C(512)	115.9(12)
C(513)-C(512)-C(511)	112.0(13)
C(512)-C(513)-C(514)	116.7(16)
C(522)-C(521)-N(5)	117.5(12)
C(521)-C(522)-C(523)	115.4(15)
C(524)-C(523)-C(522)	108(3)
N(5)-C(531)-C(532)	112.0(12)
C(533)-C(532)-C(531)	110.7(14)
C(534)-C(533)-C(532)	115.2(18)
N(5)-C(541)-C(542)	115.4(12)
C(541)-C(542)-C(543)	109.6(12)
C(544)-C(543)-C(542)	112.3(15)
C(641)-N(6)-C(631)	111.4(19)
C(641)-N(6)-C(621)	105.8(13)
C(631)-N(6)-C(621)	112.9(19)
C(641)-N(6)-C(611)	106.3(16)
C(631)-N(6)-C(611)	108.2(17)
C(621)-N(6)-C(611)	112.1(18)
C(612)-C(611)-N(6)	113.1(17)
C(611)-C(612)-C(613)	112(2)
C(614)-C(613)-C(612)	117(3)
C(622)-C(621)-N(6)	116.0(14)
C(623)-C(622)-C(621)	116.0(17)
C(622)-C(623)-C(624)	116.5(19)
N(6)-C(631)-C(632)	116(2)
C(633)-C(632)-C(631)	107(2)
C(632)-C(633)-C(634)	112(2)
N(6)-C(641)-C(642)	117.3(15)
C(643)-C(642)-C(641)	115.5(19)
C(642)-C(643)-C(644)	116(2)
N(6B)-Os(1B)-N(5B)	95.2(7)
N(6B)-Os(1B)-S(3B)	173.5(6)
N(5B)-Os(1B)-S(3B)	90.4(5)
N(6B)-Os(1B)-S(4B)	90.5(6)
N(5B)-Os(1B)-S(4B)	85.6(5)
S(3B)-Os(1B)-S(4B)	93.0(3)
N(6B)-Os(1B)-S(2B)	86.8(6)
N(5B)-Os(1B)-S(2B)	94.0(5)
S(3B)-Os(1B)-S(2B)	89.7(2)
S(4B)-Os(1B)-S(2B)	177.3(3)
N(6B)-Os(1B)-S(1B)	82.7(5)
N(5B)-Os(1B)-S(1B)	177.9(5)
S(3B)-Os(1B)-S(1B)	91.6(2)
S(4B)-Os(1B)-S(1B)	94.52(16)
S(2B)-Os(1B)-S(1B)	85.75(14)
C(1B)-S(1B)-Os(1B)	112.3(6)
N(1B)-C(1B)-S(1B)	175.6(15)
C(2B)-S(2B)-Os(1B)	110.4(5)

N(2B)-C(2B)-S(2B)	178.8(15)
C(4B)-S(4B)-Os(1B)	110.8(6)
N(4B)-C(4B)-S(4B)	171.7(15)
C(3B)-S(3B)-Os(1B)	110.1(12)
C(6B)-N(6B)-Os(1B)	171(2)
N(6B)-C(6B)-S(6B)	173(2)
N(5B)-C(5B)-S(5B)	152.5(16)
C(5B)-N(5B)-Os(1B)	140.6(16)
N(3B)-C(3B)-S(3B)	163(4)

Table 4. Anisotropic displacement parameters (A^2 x 10^3) for km3931. The anisotropic displacement factor exponent takes the form:
-2 pi^2 [h^2 a*^2 U11 + ... + 2 h k a* b* U12]

	U11	U22	U33	U23	U13	U12
Os(1A)	53(1)	76(1)	53(1)	-5(1)	13(1)	-7(1)
S(1A)	68(2)	118(3)	71(2)	8(2)	21(2)	5(2)
S(2A)	67(2)	94(3)	92(3)	-11(2)	4(2)	-3(2)
S(3A)	89(3)	71(2)	99(3)	-31(2)	15(2)	-12(2)
S(4A)	67(2)	93(3)	78(2)	24(2)	9(2)	1(2)
S(5A)	76(3)	161(4)	65(2)	-1(2)	23(2)	-13(2)
S(6A)	124(4)	78(3)	137(4)	0(3)	35(3)	-15(3)
N(1)	55(7)	76(6)	85(7)	-19(6)	7(5)	-4(5)
C(111)	72(9)	79(7)	91(10)	-3(8)	1(7)	2(6)
C(112)	80(10)	78(7)	87(9)	-9(7)	5(8)	4(7)
C(121)	90(11)	80(7)	117(12)	-8(8)	30(8)	-29(6)
C(122)	124(14)	95(9)	131(13)	35(10)	12(12)	-23(9)
C(131)	67(9)	86(10)	100(8)	4(8)	24(7)	-11(7)
C(132)	117(14)	139(15)	90(9)	-4(10)	22(9)	11(12)
C(141)	70(10)	88(10)	74(7)	6(7)	0(6)	-6(7)
C(142)	129(17)	176(18)	95(12)	-54(12)	27(12)	-18(13)
N(2)	49(7)	115(8)	66(6)	-6(6)	1(5)	-5(5)
C(211)	66(10)	108(10)	93(10)	0(9)	18(8)	-21(6)
C(212)	74(10)	124(11)	106(11)	-30(10)	7(9)	-11(8)
C(221)	52(7)	93(10)	78(7)	-3(7)	-1(6)	-20(6)
C(222)	93(12)	161(16)	66(7)	7(10)	9(8)	-27(11)
C(231)	68(9)	113(9)	70(8)	16(8)	0(7)	10(6)
C(232)	88(12)	116(10)	103(11)	-1(10)	-7(9)	18(8)
C(241)	52(9)	134(14)	81(8)	14(8)	-3(6)	12(7)
C(242)	82(14)	240(20)	93(11)	39(13)	-2(10)	-20(14)
N(3)	87(7)	49(6)	47(5)	8(4)	13(5)	-9(4)
C(311)	67(7)	55(7)	42(6)	-1(5)	-5(5)	-21(5)
C(312)	80(9)	73(9)	82(9)	-13(7)	17(8)	-15(6)
C(321)	89(9)	66(7)	64(8)	9(6)	1(6)	2(6)
C(322)	115(11)	91(11)	101(11)	-11(9)	29(9)	13(9)
C(331)	78(9)	69(7)	61(6)	0(6)	29(6)	-18(6)
C(332)	82(10)	102(11)	69(7)	-16(7)	29(7)	-35(8)
C(341)	84(10)	74(9)	49(5)	15(6)	9(6)	-11(6)
C(342)	122(13)	96(11)	47(7)	-9(7)	4(7)	-12(8)
N(4)	82(7)	55(6)	67(5)	-6(5)	25(5)	-24(4)
C(411)	95(9)	80(9)	91(9)	-26(8)	45(8)	-37(6)
C(412)	100(12)	117(13)	156(15)	-27(12)	58(12)	-8(8)
C(421)	100(9)	57(6)	63(7)	-10(6)	5(7)	-18(6)
C(422)	92(9)	65(9)	133(13)	-10(9)	5(9)	-6(7)
C(431)	75(9)	57(7)	85(7)	-17(6)	35(7)	-20(6)
C(432)	131(13)	66(9)	82(8)	-31(7)	27(9)	-33(9)
C(441)	82(9)	52(7)	65(6)	1(5)	24(6)	-7(6)
C(442)	99(11)	66(8)	65(7)	-1(6)	30(7)	-25(7)
N(5)	79(6)	84(5)	52(5)	16(4)	16(4)	-15(5)
C(511)	75(8)	82(8)	86(9)	15(7)	17(6)	-18(7)
C(512)	94(9)	80(9)	81(9)	5(8)	-2(7)	-23(8)
C(521)	92(10)	82(6)	60(7)	10(6)	10(7)	-22(6)
C(522)	115(13)	113(11)	82(9)	12(8)	38(9)	13(10)

C(531)	93(8)	99(9)	47(6)	8(7)	2(6)	-18(7)
C(532)	77(8)	106(12)	96(11)	16(9)	15(8)	3(8)
C(541)	95(10)	90(7)	45(6)	10(6)	5(6)	-15(7)
C(542)	127(13)	80(8)	63(8)	-1(7)	17(8)	-18(8)
N(6)	126(10)	133(9)	109(8)	-54(7)	56(7)	-45(7)
C(611)	158(17)	128(10)	164(14)	-85(11)	64(12)	-43(9)
C(612)	200(20)	115(13)	194(17)	-42(13)	49(15)	-27(12)
C(621)	128(12)	119(11)	90(10)	-54(10)	33(8)	-23(10)
C(622)	121(13)	131(14)	133(14)	-46(12)	42(10)	-42(11)
C(631)	86(13)	237(17)	122(9)	-46(13)	38(9)	-48(13)
C(632)	137(15)	213(16)	68(10)	-6(11)	19(10)	-81(12)
C(641)	146(13)	133(13)	112(11)	-62(11)	57(10)	-37(10)
C(642)	152(14)	173(17)	136(14)	-51(13)	83(13)	-53(13)
Os(1B)	89(1)	66(1)	59(1)	5(1)	21(1)	-2(1)
S(1B)	71(3)	118(3)	66(2)	25(2)	3(2)	6(2)
S(2B)	112(3)	90(3)	61(2)	19(2)	-3(2)	-19(2)
S(5B)	207(7)	94(3)	79(3)	3(2)	21(3)	-47(4)
S(4B)	184(6)	150(5)	68(3)	17(3)	0(3)	-91(5)
S(3B)	115(4)	106(4)	160(5)	-16(3)	-10(3)	28(3)
S(6B)	138(5)	210(7)	184(6)	-124(6)	-29(5)	42(5)

Table 5. Hydrogen coordinates (x 10^4) and isotropic displacement parameters (A^2 x 10^3) for km3931.

	x	y	z	U(eq)
H(11A)	7751	2049	192	99
H(11B)	7730	2260	1086	99
H(11C)	7335	1228	145	100
H(11D)	7384	1342	1091	100
H(11E)	7855	877	1194	123
H(11F)	7788	710	259	123
H(11G)	7748	-505	959	191
H(11H)	7445	-282	436	191
H(11I)	7510	-114	1370	191
H(12A)	7704	3633	758	113
H(12B)	7713	3457	-149	113
H(12C)	7278	4388	315	143
H(12D)	7331	4286	-580	143
H(12E)	7762	5012	764	204
H(12F)	7851	4792	-66	204
H(12G)	7736	5857	-266	492
H(12H)	7515	5829	316	492
H(12I)	7439	5412	-537	492
H(13A)	7097	2383	801	100
H(13B)	7057	3290	520	100
H(13C)	7406	3710	1585	138
H(13D)	7488	2807	1835	138
H(13E)	7020	2612	2129	138
H(13F)	6944	3521	1896	138
H(13G)	7083	3400	3334	260
H(13H)	7303	3966	3014	260
H(13I)	7385	3061	3243	260
H(14A)	7093	3060	-726	95
H(14B)	7103	2128	-526	95
H(14C)	7507	2957	-1273	159
H(14D)	7551	2048	-995	159
H(14E)	7083	1833	-1834	146
H(14F)	7133	2671	-2219	146
H(14G)	7213	1675	-2902	466
H(14H)	7460	1392	-2188	466
H(14I)	7486	2224	-2620	466
H(21A)	9617	1896	1530	106
H(21B)	9642	2230	677	106
H(21C)	10039	1210	1581	123
H(21D)	10043	1512	699	123
H(21E)	9589	908	300	148
H(21F)	9633	518	1160	148
H(21G)	9731	-433	207	291
H(21H)	10009	-293	874	291
H(21I)	9981	120	23	291
H(22A)	10286	2603	1190	91
H(22B)	10236	3515	1380	91
H(22C)	9896	3620	202	129
H(22D)	9942	2702	13	129
H(22E)	10355	3931	59	118

H(22F)	10428	3011	-27	118
H(22G)	10346	3628	-1218	200
H(22H)	10035	3866	-1106	200
H(22I)	10115	2950	-1193	200
H(23A)	9588	3256	1988	102
H(23B)	9593	3481	1089	102
H(23C)	9908	4477	1449	127
H(23D)	9993	4159	2343	127
H(23E)	9442	4819	1679	135
H(23F)	9536	4531	2579	135
H(23G)	9560	5898	2515	244
H(23H)	9773	5838	1911	244
H(23I)	9872	5546	2809	244
H(24A)	10219	2154	2368	109
H(24B)	10189	3051	2649	109
H(24C)	9804	1818	2720	170
H(24D)	9754	2721	2950	170
H(24E)	10259	2164	3807	155
H(24F)	10000	2560	4134	155
H(24G)	10046	1288	4504	339
H(24H)	10023	1018	3601	339
H(24I)	9755	1409	3879	339
H(31A)	11058	3854	768	68
H(31B)	11233	4274	1544	68
H(31C)	10850	5033	316	94
H(31D)	11046	5509	1026	94
H(31E)	10648	4304	1319	101
H(31F)	10821	4888	1978	101
H(31G)	10353	5327	1605	171
H(31H)	10386	5389	699	171
H(31I)	10560	5978	1350	171
H(32A)	11656	3659	1271	90
H(32B)	11469	3260	503	90
H(32C)	11977	4106	549	121
H(32D)	11782	3786	-255	121
H(32E)	11851	2470	216	154
H(32F)	12047	2792	1020	154
H(32G)	12345	2382	109	260
H(32H)	12381	3319	262	260
H(32I)	12186	2998	-540	260
H(33A)	11759	5158	672	81
H(33B)	11481	5654	729	81
H(33C)	11734	4615	1954	99
H(33D)	11500	5280	2002	99
H(33E)	12086	5548	1983	113
H(33F)	11863	6259	1781	113
H(33G)	12095	6366	3096	168
H(33H)	12002	5481	3279	168
H(33I)	11768	6167	3080	168
H(34A)	11480	4580	-554	84
H(34B)	11208	5061	-419	84
H(34C)	10926	3957	-632	109
H(34D)	11194	3373	-557	109
H(34E)	11026	4501	-1827	111
H(34F)	11303	3951	-1745	111
H(34G)	10922	3362	-2641	184
H(34H)	10737	3346	-1964	184
H(34I)	11013	2799	-1883	184

H(41A)	11227	510	5413	102
H(41B)	11382	1001	6172	102
H(41C)	11372	-674	6031	143
H(41D)	11504	-222	6835	143
H(41E)	11728	-131	5422	242
H(41F)	11859	324	6224	242
H(41G)	12128	-788	6072	327
H(41H)	11858	-1350	6046	327
H(41I)	11993	-888	6846	327
H(42A)	10818	1276	5479	90
H(42B)	10990	1704	6259	90
H(42C)	10450	947	6160	119
H(42D)	10622	1370	6947	119
H(42E)	10411	2163	5466	154
H(42F)	10610	2597	6204	154
H(42G)	10094	2872	6200	256
H(42H)	10240	2446	7011	256
H(42I)	10046	1941	6321	256
H(43A)	10944	-730	6157	84
H(43B)	10660	-269	6221	84
H(43C)	10625	205	4896	111
H(43D)	10906	-287	4834	111
H(43E)	10407	-1000	5153	122
H(43F)	10683	-1469	5011	122
H(43G)	10326	-1476	3837	262
H(43H)	10601	-1021	3680	262
H(43I)	10332	-524	3818	262
H(44A)	10901	352	7409	78
H(44B)	11180	-130	7326	78
H(44C)	11452	985	7538	90
H(44D)	11179	1545	7465	90
H(44E)	11345	429	8685	117
H(44F)	11084	1025	8619	117
H(44G)	11464	1442	9575	150
H(44H)	11390	2092	8885	150
H(44I)	11655	1512	8916	150
H(51A)	8396	4641	-882	97
H(51B)	8505	3933	-1365	97
H(51C)	8131	5148	-2146	105
H(51D)	8213	4347	-2550	105
H(51E)	7921	4352	-1297	128
H(51F)	7975	3599	-1812	128
H(51A)	7512	4000	-2172	199
H(51B)	7666	4131	-2905	199
H(51C)	7609	4874	-2376	199
H(52A)	8779	6205	-1663	94
H(52B)	8452	5985	-1932	94
H(52C)	8742	6180	-383	121
H(52D)	8419	5906	-626	121
H(52E)	8624	7383	-500	130
H(52F)	8457	7245	-1396	130
H(52A)	8152	7648	-622	550
H(52B)	8244	6911	-37	550
H(52C)	8078	6758	-928	550
H(53A)	8966	4214	-834	98
H(53B)	8881	4942	-329	98
H(53C)	9293	4964	-1316	112
H(53D)	9169	5780	-1043	112

H(53E)	9328	5428	287	151
H(53F)	9449	4609	19	151
H(53A)	9814	5507	406	233
H(53B)	9664	6127	-251	233
H(53C)	9785	5305	-516	233
H(54A)	8941	5191	-2362	93
H(54B)	8619	4979	-2734	93
H(54C)	8714	3611	-2355	108
H(54D)	9040	3839	-2043	108
H(54E)	8744	3977	-3678	126
H(54F)	9062	4285	-3383	126
H(54A)	9076	3050	-3964	204
H(54B)	8888	2672	-3389	204
H(54C)	9204	2963	-3035	204
H(61A)	8487	1228	-1438	175
H(61B)	8767	1507	-1729	175
H(61C)	8277	989	-2765	201
H(61D)	8551	1374	-3013	201
H(61E)	8151	2226	-2247	190
H(61F)	8446	2618	-2318	190
H(61A)	8109	3137	-3226	334
H(61B)	8004	2276	-3555	334
H(61C)	8306	2600	-3665	334
H(62A)	8381	-146	-2701	133
H(62B)	8544	-836	-2154	133
H(62C)	8312	-444	-1126	151
H(62D)	8142	213	-1701	151
H(62E)	8101	-1406	-1916	143
H(62F)	7936	-759	-2515	143
H(62A)	7632	-1294	-1733	240
H(62B)	7675	-364	-1547	240
H(62C)	7842	-1006	-941	240
H(63A)	8715	189	-670	175
H(63B)	9009	459	-885	175
H(63C)	8806	-1182	-977	167
H(63D)	9094	-923	-1250	167
H(63E)	8973	-712	241	194
H(63F)	9257	-419	-26	194
H(63A)	9337	-1608	633	243
H(63B)	9364	-1729	-272	243
H(63C)	9084	-2014	16	243
H(64A)	8794	450	-2899	151
H(64B)	8927	-347	-2478	151
H(64C)	9149	1218	-2086	175
H(64D)	9278	435	-1624	175
H(64E)	9281	743	-3244	212
H(64F)	9413	-32	-2775	212
H(64A)	9802	865	-2868	353
H(64B)	9783	818	-1951	353
H(64C)	9656	1572	-2471	353

Crystal Data of *fac*-$[N^nBu_4]_2K[Os(NCS)_3(SCN)_3]$

Table 1. Crystal data and structure refinement for osscn6.

A. CRYSTAL DATA	
Empirical formula	C38 H72 K N8 Os S6 [NBu4]2K[fac-Os(NCS)3(SCN)3]
Formula weight	1062.70
Wavelength	0.71073 A
Temperature	150(2) K
Crystal system	Monoclinic
Space group	Cc
Unit cell dimensions	a = 10.5101(17) A alpha = 90 deg. b = 31.466(5) A beta = 99.565(3) deg. c = 15.899(3) A gamma = 90 deg.
Volume	5184.9(14) A^3
Number of reflections for cell	3217 (2 < theta < 22 deg.)
Z	4
Density (calculated)	1.361 Mg/m^3
Absorption coefficient	2.814 mm^-1
F(000)	2188
B. DATA COLLECTION	
Crystal description	Red shard
Crystal size	0.30 x 0.08 x 0.05 mm
Instrument	CCD area detector
Theta range for data collection	1.29 to 26.44 deg.
Index ranges	-13<=h<=12, -39<=k<=34, -16<=l<=19
Reflections collected	13124
Independent reflections	8753 [R(int) = 0.0465]
Scan type	phi and omega scans
Absorption correction	Sadabs

(Tmin= 0.928, Tmax=0.592)

C. SOLUTION AND REFINEMENT.

Solution	Patterson (SHELXS-97 (Sheldrick, 1990))
Refinement type	Full-matrix least-squares on F^2
Program used for refinement	SHELXL-97
Hydrogen atom placement	geometric
Hydrogen atom treatment	riding
Data / restraints / parameters	8753/458/488
Goodness-of-fit on F^2	0.941
Conventional R [F>4sigma(F)]	R1 = 0.0661 [4857 data]
Weighted R (F^2 and all data)	wR2 = 0.1545
Absolute structure parameter	0.055(12)
Final maximum delta/sigma	0.024

Weighting scheme
calc w=1/[\s^2^(Fo^2^)+(0.0686P)^2^+0.0000P] where P=(Fo^2^+2Fc^2^)/3

Largest diff. peak and hole	1.712 and -0.507 e.A^-3

Table 2. Atomic coordinates (x 10^4) and equivalent isotropic displacement parameters (A^2 x 10^3) for osscn6. U(eq) is defined as one third of the trace of the orthogonalized Uij tensor.

	x	y	z	U(eq)
Os(1)	5161(1)	3576(1)	5007(1)	76(1)
S(1)	8254(4)	4713(1)	5450(2)	74(1)
C(1)	7166(11)	4347(4)	5343(9)	65(3)
N(1)	6380(9)	4086(3)	5237(7)	60(2)
S(2)	3879(5)	2941(1)	4699(4)	106(2)
C(2)	2493(10)	3085(3)	4884(9)	70(3)
N(2)	1455(9)	3164(4)	4962(10)	104(4)
S(3)	5897(4)	3452(1)	3690(3)	83(1)
C(3)	7370(9)	3602(4)	3838(9)	69(3)
N(3)	8425(9)	3710(3)	3934(8)	79(3)
S(4)	2675(5)	3857(1)	7185(3)	101(1)
C(4)	3607(12)	3763(4)	6502(8)	77(4)
N(4)	4545(14)	3713(4)	6234(12)	127(5)
S(5)	1734(6)	4506(2)	3937(5)	148(2)
C(5)	2923(14)	4192(5)	4238(11)	107(6)
N(5)	3785(10)	3987(3)	4122(11)	120(4)
S(6)	6701(5)	3102(1)	5776(3)	96(1)
C(6)	7919(14)	3384(5)	6186(11)	105(5)
N(6)	8782(14)	3573(5)	6548(11)	131(5)
K(1)	5340(4)	1080(1)	388(2)	96(1)
N(1A)	9157(10)	2519(3)	2793(7)	78(3)
C(1A)	8505(13)	2513(4)	3564(9)	76(3)
C(2A)	7655(16)	2131(5)	3660(12)	102(5)
C(3A)	6978(18)	2156(5)	4376(12)	116(5)
C(4A)	6100(20)	1803(7)	4493(17)	167(9)
C(5A)	8196(15)	2496(5)	1951(9)	98(4)
C(6A)	7197(17)	2853(6)	1819(12)	121(6)
C(7A)	6097(19)	2800(7)	1106(12)	145(7)
C(8A)	5050(30)	2588(12)	1403(18)	258(17)
C(9A)	9914(14)	2931(4)	2827(10)	83(4)
C(10A)	10784(18)	3009(5)	2187(13)	122(6)
C(11A)	11605(19)	3391(5)	2388(13)	122(6)
C(12A)	12530(20)	3491(6)	1822(18)	163(10)
C(13A)	10045(13)	2135(4)	2788(10)	90(4)
C(14A)	11069(16)	2079(5)	3559(13)	126(7)
C(15A)	11900(20)	1708(6)	3461(15)	153(8)
C(16A)	12720(20)	1581(9)	4200(20)	230(15)
N(1B)	6181(11)	5009(3)	2773(7)	69(3)
C(1B)	6645(15)	4552(4)	2731(10)	92(4)
C(2B)	7180(20)	4434(6)	1939(12)	149(7)
C(3B)	8000(30)	4103(9)	1868(14)	206(11)
C(4B)	8560(30)	4024(8)	1089(15)	197(13)
C(5B)	5062(13)	5092(5)	2039(9)	80(4)
C(6B)	3858(15)	4813(5)	1988(12)	104(5)
C(7B)	2818(15)	4970(5)	1288(11)	108(6)
C(8B)	1637(16)	4747(7)	1267(15)	139(8)
C(9B)	5741(14)	5068(4)	3622(8)	76(3)
C(10B)	5271(15)	5510(5)	3819(9)	91(4)

C(11B)	4704(15)	5510(5)	4615(10)	98(5)
C(12B)	4293(18)	5939(6)	4867(12)	133(7)
C(13B)	7250(13)	5323(4)	2652(9)	77(3)
C(14B)	8411(14)	5335(5)	3345(11)	96(5)
C(15B)	9468(15)	5596(6)	3104(11)	110(5)
C(16B)	10578(18)	5636(7)	3744(14)	148(8)

Table 3. Bond lengths [A] and angles [deg] for osscn6.

Os(1)-N(1)	2.047(8)
Os(1)-N(4)	2.198(14)
Os(1)-N(5)	2.251(13)
Os(1)-S(3)	2.382(5)
Os(1)-S(6)	2.385(5)
Os(1)-S(2)	2.415(4)
S(1)-C(1)	1.612(9)
S(1)-K(1)#1	3.332(5)
C(1)-N(1)	1.156(8)
S(2)-C(2)	1.599(9)
C(2)-N(2)	1.145(9)
N(2)-K(1)#2	2.787(12)
S(3)-C(3)	1.598(9)
C(3)-N(3)	1.147(9)
N(3)-K(1)#1	2.878(11)
S(4)-C(4)	1.606(9)
S(4)-K(1)#2	3.449(6)
C(4)-N(4)	1.148(9)
S(5)-C(5)	1.603(9)
S(5)-K(1)#2	3.462(8)
C(5)-N(5)	1.151(10)
S(6)-C(6)	1.604(9)
C(6)-N(6)	1.156(9)
C(6)-K(1)#1	3.466(16)
N(6)-K(1)#1	2.877(19)
K(1)-N(2)#3	2.787(12)
K(1)-N(6)#4	2.877(19)
K(1)-N(3)#4	2.878(11)
K(1)-S(1)#4	3.332(5)
K(1)-S(4)#3	3.449(6)
K(1)-S(5)#3	3.462(8)
K(1)-C(6)#4	3.466(16)
N(1A)-C(1A)	1.501(15)
N(1A)-C(9A)	1.519(14)
N(1A)-C(13A)	1.529(14)
N(1A)-C(5A)	1.539(15)
C(1A)-C(2A)	1.519(18)
C(2A)-C(3A)	1.442(19)
C(3A)-C(4A)	1.47(2)
C(5A)-C(6A)	1.526(19)
C(6A)-C(7A)	1.487(18)
C(7A)-C(8A)	1.43(2)
C(9A)-C(10A)	1.496(18)
C(10A)-C(11A)	1.482(18)
C(11A)-C(12A)	1.47(2)
C(13A)-C(14A)	1.501(18)
C(14A)-C(15A)	1.485(18)
C(15A)-C(16A)	1.40(2)
N(1B)-C(9B)	1.508(15)
N(1B)-C(1B)	1.521(14)
N(1B)-C(13B)	1.533(15)
N(1B)-C(5B)	1.536(14)
C(1B)-C(2B)	1.511(19)
C(2B)-C(3B)	1.37(2)

C(3B)-C(4B)	1.47(2)
C(5B)-C(6B)	1.532(18)
C(6B)-C(7B)	1.508(18)
C(7B)-C(8B)	1.42(2)
C(9B)-C(10B)	1.524(16)
C(10B)-C(11B)	1.485(18)
C(11B)-C(12B)	1.492(19)
C(13B)-C(14B)	1.503(17)
C(14B)-C(15B)	1.482(18)
C(15B)-C(16B)	1.421(19)

N(1)-Os(1)-N(4)	87.5(4)
N(1)-Os(1)-N(5)	88.9(4)
N(4)-Os(1)-N(5)	100.9(6)
N(1)-Os(1)-S(3)	90.0(3)
N(4)-Os(1)-S(3)	177.5(4)
N(5)-Os(1)-S(3)	79.3(4)
N(1)-Os(1)-S(6)	92.7(3)
N(4)-Os(1)-S(6)	86.7(4)
N(5)-Os(1)-S(6)	172.3(4)
S(3)-Os(1)-S(6)	93.23(16)
N(1)-Os(1)-S(2)	175.0(3)
N(4)-Os(1)-S(2)	96.0(4)
N(5)-Os(1)-S(2)	94.0(3)
S(3)-Os(1)-S(2)	86.41(17)
S(6)-Os(1)-S(2)	83.9(2)
C(1)-S(1)-K(1)#1	85.5(5)
N(1)-C(1)-S(1)	177.7(13)
C(1)-N(1)-Os(1)	172.9(10)
C(2)-S(2)-Os(1)	102.9(4)
N(2)-C(2)-S(2)	174.1(14)
C(2)-N(2)-K(1)#2	131.1(10)
C(3)-S(3)-Os(1)	105.7(5)
N(3)-C(3)-S(3)	179.1(16)
C(3)-N(3)-K(1)#1	135.0(11)
C(4)-S(4)-K(1)#2	83.1(6)
N(4)-C(4)-S(4)	159.1(16)
C(4)-N(4)-Os(1)	138.9(16)
C(5)-S(5)-K(1)#2	82.4(7)
N(5)-C(5)-S(5)	153.2(17)
C(5)-N(5)-Os(1)	131.4(15)
C(6)-S(6)-Os(1)	106.8(7)
N(6)-C(6)-S(6)	174(2)
N(6)-C(6)-K(1)#1	50.7(13)
S(6)-C(6)-K(1)#1	134.9(9)
C(6)-N(6)-K(1)#1	111.1(16)
N(2)#3-K(1)-N(6)#4	98.0(5)
N(2)#3-K(1)-N(3)#4	82.8(4)
N(6)#4-K(1)-N(3)#4	91.8(4)
N(2)#3-K(1)-S(1)#4	162.1(3)
N(6)#4-K(1)-S(1)#4	79.5(4)
N(3)#4-K(1)-S(1)#4	79.6(2)
N(2)#3-K(1)-S(4)#3	83.2(3)
N(6)#4-K(1)-S(4)#3	81.3(3)
N(3)#4-K(1)-S(4)#3	163.4(3)
S(1)#4-K(1)-S(4)#3	113.60(14)
N(2)#3-K(1)-S(5)#3	92.9(3)
N(6)#4-K(1)-S(5)#3	168.0(4)

N(3)#4-K(1)-S(5)#3	84.5(3)
S(1)#4-K(1)-S(5)#3	88.55(14)
S(4)#3-K(1)-S(5)#3	105.15(17)
N(2)#3-K(1)-C(6)#4	92.1(4)
N(6)#4-K(1)-C(6)#4	18.1(3)
N(3)#4-K(1)-C(6)#4	74.0(3)
S(1)#4-K(1)-C(6)#4	80.0(3)
S(4)#3-K(1)-C(6)#4	97.6(3)
S(5)#3-K(1)-C(6)#4	157.1(3)
C(1A)-N(1A)-C(9A)	106.8(9)
C(1A)-N(1A)-C(13A)	110.9(10)
C(9A)-N(1A)-C(13A)	111.1(10)
C(1A)-N(1A)-C(5A)	112.8(10)
C(9A)-N(1A)-C(5A)	109.5(10)
C(13A)-N(1A)-C(5A)	105.8(9)
N(1A)-C(1A)-C(2A)	116.5(11)
C(3A)-C(2A)-C(1A)	114.3(13)
C(2A)-C(3A)-C(4A)	117.4(16)
C(6A)-C(5A)-N(1A)	115.0(11)
C(7A)-C(6A)-C(5A)	117.0(16)
C(8A)-C(7A)-C(6A)	110.0(19)
C(10A)-C(9A)-N(1A)	119.4(11)
C(11A)-C(10A)-C(9A)	112.6(14)
C(12A)-C(11A)-C(10A)	117.7(17)
C(14A)-C(13A)-N(1A)	116.3(11)
C(15A)-C(14A)-C(13A)	111.2(14)
C(16A)-C(15A)-C(14A)	115.2(19)
C(9B)-N(1B)-C(1B)	107.8(9)
C(9B)-N(1B)-C(13B)	111.9(10)
C(1B)-N(1B)-C(13B)	110.9(10)
C(9B)-N(1B)-C(5B)	110.4(11)
C(1B)-N(1B)-C(5B)	109.8(10)
C(13B)-N(1B)-C(5B)	106.1(10)
C(2B)-C(1B)-N(1B)	115.9(12)
C(3B)-C(2B)-C(1B)	125.8(17)
C(2B)-C(3B)-C(4B)	122.7(19)
C(6B)-C(5B)-N(1B)	117.6(12)
C(7B)-C(6B)-C(5B)	110.0(14)
C(8B)-C(7B)-C(6B)	112.2(16)
N(1B)-C(9B)-C(10B)	117.1(10)
C(11B)-C(10B)-C(9B)	111.5(12)
C(10B)-C(11B)-C(12B)	113.9(14)
C(14B)-C(13B)-N(1B)	116.5(10)
C(15B)-C(14B)-C(13B)	112.1(13)
C(16B)-C(15B)-C(14B)	115.1(15)

Symmetry transformations used to generate equivalent atoms:

#1 x+1/2,-y+1/2,z+1/2 #2 x-1/2,-y+1/2,z+1/2

#3 x+1/2,-y+1/2,z-1/2 #4 x-1/2,-y+1/2,z-1/2

Table 4. Anisotropic displacement parameters (A^2 x 10^3) for osscn6. The anisotropic displacement factor exponent takes the form:
-2 pi^2 [h^2 a*^2 U11 + ... + 2 h k a* b* U12]

	U11	U22	U33	U23	U13	U12
Os(1)	89(1)	50(1)	94(1)	-7(1)	32(1)	-6(1)
S(1)	82(2)	65(2)	74(3)	7(2)	8(2)	-7(2)
C(1)	77(9)	62(8)	62(8)	-20(7)	30(7)	0(5)
N(1)	58(6)	64(5)	63(6)	3(5)	29(5)	5(4)
S(2)	106(3)	54(2)	168(5)	-14(3)	56(3)	-4(2)
C(2)	88(7)	27(6)	95(10)	-8(6)	16(9)	2(5)
N(2)	84(7)	60(7)	170(13)	-5(8)	22(9)	-7(6)
S(3)	93(3)	73(2)	87(3)	0(2)	25(2)	-1(2)
C(3)	97(8)	54(7)	57(8)	-13(7)	16(7)	1(8)
N(3)	95(7)	66(7)	76(8)	-18(6)	18(7)	-1(6)
S(4)	111(3)	91(3)	107(4)	8(2)	37(3)	11(2)
C(4)	79(9)	57(8)	98(10)	-5(7)	23(7)	-14(7)
N(4)	170(12)	31(6)	217(9)	-3(6)	145(10)	-19(6)
S(5)	139(5)	125(4)	187(6)	-1(4)	45(5)	31(4)
C(5)	139(13)	59(10)	121(14)	31(9)	13(10)	9(8)
N(5)	73(7)	42(5)	227(12)	-43(6)	-24(8)	-11(4)
S(6)	129(4)	64(3)	97(3)	0(2)	29(3)	16(2)
C(6)	123(11)	88(10)	104(14)	25(9)	19(9)	7(7)
N(6)	133(13)	116(12)	139(15)	24(10)	8(10)	-3(9)
K(1)	101(3)	94(2)	90(3)	0(2)	4(2)	-28(2)
N(1A)	81(7)	60(6)	92(7)	-27(5)	15(5)	4(4)
C(1A)	79(9)	60(7)	88(8)	-9(7)	14(6)	16(6)
C(2A)	86(11)	93(10)	133(14)	-14(10)	39(9)	6(8)
C(3A)	133(14)	87(11)	140(15)	7(10)	63(10)	23(9)
C(4A)	132(18)	180(20)	220(20)	16(19)	92(16)	-8(13)
C(5A)	118(11)	91(10)	85(8)	-25(8)	20(7)	-9(7)
C(6A)	106(12)	141(15)	106(13)	1(11)	-7(9)	12(9)
C(7A)	138(14)	183(19)	101(15)	-29(13)	-18(10)	-33(12)
C(8A)	180(20)	400(40)	200(30)	-140(30)	60(20)	-140(30)
C(9A)	92(10)	58(6)	98(11)	-11(7)	11(7)	8(6)
C(10A)	123(13)	90(10)	166(16)	-21(10)	65(10)	-1(8)
C(11A)	148(15)	72(9)	150(16)	18(10)	41(11)	1(8)
C(12A)	154(19)	98(15)	260(30)	19(15)	94(18)	8(11)
C(13A)	90(9)	62(7)	126(11)	-19(8)	43(7)	7(6)
C(14A)	94(12)	83(10)	192(17)	-33(11)	-4(10)	27(8)
C(15A)	122(15)	110(14)	230(20)	11(14)	44(13)	50(11)
C(16A)	124(19)	200(20)	340(30)	-20(20)	-40(20)	87(17)
N(1B)	85(7)	56(6)	66(6)	18(5)	8(5)	18(5)
C(1B)	96(10)	61(6)	112(11)	18(7)	0(8)	19(6)
C(2B)	217(19)	112(13)	111(13)	-27(10)	4(12)	68(12)
C(3B)	230(20)	270(20)	139(17)	65(16)	80(15)	162(18)
C(4B)	210(20)	240(30)	180(20)	106(19)	127(19)	120(20)
C(5B)	84(7)	91(9)	62(7)	6(7)	6(7)	36(6)
C(6B)	92(9)	101(12)	110(13)	-11(10)	-4(9)	26(8)
C(7B)	95(9)	114(13)	105(13)	-21(10)	-10(9)	36(9)
C(8B)	83(10)	160(19)	160(20)	-4(16)	-10(13)	46(10)
C(9B)	84(9)	81(8)	60(7)	26(6)	5(6)	-6(7)
C(10B)	89(10)	118(10)	65(9)	0(8)	6(7)	17(8)

C(11B)	78(11)	132(12)	85(10)	11(8)	18(7)	8(9)
C(12B)	119(14)	175(16)	112(14)	-26(12)	44(12)	24(13)
C(13B)	95(8)	68(7)	74(9)	4(7)	29(6)	6(6)
C(14B)	95(10)	82(10)	109(12)	14(9)	16(8)	-3(8)
C(15B)	110(10)	100(12)	124(14)	-2(10)	35(9)	-17(9)
C(16B)	107(13)	164(19)	180(20)	13(16)	31(11)	-43(13)

Table 5. Hydrogen coordinates (x 10^4) and isotropic displacement parameters (A^2 x 10^3) for osscn6.

	x	y	z	U(eq)
H(1A1)	7969	2773	3554	91
H(1A2)	9179	2530	4078	91
H(2A1)	7015	2101	3131	122
H(2A2)	8199	1873	3720	122
H(3A1)	6468	2422	4322	139
H(3A2)	7628	2180	4901	139
H(4A1)	5745	1849	5017	251
H(4A2)	6583	1535	4536	251
H(4A3)	5400	1791	4005	251
H(5A1)	8688	2502	1472	117
H(5A2)	7736	2221	1928	117
H(6A1)	6842	2887	2354	145
H(6A2)	7648	3120	1724	145
H(7A1)	5807	3082	875	174
H(7A2)	6377	2633	643	174
H(8A1)	4366	2531	920	387
H(8A2)	4720	2769	1819	387
H(8A3)	5362	2319	1674	387
H(9A1)	9284	3168	2778	100
H(9A2)	10447	2952	3401	100
H(10A)	11344	2758	2165	146
H(10B)	10252	3045	1616	146
H(11A)	11029	3639	2396	146
H(11B)	12092	3357	2973	146
H(12A)	13031	3743	2036	245
H(12B)	12066	3547	1246	245
H(12C)	13117	3250	1806	245
H(13A)	9504	1875	2722	108
H(13B)	10473	2155	2280	108
H(14A)	11606	2339	3645	151
H(14B)	10657	2039	4070	151
H(15A)	11345	1464	3247	184
H(15B)	12439	1776	3021	184
H(16A)	13203	1328	4084	345
H(16B)	12207	1516	4647	345
H(16C)	13328	1811	4398	345
H(1B1)	7319	4499	3234	110
H(1B2)	5912	4360	2777	110
H(2B1)	6427	4389	1487	179
H(2B2)	7623	4692	1775	179
H(3B1)	7544	3840	1982	248
H(3B2)	8740	4134	2342	248
H(4B1)	8977	3745	1129	295
H(4B2)	9199	4244	1031	295
H(4B3)	7872	4031	591	295
H(5B1)	4792	5392	2078	96
H(5B2)	5397	5061	1496	96
H(6B1)	4078	4515	1873	124
H(6B2)	3539	4821	2540	124
H(7B1)	2671	5276	1373	129

H(7B2)	3113	4936	732	129
H(8B1)	991	4859	805	209
H(8B2)	1332	4785	1813	209
H(8B3)	1773	4444	1171	209
H(9B1)	6467	4991	4077	91
H(9B2)	5035	4864	3654	91
H(10C)	6003	5711	3880	110
H(10D)	4614	5607	3338	110
H(11C)	5347	5395	5085	118
H(11D)	3947	5319	4538	118
H(12D)	3964	5918	5407	199
H(12E)	3612	6049	4423	199
H(12F)	5033	6133	4936	199
H(13C)	7545	5255	2108	93
H(13D)	6870	5612	2593	93
H(14C)	8158	5453	3871	115
H(14D)	8727	5042	3471	115
H(15C)	9733	5469	2590	132
H(15D)	9128	5884	2948	132
H(16D)	11216	5817	3534	222
H(16E)	10951	5355	3886	222
H(16F)	10332	5765	4255	222

Crystal Data of $[N^nBu_4]_3[Os(NCS)_6]$

Table 1. Crystal data and structure refinement for ncs066.

A. CRYSTAL DATA

Empirical formula	C54 H108 N9 Os1 S6 [NBu4]3[Os(NCS)6]
Formula weight	1265.91
Wavelength	0.71073 A
Temperature	150 K
Crystal system	Cubic
Space group	P a -3
Unit cell dimensions	a = 24.195(2) A alpha = 90 deg. b = 24.195(2) A beta = 90 deg. c = 24.195(2) A gamma = 90 deg.
Volume	14163.7 A^3
Number of reflections for cell	6536 (3 < theta < 27 deg.)
Z	8
Density (calculated)	1.187 Mg/m^3
Absorption coefficient	2.012 mm^-1
F(000)	5327.977

B. DATA COLLECTION

Crystal description	orange-brown block
Crystal size	0.27 x 0.27 x 0.36 mm
Instrument	Smart Apex
Theta range for data collection	1.46 to 28.82 deg.
Index ranges	-31<=h<=32, -25<=k<=31, -26<=l<=32
Reflections collected	88308
Independent reflections	6153 [R(int) = 0.04]
Scan type	\f & \w scans

Absorption correction	Semi-empirical from equivalents (Tmin= 0.656, Tmax=1.000)

C. SOLUTION AND REFINEMENT.

Solution	direct (Shelxs)
Refinement type	Full-matrix least-squares on F
Program used for refinement	CRYSTALS
Hydrogen atom placement	geom
Hydrogen atom treatment	noref
Data	3722
Parameters	212
Goodness-of-fit on F^2	0.9970
R	0.0574
Rw	0.0458
Extinction coefficient	74.3(296)
Final maximum delta/sigma	0.001138
Weighting scheme	Chebychev Polynomial
Largest diff. peak and hole	2.10 and -2.26 e.A^-3

Table 2. Atomic coordinates (x 10^4) and equivalent isotropic displacement parameters (A^2 x 10^3) for ncs066. U(eq) is defined as one third of the trace of the orthogonalized Uij tensor.

	x	y	z	U(eq)
OS1	1892(1)	1892(1)	1892(1)	35
S(1)	2677(1)	650(1)	560(1)	61
N(1)	2187(2)	1337(2)	1344(2)	40
C(1)	2394(2)	1053(2)	1019(2)	43
S(2)	1402(1)	3325(1)	3163(1)	55
N(2)	1627(2)	2469(2)	2436(2)	40
C(2)	1540(2)	2820(2)	2735(2)	36
N(3)	2420(2)	326(2)	-2641(2)	46
C(11)	2693(2)	565(2)	-2123(3)	56
C(21)	2925(3)	144(3)	-1730(3)	71
C(31)	3121(4)	442(5)	-1199(4)	111
C(41)	3364(5)	54(7)	-782(4)	156
C(12)	2183(2)	814(2)	-2970(2)	46
C(22)	1903(3)	661(3)	-3486(3)	77
C(32)	1632(3)	1157(3)	-3765(3)	73
C(42)	1315(4)	963(4)	-4302(4)	109
C(13)	2828(2)	-1(2)	-2990(2)	50
C(23)	3332(2)	319(2)	-3185(3)	58
C(33)	3633(3)	15(3)	-3637(3)	61
C(43)	4127(3)	340(3)	-3848(3)	79
C(14)	1955(2)	-66(2)	-2485(2)	52
C(24)	1524(3)	173(2)	-2095(3)	58
C(34)	986(3)	-124(3)	-2112(3)	66
C(44)	558(3)	122(3)	-1736(4)	84

Table 3. Bond lengths [A] and angles [deg] for ncs066.

Os(1)-N(1)	2.016(4)
Os(1)-N(1)#1	2.016(4)
Os(1)-N(1)#2	2.016(4)
Os(1)-N(2)	2.023(4)
Os(1)-N(2)#1	2.023(4)
Os(1)-N(2)#2	2.023(4)
S(1)-C(1)	1.629(5)
N(1)-C(1)	1.161(6)
S(2)-C(2)	1.635(5)
N(2)-C(2)	1.137(6)
N(3)-C(11)	1.531(7)
N(3)-C(12)	1.536(6)
N(3)-C(13)	1.523(7)
N(3)-C(14)	1.518(6)
C(11)-C(21)	1.503(9)
C(11)-H(111)	1.000
C(11)-H(112)	0.998
C(21)-C(31)	1.549(11)
C(21)-H(211)	0.999
C(21)-H(212)	1.000
C(31)-C(41)	1.498(14)
C(31)-H(311)	0.999
C(31)-H(312)	1.000
C(41)-H(411)	1.001
C(41)-H(412)	0.999
C(41)-H(413)	1.000
C(12)-C(22)	1.468(9)
C(12)-H(121)	1.000
C(12)-H(122)	1.000
C(22)-C(32)	1.524(9)
C(22)-H(221)	1.000
C(22)-H(222)	0.999
C(32)-C(42)	1.579(12)
C(32)-H(321)	1.001
C(32)-H(322)	0.998
C(42)-H(421)	0.996
C(42)-H(422)	1.000
C(42)-H(423)	1.003
C(13)-C(23)	1.519(8)
C(13)-H(131)	0.999
C(13)-H(132)	1.001
C(23)-C(33)	1.506(8)
C(23)-H(231)	1.001
C(23)-H(232)	1.001
C(33)-C(43)	1.518(9)
C(33)-H(331)	1.001
C(33)-H(332)	0.999
C(43)-H(431)	1.001
C(43)-H(432)	1.000
C(43)-H(433)	1.000
C(14)-C(24)	1.520(8)
C(14)-H(141)	1.001
C(14)-H(142)	1.000
C(24)-C(34)	1.488(8)

C(24)-H(241)	1.000
C(24)-H(242)	1.000
C(34)-C(44)	1.502(9)
C(34)-H(341)	0.998
C(34)-H(342)	1.003
C(44)-H(441)	0.998
C(44)-H(442)	1.000
C(44)-H(443)	1.005

N(1)-Os(1)-N(1)#1	91.74(16)
N(1)-Os(1)-N(1)#2	91.74(16)
N(1)#1-Os(1)-N(1)#2	91.74(16)
N(1)-Os(1)-N(2)	177.47(16)
N(1)#1-Os(1)-N(2)	90.69(16)
N(1)#2-Os(1)-N(2)	88.90(16)
N(1)-Os(1)-N(2)#1	88.90(16)
N(1)#1-Os(1)-N(2)#1	177.47(16)
N(1)#2-Os(1)-N(2)#1	90.69(16)
N(2)-Os(1)-N(2)#1	88.65(17)
N(1)-Os(1)-N(2)#2	90.69(16)
N(1)#1-Os(1)-N(2)#2	88.90(16)
N(1)#2-Os(1)-N(2)#2	177.47(16)
N(2)-Os(1)-N(2)#2	88.65(17)
N(2)#1-Os(1)-N(2)#2	88.65(17)
Os(1)-N(1)-C(1)	173.7(4)
S(1)-C(1)-N(1)	179.2(5)
Os(1)-N(2)-C(2)	171.7(4)
S(2)-C(2)-N(2)	178.9(4)
C(11)-N(3)-C(12)	107.1(4)
C(11)-N(3)-C(13)	111.8(4)
C(12)-N(3)-C(13)	110.7(4)
C(11)-N(3)-C(14)	110.6(4)
C(12)-N(3)-C(14)	109.5(4)
C(13)-N(3)-C(14)	107.2(4)
N(3)-C(11)-C(21)	114.9(5)
N(3)-C(11)-H(111)	108.045
C(21)-C(11)-H(111)	107.918
N(3)-C(11)-H(112)	108.146
C(21)-C(11)-H(112)	108.069
H(111)-C(11)-H(112)	109.655
C(11)-C(21)-C(31)	108.8(7)
C(11)-C(21)-H(211)	109.595
C(31)-C(21)-H(211)	109.750
C(11)-C(21)-H(212)	109.446
C(31)-C(21)-H(212)	109.707
H(211)-C(21)-H(212)	109.518
C(21)-C(31)-C(41)	112.7(9)
C(21)-C(31)-H(311)	108.413
C(41)-C(31)-H(311)	108.855
C(21)-C(31)-H(312)	108.400
C(41)-C(31)-H(312)	108.848
H(311)-C(31)-H(312)	109.555
C(31)-C(41)-H(411)	109.298
C(31)-C(41)-H(412)	109.578
H(411)-C(41)-H(412)	109.502
C(31)-C(41)-H(413)	109.526
H(411)-C(41)-H(413)	109.368
H(412)-C(41)-H(413)	109.555

N(3)-C(12)-C(22)	114.8(4)
N(3)-C(12)-H(121)	108.164
C(22)-C(12)-H(121)	108.122
N(3)-C(12)-H(122)	108.172
C(22)-C(12)-H(122)	108.091
H(121)-C(12)-H(122)	109.393
C(12)-C(22)-C(32)	112.2(6)
C(12)-C(22)-H(221)	108.588
C(32)-C(22)-H(221)	108.911
C(12)-C(22)-H(222)	108.634
C(32)-C(22)-H(222)	108.852
H(221)-C(22)-H(222)	109.616
C(22)-C(32)-C(42)	109.8(6)
C(22)-C(32)-H(321)	109.432
C(42)-C(32)-H(321)	109.103
C(22)-C(32)-H(322)	109.577
C(42)-C(32)-H(322)	109.378
H(321)-C(32)-H(322)	109.493
C(32)-C(42)-H(421)	109.701
C(32)-C(42)-H(422)	109.492
H(421)-C(42)-H(422)	109.732
C(32)-C(42)-H(423)	109.218
H(421)-C(42)-H(423)	109.504
H(422)-C(42)-H(423)	109.178
N(3)-C(13)-C(23)	115.4(4)
N(3)-C(13)-H(131)	108.028
C(23)-C(13)-H(131)	108.046
N(3)-C(13)-H(132)	107.919
C(23)-C(13)-H(132)	107.918
H(131)-C(13)-H(132)	109.459
C(13)-C(23)-C(33)	111.4(5)
C(13)-C(23)-H(231)	108.918
C(33)-C(23)-H(231)	109.113
C(13)-C(23)-H(232)	109.025
C(33)-C(23)-H(232)	109.048
H(231)-C(23)-H(232)	109.294
C(23)-C(33)-C(43)	111.8(6)
C(23)-C(33)-H(331)	108.852
C(43)-C(33)-H(331)	108.828
C(23)-C(33)-H(332)	108.953
C(43)-C(33)-H(332)	108.912
H(331)-C(33)-H(332)	109.514
C(33)-C(43)-H(431)	109.462
C(33)-C(43)-H(432)	109.576
H(431)-C(43)-H(432)	109.360
C(33)-C(43)-H(433)	109.535
H(431)-C(43)-H(433)	109.396
H(432)-C(43)-H(433)	109.498
N(3)-C(14)-C(24)	115.2(4)
N(3)-C(14)-H(141)	107.958
C(24)-C(14)-H(141)	108.056
N(3)-C(14)-H(142)	108.051
C(24)-C(14)-H(142)	108.105
H(141)-C(14)-H(142)	109.390
C(14)-C(24)-C(34)	113.5(5)
C(14)-C(24)-H(241)	108.496
C(34)-C(24)-H(241)	108.335
C(14)-C(24)-H(242)	108.459

C(34)-C(24)-H(242)	108.512
H(241)-C(24)-H(242)	109.467
C(24)-C(34)-C(44)	113.3(5)
C(24)-C(34)-H(341)	108.811
C(44)-C(34)-H(341)	108.404
C(24)-C(34)-H(342)	108.535
C(44)-C(34)-H(342)	108.341
H(341)-C(34)-H(342)	109.441
C(34)-C(44)-H(441)	109.856
C(34)-C(44)-H(442)	109.555
H(441)-C(44)-H(442)	109.686
C(34)-C(44)-H(443)	109.416
H(441)-C(44)-H(443)	109.239
H(442)-C(44)-H(443)	109.072

Symmetry transformations used to generate equivalent atoms:
#1 y,z,x #2 z,x,y

Table 4. Anisotropic displacement parameters (A^2 x 10^3) for ncs066. The anisotropic displacement factor exponent takes the form:
-2 pi^2 [h^2 a*^2 U11 + ... + 2 h k a* b* U12]

	U11	U22	U33	U23	U13	U12
Os(1)	35(1)	35(1)	35(1)	-2(1)	-2(1)	-2(1)
S(1)	74(1)	55(1)	54(1)	-11(1)	4(1)	15(1)
N(1)	40(2)	40(2)	39(2)	-5(2)	0(2)	3(2)
C(1)	47(3)	39(3)	44(3)	4(2)	-9(2)	0(2)
S(2)	77(1)	42(1)	45(1)	-8(1)	14(1)	-8(1)
N(2)	43(2)	38(2)	39(2)	-4(2)	1(2)	1(2)
C(2)	34(2)	38(2)	36(2)	8(2)	0(2)	-8(2)
N(3)	48(2)	35(2)	54(3)	-1(2)	7(2)	-4(2)
C(11)	53(3)	50(3)	67(3)	-7(3)	3(3)	-3(3)
C(21)	47(3)	93(5)	73(4)	4(4)	-8(3)	-2(3)
C(31)	96(6)	142(8)	94(6)	-2(6)	-30(5)	-3(6)
C(41)	135(9)	247(15)	85(7)	-16(8)	-21(7)	40(10)
C(12)	43(3)	36(2)	59(3)	4(2)	11(2)	-1(2)
C(22)	104(5)	62(4)	64(4)	4(3)	4(4)	28(4)
C(32)	65(4)	70(4)	83(5)	20(4)	15(4)	17(3)
C(42)	99(6)	139(8)	88(6)	22(6)	0(5)	25(6)
C(13)	49(3)	39(3)	62(4)	6(2)	8(2)	6(2)
C(23)	50(3)	52(3)	72(4)	10(3)	5(3)	1(2)
C(33)	57(3)	63(4)	64(4)	22(3)	12(3)	16(3)
C(43)	43(3)	98(5)	95(5)	21(4)	10(3)	9(3)
C(14)	48(3)	40(2)	67(3)	-2(2)	10(3)	-8(2)
C(24)	64(4)	43(3)	66(3)	-11(3)	19(3)	-9(3)
C(34)	54(3)	63(4)	81(4)	-11(3)	6(3)	1(3)
C(44)	60(4)	73(4)	117(6)	-24(4)	24(4)	-6(3)

Table 5. Hydrogen coordinates (x 10^4) and isotropic displacement parameters (A^2 x 10^3) for ncs066.

	x	y	z	U(eq)
H(111)	3002	811	-2243	68
H(112)	2411	788	-1920	68
H(211)	3243	-50	-1907	85
H(212)	2631	-132	-1634	85
H(311)	3407	721	-1304	133
H(312)	2796	634	-1030	133
H(411)	3483	269	-449	188
H(412)	3690	-138	-946	188
H(413)	3080	-225	-671	188
H(121)	2495	1069	-3064	55
H(122)	1912	1012	-2730	55
H(221)	2181	498	-3744	92
H(222)	1612	382	-3400	92
H(321)	1923	1431	-3872	87
H(322)	1365	1334	-3505	87
H(421)	1138	1287	-4484	130
H(422)	1582	785	-4563	130
H(423)	1023	688	-4196	130
H(131)	2629	-141	-3323	60
H(132)	2961	-322	-2764	60
H(231)	3210	687	-3328	70
H(232)	3589	374	-2866	70
H(331)	3373	-50	-3952	74
H(332)	3765	-348	-3490	74
H(431)	4316	126	-4147	95
H(432)	3999	703	-3999	95
H(433)	4392	405	-3537	95
H(141)	1763	-181	-2833	62
H(142)	2122	-398	-2304	62
H(241)	1458	568	-2198	69
H(242)	1672	154	-1709	69
H(341)	841	-114	-2498	79
H(342)	1049	-518	-1998	79
H(441)	207	-94	-1762	104
H(442)	488	515	-1844	104
H(443)	696	111	-1344	104

Courses and Conferences Attended

Inorganic Seminars and Colloquia.

Butler Electrochemistry Meeting, University of St. Andrews, July 1999.

The Chemistry of the Platinum Group Metals, University of Nottingham, July 1999.

ICCC, University of Edinburgh, July 2000.

1st Chianti Electrochemistry Meeting, Certosa di Pontignano, Siena, 2000.

Introduction to Electrochemistry Lecture Course, Siena, 2000.